The Institute of Paper Science and Technology

Atlanta, Georgia

Doctor's Dissertation

An Investigation of the Role of Mixing Conditions During Polymeric Retention Aid Addition on the Adsorption Homogeneity

Christopher O. Luettgen

March, 1992

INSTITUTE OF PAPER SCIENCE AND TECHNOLOGY
Atlanta, Georgia

AN INVESTIGATION OF THE ROLE OF MIXING CONDITIONS DURING POLYMERIC RETENTION AID ADDITION ON THE ADSORPTION HOMOGENEITY

A-490 thesis final copy submitted by

Christopher O. Luettgen

B.S. 1985, Western Michigan University
Kalamazoo, Michigan

M.S. 1987, Lawrence University - The Institute of Paper Chemistry
Appleton, Wisconsin

in partial fulfillment of the requirements
of the Institute of Paper Science and Technology
for the degree of Doctor of Philosophy

March 6, 1992

"for I have dream'd of bloody turbulence, and this whole night hath nothing been but shapes and forms..."

William Shakespeare

TABLE OF CONTENTS

LIST OF FIGURES AND TABLES

Figure:

Table:

ABSTRACT

Many techniques have been used for introducing a polymeric retention aid to a pulp furnish. The mixing conditions during this dispersion process may play a role in the uniformity of the polymer adsorption and thus the efficiency of the retention aid addition. An investigation of the relationship between mixing conditions during the polymer introduction, polymer adsorption uniformity, and retention efficiency has been undertaken. Laboratory- and pilot-scale equipment have been employed to quantify a dispersion of an injected material into a turbulent flow of pulp and to study the adsorption characteristics.

On a pilot scale, a side-port injection into a turbulent pipeline flow of a dilute fiber suspension was studied for the influence of pipe and jet velocity conditions on dispersion. Adsorption homogeneity was examined using an automated electrophoresis device. Laboratory mixing conditions were found to alter the adsorption characteristics; however, adsorption was independent of the dispersion capabilities of the single side-port injection method. The adsorption created by the side-port injection may have occurred too quickly for dispersion differences to cause changes in adsorption or too slowly as adsorption may have occurred downstream.

An additional finding from this work came from the on-line tracking of the injected polymer solution. The solution dispersion in the turbulent pulp suspension occurred to a greater extent than in a pure water flow at the same flow rates. For drag-reducing flow, this result is counterintuitive. An attempt has been made to rationalize this finding in light of recent studies on turbulence intensity in suspension flows.

Further work using electrophoresis has suggested a time scale necessary for adsorption to reach an equilibrium state of a plateau mobility. Untreated latex spheres and polyelectrolyte were mixed in a Y-junction and injected directly into an electrophoresis cell. Initial changes of mobility with time were found to be dependent on concentration and mixing condition. The fastest equilibrium electrophoretic mobility (EM) was obtained in seven to 10 seconds; for the slowest rates, equilibrium was not yet obtained in 10 minutes. Also, the width of the EM distribution was found to be more broad for lower concentrations and lower Reynolds number mixing conditions; a dependency on collision rate seems to occur. Additional laboratory mixing studies have shown an optimum retention at a relatively low level of mixing at which an inhomogeneous adsorption state was found to occur.

INTRODUCTION

Many techniques are used for introducing polymeric retention aids to pulp furnishes. The mixing conditions during the dispersion process may play a role in the uniformity of polymer adsorption and thus affect the efficiency of the retention aid addition process. An investigation of the relationship between mixing conditions during polymer introduction, polymer adsorption uniformity, and retention efficiency has been undertaken.

Intuitively, the procedure used for polymer addition has a significant effect on the uniformity of the polymer adsorption due to a shear rate and adsorption time interaction. Adsorption kinetics are likely to be governed by collision theory. The distribution of polymer throughout the pulp sample would therefore be influenced by the mixing conditions during the polymer addition. Measuring the homogeneity of polymer adsorption onto furnish particles would reveal the relationship between the precise conditions for polymer addition and retention efficiency. Through new instrument methods, a distribution of the mobility, or zeta-potential, of particles in a sample is measured. The homogeneity of this distribution describes the polymer adsorption uniformity. A significant advancement would be to understand the role of the polymer addition process on adsorption homogeneity and the resultant retention efficiency; this thesis attempts to make such a contribution.

The literature review following focuses on existing theories of polymer adsorption and particle flocculation. The relevance of suspension flow characteristics, turbulent flows of suspensions, and the geometry of polymer addition on the problem statement are also discussed.

REVIEW OF THE LITERATURE

In order to prepare the reader for a better understanding of the design considerations of the experimental procedures, the literature is presented in several sections. The topics discussed are electrokinetic phenomena, polymer adsorption theory and particle flocculation mechanisms, adsorption behavior under shear flows, and fluid dynamic aspects of the problem statement.

THEORY OF ELECTROKINETIC PHENOMENA

The Zeta-potential Concept

Most materials develop a surface charge when immersed in water. Due to the nature of cellulosic and ligneous material in wood pulp, fiber surfaces obtain a negative charge. Positive ions in the solution are preferentially adsorbed onto the surface, thus decreasing the magnitude of the electric potential. A layer of these ions not removed by a shearing flow surrounds the particle and is referred to as the shear layer. Outside this layer is a diffuse atmosphere of ions which will decrease the electric potential exponentially to zero. This concept of a layer of shear gives rise to a potential that is not equal to the surface potential but can be measured across the diffuse layer. The electric potential at the shear layer is referred to as the zeta-potential, ζ.

The notion of a shear layer of adsorbed ions and a diffuse layer of ions was suggested as a model by Gouy[1] and Chapman[2] and extended later by Stern[3] to describe the repulsive and attractive forces between colloidal particles in solution. Figure 1 is a depiction of this model. Many important properties of colloidal systems are determined by the electrical

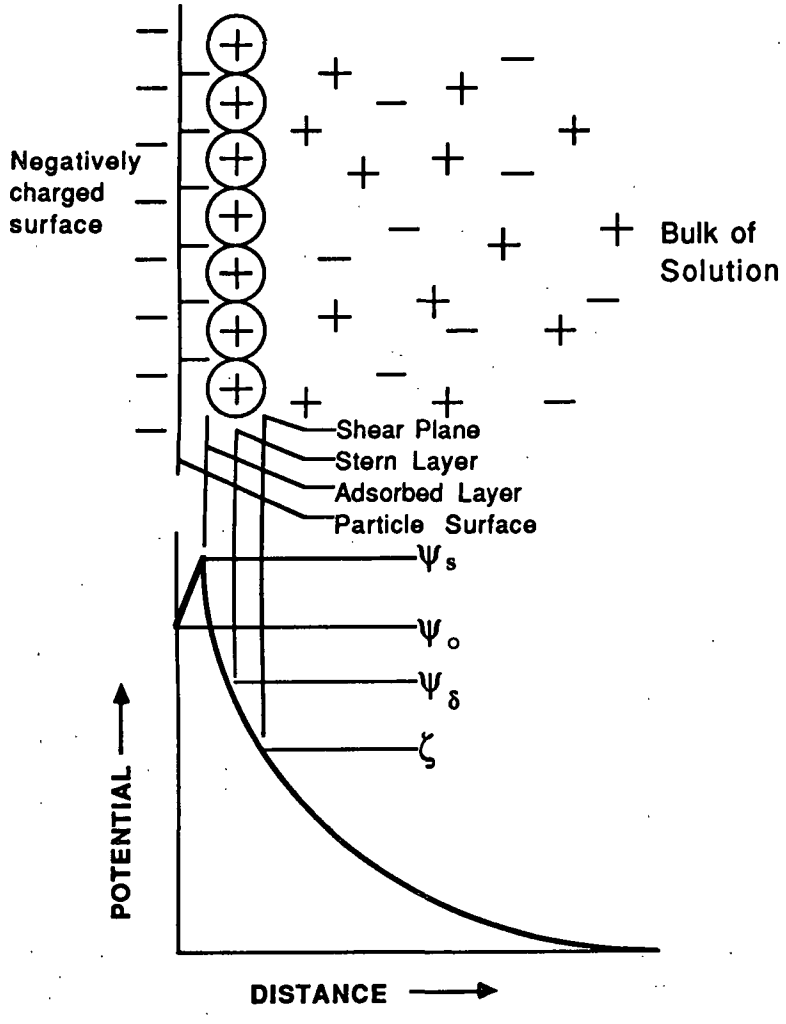

Figure 1. A model for the electrokinetic double layer showing an adsorbed layer of ions.

potential about the particles. The electrical potential distribution determines the interaction energy between particles and is responsible for the stability of particles toward coagulation and for many aspects of the rheological and hydrodynamic flow behavior of suspensions.

Papermakers have attempted to correlate ζ-potential with the cationic demand of pulp furnish[§] in order to optimize the machine retention. Zeta-potential has, in some cases, been found to be a good indicator of paper machine upsets.

Zeta-potential can give an indication of an effective charge density for a particle surface. Thus, the assumption that all surfaces within the same furnish are of equal charge density is used in a significant role when explaining the mechanisms of electrolyte and polymer adsorption. The ζ-potential has been measured for colloidal materials by electrokinetic methods. These methods will now be discussed so that their application may be better understood.

Application of Electrokinetic Phenomena

Electrokinetic phenomena have been reviewed extensively in the literature.[4,5,6,7,8] The surface charge of a colloidal particle is difficult to measure due to the surrounding Stern layer. The potential at the layer of shear with respect to the bulk solution, or the ζ-potential, is measured instead. The zeta-potential is calculated from the results of four types of electrokinetic phenomena measurement. Electroosmosis is the movement of a liquid with respect to a stationary charged surface (e.g., a capillary wall or a porous plug) resulting from an applied electric field. If a surface is negatively charged, there will be a net excess of positive ions in the adjacent liquid. As the ions move under the influence of the applied field, they will draw the liquid along with them. Measurement of the velocity of the liquid, or the volume of liquid transported per unit current flow, gives information regarding the

[§] Cationic demand may be defined as a dosage of cationic molecule that can neutralize the negative surface charges of a colloid in solution to an isoelectric point, or a point of zero remaining surface charge.

electrical potential in the neighborhood of the stationary charged surface.

Instead of applying an electric field to cause liquid to move through a capillary or plug, one can force the liquid to flow using a pressure gradient. The ions near a wall are carried along with the liquid and their accumulation downstream causes the buildup of an electric field. The induced electric field drives an electric current back, via ionic conduction through the liquid, against the direction of liquid flow. A steady state is quickly established, and the measured potential across the capillary or plug is called the streaming potential.

Electrophoresis is the movement of particles in an electric field. The surface of the shear plane forms a sheath which envelops the particle. The materials inside this sheath form a unit such that the particle moves with its contained charge. Measurement of the mobility of the particle under electrophoresis (i.e., the velocity per unit electric field strength) gives a measure of the electric charge of the solid particle.

The converse of electrophoresis is the development of a potential from a particle moving by some external means. When charged particles are allowed to settle (or rise) through a fluid under a gravitational or centrifugal field, a potential gradient is generated. This potential is called the sedimentation potential. As the particle moves, it leaves behind an atmosphere of charge from the diffuse layer. The potential which is developed is thus related to the zeta-potential. The potential generated by falling particles is the Dorn effect.

Electrophoresis is the most commonly used method for measuring zeta-potential for a wide range of materials. The paper industry has relied on the microelectrophoresis method

for electrophoretic mobility (EM) measurements of pulp fines* and filler particles. It has been suggested that fines have surface properties which are identical to larger particles within the pulp slurry.[9,10,11] For example, Jaycock et al.[10] found that a group of fillers taken separately have different EM versus pH curves and different isoelectric points; when each was exposed to fiber fines, the curves changed, and each filler had more similar isoelectric points.

Attempts to apply electrokinetic phenomena other than electrophoresis to pulp measurements have been unsuccessful due to specific problems associated with wood pulp. These problems have been discussed elsewhere[8,11] and have been the subject of much debate. Electrophoresis has been used in this work.

The force acting on the double layer as the result of an applied electric field produces a translation; the electrophoretic velocity is given by

$$v_E = \frac{\epsilon_r E \zeta}{4\pi\eta} \qquad [1]$$

where ϵ_r is the dielectric constant (or relative permittivity); E is the applied potential; and η is the solution viscosity. Equation [1] is the Smoluchowski equation. It is customary to refer to $1/\kappa$, the distance over which the potential decreases by an exponential factor at low potentials, as the thickness of the double layer. Equation [1] applies when 1) the thickness of the double layer must be thin compared with the dimensions of the particle ($\kappa a >> 1$, where a is the particle radius of curvature) and 2) the surface conductance must be small.[12] The reciprocal of the double layer thickness, κ, is given by[5]

---

* Fines are traditionally defined as that component of the furnish which will pass through a 200 mesh screen. Such a screen has 76 μm openings.

$$\kappa \quad \left[\frac{2e^2 N_A c z^2}{\epsilon_r \epsilon_0 kT}\right]^{1/2} \qquad [2]$$

where e is the elementary charge; N_A is the Avagadro number; ϵ_0 is the permittivity in a vacuum; c is the electrolyte concentration (moles/L); z is the charge number of the counter-ions; k is the Boltzmann constant; and T is the absolute temperature. For an aqueous solution of a symmetrical electrolyte at 25°C, Equation [2] becomes

$$\kappa \quad 0.328 \times 10^8 \, (cz^2)^{1/2} \text{ cm}^{-1} \qquad [3]$$

For a 1:1 electrolyte, the double layer thickness is therefore about 100 Å for a 10^{-3} M solution, 30 Å for 10^{-2} M solution, and 10 Å for a 10^{-1} M solution.

For certain values of the ratio of particle diameter to reciprocal double layer thickness, a/κ^{-1}, we are concerned with a retardation effect due to electroosmotic slipping at surfaces (the ions in the diffuse double layer are also moving due to the electric field but in the opposite direction due to the net charge in the fluid region being opposite in sign to that of the surface; the ions entrain solvent with them so that there is a local motion of the medium opposing the motion of the charged particle), and a relaxation effect originating from a polarized double layer around particles in a flow (the electrostatic double layer is distorted under the action of an external electric field). These effects alter the result of the electrophoretic field on the particle mobility. Overbeek[12] states that the relaxation effect may be neglected as long as the electrical double layer is thin compared with the size of the particle. Shaw[5] states that relaxation may be neglected when κa is either small ($<$ca. 0.1) or large ($>$ca. 300). It is significant for intermediate values of κa, especially at high potentials and when the counterions are polyvalent and/or have low mobilities.

For a fiber system, the particle diameters of fines vary from submicron colloidal matter to 80 μm. The approximate range of values for the ratio a/κ^{-1} for fines in 0.01 M KCl would be 30 to 30,000. The latex particles in this study are 0.40 μm average diameter, and for operating electrolyte concentrations, the κa value was 130.

A simple microelectrophoresis apparatus consists of a transparent cell, with a microscope focused on the particles inside the cell, and a system of electrodes and devices for filling and cleaning the cell. The design of microelectrophoresis instruments varies with regard to all of these items. The cell may be open or closed.[4,13] The liquid moves in an electrophoresis cell due to electroosmotic slipping relative to the cell wall. In a closed cell, liquid that flows along the surface returns in the center of the cell. Thus, in a cylindrical cell, there exists a concentric cylinder in the cell, where the flow of liquid is zero, and the EM of a particle may be measured directly; as we go from wall to wall, there are two points of measurement. These points of zero electroosmotic flow in a cylindrical cell are given by[14]

$$X = R\left[1 \pm \frac{\sqrt{2}}{2}\right] = 0.293\ R \text{ or } 1.707\ R \qquad [4]$$

in which R is the radius of the cell, and X is the distance from a wall.

Recently, procedures have been presented to eliminate or substantially reduce the electroosmotic slip by coating the cell surface with a charge reducing material. Herren[15] has reported promising results with covalently bonded coatings of polyethylene glycol. Figure 2[15] shows that the electroosmotic flow was virtually eliminated for polystyrene latex spheres that were uncoated or coated with poly(ethylene glycol). The profiles were reported

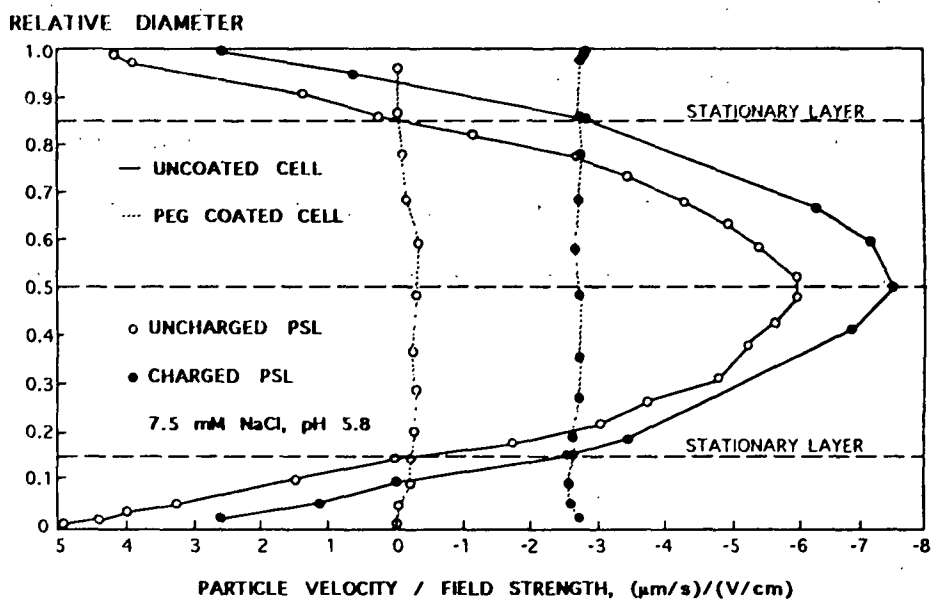

Figure 2. Comparison of degree of electroosmosis in uncoated and poly(ethylene glycol), 20,000 molecular weight, coated capillaries using uncoated and methylcellulose-coated polystyrene latex spheres.[15]

as symmetrical and reproducible in each case. Others have reported equal success with methylcellulose coatings, including Goulet[16] and Miller.[17] In this study, cells coated with methylcellulose were successful in reducing the electro-osmotic effect.

Several commercial instruments are available which automate measurement of microelectrophoresis to give EM distributions for a large number of particles in a sample. The benefit of obtaining the distribution of particle mobilities, rather than the mobility of individual particles, has been made possible by recent advancements in laser illumination and light scattering. Laser Doppler Anemometry (LDA) has been applied to particle velocity measurements[18] and has been adapted to measure the electrophoretic mobility. This technique operates on the principle of detecting light pulses scattered by small particles in a

flow while passing through the region where two laser beams cross. The coherent, monochromatic nature of the laser beams creates a well-defined fringe pattern, depicted in Figures 3 and 4.[19] Thus, particles passing through the region scatter light in pulses at a frequency proportional to the particle velocity. These light pulses are detected by a photodetector outside the flow and converted to a velocity, v, according to the formula:[18]

$$v = \frac{\lambda f_p}{2 \sin(\alpha/2)} \qquad [5]$$

where λ is the wavelength of the laser light; α is the angle between the beams; and f_p is the frequency of the light pulses scattered from the measuring volume. A schematic diagram of a Doppler anemometer is shown in Figure 5.[18]

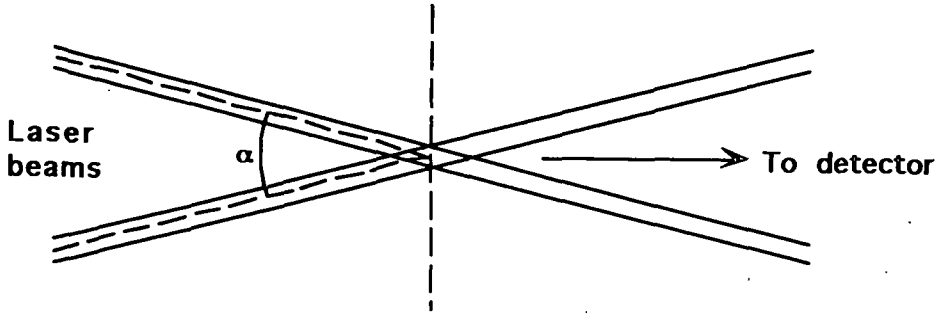

Figure 3. Arrangement of illuminating beams in the differential Doppler technique.[19]

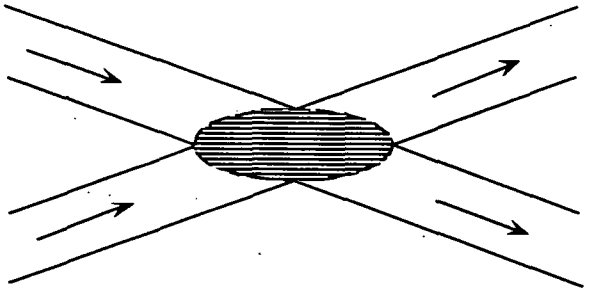

Figure 4. Fringe pattern produced by crossing beams in the differential Doppler technique.[19]

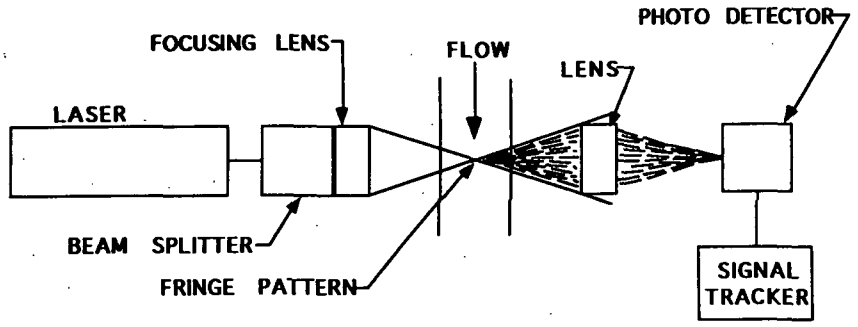

Figure 5. Schematic diagram of the laser anemometer arrangement. The two laser beams from the beam splitter are focused to form a fringe pattern at the beam crossing point. The fringe pattern is imaged on a photodetector and the Doppler signal produced by particles crossing the fringes is analyzed by a frequency tracker.[18]

Examples of the time variation of scattered light from a particle moving through a fringe are shown in Figure 6.[19] The ideal signal for a particle is shown in (a). An imperfect signal (b) can result if the intersecting beams are not of equal intensity or if a particle is not small compared with the fringe spacing. A particle following a path that is not along the axis of the cell would give the intensity variation in Figure 6(c).

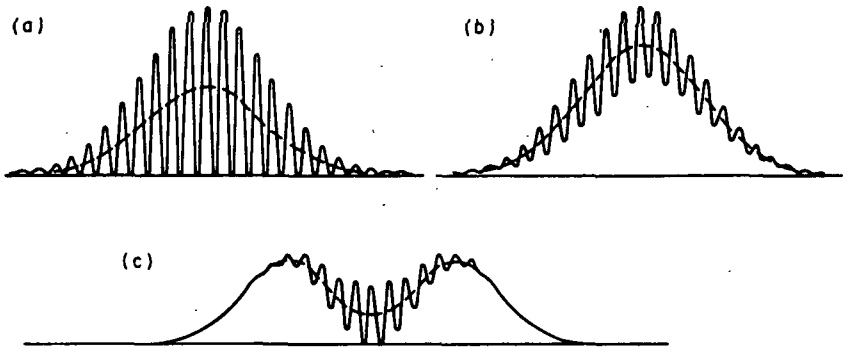

Figure 6. Types of signals from particles crossing a region of intersection of light beams.[19]

An important factor in the LDA technique is the degradation of signal quality for a particle whose diameter is large when compared with the fringe spacing. Large particles span light and dark bands of a fringe pattern and average out the variations in light intensity. The quality of a signal from the passage of such a particle is reduced. Drain[19] reports that the optimum ratio of particle diameter to fringe spacing is 0.586. The fringe spacing is given by[19]

$$s = \frac{\lambda}{2 \sin\alpha/2} \qquad [6]$$

Any particle with dimensions larger than the fringe spacing will form a pedestal signal, where the frequency of the hills and valleys become indiscernible.

Recently, IPST obtained an LDA electrophoresis instrument by Malvern Corporation: the Zetasizer IIC. A schematic specific to the Zetasizer IIC is shown in Figure 7.[20] The incident light angle is set at 45° for mobility measurements and 59° for particle size measurements. The top incident beam is modulated by a ramp function so that fringes may move with the same velocity, and in this manner, not only the magnitude, but the direction of velocity may also be calculated.

Fringes for this geometry (at the 45° angle operation) are spaced 0.827 μm apart (a 633 nm wavelength laser is used). The optimum particle size for an accurate mobility distribution measurement is thus 0.485 μm. Latex particles in this size range were used throughout this project to test the effect of system variables on mobility (EM) and EM distribution.

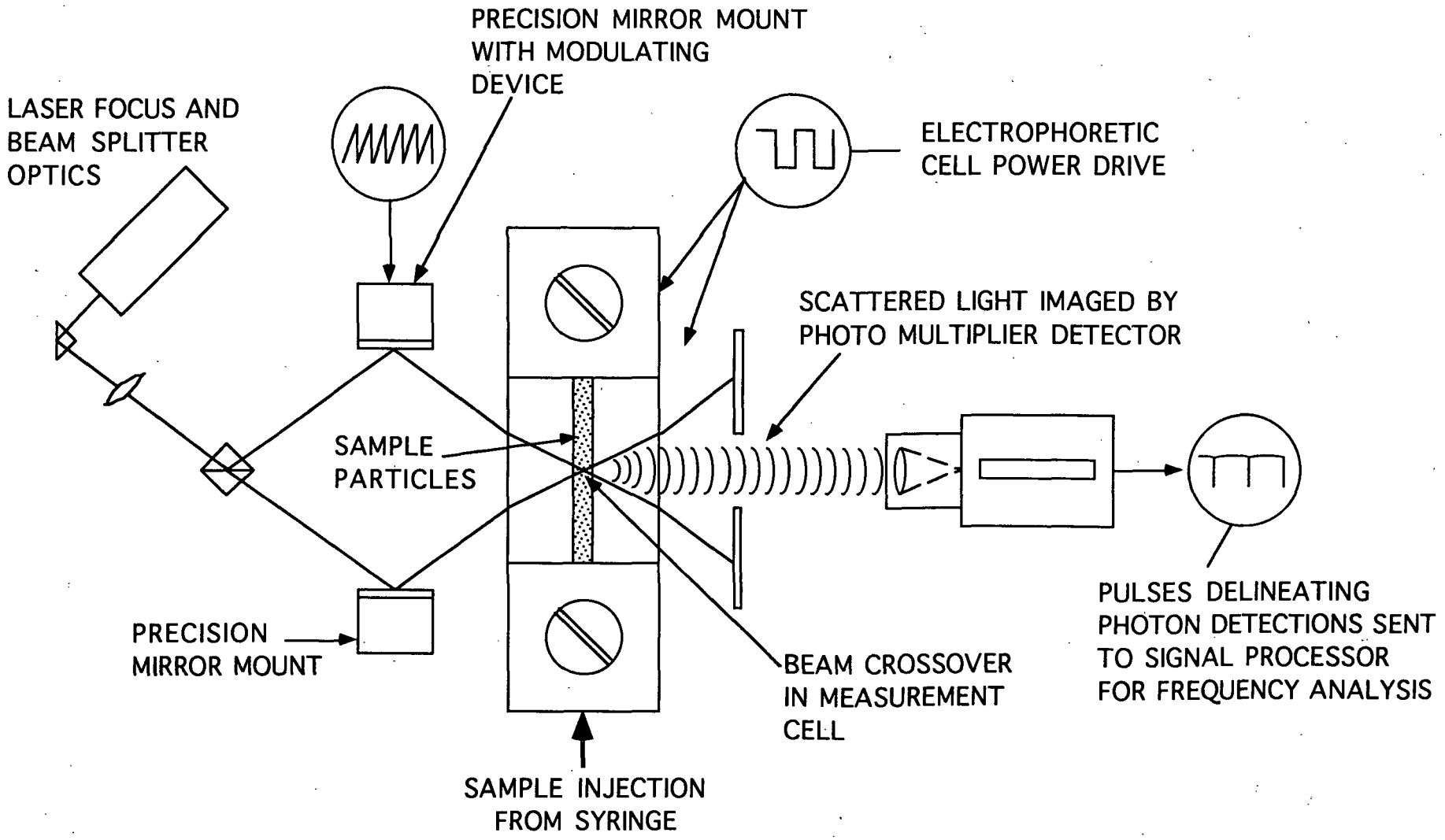

Figure 7. Malvern Zetasizer IIC principle operating schematic.[20]

Calculation of Zeta Potentials

In this section, the relation of EM to the ζ-potential and to the charge density at the surface of shear will be considered. The Smoluchowski equation has been applied to large κa values.[21] Equating the electrical and viscous forces on a liquid layer of unit area, thickness dx, distance x from the surface with electrophoretic velocity υ gives:

$$E\rho dx = \left[\eta \frac{d\upsilon}{dx}\right]_{x+dx} - \left[\eta \frac{d\upsilon}{dx}\right]_{x} = \frac{d}{dx}\left[\eta \frac{d\upsilon}{dx}\right] dx \qquad [7]$$

where E is the potential gradient, and ρ is the charge density at a point. Inserting the Poisson equation which relates the divergence of the gradient of the electrical potential at a given point to ρ [22] and assumes a continuous charge distribution:†

$$\left[\rho = -\frac{1}{4\pi}\frac{d}{dx}\left[\epsilon_r \frac{d\psi}{dx}\right]\right] \qquad [8]$$

yields

$$-\frac{E}{4\pi}\frac{d}{dx}\left[\epsilon_r \frac{d\psi}{dx}\right] = \frac{d}{dx}\left[\eta \frac{d\upsilon}{dx}\right] \qquad [9]$$

Integrating twice with the assumption that ϵ and η are constant throughout the double layer gives:

$$\frac{E\epsilon_r}{4\pi}\psi = \eta\upsilon + \text{constant} \qquad [10]$$

The boundary conditions for electrophoresis are $\psi = 0$, $\upsilon = 0$ at $x = \infty$, and $\psi = \zeta$, $\upsilon = \upsilon_E$ at the surface of shear. Therefore,

---

† The integral of ρ out to infinity gives the total excess charge in the solution, per unit area, and is equal in magnitude but opposite in sign to the surface charge density.

$$\frac{E\epsilon_r}{4\pi}\zeta = \eta v_E \qquad [11]$$

or

$$u_E = \frac{v_E}{E} = \frac{\zeta\epsilon_r}{4\pi\eta} \qquad [12]$$

Thus, the EM of a nonconducting particle for which κa is large should be independent of its size and shape provided that the ζ-potential is constant. To convert from electrostatic units of potential difference to volts, both κ and E must be multiplied by 300.‡ For an aqueous medium at 25°C, the Smoluchowski equation becomes

$$\zeta = 12.85\, u_E \text{ millivolts} \qquad [13]$$

with u_E expressed in micron sec^{-1} per volt cm^{-1}.

Henry[23] derived a general equation for conducting and nonconducting spheres:

$$u_E = \frac{\zeta\epsilon_r}{6\pi\eta}[1 + \Lambda F(\kappa a)] \qquad [14]$$

where $F(\kappa a)$ varies between zero for small values of κa and 1.0 for large values and

$$\Lambda = \frac{k_0 - k_1}{2k_0 + k_1} \qquad [15]$$

where k_o is the specific conductance of the bulk electrolyte solution, and k_1 is the specific conductance of the particles. For nonconducting particles ($\Lambda = ½$), the Henry equation can be written in the form

‡ In cgs/esu system of units, one esu of potential equals 300 volts.

$$u_E = \frac{\zeta\epsilon}{6\pi\eta} f(\kappa a) \qquad [16]$$

where $f(\kappa a)$ varies between 1.0 for small κa and 1.6 for large κa (Smoluchowski equation). $f(\kappa a)/6$ is equal to 1/4 for a cylindrical particle with its axis in the direction of the field, varies between 1/4 and 1/8 for a cylinder perpendicular to the field and varies between 1/4 and 1/6 for a spherical particle, as illustrated in Figure 8.[4]

It can be seen in Figure 8 that all nonconducting spheres merge to the Smoluchowski equation (Equation [12]) for large κa. For practical purposes, however, it offers no advantages to convert EM values into ζ-potentials. Papermaking systems for instance are always polydisperse, and electrolyte composition is unknown. Since the degree of validity of equation [17] is uncertain, we will report experimental EM values without conversion to ζ-potential.

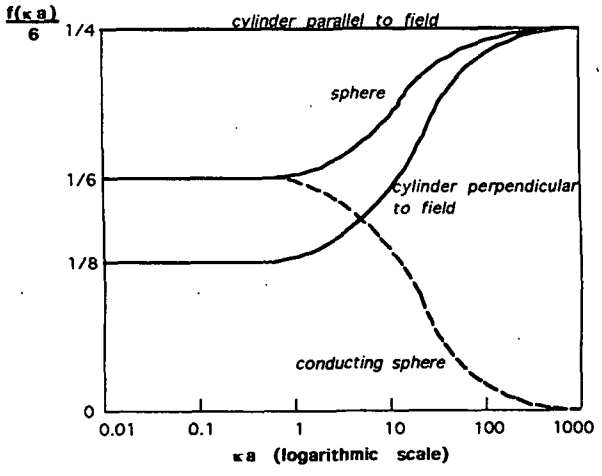

Figure 8. Dependence of the electrophoretic velocity on the ratio between the radius, a, of the particle and the thickness, $1/\kappa$, of the double layer.[4]

POLYELECTROLYTE ADSORPTION AND PARTICLE FLOCCULATION MECHANISMS

The classic coagulation theory for the stability of lyophobic colloids has been the DLVO theory (Derjaguin-Landau-Verwey-Overbeek).[24,25] The theory considers two kinds of forces between dispersed particles:

1. Electrostatic repulsive forces from the overlapping of the electrostatic double layers when two particles come in close contact.
2. van der Waals[26] attractive forces.

Additional forces may be due to adsorbed polymer interactions. The energy of interaction between two particles is a superposition of the repulsive and attractive forces:

$$V_{int} = V_R + V_A \qquad [17]$$

It is customary to sum the total interaction between an atom and a slab of infinite dimensions over all atom-atom interactions. We refer to the van der Waals forces as those intermolecular interactions which give rise to an attractive potential; these forces between individual atoms (or molecules) vary with the inverse sixth power of the intermolecular distance.

$$V_{disp} = -\frac{C_1}{a^6} \qquad [18]$$

where C_1 is a term to describe the three components of van der Waals forces[27] (Keesom[28] attraction - due to orientation of dipoles; Debye[29] attraction - due to a field inducing a dipole moment; and London[30] dispersion forces - attractive forces due to the presence of a positive nucleus and negative electrons).

The DLVO theory can be extended by considering additional forces between particles.

The van der Waals force dominates at short and long distances, and the energy of interaction is negative or attractive. At intermediate distances the forces are repulsive, provided the electrostatic repulsion is sufficiently large. The height of the repulsion barrier determines the stability of the suspension. When the barrier is high ($V_{max} > \sim 10kT$), few particles can overcome it, and coagulation does not occur. The height of the energy barrier can be altered by changing the surface potential, ψ_o, or the electrolyte strength (which influences the double layer thickness, $1/\kappa$). At low potentials or high ionic strength, the barrier is reduced.

Particles flocculate by diffusion but must have the activation energy to pass a potential energy barrier. Paper manufacturers attempt to achieve optimum retention of negatively charged fines and fillers by adding synthetic products, usually positively charged polymeric material, to destabilize the suspension and create flocculation. Two theories of adsorption of polyelectrolytes, the bridging model[31] and the electrostatic patch mosaic,[32,33] provide a conceptual framework for understanding polymer-assisted flocculation. In the bridging model, the polymer adsorbs in a configuration producing long loops and tails dangling in solution. High molecular weight polymers which can extend beyond the repulsive electrostatic double layers[6,34] keep particles of like charge separated. A near collision with a second particle provides a new surface for adsorption of the extended loops and tails. The bridging phenomenon has been supported by those studies involving high molecular weight, low charge density polymers. One may visualize that this type polymer would be advantageous to a bridging flocculation.

In mosaic adhesion, the polymer chains rest in individual patches on the particle surface and create, by means of a partial charge neutralization, an electrostatic attraction. The resulting force of attraction depends upon the strength of the charge (charge density) and

the degree of coverage. Thus, high charge density polymers are said to flocculate a furnish by the patch mechanism.

Polymer adsorption and subsequent particle flocculation are subject to collision rate control. In turbulent flow there are two mechanisms of transport and possible collision: Brownian motion and turbulent diffusivity. The aggregation of an initially monodisperse suspension produces a range of aggregate sizes depending on conditions such as concentration of the particles and the flocculation aid, double layer interactions, and mixing parameters. We assume that the aggregate size distribution is given by the Smoluchowski expression[35,36] for perikinetic (diffusion-controlled) flocculation. If there are initially N_0 spherical particles per unit volume, then the Smoluchowski result for the total particle concentration, N_T, remaining at time, t, is

$$N_t = N_0/(1 + t/t_F) \qquad [19]$$

where t_F is the half-life.

For orthokinetic flocculation, the rate of flocculation of an initially uniform suspension in a uniform shear field[4] is described by

$$\frac{dN_t}{dt} = \frac{16}{3\sigma N_c^2 \gamma a^3} \qquad [20]$$

where

N_t = particle number concentration at time, t
γ = shear rate
a = radius of the primary particles
σ = collision efficiency factor

The attractive and repulsive forces between particles are introduced by σ. van de Ven and Mason[37] have suggested σ to be of the form

$$\dot{\sigma} = f(\lambda_L/a)\,(H/36\eta\gamma a^3)^{0.16} \qquad [21]$$

where λ_L is the London retardation wavelength, and H is the Hamaker constant (equal to $\pi^2 C_1 n^2$ where n is the number of molecules per unit volume; typically, H is of the order of 10^{-19} to 10^{-21} J).

Levich[38] has shown that the ratio of the rate of coagulation resulting from turbulent agitation, $N_{(turb)}$, to that resulting from Brownian diffusion, $N_{(Br)}$, is given by

$$N_{(turb)}/N_{(Br)} = 9.0 \times 10^{12}\,\epsilon^{1/2}\,d^3 \qquad [22]$$

where ϵ is the rate of turbulent energy dissipation per unit mass, and d is the diameter (in cm) of the particle (constant has been corrected by Stratton[39]). Delichatsios and Probstein[40] have reviewed the calculation of ϵ for turbulent flow in pipes. These equations suggest that polymer addition can enhance the flocculation rate if the adsorbed polymer increases the collision radius of the particle.[41]

In addition, we see the degree of flocculation is related to the scale of turbulence. Stratton[39] points out the importance of good mixing at the point of polymer addition. Turbulence is necessary to provide both even polymer distribution and the mechanism of transport of fines and filler leading to collisions and aggregation.

Hesselink[42] has shown that polymer adsorption onto oppositely charged surfaces is virtually irreversible. This is the result of multiple point attachment of charged polymer chain sites. The Scheutjens-Fleer theory[43,44] and Norde[45] show that this lack of desorption is to be expected when a polydisperse polymer sample is in equilibrium with an adsorbing surface. Thus, the first surface upon which a polymer adsorbs will also be its

last[39]. The dilute polymer solution is typically introduced through a single port in the wall of the pipe transporting the pulp slurry. Polymer distribution onto the pulp is dependent on a competition of mixing rate and adsorption rate. Due to the electrostatic attraction in the dispersion, virtually every collision should lead to adsorption. The polymer should adsorb onto all negatively charged surfaces in proportion to their external specific* surface areas.[39]

Under favorable conditions, flocs can grow by further collisions. However, growing flocs will be subjected to disruptive stresses arising from the shearing action of the fluid. One would expect the equilibrium to shift in the direction of higher dispersion as γ (the shear rate) is increased.

POLYELECTROLYTE ADSORPTION KINETICS

For most polymer adsorption kinetics studies, two distinct regions of adsorption rate have been found: typically, an initial region of rapid adsorption characterized by a linear increase of polymer adsorption with time followed by a "plateau region"[46] of near zero incremental polymer adsorption with time. Surface saturation causes the rate of adsorption to decrease and eventually become zero. In the case of polyelectrolytes, further adsorption is also deterred by the repulsion between like charges along the polymer chain extending out from adsorbed sites and the unadsorbed polymer. This two-regime behavior has been demonstrated for the adsorption of cationic polyelectrolytes onto cellulosic substrates,[47,48,49,50,51,52] that of polyelectrolytes onto nonporous, charged materials,[53,54,55,56] and for adsorption of nonionic polymers onto nonporous charged and

* For porous structures we are speaking of the specific area where polymer chain dimensions allow for adsorption.

uncharged surfaces.[46,57,58]

Several factors can influence the rate of adsorption; however, none of these factors has been studied independently. These factors may include the following: initial polymer concentration, particle concentration, mixing conditions, hydrodynamic size of the polymer, and the magnitude of attraction due to electrostatic forces. It has been observed that the rate of adsorption increases as the initial concentration of polymer is increased. Studies have concluded that the initial rate of polymer adsorption is first-order with respect to polymer concentration;[47,52,57] however, this dependence may be referred to as "pseudo" first-order as excess surface area existed in these adsorption experiments.[59] The surface area of the adsorbent remained essentially constant throughout the experiments.

Gregory[60] has derived a relationship describing the kinetics of adsorption based on the number concentration of particles inversely proportional to the adsorption time.

$$t_a = -\ln(1-f)/k_{12} N_c \qquad [23]$$

where t_a is the time required to adsorb a fraction, f, of the polymer; k_{12} is the rate constant; and N_c is the number concentration of particles. This model predicts that adsorption can be slow for dilute suspensions. However, to our knowledge, there are no experimental data which conclusively verify this dependence on particle concentration. Some indirect evidence presented by Wigsten[61] suggests that adsorption can occur much slower in dilute solutions than predicted by other works performed at higher concentrations. Some conclusions on adsorption rate have been based on polyelectrolyte-induced flocculation rates. These flocculation rates have been shown to be directly related to particle concentration.[62] (For a further discussion, see the Flocculation Kinetics Section below.)

Lindström and Soremark[63] have presented data suggesting that varying the absorbent concentration by a factor of 10 (fiber concentration varied from 1 to 10 g/l or 0.1 to 1.0%C) does not alter the rate of polymer adsorption. It is unclear from their report, however, if the initial ratio of adsorbent to adsorbate was held constant and if the reaction vessel mixing conditions were turbulent. Very high polyelectrolyte dosages of one to two percent (20 to 40 #/T) were used and resulted in adsorption times to a plateau region of one minute for fiber fines (as measured by the rate of change of EM) and in excess of 60 minutes for long fiber. These adsorption times to a plateau were verified for pulp fibers by Horn and Melzer.[64]

For nonporous substrates, the adsorption times to a plateau region have been found to be less than for porous substrates. Black[53] found that 85 percent of a cationic polymer added to kaolite clay particles in a stirred reactor (100 RPM) adsorbed within 30 seconds after addition. Somasundaran[54] found that a cationic PAM completely adsorbed onto a glass slide within 5 to 20 seconds under quiescent conditions.

The rate of polymer adsorption has been found to have a strong dependency on the degree of mixing, that is, whether the initial and/or final conditions are perikinetic or orthokinetic. Workers who have investigated the effect of mixing conditions on adsorption have concluded that a shear rate increase will increase the adsorption rate.[57,65,66,67,68]

Dijt et al.[57] measured the adsorption of a nonionic polymer onto silica using a reflectometric technique. A jet of solution was impinged onto a surface at 90° to create a stagnation point. Polymer deposition was detected continuously by means of a polarized laser beam. Initial adsorption rate was found to increase with Reynolds number and polymer concentration. Plots of initial rate versus concentration (log-log) for three values of Reynolds

number were linear with slope near unity. The intercept values increased with Reynolds number.

In a series of works by Wågberg et al.,[49,69,70] adsorption rate studies were performed using a flow loop. A pulp suspension of 2 g/L (0.2%C) was pumped from a pulp chest into a pipe of 24 mm (0.94 in) diameter, at a flow rate of 0.62 m/s (2.03 ft/s). Polymer (either a PAM of high molecular weight ($>10^6$) or a medium molecular weight dimethyldiallylammonium chloride [DMDAAC]) was injected (at 0.1 g/L or 0.01% addition) into the pulp suspension at a constriction. Injected dye experiments showed that the visible mixing length was less than 30 mm. Contact times were made between 0.5 and 2.5 s by exchangeable pipe sections and different sampling ports. The stock passed through a filter cloth which removed the fibers, while the unadsorbed polymer was collected and evaluated.

This research concluded that a constant adsorption level was already established within 0.5 seconds and that the amount of adsorbed polymer did not change. In some experiments an extra constriction in the flow loop acting as a static mixer was placed in-line after the polymer addition (0.7 m). This additional mixing had no influence on the adsorption results. The collision efficiency was determined to be sufficient without its addition.

A sample from the flow loop experiments examined many hours later was found to have a much higher level of adsorbed polymer than that measured within 2.5 s after the injection. The authors suggest that this additional adsorption is not related to the collision frequency but rather depends on the rate of reconformation of the adsorbed polymer and on the rate at which other polymer molecules penetrate the already formed polymer layer.

Evidence for this theory comes from stoichiometric measurements of released counterions; the rate of release continued beyond the plateau of polymer adsorption. This result was attributed to polymer structures reconforming on adsorption sites. The time scale for reconformation was said to exceed 60 s.[69]

Rearrangement of polymer conformation has been reported to be a more rapid process on nonporous materials when compared to polymers on cellulose fiber surfaces.[71] Conductivity measurements on polystyrene latex, bentonite, and carboxymethylated cellulose fibers show that in the case of cellulose fibers the release of counterions is much slower. This result was attributed to the surface characteristics of the materials -- porous fibers allowing for penetration during the reconformation process.

Some other useful techniques have been reported for measuring polymer adsorption kinetics. Döll[72] utilized electrophoretic mobility (EM) measurements to monitor the charge neutralization of suspended silica particles as a function of time after polymer addition. Mixing conditions created by T-, Y-, and Jet-mixers were used to introduce cationic polyelectrolytes to a pipe suspension flow. The time required to complete neutralization of the surface charges (isoelectric point) was considered the characteristic reaction time; the reciprocal of this time was defined as the characteristic reaction rate. Shorter reaction rates were obtained at higher Reynolds numbers. However, the polymer dosage used and the method for instantaneous EM measurement were not discussed.

Klute[73] has also measured the changes of electrophoretic mobility (EM) with time to determine polymer adsorption kinetics. A cationic polymer was used to destabilize a dilute silica suspension (concentrations not mentioned) in laminar and turbulent pipe flow. For the

high Reynolds number conditions, the electrophoretic mobility (EM) decreased over five seconds following polymer addition. For the lowest Reynolds number condition (laminar flow), little change in EM was seen after 50 seconds. Particle counting (method was not revealed) was used to determine the extent of flocculation and results were applied to a form of Equation [19]. The relative number of particles, N_t/N_0, was found to decrease in seconds. As the Reynolds number increased, the reaction rate for polymer aggregation increased along with the adsorption rates as determined from the EM curves.

FLOCCULATION KINETICS

Indirect evidence of enhanced adsorption rates due to increased particle concentration and mixing intensity has been derived from flocculation kinetics studies. The results of flocculation rate studies typically have been used as a measure of polymer adsorption rate; adsorption must be a precursor to particle flocculation; therefore, adsorption occurred within the time frame of flocculation. We will now discuss the flocculation rate studies that have been used for this argument.

Franco[39,74] concluded that adsorption onto TiO_2 particles under turbulent conditions occurs rapidly. When a high molecular weight, low charge density polymer was used, 70 percent of the particles flocculated in 0.06 s, and the flocculation was completed in less than 1 s. It was proposed that polymer adsorption, a precursor to flocculation, must have occurred within the 0.06 s time span.

Stratton[39] conducted experiments with the IPC web former in order to study the importance of good mixing at the point of polymer addition. A high molecular weight, high

charge density cationic polymer was introduced to a furnish comprised of a bleached kraft pulp with 5 percent TiO_2 (based on o.d. pulp). Figure 9[39] gives the schematic of the flow system.

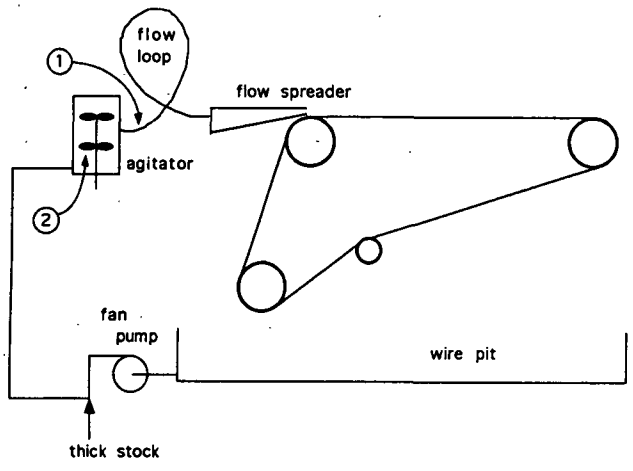

Figure 9. Schematic diagram of the modified web former. Numbered areas indicate points of polymer addition.[39]

The polymer was introduced in one of three ways:

1. After the agitator (point 1) with the agitator off.
2. After the agitator (point 1) with the agitator on at 1730 RPM.
3. Into the agitator (point 2) with the agitator on at 1730 RPM.

This sequence provides increasing degrees of agitation and, therefore, increasing distribution of the polymer over the total volume of the furnish. Headbox ash and white water ash decreased with better mixing conditions; single-pass retention improved upon changing from conditions 1 to 3; and pigment distribution improved as evident from the increase in pigment scattering coefficient.

In a related work, Luettgen[75] has noted the effect of shear enhanced collisions in a

concentric cylinder shear field of dilute TiO_2 particles. Three levels of shear during polymer addition were studied by adjusting the inner cylinder rotational speed. The high shear level required the least time to initiate a change in the degree of flocculation, as seen in Figure 10.

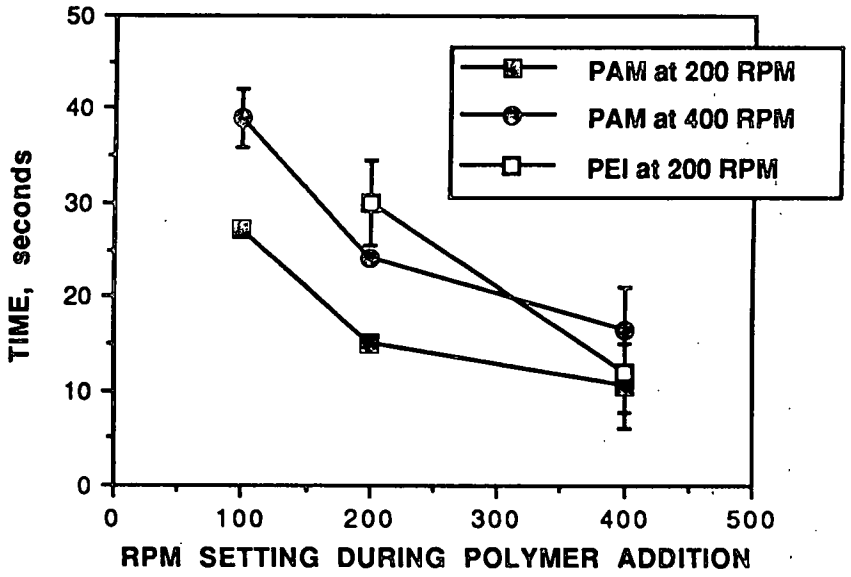

Figure 10. Time to initiate flocculation versus RPM setting for a TiO_2 solution in a couette shear field.

Wågberg and Lindström[68,76] point out that the flocculation process for fibers, upon the addition of a cationic PAM, was complete in less than two seconds with substantial flocculation within 0.45 s, which suggests rapid polymer adsorption. It was assumed that the turbulence affects the transport of polymer molecules toward the fibers; thus, adsorption times of less than a second would be expected.

Their experiments also indicated that the size of the flocs formed was controlled by

the macroscale of the turbulence in the pipe. Wågberg and Lindström further develop an earlier discussion by Saffman and Turner[77] on an expression for the number of collisions per second per unit volume:

$$N_{12} = 1.294\,(a_1 + a_2)^3 \left[\frac{\epsilon_t}{\nu}\right]^{1/2} n_1 \cdot n_2 \qquad [24]$$

where a_1 and a_2 are the respective radii of the colliding particles; ϵ_t is the energy dissipation per unit mass per unit time; and n_1 and n_2 are the numbers of particles per unit volume. Equation [24] is valid when the microscale of turbulence is larger than the particles. Considering a fiber to be an equivalent sphere of the same volume, and estimating the microscale of turbulence to be 40 μm, the resultant collision frequency was $N_{12} = .120 \times 10^{16}$ /sm^3. The number of polymer molecules present, 12×10^{16} /m^3, suggested that each polymer will, during one second, have many chances of being adsorbed onto a fiber surface. Thus, it appeared that significant polymer adsorption occurred at very short times in a turbulent flow.

Wigsten[78] presented data which conflict with the conclusions of Wågberg for the initial stages of polymer adsorption. A linear, high molecular weight polyamine was adsorbed onto polystyrene latex, diameter 1.07 μm in turbulent tube flow. Reaction times varied from 0.16 to 2.4 seconds. The adsorption reaction was quenched in excess surfactant solution, and adsorption rates were determined by measuring the amount of unadsorbed polymer. Floc size was determined using a Coulter Counter. Orthokinetic flocculation was found to be adsorption rate-limited; however, adsorption was found to occur much slower than indicated by the studies we have mentioned previously. The concentrations examined were much lower in the Wigsten study. Thus, the slow adsorption results are probably due

to the concentration dependency for polymer to particle collisions.

In summary, a thorough understanding of the individual parameters which determine adsorption and flocculation rates has not yet been achieved. Neither experimental nor theoretical evidence has been reported concerning the relation between adsorption conditions and the homogeneity of adsorption. A typical papermaking furnish of cellulose fiber and filler suspension flowing under turbulent conditions complicates the situation. A reasonable correlation from the literature would be that adsorption must occur on a millisecond time scale, and that heterogeneous adsorption prevails under poor mixing conditions. However, actual rates of adsorption of a polyelectrolyte have not been determined when concurrent flocculation occurs in a turbulent suspension flow.

FLUID DYNAMIC ASPECTS

Suspension Flow

Several authors have attempted to categorize the flow behavior of suspensions by visual observation and modeling in order to determine which parameters are significant. The discussion that follows was obtained from two excellent reviews on flow regimes authored by Duffy et al.[79], and Norman et al.[80].

Friction losses associated with the pumping of wood pulp suspensions are considerably different from those associated with the pumping of pure water or suspensions of noninteracting fibers. Part of the complexity is due to the different flow regimes evident with changes in velocity. Above a certain finite velocity, the fibers will flow in a plug network. Increasing the velocity further causes the flow to undergo transition to a regime in

which the fluid shear stresses are insufficient to disrupt the fiber plug completely. This transition flow is characterized by a turbulent fiber/water annulus and a central fiber plug. Still higher velocities result in a disruption of the fiber network and development of a turbulent core (the annulus maintains turbulence). This fully-turbulent regime is characterized by a drag below that of pure water.

Pulp Flow Regimes

At low fiber concentrations, fibers and fines are free to move in a suspension with little interaction. At higher fiber concentrations, fibers collide and produce flocs by mechanical entanglement. These flocs will interlock at low flow rates to form coherent networks. Networks will interact with the solid boundaries by direct contact or hydrodynamic shear. At higher velocities, flocs are dislodged from the network, and a complex interaction results between the turbulent eddies, flocs, fibers, and the network itself.

Most pipe friction data for chemical pulps have been represented in one of two forms shown in Figure 11. Alternatively, the Reynolds number may replace the velocity as the abscissa as shown in Figure 11(b). The letters shown in Figures 11(a) and 11(b) denote various critical points in the flow regimes. The literature contains several apparent misinterpretations of the relationships which exist between Figures 11(a) and 11(b). It can be shown from the definition of the friction factor that:

$$\frac{d(\log\ (\Delta H/L))}{d(\log\ V)} = \frac{d(\log\ \phi)}{d(\log\ V)} + 2 \qquad [25]$$

where $\Delta H/L$ is the head loss per unit length of pipe; V is the bulk velocity; and ϕ is the friction factor. Thus, at corresponding points, the slope of the curve in Figure 11(a) is

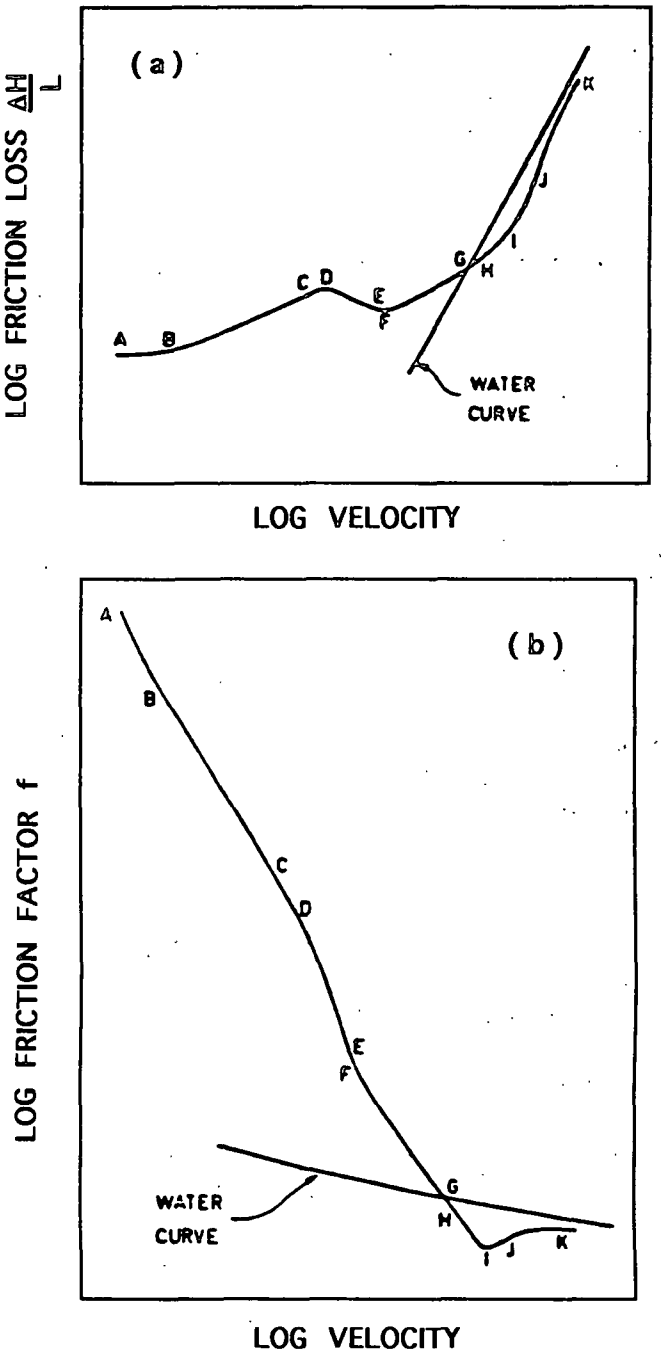

Figure 11. Typical friction curves for chemical pulps.[79]

always greater than the slope of the curve in Figure 11(b) by a constant value of two. At high concentrations, the high negative slopes in region ABCDEF in Figure 11(b) tend to

obscure the important changes of slope in Figure 11(a). For example, Forgacs, Robertson, and Mason[81,82] represented the data points for a 0.58% pulp by a single straight line from the lowest velocities they investigated, to a sharp transition point below the water curve, which they assumed to represent the onset of turbulence in the water annulus. Figure 11(a) and Equation [26] show that this would not be possible for higher concentrations. A single straight line followed by a sharp transition point implies that one mechanism of flow persists up to the transition point and then changes abruptly. Several distinct changes have been shown to occur in the "linear" portion up to the first transition point.

The following is a brief outline of the mechanisms of flow proposed for chemical pulps.[83,84] Each letter refers to the appropriate point in Figure 11:

Before A...porous media flow

The fiber plug does not move, but water passes through the network in accordance with Darcy's Law.

AB...plug flow where plug-wall contact predominates

Constant head loss with increasing velocity, indicating little or no hydrodynamic shear. At a given consistency, friction losses are higher in a rough pipe than in a smooth pipe.[83] Fibers and flocs embedded in the plug interact with the wall at these low rates, thereby increasing the drag on the plug. Since water is present, the high friction losses (relative to water alone) are considered to be caused by boundary friction and not direct solid-solid friction as proposed by Durst and Jenness.[84] Moderate flow rates are needed to maintain a coherent plug in small diameter pipes. An annulus has not fully developed in this regime, although thinned volumes exist adjacent to the wall as a result of the flocculated

nature of the fiber network.

BC...plug flow with combined hydrodynamic shear and plug- wall interaction

Fiber-wall interaction occurs between the coherent plug and the pipe wall due to network asperities being progressively broken from the plug. A water annulus is partly developed in this regime.

Flocs protruding from the plug are observed to break off and roll along the surface of the plug between the plug and the wall. The velocity of these flocs is lower than the bulk. Other flocs embedded in the plug are not disturbed. Some of the rolling flocs pick up fibers from the plug and grow in size. The rolling flocs are caught and held again by flocs embedded in the moving plug.

A large number of rolling flocs are found in a rough pipe. As the flow rate is increased, the number of flocs torn from the plug first increase, and then decrease, until there is no sign of such flocs at D.

Friction loss in the region ABCD increases with greater pipe roughness. Hydrodynamic shear and plug-wall interaction both contribute to the friction head loss.

C...plug-wall interaction ceases

DE...plug flow with water annulus in laminar shear

The annulus is continuous and there is no evidence of disturbances on the plug surface. Friction is purely hydrodynamic.

E...onset of turbulence in the water annulus

A change from a positive to a negative slope at the maximum

point D indicates a change in the mechanism of flow. A thin, continuous water annulus develops. Rolling floc action ceases at C just before the maximum. There are no obvious signs of fiber or floc disturbances on the surface of the flowing plug between C and F.

The reasons for the formation of the water annulus beyond C are unknown. However, it is thought that the flow stresses cause internal network deformation and deflection of protruding fibers and flocs at the edge of the plug,[85] these movements being sufficient to form a continuous water annulus at the pipe wall. If this is correct, a decrease in fiber and network stiffness (caused for example by refining or bleaching) would be expected to move the position of point C to lower velocities. An increase in pipe roughness also moves point C to lower velocities, presumably because the annulus now needs to develop only at the asperities of the pipe wall.

FH...plug flow with an essentially fiber-free turbulent water annulus

The change in the slope of the head loss curve from negative to positive at F indicates a change in the mechanism of flow. The water annulus changes from laminar to turbulent flow. The only superficial difference from regime DE is that a few fibers are dislodged from the network into the sheared annulus.

G...onset of drag reduction

The point at which the friction loss curves for pulp and water cross.

H...onset of permanent disruption of the plug

The removal of weakly bonded surface flocs from the plug in a manner similar to that described for BC is observed. The dislodged flocs move along the plug surface and are trapped by other protruding flocs. A small increase in velocity produces permanent

disruption at H. Individual fibers and small flocs are torn from the plug, while the bulk of the plug is still undisturbed.

H is often close to the onset of drag reduction, point G, but can also be at a significantly higher velocity.[86] The wall shear stress (i.e., the shear yield stress of the plug network) and the mean flow velocity at point H are exponentially related to the pulp concentration.

HJ...transition regime characterized by increasing turbulence in the fiber/water annulus and a decreasing size of the plug core with increasing velocity

The fiber/water annulus grows at the expense of the fiber plug. However, the plug is found still to exist at I, the point of maximum drag reduction or minimum friction factor.

I...maximum turbulent drag reduction with the plug core still present

Mih and Parker[87] and Lee and Duffy[88] have measured velocity profiles for the mixed flow regime using special impact probes. These showed that an intact plug of about 0.2 D still exists at I, the point of maximum drag reduction or minimum friction factor.

JK...fully-developed turbulence with progressive decrease in drag reduction and damping of turbulence

At high velocities in the upper portion of the regime JK, reduced velocity profiles approach a common curve which is distinct from the water curve and a function of consistency. At very low consistencies, the profile approaches the water curve. From K on to higher Reynolds numbers, the curve runs parallel to the water curve.

The velocity for onset to turbulence is a function of several factors. These include pulp consistency, fiber morphology, and pipe diameter. For the present study, a hardwood fiber at 0.5 percent consistency (%C) was examined in a 7.6 cm (3 inch) inner diameter (ID) pipe at Reynolds numbers that varied between 6×10^4 and 3.2×10^5 (pipe velocities of 0.9 to 4.6 m/s or 3 to 15 ft/s). Robertson and Mason[81] studied fiber flows in a 7/8" ID glass tube and found a transition to turbulence above 60 cm/s (2 ft/s or a Reynolds number of 1.3×10^4). In a comparison of softwood and hardwood chemical pulps, they found the flocculating tendency to be greatly reduced for the shorter stiffer hardwood pulps. It would thus appear reasonable to conclude that the flow conditions examined in the present study were fully turbulent, although friction factor data were not acquired.

Other studies can be compared to the present experiments to assess the flow state. Experimental data of low consistency fiber flows in two-inch pipes have been presented by Daily and Bugliarello.[89,90] Between consistencies of 0.50 and 1.00 percent, the transition to turbulence (point J in Figure 11) could range in Reynolds number from 1×10^4 to 9×10^4 depending on the pulp type. For suspensions of increased length to diameter ratio and flexibility, there were increased departures from Newtonian behavior. Long fibered, flexible pulps such as a southern pine bleached kraft had extended transition regimes. Short fibered pulps that were less flexible such as poplar groundwood (fiber length 0.49 mm) had abrupt transitions to turbulence at a relatively low Reynolds number, becoming fully turbulent at approximately 4×10^4.

Mih and Parker[87] obtained friction factor data for hardwood kraft; characteristic curves were found for a 0.5%C pulp suspension in two- and four-inch pipes. The point of maximum drag reduction was found at Reynolds numbers of 8×10^4 and 1.5×10^5, and the

point of turn toward the water line at 2×10^5 and 5×10^5 for the two- and four-inch pipes, respectively.

Moller and Duffy[91] present empirical equations to describe the inflection points for the friction loss curve. The minimum in the friction curve (point F), the onset of drag reduction, and the maximum drag reduction equations were each given; these values for the present study were calculated as 0.4, 1.5, and 3.4 ft/s, respectively. The minimum velocity examined (3 ft/s) is thus expected to be near the point of maximum drag reduction, at point I in Figure 11.

Turbulent Flow

The addition of fiber to water produces a lowering of the longitudinal pressure gradient at the same flow rate when turbulent flow exists. This phenomenon is termed drag reduction. The ability of certain particulate additives to reduce turbulent flow resistance has been reported in numerous publications.[92,93,94,95] It has been established that the effectiveness of particulates as drag reducing additives increases as their aspect ratio increases and is appreciable only for fibrous additives (Radin et al.[95] established that drag reduction could always be obtained with fibrous additives having aspect ratios greater than about 30). Vaseleski and Metzner[96] measured flow resistance data for fiber suspensions in pipes with different diameters and inferred that the presence of fibers in the turbulent core region of flow was important for drag reduction. This is in contrast to drag-reducing polymer solutions, in which the mechanism of drag reduction has been shown to occur near the wall.[97]

Daily et al.[98] performed the first turbulence measurements in pulp suspensions using an impact probe mounted in a pipe. They concluded that turbulence is strongly suppressed by the addition of fibers to water. Although this result has been verified, their measurements were not conclusive. A closer study of their reported turbulence spectra by Norman et al.[80] revealed that practically all the turbulence energy fell within a frequency range below (thus, a wavelength range above) that corresponding to the pipe diameter. Large-scale variations were measured, and not what is usually defined as turbulence.

Bobkowicz and Gauvin[99] measured the turbulence characteristics of a nylon fiber suspension by means of a diffusion technique. Hot water was injected from a point source at the pipe axis, and a temperature profile was measured downstream by a thermistor. The data indicated an increase in radial turbulence intensity with fiber length to diameter ratio (L/D) and concentration, including greater dispersion above that of pure water flow. The authors point out that the work by Daily[98] measured turbulence intensity decreases in the longitudinal direction. Later, this work received criticisms as being inconsistent with generally accepted beliefs of fiber turbulence damping. Possible reasons reported were that the flow was not fully turbulent and that there may have been particle interference with the sensing probe.[100,101] This author finds no such grounds for criticism; the flow conditions were probably turbulent given the reported parameters and the evidence of dispersion. Also, particle interference does not explain a larger dispersion area measured by the thermistor probe.

Mih and Parker[87] used their annular purge impact probe to measure velocity profiles for turbulent flow of aqueous suspensions of papermaking fibers (average length 2.7 mm, average fiber diameter 0.03 mm) in a 50 and 100 mm diameter hydraulically smooth pipe at

bulk velocities up to 9.17 m/s. At low flow rates and high concentrations, they found a region near the pipe axis where local velocity was independent of position. The region corresponded to a central undisrupted plug of fibers. The size of the plug decreased with increasing bulk velocity and with decreasing fiber concentration. At high flow rates and low concentrations, they did not detect a plug, although they reported an apparent flattening of profiles near the pipe axis. Velocity profiles for regions of turbulent shear were linear when plotted on the reduced velocity (U^+) versus the logarithm of distance from the wall (ln y) coordinates. U^+ is defined as:

$$U^+ = \frac{u}{U^*} \qquad [26]$$

where

$$U^* = \sqrt{\tau_w / \rho} \qquad [27]$$

and U^* is referred to as the reduced shear velocity, where τ_w is the wall shear stress, and ρ is the fluid density.

The gradients appeared to be independent of flow rate and were a function of fiber type and concentration. Moreover, they found that at high flow rates velocity profiles for a given suspension in both diameter pipes could be approximately represented by a single line on these coordinates. They associated this behavior with a regime of turbulent flow characterized by values of friction factor independent of flow rate.[102]

Seely,[103] who studied softwood sulfite pulp fibers, confirmed that velocity profiles in regions of turbulent shear were linear when plotting the reduced velocity U^+ versus the logarithm of dimensionless distance from the wall S^+ defined by:

$$S^+ = \frac{yU^*}{\nu} \qquad [28]$$

where ν is the kinematic viscosity of water at the same temperature as the suspension. Seely extrapolated the reduced velocity profiles and found that most intersected the water curve somewhere near the coordinates $S^+ = 30$, $U^+ = 14$. The gradient of these profiles increased with bulk velocity (conflicting with the Mih and Parker results). Seely was unable to distinguish the velocity profiles he obtained for dilute fiber suspensions at high flow rates from those he obtained for water. This apparent Newtonian behavior at high flow rates was also observed in measurements of flow resistance, which corresponded to accepted values for water.

Lee and Duffy[104,105] were also able to intersect S^+ and U^+ data to the same coordinates. These coordinates correspond with the outer layer of the buffer zone in turbulent Newtonian fluids. They suggested that the addition of fibers to water did not modify the wall layer in flow through smooth pipes, and the cause of drag reduction was attributed to the turbulent core region;[104] drag reduction occurred as a result of fibers reducing momentum transfer in the turbulent core. In addition, there was no significant dependence of the values for U^+ at $S^+ = 30$ on fiber concentration, fiber aspect ratio, bulk velocity, or pipe diameter.[100]

The expression for a linear, reduced velocity profile that passes through the point $U^+ = 14$, $S^+ = 30$ is given by:[100]

$$U^+ = \frac{1}{K} \ln S^+ + \left[14 - \frac{3.4}{K} \right] \qquad [29]$$

where K is the gradient and called the apparent von Kármán constant. In the turbulent regime, the value of K was found to be constant for a particular suspension concentration.

Equation [29] can also be used to calculate the von Kármán constant K for a suspension from flow resistance data:[102]

$$\frac{1}{\sqrt{\phi}} = \frac{1}{K}\ln(Re\sqrt{\phi}) + \left[14 - \frac{5.6}{K}\right] \qquad [30]$$

where the dimensionless quantities, Reynolds number, Re, and friction factor, ϕ, are defined by:

$$Re = \frac{DV\rho}{\mu} \qquad [31]$$

$$\phi = \frac{(\partial P/\partial \ell)\, D}{2\rho V^2} \qquad [32]$$

where

D = pipe diameter
V = average fluid velocity in the pipe
ρ = mass density of the suspending fluid
$\partial P/\partial \ell$ = longitudinal pressure gradient in the pipe

Equation [30] can reduce to the Kármán-Prandtl Law for water in a smooth pipe if K = 0.4. Lee and Duffy also showed that values of K characterizing a turbulent suspension can be predicted from data for the torque resistance measured with a rotational disk apparatus based on an analysis performed by Goldstein.[106]

Lee and Duffy[107] further postulated that variations of K can be explained in terms of the relationship between intensity of turbulence and the scale of fiber agglomeration in a suspension. In fully-developed turbulent flow, two regimes could be recognized from the

variations of K with bulk velocity. At low turbulence intensities, values of K for a particular suspension increase with increases in bulk velocity. The behavior corresponds to the regime in which friction factor is largely independent of flow rate. At high turbulence intensities, there is a regime in which K is independent of flow rate. As concentration decreases in this regime, the lower bulk velocity limit decreases, and the limiting value of K increases to approach that for water. This corresponds to a regime in which the flow resistance curves are approximately parallel to the water curve.

They suggested that a significant portion of the momentum transfer in turbulent fiber suspension is the result of radial movement of fiber flocs. Shear in turbulent fiber suspensions is restricted to a small volume of water between adjacent flocs. Consequently, the relative velocity between adjacent eddies in a pulp suspension is less than that for pure water. In addition, there is the probability of direct contact between flocs that further restricts relative motion. The three-dimensional fiber network that comprises a floc possesses properties similar to those normally encountered in solid materials. Fiber networks can transmit forces from one point to another within their structures and can enhance momentum transfer by providing a solid link between adjacent fluid layers. The larger the fiber floc, the greater is the distance over which it can transfer momentum. Thus, fiber flocs affect momentum transfer in two opposing ways: they tend to lower it by damping the turbulence of the suspending phase, and also tend to enhance the momentum transfer by providing a solid link between adjacent fluid layers. The concept of two opposing mechanisms to control the momentum transfer was presented to explain the variation of K with bulk velocity and distance from the pipe axis.

Since the pioneering work of Duffy and co-workers in the 1970s, the debate on the

influence of fibers on the momentum transfer has continued. Gore and Crowe[108] recently performed an analytical review of the literature to describe the conflicting conclusions dealing with various particle flows in gas streams. Various researchers have worked with the addition of particles to turbulent gas flows and found the turbulence intensity to increase (eight references cited) and decrease (six references cited) from that of the carrier phase. Gore discovered that a critical parameter appears to be the ratio of particle diameter to a turbulent length scale, d_p/l_c. The length scale associated with the fluid phase, l_c, was the integral length scale or the characteristic length of the most energetic eddy when only one phase is present. Hutchinson et al.[109] demonstrated that the l_c/r ratio across a pipe in fully-developed flow was approximately constant ($l_c/r \simeq 0.2$) except near the pipe wall. A critical demarcation value of $d_p/l_c \simeq 0.1$ caused the turbulent intensity of the carrier phase to either increase or decrease with the addition of particles. For a value greater than 0.1, the addition of particles caused an increase in the carrier-phase turbulence intensity. There was no reference made to cylindrical particles, but by using the length-weighted fiber length to be the characteristic particle diameter, we may calculate a critical ratio of 0.092 for the present study -- approximately on the Gore and Crowe demarcation line. Note, however, that results from solid-gas flows are not directly applicable to solid-liquid flows. For instance, drag reduction with spherical particles is possible in gas, but not in liquid flows.

Several works have involved utilizing new technology in laser Doppler velocimetry (LDV) to determine the influence of particles on turbulent flows. Park et al.[110] examined a silica suspension in Stoddard solvent (a yield-power-law fluid, which resembles the rheological properties of pulp suspensions) with an LDV system for measuring the mean velocity and turbulent properties through a pipe flow. The root-mean-square (rms) longitudinal velocity profile was similar to a classical turbulent Newtonian fluid. However,

the relative turbulence intensity for the tangential component was higher at the wall and lower at the center for the slurry. Near the wall the ratio of rms tangential velocity to rms axial velocity was approximately 70 percent higher for the slurry.

Results were reported for 0.5 %C fiber suspension flows when compared to pure water by Ek.[111] Combined LDA and light reflection techniques were used for simultaneous measurement of local velocity and local concentration in a glass tube. The longitudinal turbulent intensity was higher than for water at locations close to a wall ($1 < r/R < 0.5$) and decreased near the center.

Liljegren and Vlachos[112] present LDV data for four volume fractions (0.0001 to 0.001) of glass spheres in air. Consistently higher turbulence intensities were measured at all radial positions for the highest particle volume fraction loading. The authors suggested that the particles were enhancing the largest eddy disturbances in the flow leading to additional production of turbulent energy.

McComb and Chan[113] made single-component laser-Doppler measurements in drag-reducing suspensions of asbestos fiber with extremely high l/d ratios (ca. 10^5). Tangential and longitudinal components were measured. At the lowest Reynolds number examined, $Re = 1.4 \times 10^4$, 70 percent drag reduction was observed. The longitudinal fluctuating component, u', decreased compared to the fiber-free turbulent flow, but the tangential component, w', increased. Similar results were reported for $Re = 9.0 \times 10^3$. This represents a profound modification of the turbulent structure, much more than simply a suppression of turbulence. (The decrease in u' is the opposite effect seen in drag-reducing polymer flows, where u' increased dramatically, and radial component, v', is decreased.) As

the same solution was repeatedly passed through the flow system, there was a transition from "fiber-like" drag reduction to "polymer-like" drag reduction, with u' increasing and then decreasing back to that of the pure carrier fluid alone, and with drag reduction also decreasing. Examination of energy spectra, however, showed no evidence of a transition from one kind of drag reduction to another. Drag reduction magnitude also showed no obvious transition. These findings show that fibers can affect turbulence in complex ways.

At higher Reynolds numbers (3.2×10^4 and 5.3×10^4), u' was higher than in the carrier fluid alone even at high levels of drag reduction. Energy spectra showed a dip at length scales on the same order as the fiber length, suggesting resonant energy adsorption by the fibers.

Counter to the work of Gore and Crowe,[108] Steen[114] found that long fibers (length of 3 mm) decreased and short fibers (1 mm) increased the turbulence levels when compared to water flows. Radial profiles of axial velocity and turbulence spectra were recorded using an LDV technique on vertical upward pipe flow. An increase in velocity and turbulent energy when compared with a pure fluid could be observed for the short fibers at a low consistency level of 1.2 g/L (0.12 %C). Near the wall the turbulence levels were found to be higher than for pure fluid. Steen[115] cites qualitative comparisons with results of Ek.[111]

At present, a great deal of research has involved unravelling the aspects of turbulent suspension flows, particularly the causes of drag reduction. Unfortunately, the results often do not lend themselves to quantitative analysis. The complexity of turbulent suspensions of fibers has continued to challenge researchers. As illustrated in this discussion, further work is required on the fundamental nature of momentum transfer and turbulent fiber flows.

Side-port Injections

Process additives are often introduced by direct injection into a turbulent pipeline flow. A side-port or side tee is often used for this addition. Effective use of the turbulence increases reactant contact which has, in many cases, been shown to give a desired effect. Several authors have discussed the parameters for efficient pipeline tee mixing. Chilton and Genereaux[116] undertook one of the first pipe mixing studies by visually observing a secondary smoke gas injected into a glass tee. Good mixing could be achieved in two to three pipe diameters if proper velocity ratios were used (velocity ratio defined as jet velocity, u, versus pipe velocity, U, as presented in Figure 12). Small mass velocities prevented the injected gas from penetrating into the mainstreams, and higher ratios caused the injected gas to overpenetrate.

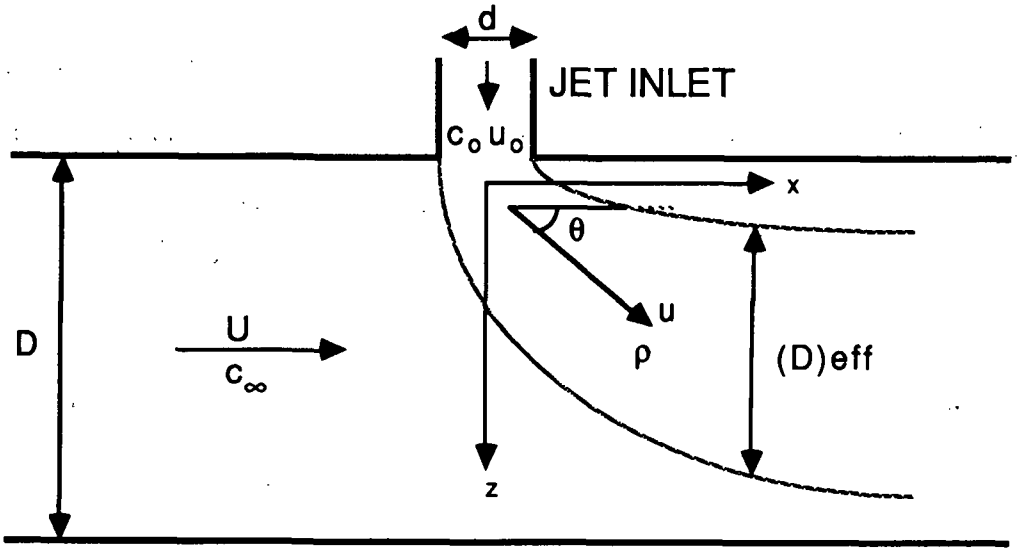

Figure 12. Jet geometry of a side-port injection with parameters defined.

Forney and co-workers[117,118,119] have used scaling factors to optimize the far field[§§] mixing results by manipulating the near field[**] jet conditions. These studies showed that mixing efficiency is optimized when the injected jet is geometrically centered along the pipe axis at some distance between two and 10 diameters downstream. Velocity ratios for the tee dimensions could be calculated in order to obtain the optimum conditions based on this assumption.

Recent data by Maruyama et al.[120,121] attempted to minimize the variance (second moment) in concentration across the pipe of the injected tracer material. These works suggested that optimum mixing is achieved in a short pipe length by impacting the jet against the opposite pipe wall between two and three pipe diameters from the injection. Although the mixing criteria used by Maruyama and by Forney were quite different, the measured results of all studies were identical for optimum mixing further downstream. One exception was that the second moment method encouraged jet impingement for optimum mixing when the measurement point was close to the injection.[122] Sroka and Forney[123] have developed the scaling laws which optimize the dispersion over the first 15 pipe diameters by using the second moment minimum method. In some cases this method determines that mixing is optimized at velocity ratios that place the jet in the center to upper half of the main pipe.

Cozewith and Busko[124] have presented experimental data suggesting impingement against the opposite wall will promote mixing for small distances ($L/D < 3$), and plumes

---

[§§] The region downstream from the injection port where ambient turbulence predominates.

[**] The region near the injection port where the mixing is dominated by jet-induced turbulence.

formed in the lower half (refer to Figure 12) will promote mixing for intermediate distances ($3 < L/D < 15$). Also, the impingement flow pattern was described; some of the fluid hitting the far wall spreads out circumferentially and forms a layer, coating the wall, that flows downstream along the pipe surface. The remaining side-stream fluid flows downstream as a jet in the far wall half of the pipe.

In summary of the present state of knowledge for side-port tee injections into turbulent flows, optimum mixing over short mixing distances, within three pipe diameters, occurs when velocity conditions create an impingement flow against the opposite wall. For intermediate mixing distances, between three and 15 pipe diameters, the mixing is optimized by setting near field geometry parameters to minimize the second moment at the desired far field location, and slower mixing, that which occurs beyond 15 pipe diameters, can be optimized by near field conditions which geometrically center the injected jet along the pipe axis at some distance downstream. One can visualize that the near field geometry conditions can be used to optimize adsorption, once we know the relavant kinetics of the adsorption.

PRESENTATION OF THE PROBLEM AND GENERAL APPROACH

In the preceding discussion, we have raised several questions about the process of polymer injection to a turbulent pulp flow. This action is of interest for retention aid additions as well as many other wet stock additive injections. Key to the retention process, from a papermaking optimization standpoint, is the efficiency of the polymer adsorption onto stock surfaces. We present the hypothesis that optimum retention of particulates occurs when the adsorption is most uniform. Due to the high collision efficiency in turbulent conditions, and the irreversibility of polymer adsorption, the most uniform adsorption of polymer chains onto a flowing stock will occur when certain conditions are met: (1) mixing is most uniform and (2) dispersion of the injected material is uniform sooner than adsorption of the polymer is complete.

Polymer adsorption homogeneity can be studied by examining the effect that adsorbed polymer has on the zeta-potential of a particle. By new instrument developments, the electrophoretic mobility of a whole sample can conveniently be measured. With the acquisition of the Zetasizer IIC (Malvern Corporation), we may study the effect of operating variables on the homogeneity of the distribution for small particles in the sample.

In order to examine the rate effects in a turbulent dispersion, some knowledge of that dispersion must be initially obtained. We have seen that the flow properties and flow regime transitions are greatly dependent on fiber characteristics. Also, we may think of the injection of polymer to such a flow in turbulence as highly complex. A phase of this study will examine dispersion properties of a tracer in the injected polyelectrolyte solution. The dispersion profiles obtained will give an indication of the coverage or exposure rate of

injected material downstream from the introduction point. This dispersion rate when compared with adsorption homogeneity may give some insight for adsorption rate phenomena in turbulent pulp flows.

The purpose of this work, therefore, will be to investigate the role of mixing conditions during the introduction of polymer on adsorption homogeneity. Data will be obtained from mobility distributions which are correlated with (1) turbulent dispersion rates to examine the adsorption rate behavior and (2) particulate retention results to examine the efficiency of the flow conditions. The results obtained will extend our understanding of adsorption kinetics and electrophoretic mobility of similar systems for optimizing additive efficiency.

THESIS OBJECTIVES

The underlying objectives of this project are to examine conditions for polymeric retention aid cost-effectiveness and reduction in particulate matter losses. In particular, what are the optimum conditions for polymer introduction to an adsorbing medium. The immediate objectives are:

1. To determine the effect on dispersion of an injected material into a turbulent pipeline flow of pulp, at one consistency typical of that in a headbox (0.5%), various turbulent mixing conditions (as varied by pipeline velocity), and one injection method (a side-port injection).

2. To determine the effect of mixing conditions during polymeric retention aid addition on the adsorption homogeneity on both pilot- and laboratory-staged conditions.

3. To determine the relationship between dispersion of the injected material and adsorption homogeneity, in order to make specific conclusions about adsorption rate at the described conditions.

4. To determine the retention efficiencies as a function of mixing conditions during polyelectrolyte addition.

EXPERIMENTAL

DESIGN

The experimental approach is divided into the following steps:

1. Examine the magnitude of influence for mixing conditions during polymer addition on the electrophoretic mobility (EM) distribution by running preliminary Dynamic Drainage Jar (DDJ) studies at different levels of shear.
2. Modify the existing flow loop so that turbulent dispersion rates may be measured and controlled, and stock sampling may be made.
3. Prepare a model pulp system and characterize its components.
4. Design a sensor/data acquisition system for measuring dispersion rates in turbulent flow, on-line.
5. Test samples for EM mean and distribution and retention efficiency as a function of pipeline velocity parameters.
6. Use the Malvern Zetasizer IIC manual mode of operation for a dual syringe injection system to uncover details of adsorption equilibrium rates.
7. Re-examine DDJ shear levels and the influence that addition conditions may have on EM distribution and retention efficiency. Couple these results with the preliminary DDJ work and the flow loop findings.

MATERIALS

Latex

We have defined an optimum particle size for a Malvern Zetasizer IIC measurement as 0.48 μm. The latex we used as a tracking material for EM measurement is a polystyrene sphere (Morton Thiokol Corporation, plastic pigment product Lytron® #2501) which was donated to this thesis project. The particle size average and distribution were characterized by several instruments and methods. These methods and the results are summarized in Appendix III. The results of these experiments suggested that the latex was suitable for electrophoretic mobility (EM) measurements on the Zetasizer IIC both with regard to the size and distribution, and for DDJ retention measurements because of the capability to model filler materials in a stock furnish. Although the various methods used are based on different technologies and report different parameters, we may say that the particle size is approximately 0.40 μm in diameter. The distribution data suggest that insignificantly few particles fall in the larger size ranges that would approach the width of one fringe spacing (0.827 μm) in the Zetasizer laser geometry.

The EM was characterized for both pH and background electrolyte dependency as well as for reproducibility at pH 9.0. Figure 13 is a plot of EM versus pH for two electrolyte concentrations. The latex mobility is independent of pH above 7.5. At pH 9.0, the EM of the latex was determined to be -6.10 (μm/s)/(V/cm) in a 0.01 M KCl background. The pH dependency curve is typical of a latex which has carboxyl functional groups as shown in the inserted plot in Figure 13.[125] The standard deviation of the EM distribution was found to be independent of pH with a value of 0.83 (μm/s)/(V/cm).

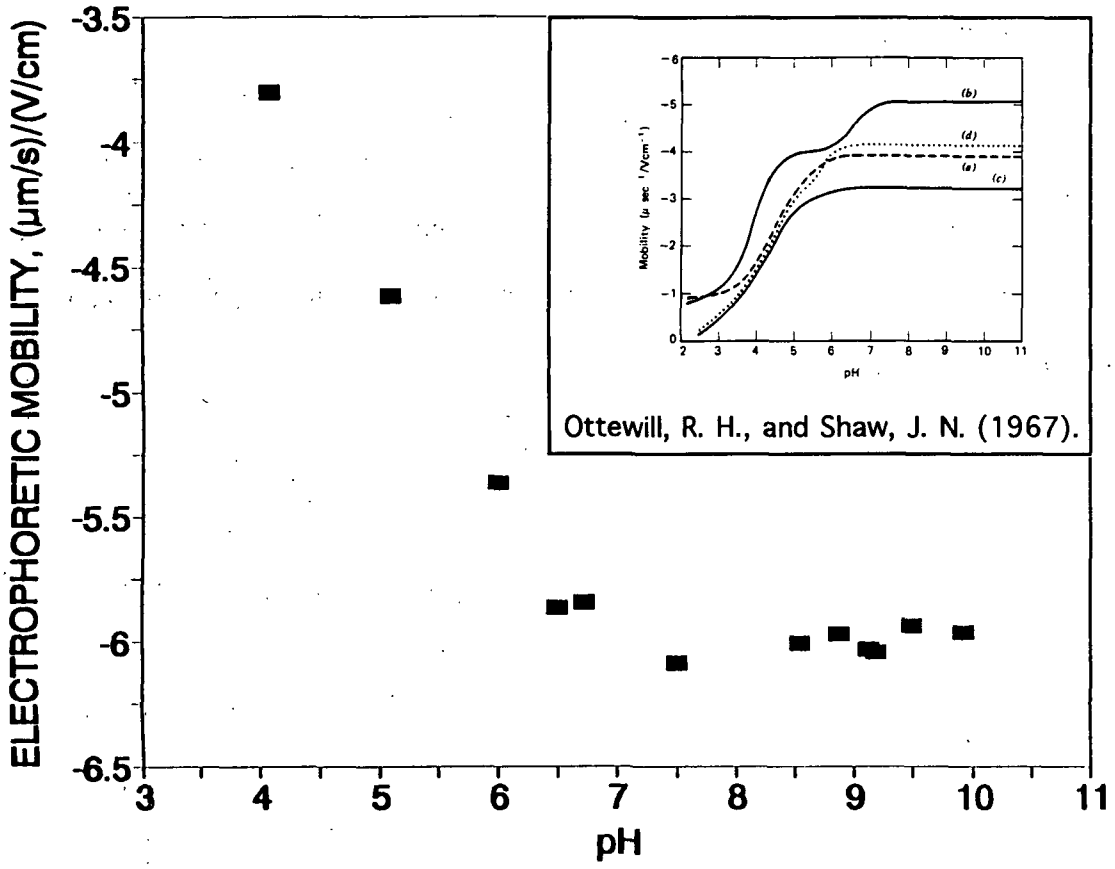

Figure 13. Electrophoretic mobility versus pH for a 0.01 M KCl background electrolyte solution for the polystyrene latex used in this project. The insert gives the typical curves expected for polystyrene particles of different functional groups suspended in 5×10^{-4} M NaCl solutions at 25°C as reported by Ottewill and Shaw.[125] (a) Carboxyl and sulfate groups; (b) carboxyl and phosphate groups; (c) carboxyl groups; (d) two types of carboxyl groups.

The flow loop experiments to be described later required the use of large quantities of Appleton city tap water which typically had a pH between 9.0 and 9.5. Since the latex was EM insensitive at this pH range, it was decided to maintain all laboratory experiments at pH 9.0.

Polymeric Retention Aid

A commercial cationic polyacrylamide (PAM), Allied Colloid Percol® 175, was used throughout this project for adsorption and dispersion experiments. The polymer arrives in dry bead form. The manufacturer's suggested dissolution procedure was followed; an initial solution was made of 0.5 percent dry solids and mixed at high shear for two hours followed by a final dilution to 0.05 percent for one hour of mixing.

The molecular weight and charge density of the PAM have been characterized by the manufacturer to be 9×10^6 by intrinsic viscosity in 1 M NaCl (at 25°C) and 10 mole percent by conductometric titration, respectively. The retention aid may be characterized as a high molecular weight, medium charge density polymer for wet-end flocculation. Using the empirical equations for the molecular weight derived by Mabire et al.[126] based on intrinsic viscosity measurements in 1 M NaCl

$$R_G = 0.56\,\overline{M}_w^{0.50} \qquad [33]$$

the polymer radius of gyration, R_G, is calculated to be 1680 Å.

Pulp

A hardwood pulp was donated for this project from Mead Corporation, Escanaba, Michigan. The pulp was a bleached kraft in dry lap form. A species identification was performed on the pulp, and the results are presented in Appendix II. In order to prepare the pulp, we wished to eliminate as much of the fines material as possible. By doing this we would reduce the complication that fines would cause in laboratory retention studies.

A discussion of the fiber length characteristics and the effect of fractionation is given in Appendix I. The reduction of the fines fraction was facilitated using the pilot paper machine at IPC. A fine tissue was made on the machine so as to reduce retention by filtration. The fines were successfully reduced from 14 to 18 arithmetic percent in the original pulp to 4.4 to 7.5 percent in the tissue. The tissue was stored at approximately 30 percent solids in refrigeration (40°C) until needed.

In addition, a carbohydrate analysis of the pulp was determined by IPC analytical services. The following analysis was based on a single determination. Lignin content must be less than 1.0 percent, but was not measured.

Table 1. Carbohydrate analysis for bleached hardwood sample.

Araban, %	Xylan, %	Mannan, %	Galactan, %	Glucan, %
0.3	21.7	1.4	0.2	75.5

EQUIPMENT

Dynamic Drainage Jar

Two phases of the experimental design make use of a modified Dynamic Drainage Jar (DDJ) or Britt Jar. A first modification involved an air line added to create an air pad underneath the screen to prevent premature drainage through the wire.[127] Second, there were four one-half-inch baffles in the DDJ at 90° increments to increase mixing in the jar. A representation of the DDJ used is given in Figure 14. Mixer setting was maintained by a Servodyne controller.

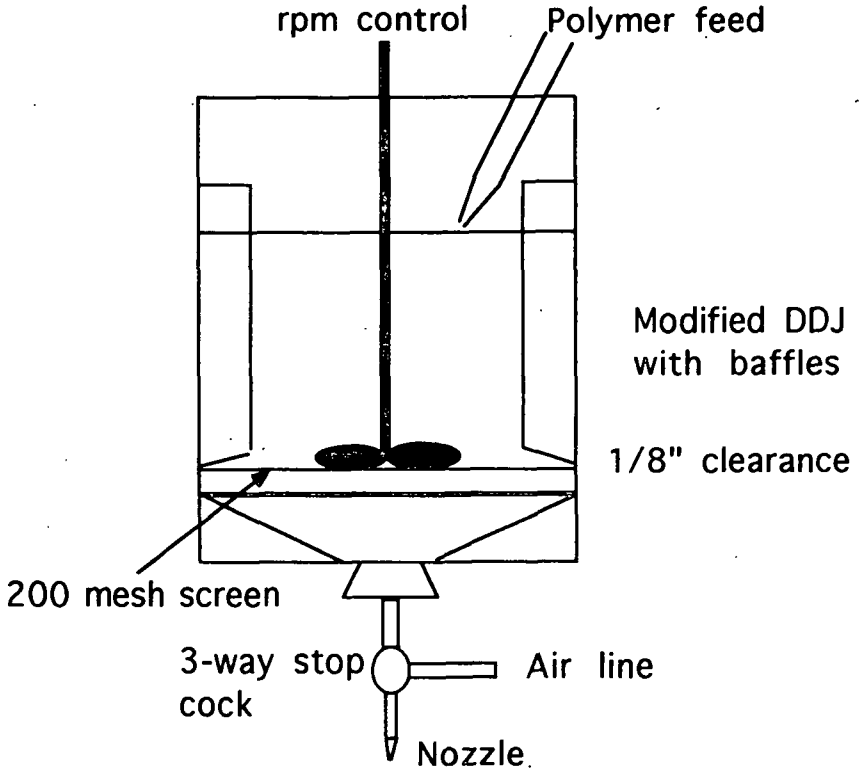

Figure 14. Modified Dynamic Drainage Jar.

Flow Loop

An existing flow loop in the IPC pulp laboratory was modified to include a testing section with polymer preparation station and sampling and sewer loops. An operating schematic is shown in Figure 15. The flow loop consisted of a stock dilution tank (2500 gal.) for dispersing the fiber and latex. Flow from the dilution tank maintained a constant level in a mix tank (960 gal.). The mix tank was fitted with steam and cold water pipes so that a constant temperature of 23°C (73°F) could be maintained. PVC piping, 7.62 cm inner diameter (3" Schedule 40), was fitted throughout the flow loop. A variable speed pump on the bottom of the mix tank could maintain a constant flow rate between 0.6 and 5.5 m/s (2

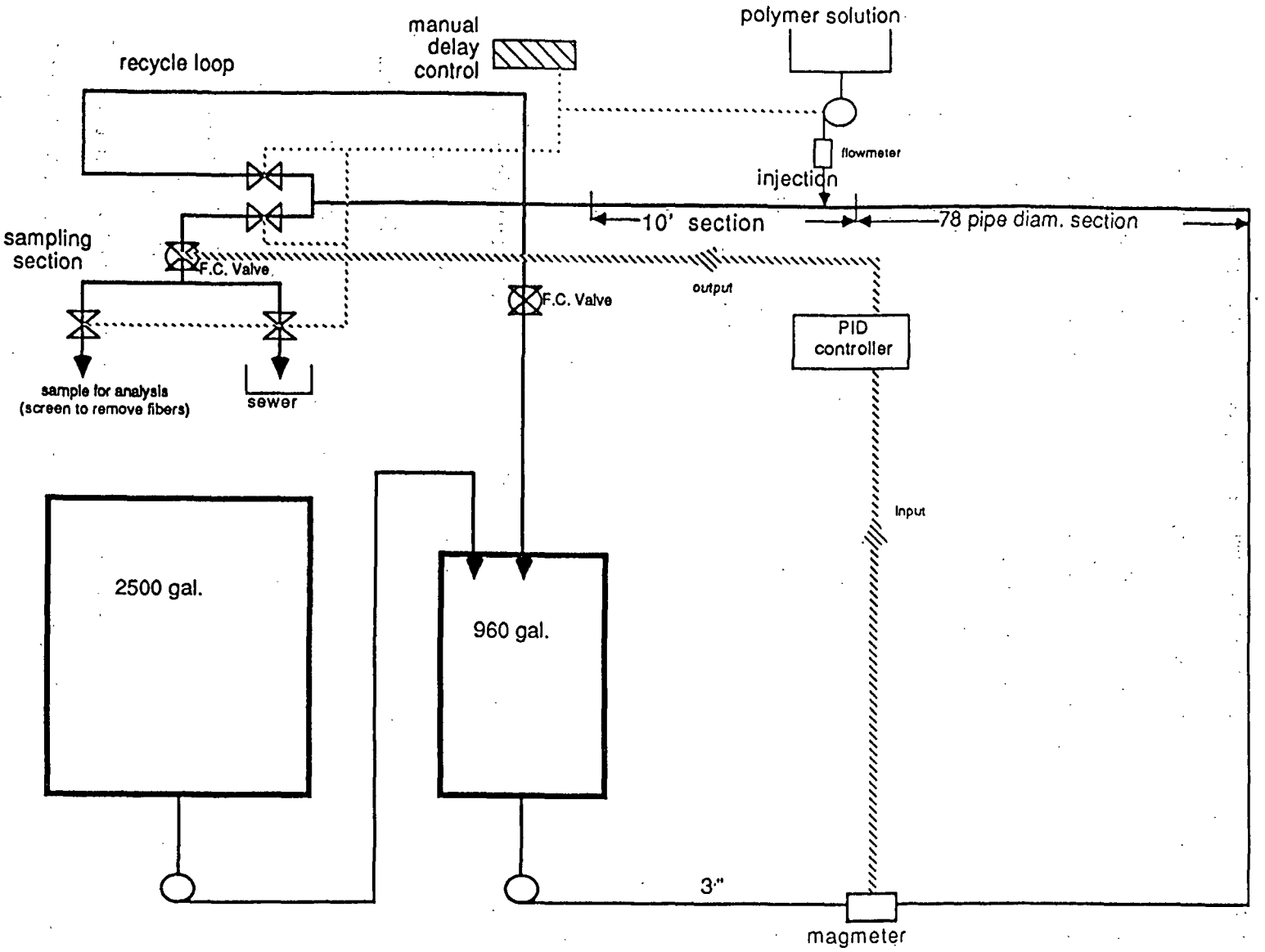

Figure 15. Operating schematic of modified flow loop for side-port injection experiments.and 18 fps). A magnetic flowmeter (Rosemount) with a digital output was used to control and maintain flow rates.

A 3.05 m (10 ft) pipe test section, installed 78 pipe diameters from an elbow, consisted of a polymer injection port and seven "hot-tap" mountings. The fittings connecting the test section piping were smooth routed to reduce disruptions to the flow pattern. Flow could continue through a recycling loop and back into the mix tank. During experiments involving an injection of material through the test section port, air-actuated ball valves (DeZurik) were manually switched to close off the recycling loop and open the sampling/sewer section. A computer-controlled air-actuated V-port ball valve using a PID (proportional-integral-derivative) algorithm controller (written in Turbo Pascal and discussed in Appendix X) was used to stabilize and maintain a set-point flow rate. Sampling and sewer legs of the loop were also controlled by air-actuated manually-controlled ball valves.

Sensor/Data Acquisition System

In order to quantify the dispersion of the injected polymer, a conductivity probe was sequentially placed in seven hot-tap mountings along the pipeline test section downstream from the injection port. A prototype conductivity probe and meter were designed and built by TBI-Bailey Controls Company (a Division of Babcock and Wilcox) for an on-line measurement application. The meter was modified by IPC electronics personnel to output 1000 data samples per second. The data were input and stored using a computer data acquisition system which consisted of a personal computer (80286 processor), with analog to digital (A/D) interface board (Metrabyte DAS-16F), and a second board for continuous real-time display and disk storage (Metrabyte WFS-200 Waveform Scroller Board with CODAS software). This combination allowed for viewing the data in scrolling chart recorder fashion while saving the data to disk. A discussion of the software is given in Appendix XI.

Flow Loop Control System

The velocity conditions of the flow loop operation were controlled with the aid of a second computer, an analog to digital (A/D) interface, and a PID algorithm controller. The signal from the magnetic flowmeter was inputted to the computer. Using an algorithm based on Turbo Pascal V4.0 (discussed in Appendix X), a control signal was output to an air-actuated V-port ball valve in the sampling section of the flow loop. During experimentation, velocity conditions were adjusted to a set-point; when an injection was started, the manually-controlled air-actuated valves were switched over to sampling section flow, and the computer controlled valve maintained flow conditions.

Polymer Preparation/Injection System

The polymeric retention aid solution was prepared to specifications of the manufacturer. Equipment for polymer preparation and mixing was obtained from existing parts at IPC. A stainless steel tank and two side-mounted mixers were used for initial dissolution at 0.5 percent (see Figure 16). A mixing tank with bottom feed to a pump was used for the final dilution to 0.05 percent. One side-mounted mixer was used on this tank.

A schematic of the polymer injection system is shown in Figure 17. A constant speed centrifugal pump (Roth Manufacturing Corp.) was obtained for the pipeline injection. The pump was required to deliver 1 to 4 gpm injecting into the pipeline flow of 20 to 30 psi. The polymer solution was pumped through a recycling loop; a small fraction of polymer was removed from the loop for the injection; this reduced the pulsations in flow caused by the pump. The injection flow went through a tapered rotometer for flow indication. The rotometer was calibrated for volumetric flow rate using a stopwatch and bucket method (see

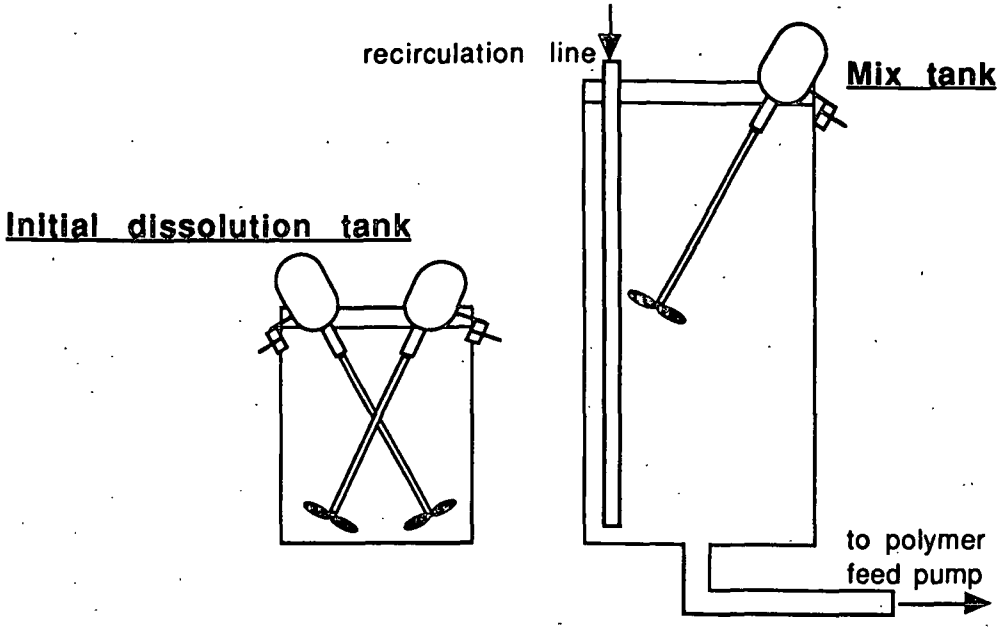

Figure 16. Polymer initial dissolution and mixing tank.

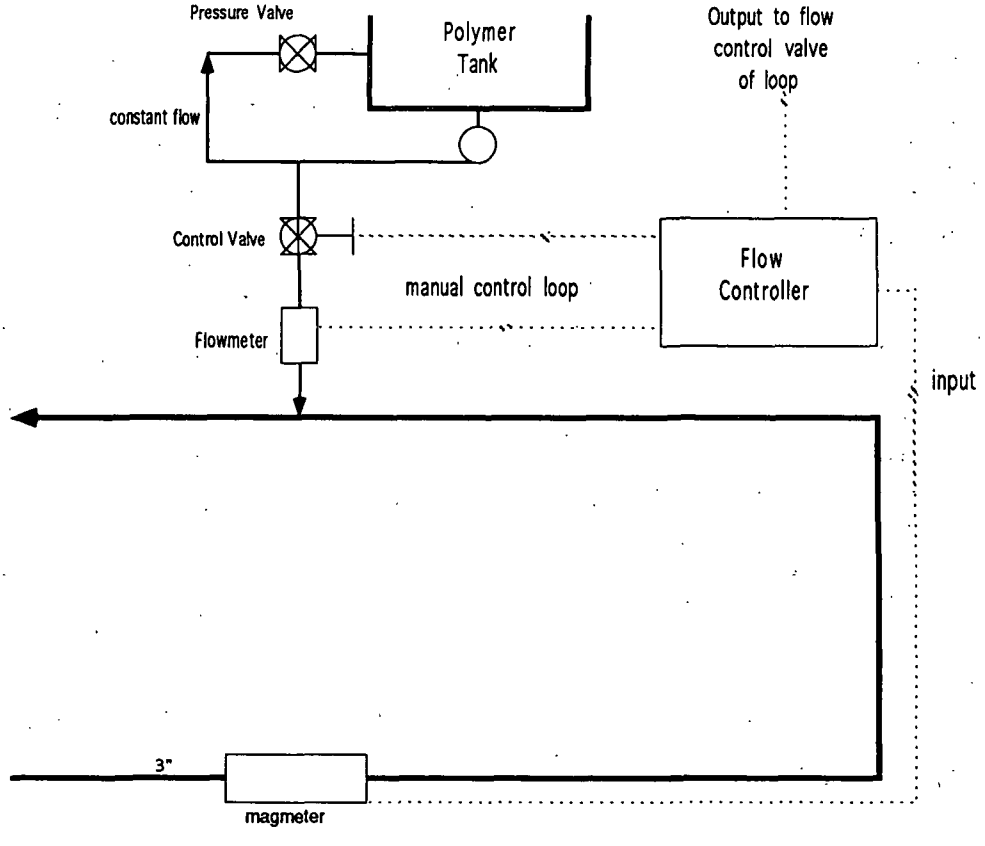

Figure 17. Polymer dilution, injection and, control system.

Appendix VIII). A check valve was used to eliminate reverse flow through the rotometer and into the polymer tank.

Pipeline Test Section

The test section consisted of the 10-foot length of piping, 78 pipe diameters from an elbow, the injection port, hot-tap probe mountings, and the surrounding area of the flow loop platform. PVC unions were fitted to both ends of the pipe and routed to reduce obstructions to the flow. Seven probe mountings were placed on the pipe downstream from the port. A schematic of the pipe section is given in Figure 18. The conductivity probe and meter could be moved from one mounting to the next and was suspended by rope from a beam.

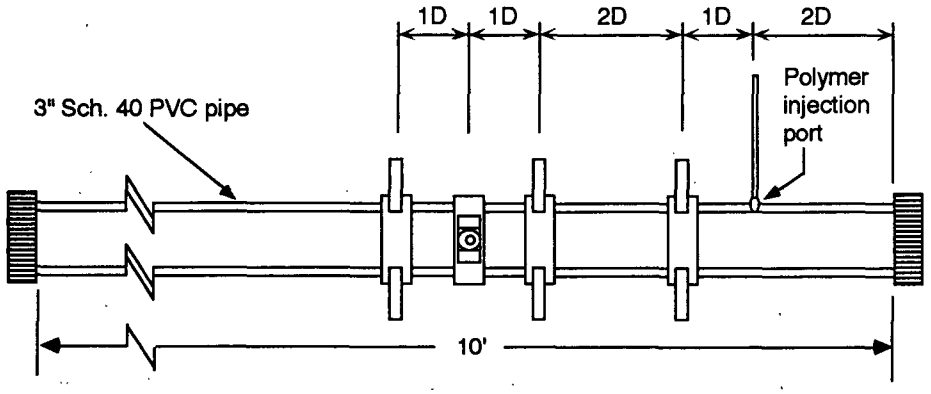

Figure 18. Pipeline testing section schematic showing injection port and probe mountings.

Probe mountings not in use were fitted with dummy probes; these probes were of proper length and curved tip shape as to fit flush with the inner pipe wall and not disrupt the flow. A single probe mounting is diagrammed in Figure 19. When the probe was to be

inserted into a particular mounting, a particular sequence of events took place: the dummy probe was first removed; the teflon ferrule fitting was loosened, and the dummy probe was pulled out beyond the sliding gate valve; the valve was closed to prevent escaping fluid; the dummy probe was completely removed; the conductivity probe placed into the fitting; the sliding gate valve opened; the probe inserted to the proper depth for a specific data position; and finally, the ferrule fitting tightened. The operation of this procedure became fail-proof following only a few dousings from 15 fps flow rates.

Electrokinetic Measurement

Measurements of electrophoretic mobility (EM) were made with the Malvern Zetasizer IIC; the theory of which was discussed in the preceding literature review. A representation of the instrument is given in Figure 20.[20] The optical unit consists of a laser light source, a sample chamber alignment mechanism, and a photomultiplier. The optical system is operated on an anti-vibration mount which comprises a heavy mass mounted on a pneumatic damping system.[20]

Signals from the optical unit were processed by the digital correlator, which was interfaced with a computer system. The computer provides further signal processing and results. Power supplied to the laser, photomultiplier, and EM sample cell was contained in the PC16 Power Supply Unit. An additional power supply, the PC7 unit, provided temperature regulation to the Joule-Peltier device mounted under the sample cell.

Adsorption Kinetic Measurement

For the work on equilibration rates using the Zetasizer, a simple Y-junction with dual

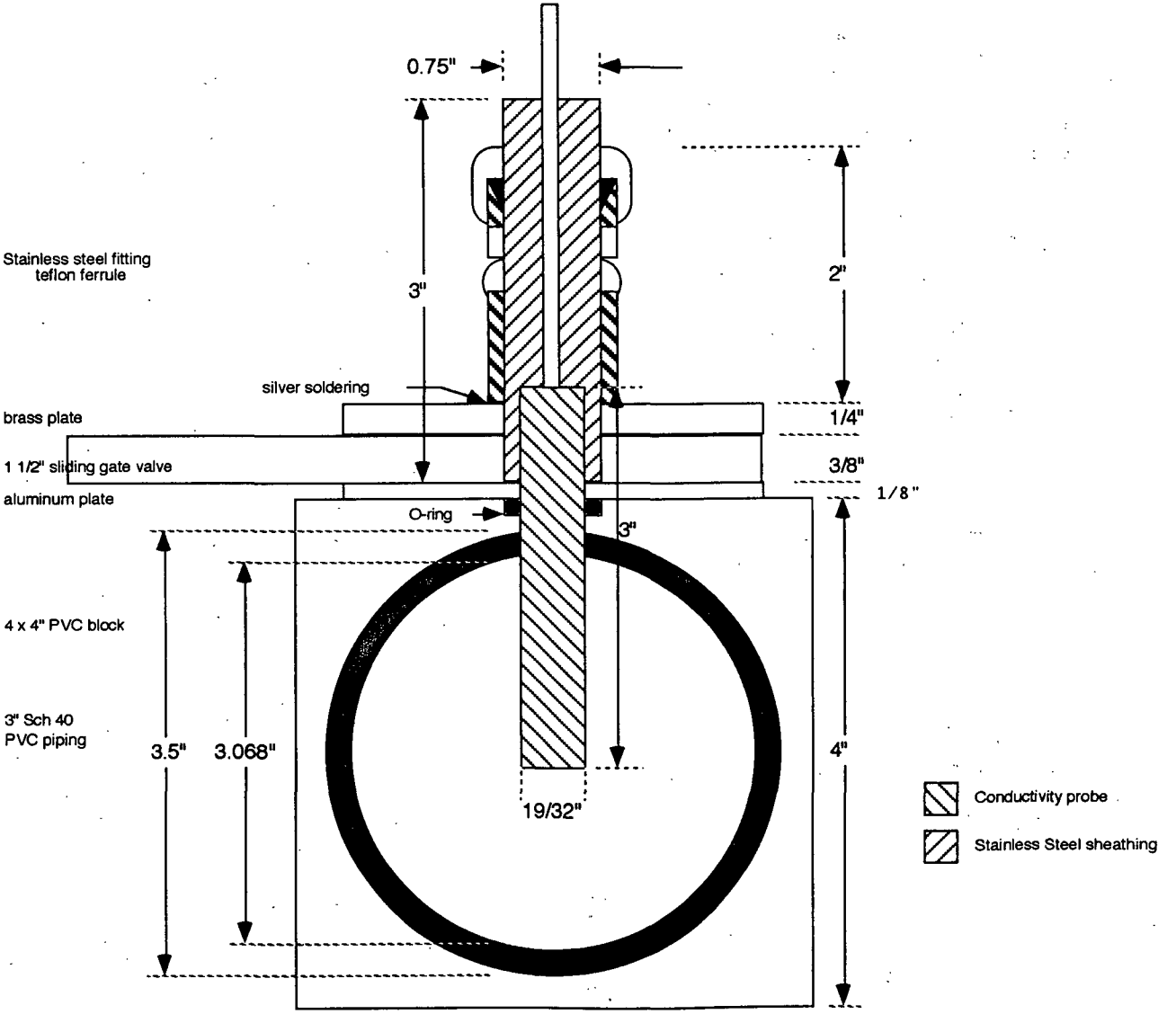

Figure 19. Schematic diagram of a single "hot-tap" probe mounting with conductivity probe in fully-inserted position.

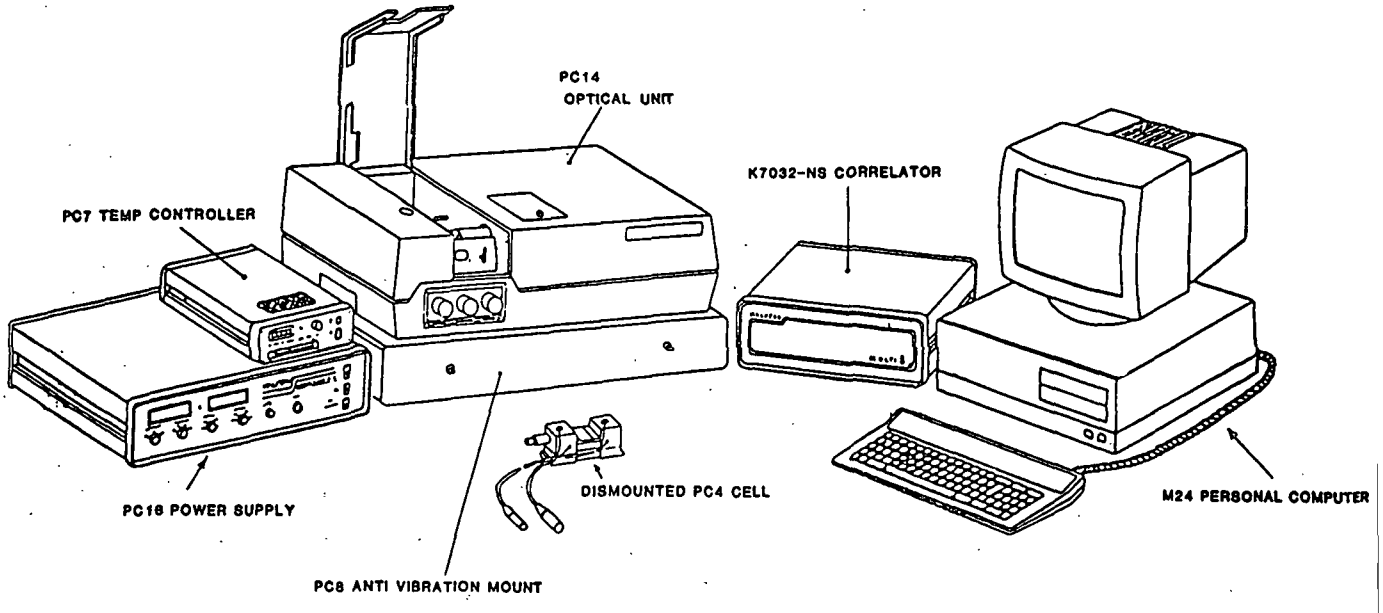

Figure 20. Malvern Zetasizer IIC system components.[20]

syringe injection system was used to combine untreated latex with cationic polymer and introduce the mixture to the quiescent chamber of the EM cell. Two different sized Y-junctions were used. A schematic of the larger size Y-junction is shown in Figure 21. The Y-junction was fabricated from a polypropylene junction and tygon tubing with connectors fashioned from syringe tips. These tapered tips were important in allowing an airtight seal with the Zetasizer. The Reynolds numbers for the Y-junctions, used to describe the mixing conditions, were calculated from the inside diameter at the tube junction, in this case, 5/32 inch. An adjustable elevated stand held the dual syringe system horizontal and level with the inlet port to the EM cell. An antivibration pad under the stand was found to be essential due to vibrations causing erroneously broad EM distributions.

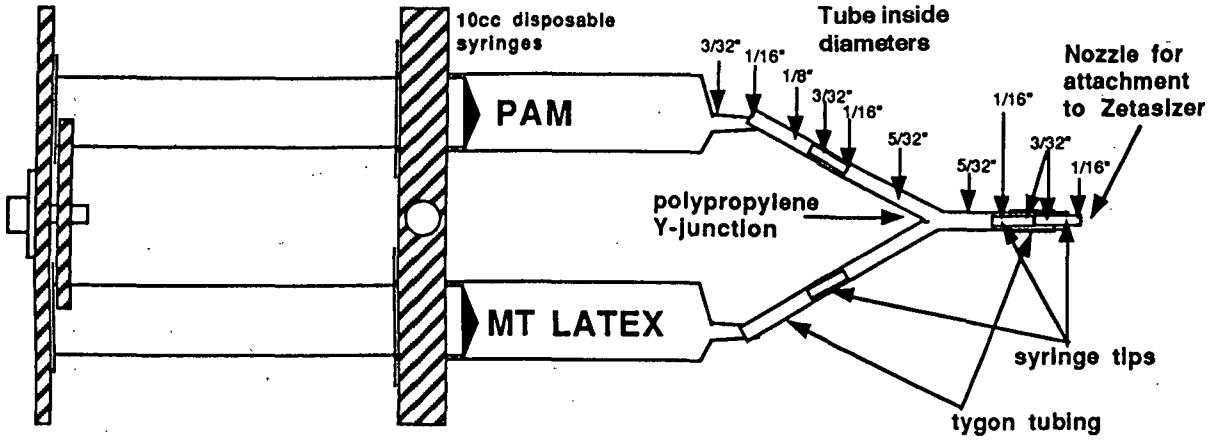

Figure 21. Dual injection syringe with Y-junction for mixing untreated latex with polyelectrolyte in equal volumes and ejecting into the EM cell.

PROCEDURES

DYNAMIC DRAINAGE JAR EXPERIMENTS

The modified Dynamic Drainage Jar (DDJ) was used for two phases of experimentation. A preliminary study examined the magnitude of influence that mixing conditions during the polymer addition could have on the ζ-potential mean and distribution. Later, a more extensive study was performed using the DDJ and involving greater diversity in the level of addition mixing. A subtle but significant procedure change separates these two experimental techniques. Both experimental procedures will be discussed in this section.

A DDJ station was set up as described in the Equipment Section and in Figure 14. Five hundred-gram samples of 0.45 percent solids pulp fiber and 0.05 percent latex solids were added per run to the DDJ, while the agitator was set to a specific RPM setting. Thirty seconds elapsed, and the retention aid was injected near the surface of the stirred slurry with an automatic pipette. The retention aid solution at 0.05 percent concentration was injected at a rate of approximately 2.5 mL per second. The different volumes of retention aid solution, corresponding with the dosage levels, were injected at constant volumetric rate rather than over a constant time sequence. The retention aid was allowed to mix with the slurry for another 30 seconds at the prescribed RPM setting.

For the preliminary DDJ experiments, where we were primarily concerned with determining the magnitude of influence that different mixing conditions could create, the next step of the procedure was to drain the jar and capture white water samples for EM and retention measurements. The retention was thus inadvertently biased due to the RPM setting; the high shear level expectedly gave lower particulate retentions. For the final DDJ

experiments, where we were interested in substantiating our conclusions about the adsorption homogeneity due to mixing and the resultant retention, we turned the mixer to a low RPM setting (300 RPM) for another 30 seconds, and then drained the jar. This allowed studying the effects of the mixing during the addition rather than the influence of subsequent mixing conditions.

Tables 2 and 3 summarize the designs of the two DDJ experimental phases. During the jar draining, three weigh dish samples for gravimetric retention determination, one sample for an EM experiment, and one sample for UV absorbance retention determination were captured from the stopcock. The EM sample was diluted with background electrolyte (0.01 M KCl) and placed on a magnetic stir table; the UV absorbance sample was diluted with a weighed amount of background electrolyte; and the three weigh dishes were closed, weighed individually, and placed in an oven.

Table 2. Experimental design for preliminary Dynamic Drainage Jar runs.

Polymer Dosage Random testing between 0 and 8 lbs dry polymer per ton of dry pulp and latex solids.
RPM Setting During Polymer Addition and Draining 750 and 1500 RPM servodyne settings.

Table 3. Experimental design for final Dynamic Drainage Jar runs: A randomized block design of RPM setting with four replications.

Polymer Dosage, lbs./T
0
1
2
RPM Setting During Polymer Addition
0
500
1000
1500
RPM Setting During Jar Draining
300 RPM for 30 seconds prior to draining.

MEASUREMENTS ON THE MALVERN ZETASIZER IIC

After one weigh dish was filled from the draining DDJ, approximately 20 mL of white water was captured in a polypropylene beaker. This sample was diluted with approximately 200 mL of 0.01 M KCl and gently stirred. The surface of the liquid was flushed with nitrogen gas to deter adsorption of CO_2 which would lower the pH. The beaker was covered with a watchglass.

A syringe was filled and flushed into a waste receptacle twice and then filled and injected into the prepared Zetasizer unit. The walls of the EM cell were located using an optical focusing device and gauge positioner; thus, the positions of the two stationary layers were located. An automatic mode 30-second measurement was taken at each stationary layer. The error in locating correctly the stationary layer was reduced by averaging the results from the two stationary layers. A hard copy of the distribution was output and the sample cell flushed with background electrolyte solution.

DETERMINATION OF RETENTION

Two methods were used to test the retention of latex particles from DDJ runs: UV absorbance spectrometry and gravimetric measurement of white water concentrations. Early in this project, consistent with findings by Miller,[17] the UV absorbance method was found to give falsely high calculated retentions when a cationic polymer was present and had adsorbed onto the latex particle surfaces. Therefore, a gravimetric determination of white water concentration was undertaken.

UV Absorbance Spectrometry

An absorbance method was initially used to determine the concentration of latex in the DDJ white water samples. A calibration curve was made of UV absorbance at a peak wavelength (typically at approximately 246.7 nm) using untreated latex (presented in Appendix VI). A sample drawn from the draining DDJ was diluted with a known amount of background electrolyte and ultrasonicated for five minutes. The suspension was placed in a quartz cell (by automatic pipette) and the absorbance measured with a UV/Vis Spectrophotometer (Perkin-Elmer 320 Spectrophotometer in Appleton; Perkin-Elmer Lambda 4b UV/Vis Spectrophotometer in Atlanta). The retention values obtained from the calibration curve were biased high, particularly when compared with gravimetric retention values. Miller[17] notes the error involved with using a calibration curve made from experiments of untreated latex. The absorbance was found to decrease with polymer present. Since less latex was detected in the white water with polymer present, the retention results were biased upward.

Gravimetric Retention Measurement

Pyrex weighing jars were used for gravimetric retention determinations. Numbered sets of dishes and lids were periodically washed, dried (105°C oven), cooled in a desiccator, and tared (using a Sartorius Research balance to ten thousandths of a gram). Each DDJ experiment involved three dishes containing approximately 70 wet grams of white water each. They were immediately covered, weighed, and dried.

The weigh dishes and lids weighed approximately 100 g each. The dry weights were often 0.08 g or less depending on the retention. Therefore, cleanliness and accurate tare weights were crucial for test reproduction. Cotton gloves were worn for all glass handling to eliminate transfer of oils.

One problem which arose from this method was from the significant contribution to dry weight from the background electrolyte present in the pulp, latex, and retention aid solutions. All volumes of solutions were recorded so that the amount of salt in the white water samples could be calculated and subtracted from the weigh dish dry weights. In the final DDJ experimental phase, replicates of constant polymer dosage and mixing condition allowed for the study of data reproduction. For each mixing condition, a standard deviation of the data is reported in the Results Section.

FLOW LOOP PROCEDURES

The various stages of flow loop experimental procedures are discussed individually with much of the corresponding data presented in Appendices XIII and XIV. Table 4 describes the conditions tested and their corresponding parameters. Velocity conditions for

the remainder of this report will be referred to by their code numbers. Those conditions represented by a letter code were tested for water flows; those with a number code were also tested for dispersion into a pulp/latex slurry.

Table 4. Description of the different injection conditions for flow loop experiments.

Code Letter	Injection Port size, in	Pipe velocity, fps	Polymer feed rate, #/T	Jet velocity, fps	Velocity Ratio	Pipeline $Re(\times 10^4)$	Jet $Re(\times 10^3)$[††]
A(1)	1/4	3	1	2.25	0.752	6.306	1.554
B	1/4	6	1	4.51	0.752	12.611	3.115
C	1/4	9	1	6.76	0.752	18.917	4.668
D(2)	1/4	15	1	11.27	0.752	31.528	7.783
E(3)	1/8	3	1	9.02	3.007	6.306	3.115
F	1/8	6	1	18.04	3.007	12.611	6.229
G	1/8	9	1	27.06	3.007	18.917	9.334
H(4)	1/8	15	1	45.10	3.007	31.528	15.573
I(5)	1/16	3	1	36.09	12.030	6.306	6.231
J(7)	1/8	3	2	18.04	6.013	6.306	6.229
K(6)	1/4	3	2	4.51	1.503	6.306	3.115
L(8)	1/4	3	3	6.76	2.252	6.306	4.668
M(9)	1/8	3	3	27.06	9.020	6.306	9.344

[††] Reynolds numbers calculated by taking viscosity measured as 2.80 cP.

A variety of velocity conditions were studied. Three injection port sizes and four pipe velocities enabled the study of several velocity ratios (equal to the ratio of jet-to-pipe velocities) to maintain a polymer dosage rate of 1, 2, or 3 #/T (1 #/T is equivalent to 0.05%). Low, intermediate, and high velocity ratios were studied at a 1 #/T dosage as well as a low and high level for both higher dosage levels. The resultant Reynolds numbers were calculated to be in the turbulent regime.

Pulp Preparation Methods

Pulp suspension experiments throughout this project were performed with slurries of 0.50 percent total solids: 0.45 percent fiber solids and 0.05 percent latex solids. The stock preparation procedures consistently involved careful solids determinations. For DDJ experiments, master batches of fiber slurry and latex solution were made, tested for solids, adjusted, and retested until proper solids contents were established. Individual batches were combined (approximately 500 g total for each DDJ experiment) and immediately poured into the jar.

Flow loop experiments used much larger amounts of the raw materials. The 2500-gal mix tank required almost 100 pounds of dry fiber and 10 pounds of dry latex. The pulp was added first by bucket hoist from the drums of wet tissue. Solids were checked, adjusted, and rechecked until proper conditions were met. The addition of latex was the last step prior to experimentation.

The dilution water for all DDJ and Zetasizer EM experiments was distilled water with 0.01 M KCl adjusted to pH 9.0 with 1.0 M KOH (final conductivity of 1550 μmho/cm). In Appleton, water was obtained from the Analytical Group still, until it was shut down just prior to the move. Thereafter, water was obtained from the Krannert Building still. From both stills the water was evaluated to maintain a pH of 5.4 to 5.6 with a conductivity of 0 to 2 μmho/cm. In Atlanta, the water used for DDJ and adsorption equilibrium experiments was deionized, distilled, reverse osmotized, and 0.22 μm filtered. This water was consistently 5.8 pH with 0.2 μmho/cm conductivity.

The water for flow loop experiments was not as easily controlled. This water came

directly from city water sources and was filtered through a bank of cores to remove sand and particulates. The pH of this water was variable, between 9.2 and 9.9 with a conductivity of 110 to 220 μmho/cm. The latex was shown to be EM insensitive at this pH range, and the baseline conductivities were removed from consideration from the dispersion data.

Data Acquisition

Conductivity probe data acquisition was primarily handled by the CODAS software package. Gain settings for on-screen monitoring were software selectable. At the beginning of each data collection, a zero baseline was stored at the start of a data file followed by a calibration of the meter and acquisition system with 0.00125 M and 0.0025 M KCl solutions of 230 and 440 μmho/cm, respectively. Data collection could be turned on and off with the push of one button, and markers could be placed in data files with the space bar.

With flow at a set condition, the probe was placed in a particular downstream mounting location and at a particular position in the crosssection of the pipe. A baseline conductivity without polymer injection was taken and stored. The manual valves were switched from recycle to sewer loop and the injection begun. While polymer feed rate was being adjusted, the flow loop control scheme was stabilizing to the velocity set-point. Once conditions stabilized properly, data acquisition was activated. Each data set, representing a velocity condition, probe mount location, and probe position, consisted of 3000 to 30,000 data values (3 to 30 seconds of data acquisition). Data acquisition for a position ended when it appeared that the values had stabilized and were redundant.

Data sets from each of the eight probe positions at a mounting location could be

obtained without system adjustment. Once a set was completed, the injection line off the polymer recycle loop was turned off and manual valves on the flow loop switched back to recycle. The probe could then be moved to its next location for further data collection.

Flow Control

A PID algorithm written in Turbo Pascal (V4.0) and run by a personal computer (XT-processor) handled the flow rate control system to a set-point volumetric flow rate. A signal from a magnetic flowmeter was input to the computer (4 to 20 mA converted to a 0 to 5 V signal). The algorithm calculated the correct output signal to the sampling loop V-port ball valve (0 to 5 V output signal converted to a 4 to 20 mA signal for the electropneumatic operator on the valve). The program also output to the screen a chart of the set-point and offset values used to calculate the individual proportional gain, reset minute (integral), and derivative minute components of the output signal.

Some attempts were made with published methods to fine-tune the algorithm response. It was found, however, that more important for this application was achieving the set-point flow conditions as soon as possible after the switch from recycle to sampling loops to reduce raw material waste. Of secondary importance was the amount of fluctuation around the set-point once achieved. This was especially true after some initial tests showed that the amount of offset after achieving the set-point was insignificant. A series of experiments with water tested the response time to set-point and to stability. It was determined that the optimum values were a proportional gain of 7.0, reset minute equal to 10.0, and no derivative control.

Polymer Preparation

The polymer injection was to be used as a tracer for the efficiency of pipeline mixing. The conductivity of the polymer solution was higher than that of the pipeline upstream flow and was tracked by the on-line conductivity probe. For flow loop experiments, the retention aid was diluted in 0.05 M KCl (made in filtered tap water). Mixing in the double agitator tank took two hours; this was enough time to solubilize the swollen polymer beads. This 0.5 percent solution was poured into the mix tank and diluted with a 0.05 M KCl solution. The solution was mixed with a single agitator for one hour before injection studies were performed.

Sampling/Testing Procedures

A sample for adsorption and retention experiments was taken by switching manual valves from sewer loop to sampling loop. The flow control was allowed to stabilize, and a polypropylene jar was filled with stock. The polymer injection was stopped and the flow loop switched back to recycling. The sample jar was taken to the Zetasizer laboratory and poured into a DDJ with mixer set to 300 RPM. After 30 seconds, the DDJ was drained, and samples for gravimetric and UV absorbance retentions and EM measurements were taken. The electrophoretic mobility test sample was diluted for Zetasizer analysis with 0.01 M KCl solution.

Data Handling and Analysis

The data files from the on-line conductivity probe were saved in CODAS binary files for later analysis. We wished to use these files to calculate several parameters for the

separate probe positions and locations under different velocity conditions: the mean, root mean square, maximum, minimum, and baseline subtraction conductivities. These values are tabulated in Appendix XIII. An attempt was made to characterize the turbulence by analyzing the frequency of the signal. Finally, by testing the replicate velocity conditions, we could test the reproducibility of flow loop operation.

The CODAS files were written into segregated ASCII files for importing into an analysis package called W.A.V.E. (Vespine Software a Division of Electronic Decisions Incorporated). Fourier transforms of the data were minimally successful due to the high level of noise. A 60 Hz electronic noise signal was constantly present during data acquisition; the amplitude of which was 9 to 11 μmho/cm. An autocorrelation of the files was performed followed by a Fourier transform, which resulted in a cleaner frequency spectrum. A presentation of these techniques and the programs within W.A.V.E. which performed them are given in Appendix XI.

The mean conductivities were used to create graphical representations of the jet dispersions. These time-averaged conductivities from the probe mounting locations were extrapolated to give two- and three-dimensional shapes to the data. In this manner, we were able to visualize the quality of the dispersions under the different velocity conditions.

ADSORPTION KINETICS EXPERIMENTS

As described in the Experimental Materials Section, a Y-junction was fashioned for making dual injections into the EM cell. Three such devices were used to vary the Reynolds number at the mixing joint. Lang[59] found that by using the Zetasizer manual mode, one

could change the EM experiment time and run successive measurements (up to 20 with a manually-set delay time between measurements). The manual mode commands used for these operations are described in Appendix V.

The files from these experiments were written to binary files, imported into computer spreadsheets, and manipulated for calculation of EM distribution mean and standard deviation. Ten replicates of each latex concentration and mixing condition were made. A constant polymer dosage was maintained throughout these experiments; a dosage was decided upon which would yield an EM result analogous to one pound per ton polymer addition to a stock of pulp and latex. A 1 #/T addition to a pulp/latex slurry consistently resulted in an EM of -2.6 (μm/s)/(V/cm) in DDJ experiments. With latex alone, the dosage to achieve this EM was 19 #/T.

The latex solutions of the correct concentrations were taken from a 5 percent solids master batch. Retention aid was prepared in the laboratory using a magnetic stir bar, with an initial concentration of 0.5 percent followed by dilution to 0.05 percent. A background electrolyte of 0.05 M KCl was used for retention aid dissolution and dilution. Further dilutions to the correct concentration in order to fill a 10 cc syringe and fulfill the dosage requirement were made with 0.01 M KCl.

A preliminary experiment was performed to determine whether the polymer dosage was correct. We took 10 cc syringes of latex and polymer solution and ejected them into a polypropylene beaker with a turning stir bar. The solution was flushed with nitrogen gas, covered, and allowed to stir for 10 minutes. A syringe was filled with this mixture and injected into the EM cell for an automatic mode experiment. For low concentrations, the

time for stirring was extended to allow for the slower equilibrium rates discovered. Once a correct polymer concentration was achieved, the Zetasizer unit was switched to manual mode for variable time experiments. Three-second experiment times were found to be the most practical; shorter times were found to give noisy distributions. A typical experiment would make 20 measurements of three-second length each with zero delay time between measurements.

Injection of the dual 10 cc syringes would take approximately 3 seconds. This was manually driven, thus variable; however, every effort was made to maintain this injection rate. When the injection was completed, the dual syringe device was laid on the elevated platform and the measurement of mobilities begun.

The upper and lower limits of these experiments were determined from operation of the Zetasizer instrument with the Lytron latex particles. At the high concentrations, it becomes difficult to determine the location of the cell walls due to high laser light scattering within the cell. This causes inaccuracies in placing the laser crossing pattern correctly on the stationary layer. Also, we have seen that the "counts" level -- the arbitrary number the instrument outputs in order to give an indication of the number of particle measurements -- is typically linear with particle concentration for the reasonable concentration measurements performed in the past. However, at the high concentrations (such as 0.1 to 0.025%), the count level was found to decrease with concentration. This is probably due to the level of scattered light within the cell at these higher concentrations.

The low end for concentration experiments was due to the minimum counts the instrument requires for a measurement. If the instrument does not detect 10 counts during a

preliminary measurement, it will not begin taking data. Experiments at 0.00025% were marginal using a 400 μm pinhole aperture for the photomultiplier tube. We have the option of using a 200 μm aperture which in effect doubles the count level. Therefore, we believe a concentration of 0.0001% is possible, though not attempted for this project.

RESULTS

The results section will discuss the five experimental portions of this thesis: preliminary laboratory-scale (Dynamic Drainage Jar) experiments; flow loop dispersions; flow loop adsorptions; equilibrium adsorptions; and, finally, Dynamic Drainage Jar laboratory-scale experimental phase II.

PRELIMINARY DYNAMIC DRAINAGE JAR EXPERIMENTS

Initially, we were interested in detecting changes in EM and EM distribution with different laboratory mixing conditions during polymer addition. A DDJ and two levels of mixing, 750 and 1500 RPM settings, were chosen. Polymer dosage varied from zero to 8 #/T. The results of average EM, shown in Figure 22, show a typical trend with cationic polymer dosage; the EM decreases in negative magnitude sharply between zero and 2 #/T, reaches an isoelectric point at approximately 2.5 #/T, and levels off with increased dosage at about +1.1 (μm/s)/(V/cm).

We also see an indication that the presence of fibers has an effect on the EM of the latex. The untreated latex alone has a mobility of -6.10 (μm/s)/(V/cm); latex exposed to the fiber in the DDJ has an untreated EM of -5.90 (μm/s)/(V/cm). We may predict that the effect reported by Jaycock et al.[10] of soluble hemicellulose adsorption has occurred in this system to make the latex less negative.

The effect on EM of the two levels of mixing during the addition is not significantly different. However, the standard deviations of these EM distributions do show differences,

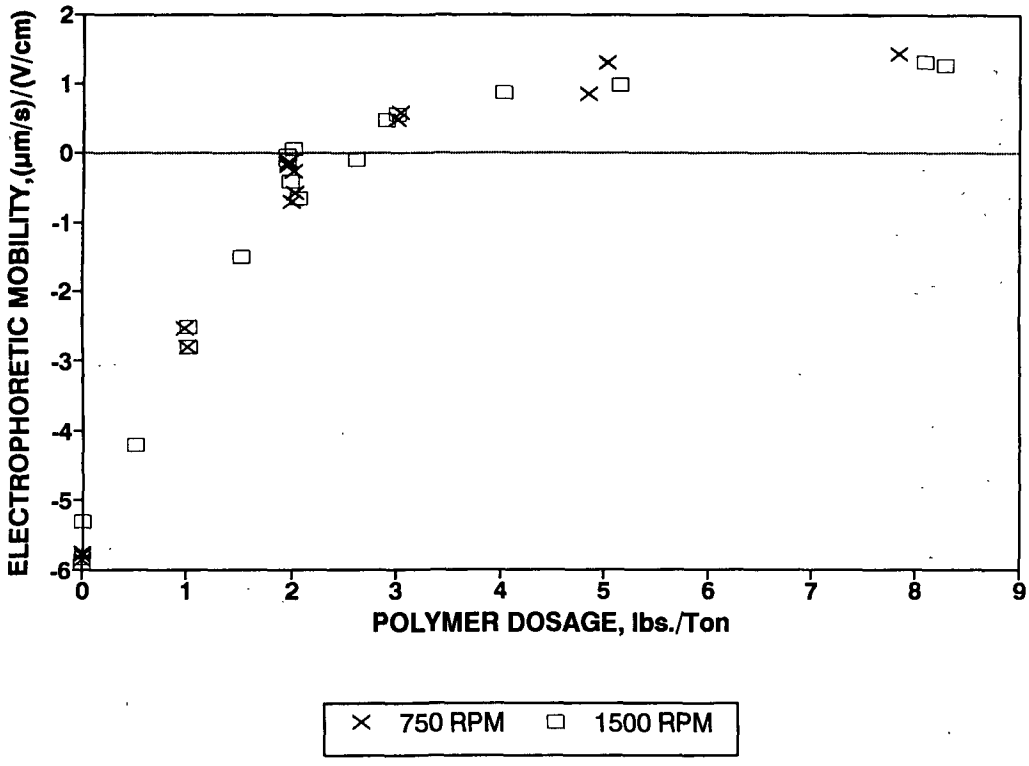

Figure 22. Average electrophoretic mobility versus PAM polymer dosage for DDJ addition at two different RPM settings.

as illustrated in Figure 23; the higher mixing level resulted in a more narrow EM distribution (α = 0.20; the statistics of this analysis are discussed in Appendix XV). The results from this early DDJ work gave encouragement for the next step of the thesis; if we could generate different mixing conditions with the side-port injection, we would see similar results with flow loop pilot-scale adsorption experiments.

FLOW LOOP DISPERSION

The on-line conductivity probe data were compiled to show the time-averaged

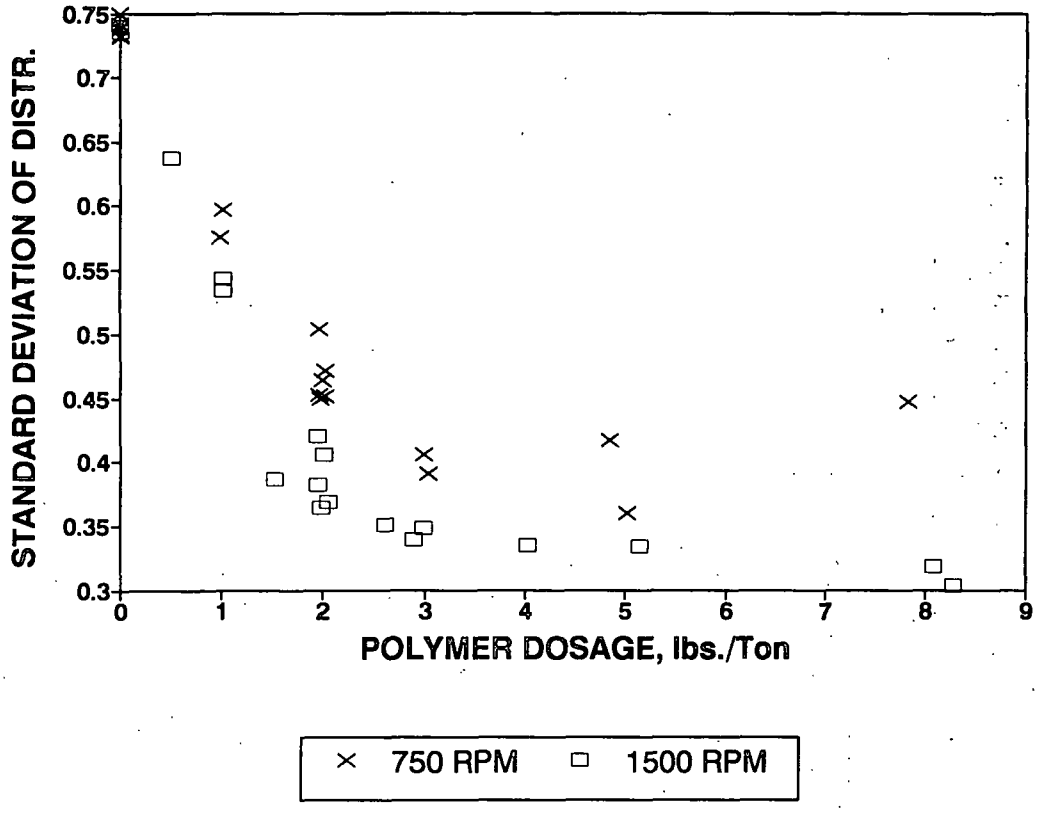

Figure 23. EM standard deviation of distribution versus polymer PAM dosage for two DDJ addition mixing conditions.

dispersions of the jet into the pipe flow with varying velocity conditions (these conditions can be reviewed in the Flow Loop Procedures Section, Table 4, Page 73). Upstream baseline conductivities were subtracted from each probe position. Two-dimensional plots of the different velocity conditions illustrate the effect of velocity ratio on the injection shape. Figures 24 through 28 show a few of the more striking differences, with the remainder of these plots presented in Appendix XIV. In each of these graphs we represent the vertical probe data and show the cross-sectional position with zero on the abscissa representing the wall at the location of the injection port. These graphs illustrate the dispersion of the jet as we go farther away from the port.

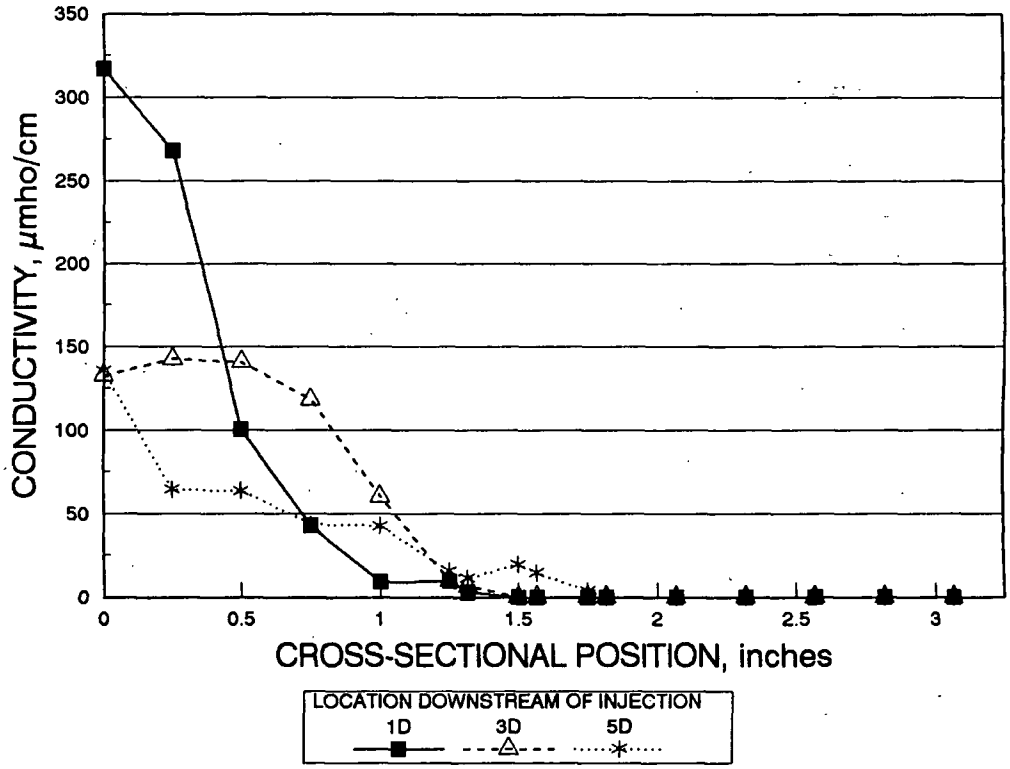

Figure 24. Three cross-sectional views downstream from the injection port showing the dispersion into a pulp suspension flow for velocity condition A.

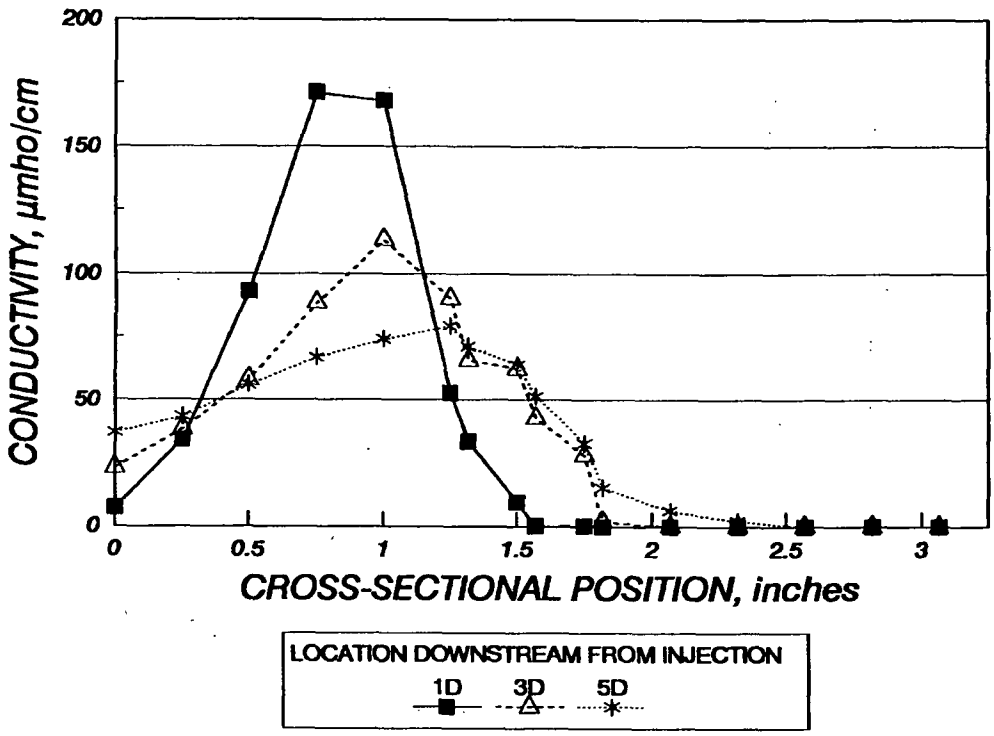

Figure 25. Three cross-sectional dispersion profiles into a water flow for condition H.

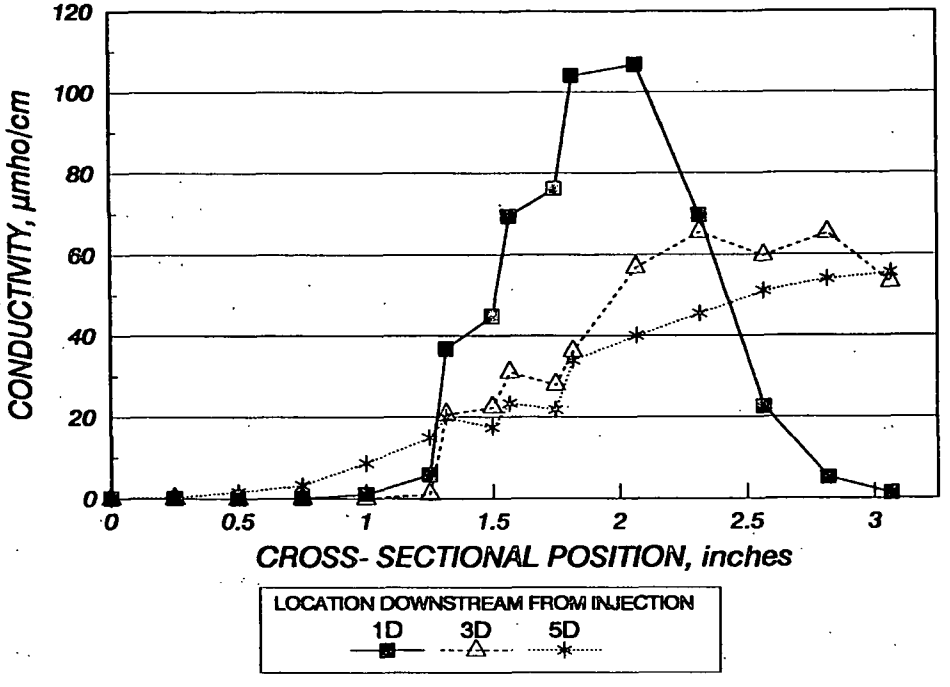

Figure 26. Three cross-sectional dispersion profiles into a water flow for condition I.

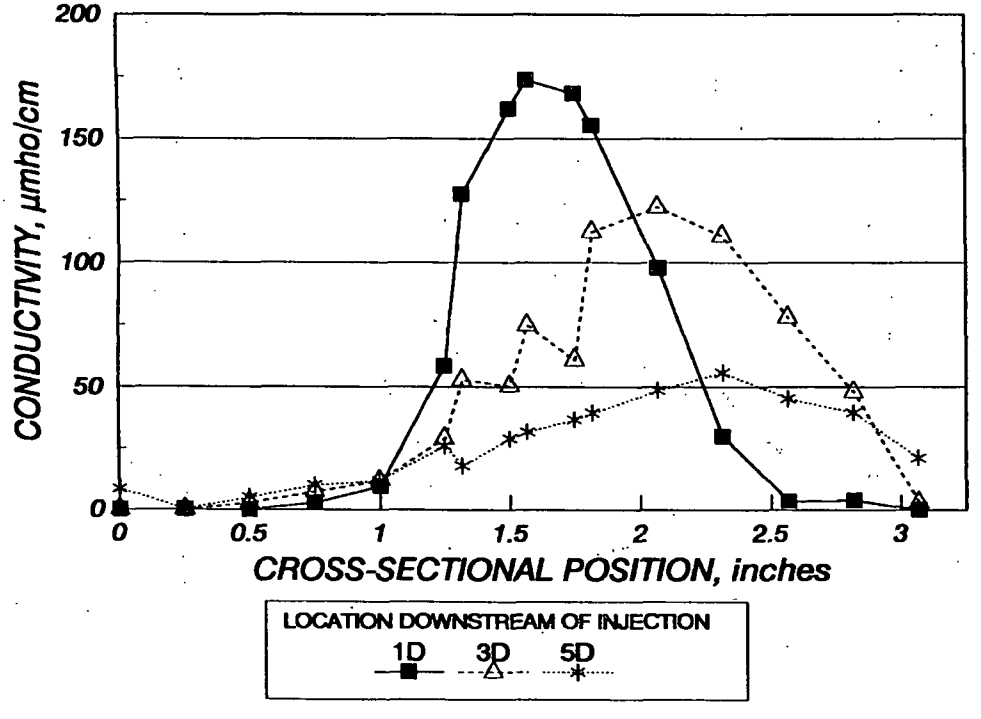

Figure 27. Three cross-sectional dispersion profiles into a pulp flow for condition J.

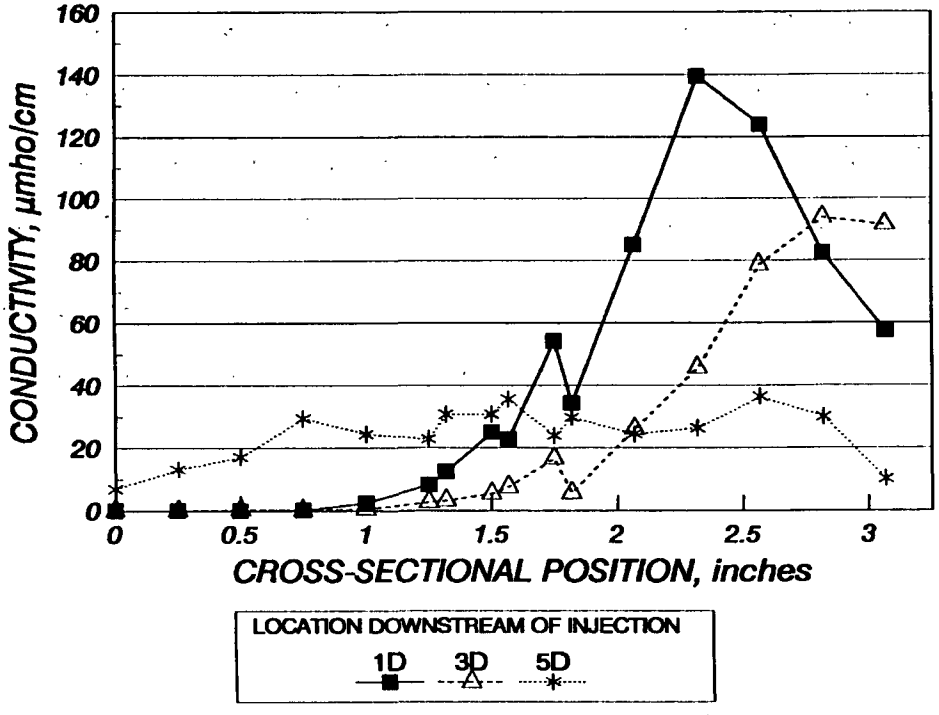

Figure 28. Three cross-sectional dispersion profiles into a pulp flow for condition M.

In order to determine the influence that the velocity ratio had on the dispersion, methods were used to quantify the mixing from the conductivity data. One method employed a mass balance to quantitatively determine the "quality of the mixing" for the different velocity conditions. This method assumes that the conductive material is injected at the pipe vertical centerline, and the plume flow is vertically symmetric. It also initially assumes that the cross section of the dispersion plume is circular. Finally, any method using the conductivity data must assume that the probe negligably perturbed the flow conditions. This assumption may be considered reasonable for this evaluation due to the smoothness of the data lines shown in Figures 24 through 28 for probe data taken from opposite sides of the pipe.

In turbulent flow, we expect both velocity and concentration to fluctuate. In our situation the concentration fluctuations are measured by the conductivity probe. The time average of the fluctuations is however zero. The background electrolyte of the injected polymer solution is not depleting by reacting with the system. Therefore, we may write a mass balance of the concentration of tracer fluid injected into the pipeline by the side-port jet and the concentration within the cross section of the pipeline at the measured points downstream.

$$u_j A_j c_j = u_p (A_{eff})_p \overline{c_p} \qquad [34]$$

where

u_j = jet velocity, cm/s
A_j = jet area, cm^2
c_j = concentration of conductive material in the jet stream, g/cm^3
u_p = pipe bulk velocity, cm/s
$(A_{eff})_p$ = effective area of pipe exposed to conductive material, cm^2
c_p = average concentration of conductive material in pipeline, g/cm^3

We calculate the average value c_p from the pipeline cross section concentration data. The conductivity is proportional to a KCl solution concentration as discussed from reference data presented in Appendix IX and in Figure A7. By taking the area under each injected KCl concentration versus cross-sectional position curve (which we can approximate by the trapezoidal rule), we can calculate an average concentration of injected conductive material in the pipeline at each measured position downstream.

$$\overline{c_p} = \frac{1}{D}\int c_p \, dr \qquad [35]$$

Thus, we may calculate the effective area of the shape that the dispersed jet makes in the pipeline cross section:

$$(A)_{eff} \quad \frac{c_j u_j A_j}{u_p \left[\frac{1}{D} \int_0^D c_p \, dr \right]} \qquad [36]$$

The results of these calculations are shown in Table 5. The pulp flows consistently gave higher values for the calculated effective areas than those for water flow (denoted by _W). It is counterintuitive that at equal bulk velocities a suspension flow would yield greater dispersion than for pure water flow.

As we view Table 5 from top to bottom, we note that the calculated dispersion values increase substantially. The effective area for all positions downstream increases as we go from velocity conditions A to I; the 2 #/T levels show an increase from K to J; the 3 #/T dosage levels show an increase from L to M. Those conditions that are of constant velocity ratio, A through D (0.75 velocity ratio) and E through H (3.01), did not show significant differences in the calculated pipeline area.

Another way of representing this is to plot the area versus the velocity ratio as in Figure 29. The calculated effective area increased with velocity ratio for all flow conditions and distances downstream. This conclusion coincides with the results presented by Forney[117,119] and Tosun.[128]

The magnitude of the calculated values has raised some concern. The total cross-sectional area of the 3" Sch. 40 pipe was 47.694 cm^2, yet the calculated effective areas are as high as 333 cm^2. For these results, we have examined the horizontal probe data. The

Table 5. Effective areas of the pipeline exposed to injected material for velocity conditions studied.

DATE AND VELOCITY CONDITION	$(A)_{eff}$ [cm^2] x/D = 1	3	5
JL13A_W	10.32	18.87	33.84
JL27A	20.33	26.49	56.15
AU8A	14.52	30.41	61.21
JL3B_W	14.70	22.94	34.55
JL14B_W	10.68	17.56	36.20
JL18B_W	10.85	21.49	36.09
JL15C_W	11.02	17.44	35.11
JL6D_W	10.06	17.40	35.11
JL15D_W	10.76	20.69	35.46
JL27D	15.07	37.40	57.00
AU9D	16.81	41.77	50.95
JL16E_W	26.94	30.05	71.81
AU3E	48.26	78.71	104.55
AU14E	40.80	73.40	89.35
JL6F_W	16.24		47.33
JL16F_W	29.61	37.34	51.91
JL16G_W	31.06	37.69	59.64
JL18H_W	31.70	44.16	60.13
AU4_7H	41.01	58.53	105.32
AU12H	37.29	58.76	98.56
JL20I_W	53.14	53.82	98.64
AU8I	59.24	80.13	208.46
AU21I	66.04	82.78	198.39
S27J	65.78	85.95	182.97
S27K	28.32	51.24	81.57
S27L	49.41	114.22	163.82
S27M	124.58	249.59	333.46

purpose of placing a mount on the side of the pipeline test section was to test the symmetry of the injected jet into the pipe. By testing the conductivity at the centerline and one position

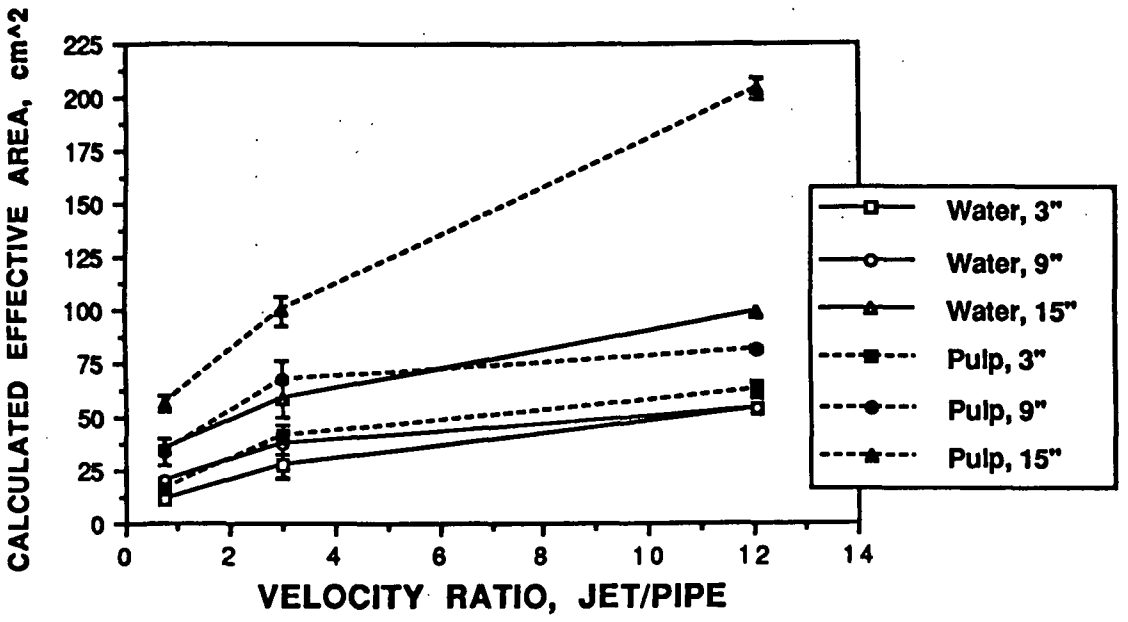

Figure 29. Calculated effective area versus the ratio of jet-to-pipeline velocities. Water and pulp flows at the three downstream positions are shown.

beyond the centerline, we could evaluate whether the magnitude of the conductivity was in fact highest at the centerline. The results from the horizontal probe data (that is, at a right angle to the injection port), some of which are shown in Figures 30 through 32, and others in Appendix XIV, suggest that the jet was probably not perfectly symmetric with the pipe centerline. We also see that the conductivity in most cases dropped at the centerline and increased at the probe position beyond the occurring at the center beyond the lack of symmetry (perhaps swirling patterns upstream).

The Fourier transform and autocorrelation analysis with W.A.V.E. has been run through an automatic peak finding algorithm in LabCalc. The predominant frequency peak in most probe positions was the 60 Hz electronic noise signal.

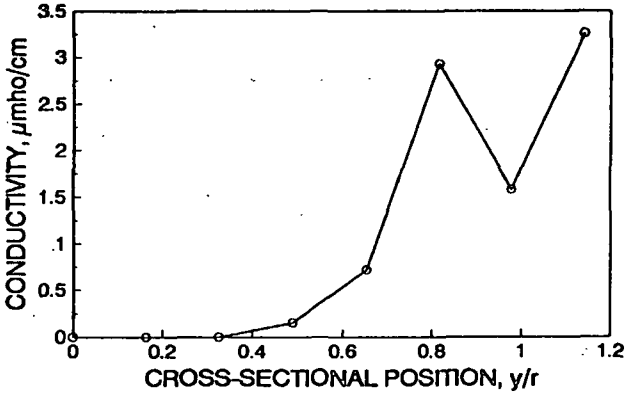

Figure 30. Horizontal probe data for water flow velocity condition A.

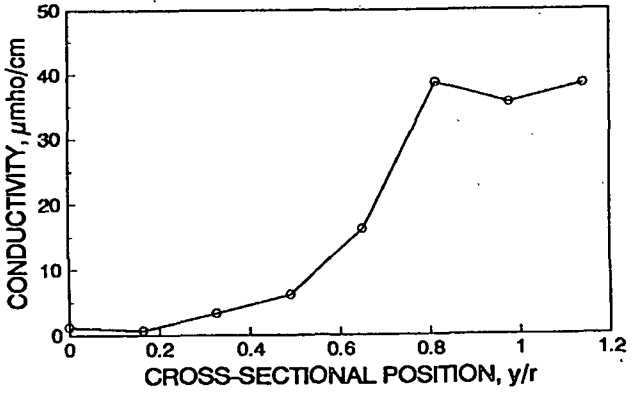

Figure 31. Horizontal probe data for pulp flow velocity condition E.

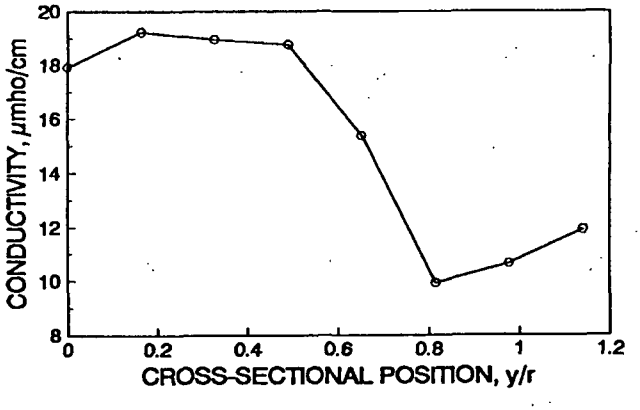

Figure 32. Horizontal probe data for pulp flow velocity condition I.

centerline. The reproducibility of this drop at the centerline suggests that something is

Another method for presenting the dispersion data compares the uniformity of the plume at the measured locations downstream with that of a perfectly dispersed condition. Rather than presenting an effective area exposed, this analysis compares the concentration in the exposed area to a perfect mixing condition concentration. Starting with a mass balance

$$c_j A_j u_j = c_p A_p u_p \qquad [37]$$

where c_p is the equilibrium concentration of the injected material if it were completely homogeneous, and A_p is the total cross-sectional area of the pipe, 47.695 cm^2. For 1, 2, and 3 #/T, the c_p parameter would be 53.87, 101.23, and 146.40 μmho/cm respectively. An average conductivity over the plume area can be calculated from

$$\bar{c} = \frac{1}{(b-a)} \int_a^b c(x)dx \qquad [38]$$

where a and b are shown in Figure 33.

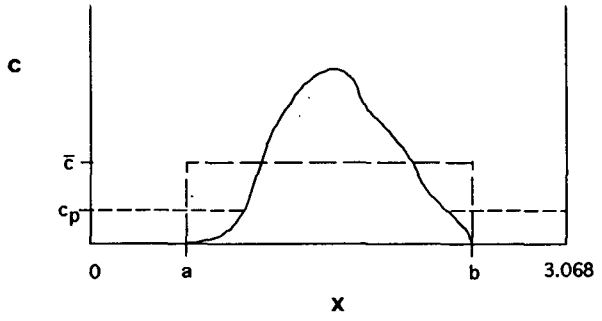

Figure 33. Typical conductivity profile from vertical probe data showing the parameters for calculating the average conductivity, and the conductivity for completely homogeneous mixing, c_p.

Table 6 shows the calculated average conductivity for the three downstream locations, for water and pulp flows, and for constant velocity ratio conditions; all the values shown in the table are for the 1 #/T dosage level. The values for the pulp case are much lower than for the water case. These results imply that mass transport in the tangential direction is much greater in the case of the pulp.[129]

Table 6. Average conductivities for water and pulp flows. Flow conditions A through D, velocity ratio = 0.75; E through H, velocity ratio = 3.0; I, velocity ratio = 12.0.

Velocity Ratio	Water			Pulp		
	1D	3D	5D	1D	3D	5D
0.7	158.7	117.4	65.0	128.5	69.3	41.8
3.0	81.1	61.9	39.0	56.3	34.8	24.6
12.0	42.0	42.1	24.8	33.4	30.1	12.8

FLOW LOOP ADSORPTION

Adsorption studies were performed on the flow loop injection configuration by reproducing the velocity conditions experienced in the dispersion experiments. Samples were drawn from the loop and taken to a DDJ to remove the long fiber and retained latex particles. The white water was examined for retention and EM.

Initially, an RPM setting of 750 was used to drain the long fiber from the DDJ. This was found to give very low gravimetric retentions. A 300 RPM setting was chosen for further studies. The EM data surprisingly did not show any significant differences in

average or standard deviation of distribution for constant polymer dosage levels. Figures 34 and 35 show that velocity conditions A, D, E, H, and I of constant dosage, 1 #/T, have no statistical differences within the standard deviations of eight replicates; likewise, conditions K and J, 2 #/T addition, and L and M, at 3 #/T, are invariant. The retention data also did not show a significant difference between mixing conditions as Figure 36 illustrates.

The values obtained for EM and retention are well in line with those obtained for similar dosages from the DDJ experiments; the standard deviations of the data are larger, which is understandable given the upscale to the pilot-scale flow loop. The values for the blank, or untreated, latex EM did not fall within expected values when compared with DDJ and Zetasizer experiments. Flow loop experiments gave an untreated latex EM of -4.0 μmho/cm, while DDJ and Zetasizer experiments gave -6.1 μmho/cm. The latex was from a

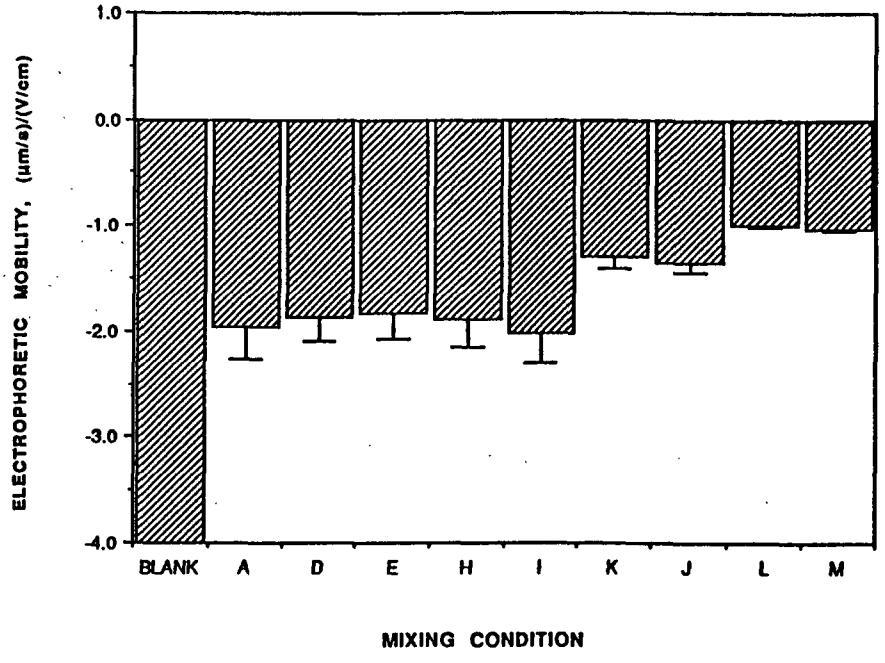

Figure 34. Electrophoretic mobility distribution average versus flow loop mixing condition.

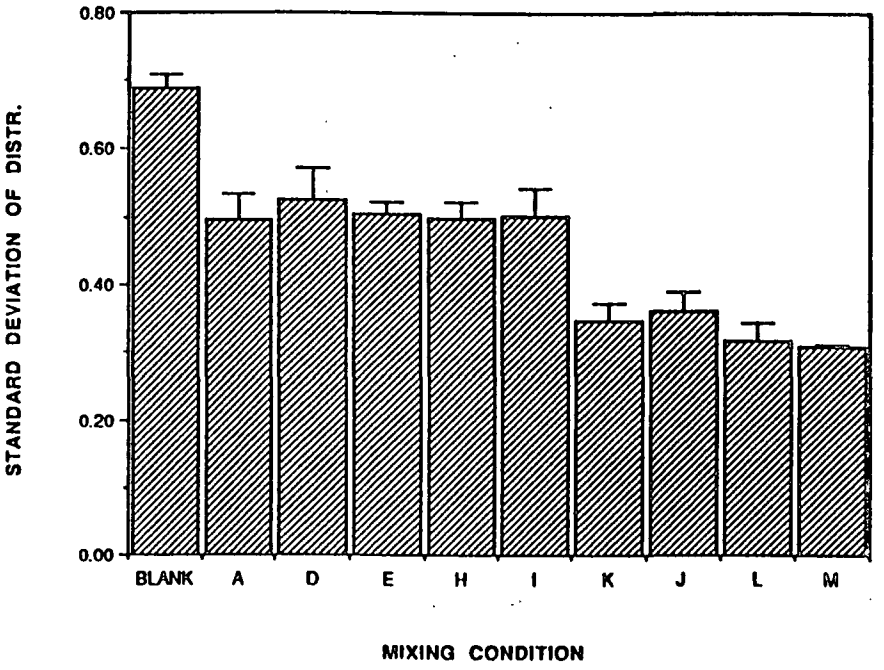

Figure 35. Electrophoretic mobility standard deviation of distribution versus flow loop mixing condition.

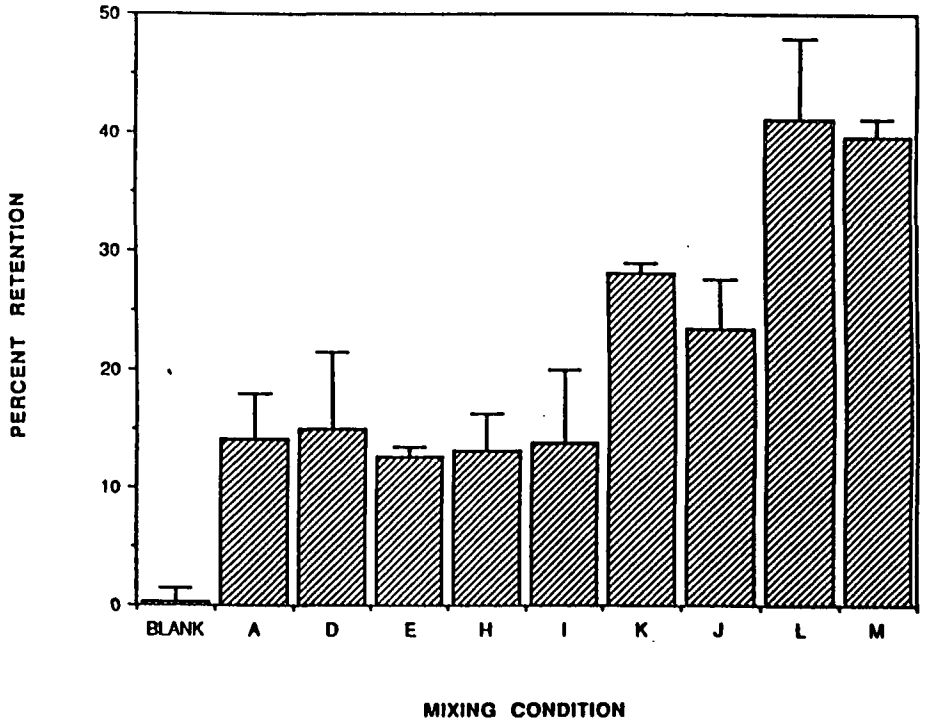

Figure 36. Gravimetric retention results versus flow loop mixing condition.

consistent source, and the same fiber was present for both flow loop and DDJ experiments. The Zetasizer operation was consistent with normal operation as determined by a standard latex measurement prior to each set of experiments. The same background electrolyte was used for each Zetasizer EM measurement. The water used during the experiment however was different; in flow loop experiments city water was used, while 0.01 M KCl solutions made from distilled water was used for all laboratory experiments. One possibility for the less negative EM results from flow loop untreated latex would be the presence of multivalent ions, such as Ca^{++}, which would have adsorbed onto the particle surfaces. The surface would become more positive and the multivalent ions would not be displaced by the Potasium ions. This is one feasible explanation for these results.

These findings, together with the early DDJ work, suggested that the mixing conditions in the pipeline, however altered by the velocity ratio, did not have an influence on the adsorption characteristics. One conclusion that was made at this point was that adsorption was determined by either the port itself and the initial introduction into the pipe, or that the adsorption occurred many pipe diameters downstream and was not influenced by the initial cone size. Another way of stating this is that the rate of reaction was fast, defined by the jet prior to deviations in cone size caused by velocity conditions, or that the rate was slow and equilibrium was eventually reached downstream subsequent to the dispersion differences.

Table 7 presents the half-height width data for the 1D data set. These data suggest that the plume width is independent of the injection port size and the velocity conditions. Thus, we conclude that the majority of plume shape deviations caused by velocity conditions 2occurred after one diameter downstream of the jet, which corresponds to residence times

Table 7. Calculated half-height widths of the 1D conductivity data from on-line probe measurements. Note the values vary between 1.7 and 2.3, independent of flow conditions or pipeline medium.

Data Set	Half-height width, cm	Data Set	Half-height width, cm
JL13A_W	2.13	JL16F_W	1.91
JL27A	2.10	JL16G_W	1.83
AU8A	2.29	JL18H_W	1.83
JL3B_W	1.73	AU4H	1.78
JL14B_W	2.03	AU12H	1.85
JL18B_W	2.29	JL20I_W	2.24
JL15C_W	2.18	AU8I	2.11
JL6D_W	2.03	AU21I	2.03
JL15D_W	2.03	S27K	2.13
JL27D	2.24	S27J	2.11
JL16E_W	2.11	S27L	2.24
AU3E	1.78	S27M	2.24
AU14E	1.65		

greater than 0.017 seconds for 15 fps flow rates and 0.083 seconds for 3 fps flow rates. This point is further evaluated in the Discussion Section below.

Several questions were raised by the DDJ and flow loop experiments involving adsorption kinetics and the role of turbulent mixing conditions. Further work at discovering the aspects governing adsorption criteria were proposed: 1. A mixing junction into the

Zetasizer EM cell would indicate an adsorption rate under in-line conditions similar to those of the flow loop configuration, and 2. More extensive DDJ experiments over a more broad range of mixing levels would further substantiate our findings on homogeneity of adsorption.

ADSORPTION KINETICS

Dual injection of cationic polymer and latex into the Zetasizer was discovered by Lang[59] to be a useful experiment for examining equilibration of EM. It may be speculated that this measurement is tracking the rate of adsorption to approximately an equilibrium state. The objective of these experiments was to determine the time to reach an equilibrium EM over a concentration range appropriate for Zetasizer operation. The first stage of these experiments examined the influence of concentration of latex, at constant latex-to-polymer concentration ratio, on the EM and distribution. Six latex concentrations at 1 #/T cationic PAM addition were chosen. The manual mode commands facilitated measurement at three-second intervals.

Single injections of untreated latex during manual mode three-second measurements showed that an equilibrium EM and standard deviation of EM distribution were obtained at the first measurement, at three seconds, and throughout the 60-second time period. Figures 37 and 38 give the results of such an experiment as the EM stabilizes at -6.33 (μm/s)/(V/cm) with a standard deviation of the EM distribution of 0.83 (μm/s)/(V/cm) with some fluctuation about these lines. These lines became stable after some experimentation uncovered that antivibration material under the syringe platform would decrease the fluctuations and narrow

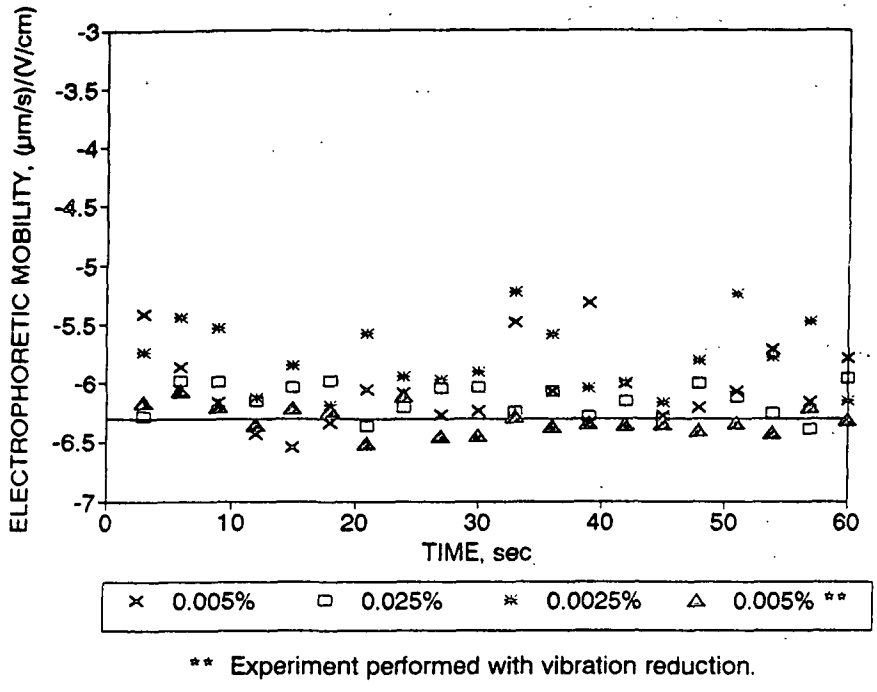

Figure 37. Electrophoretic mobility distribution average versus time for a manual mode three-second interval measurement on the Morton Thiokol latex.

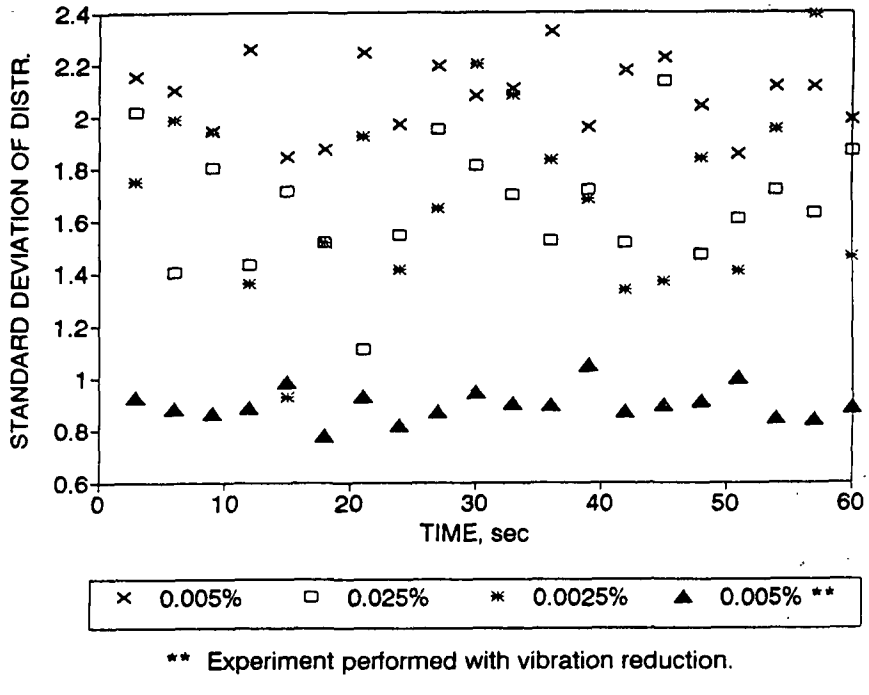

Figure 38. Electrophoretic mobility standard deviation of the distribution versus time for a manual mode three-second interval measurement on the Morton Thiokol latex.

The values for the electrophoretic mobility of the Morton Thiokol latex changed from -6.10 to -6.33 μmho/cm for experiments conducted in Appleton and experiments conducted later for the thesis in Atlanta. Since the standard latex values did not change over this period of time, we may attribute the shift to a change in the Morton Thiokol latex character. As to the reason for such a change, one possibility is that while drawing samples from the original latex drum for transport to Atlanta, it was noted that some solids had settled. One would expect that the least negative particles would have preferentially settled leaving the more negative particles remaining in colloidal solution.

The six latex concentrations studied were 0.05, 0.025, 0.01, 0.005, 0.001, and 0.0005 percent. The 0.0005 percent level was found to decrease in EM magnitude so slowly that 10-minute experiments were conducted with 30-second measurement times. For each concentration, the experiments were replicated 10 times, and the averages of each experiment are given in Figure 39. The results suggest a strong dependency of EM equilibration rate on concentration. The distribution was also influenced by concentration as given in Figure 40; each concentration had a standard deviation of distribution of about 1.6 to 1.8 at the three-second data point. The lowest concentration maintained a more broad distribution throughout the 60 second measurement, but the distributions for each concentration narrowed after the three-second measurement point. The highest concentration resulted in the most narrow equilibrium distribution. This would suggest a more homogeneous adsorption state for the high concentration mixing conditions.

The data points shown in Figures 39 and 40 are averages of 10 replicates of each of the five concentrations. Experimental error is introduced to the procedure by the inaccuracies in matching a one pound per ton dosage. The multiple dilutions necessary for

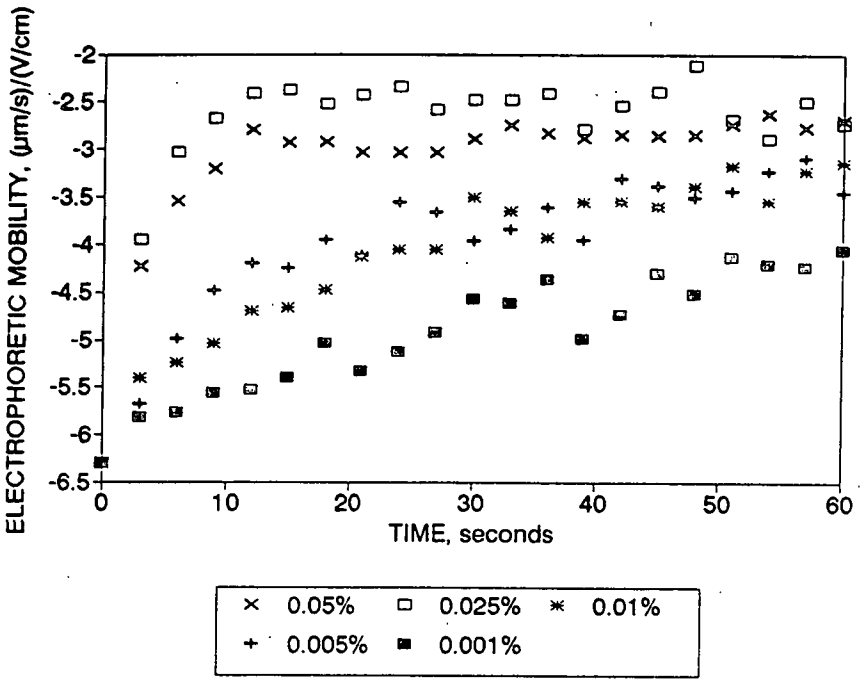

Figure 39. Electrophoretic mobility distribution average versus time for five separate latex concentrations.

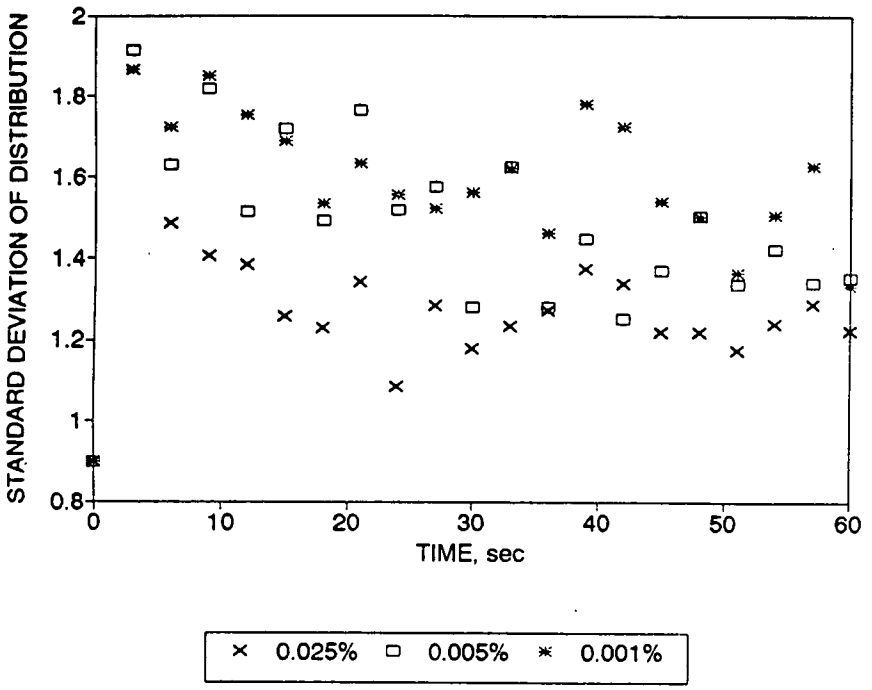

Figure 40. Electrophoretic mobility standard deviation of the distribution versus time for three latex concentrations.

these low concentrations of latex and retention aid make it difficult to know the dosage exactly. This error results in a different equilibration line for each replicate. If we drew standard deviation bars on the five concentration curves in Figure 39, we would find that they overlap. However, a trend is evident with concentration. Figure 41 shows that the high, intermediate, and low concentration curves are quite different in slope.

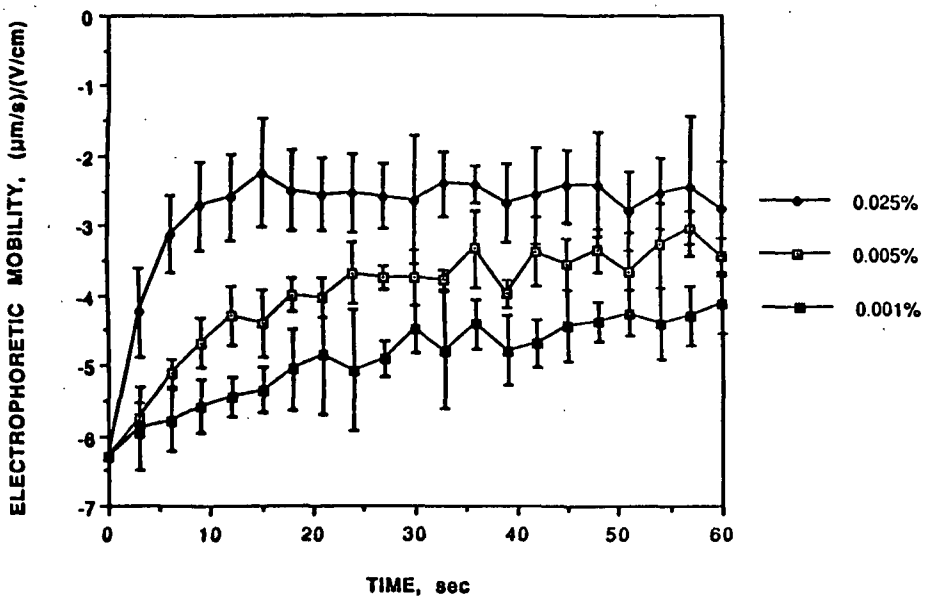

Figure 41. Electrophoretic mobility versus time for three different latex concentrations showing the standard deviation bars from ten replicates.

The question of what these EM equilibration experiments were measuring is a point for discussion. We may propose that we are measuring the approach to an equilibrium adsorption state; the alternative would be a conformational change analogous to the work performed by Wågberg. However, there is no reason to believe that there should be a concentration dependency to achieve an equilibrium conformation at these dosage levels. Also, some work by Lang[59] on buffered dual injections, where pH adjustment should cause

conformation changes, found that these changes occurred within the first three-second measurement point. Thus, we strongly believe that equilibration rates are measuring the approach to an adsorption equilibration. The significance of these findings warranted closer examination of the findings; thus, further experimentation with alternative Y-junction mixing conditions was proposed.

First, some rigorous kinetics analysis revealed more about the concentration relationship to equilibration rates. A Savitzky-Golay[130] first derivative regression smoothing was performed (discussed in Appendix XI) on the five data sets in Figure 39. The initial slope of the EM versus time curve was plotted versus initial latex concentration in order to fit the equation

$$\ln\left[\frac{dEM}{dt}\right]_0 = \ln k' + n \ln C_0 \qquad [39]$$

By fitting this line with the data sets, an R^2 of 0.92 was found with the rate constant, k, equal to 860 and the slope, n, or the reaction order, equal to 1.2. This result seemed to agree with those of Dijt et al.[57] and would bear further study with alternative Y-junction conditions.

A different mixing condition, created by changing the Reynolds number at the Y-junction, would be expected to result in a different rate constant with a similar reaction order. Further experiments were proposed to examine a smaller Y-junction, with fluid injected at the same volumetric rate, and a third mixing reactor consisting of an in-line static mixer. Calculations of the latex flow line into the Y-junction gave Reynolds numbers for 10cc injected over three seconds of 3×10^3 and 9×10^3 for the large (shown in Figure 21)

and small Y-junctions, respectively. A static mixer placed in an identical large Y-junction just past the joint was made of 1/16 inch diameter stainless steel bearings made into a packed bed one inch in length. These three mixing conditions were studied for their influence on rate to EM equilibrium and distribution. Five latex concentrations, again at 1 #/T PAM dosage, were studied: 0.1, 0.025, 0.005, 0.001, and 0.0005 percent latex, for the three mixing Y's, with 10 replicates each (the low level, 0.0005% was again only tested at 30-second measurement times for 10 minutes).

The results of these mixing/concentration experiments are given in Figures 42 through 51. The three mixing junctions resulted in similar EM curves; however, the static mixer consistently gave a higher initial slope, as seen by the three- and six-second data points giving a less negative EM. The standard deviations of these points, averaged from 10 replicates, slightly overlap those from the other mixing chambers; however, the result is consistent through five concentrations. The distributions were also strikingly different; the high Reynolds number and static mixer conditions resulted in more narrow distributions than that of the low Reynolds number condition. We also see that by going from the high to low concentrations the magnitude of the distribution standard deviation decreases (from Figures 43, 45, 47, 49, and 51). This supports the earlier findings given in Figure 40.

Another way of representing this data would be to plot the three-second data point for the four concentrations and three mixing junctions as given in Figure 52. The concentration and mixing condition interact to give a higher initial reaction slope and more homogeneous distributions; this result supports a collision theory in which available particles and turbulent mixing play key roles.

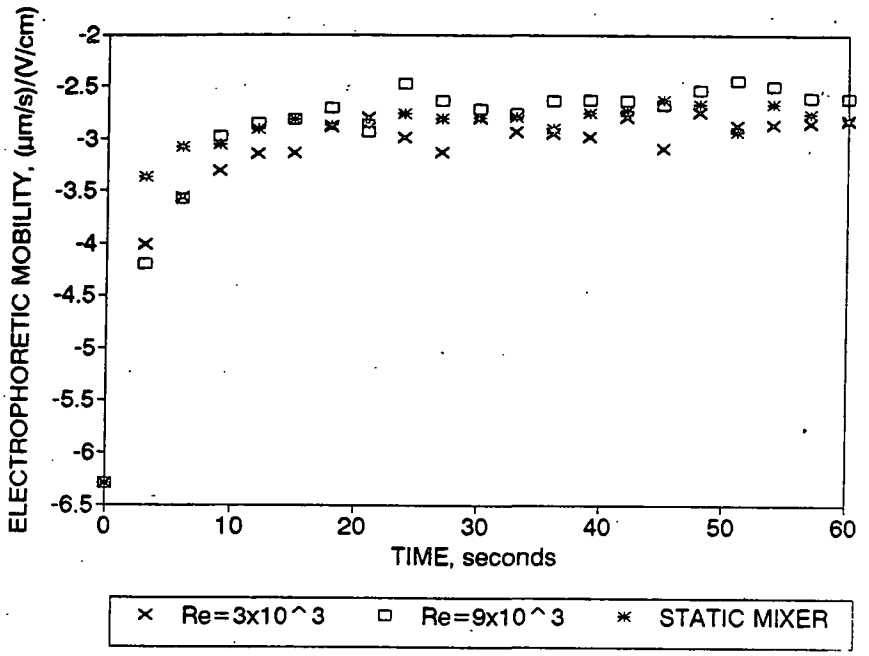

Figure 42. Electrophoretic mobility distribution average for latex concentration 0.1 percent for three mixing conditions.

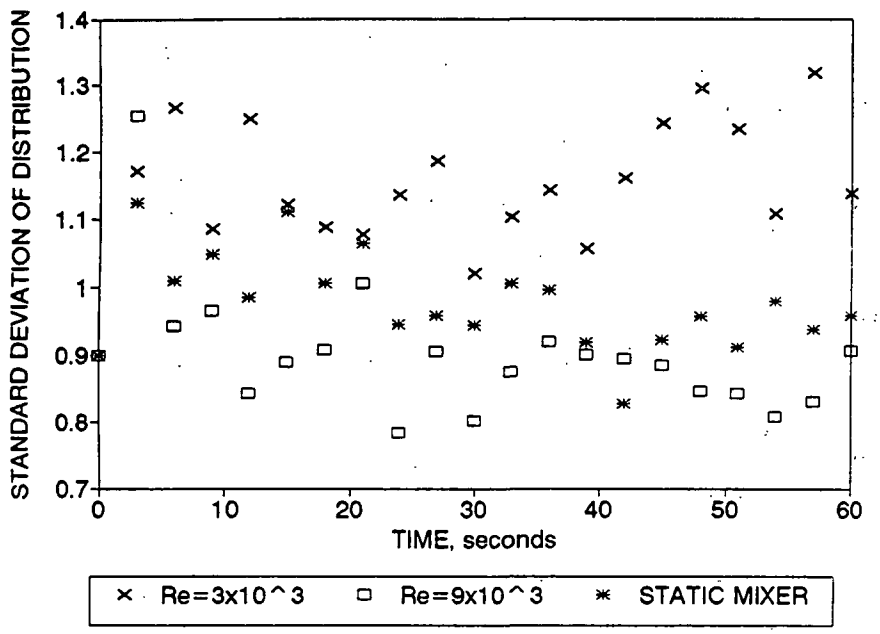

Figure 43. Electrophoretic mobility standard deviation of distribution for latex concentration 0.1 percent for three mixing conditions.

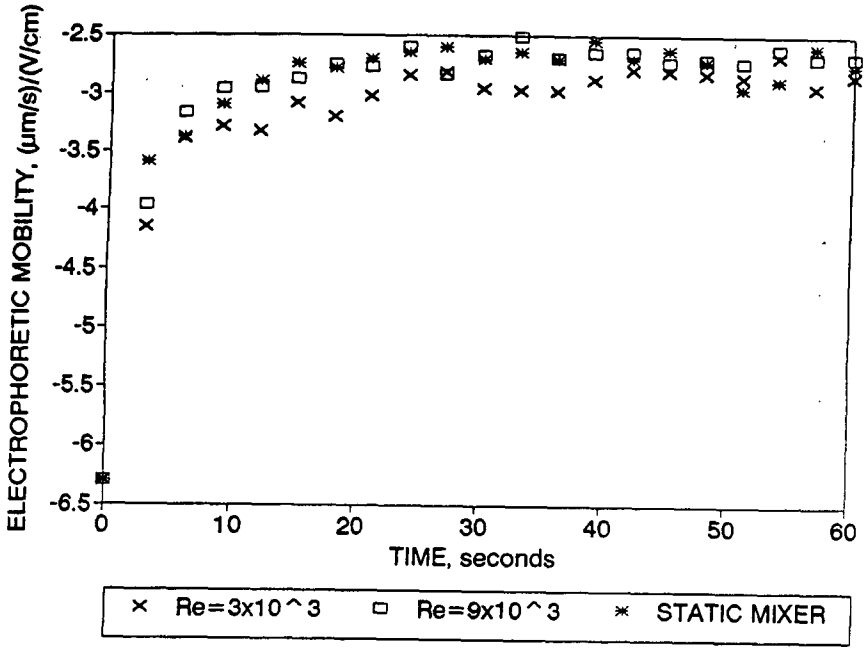

Figure 44. Electrophoretic mobility distribution average for latex concentration 0.025 percent for three mixing conditions.

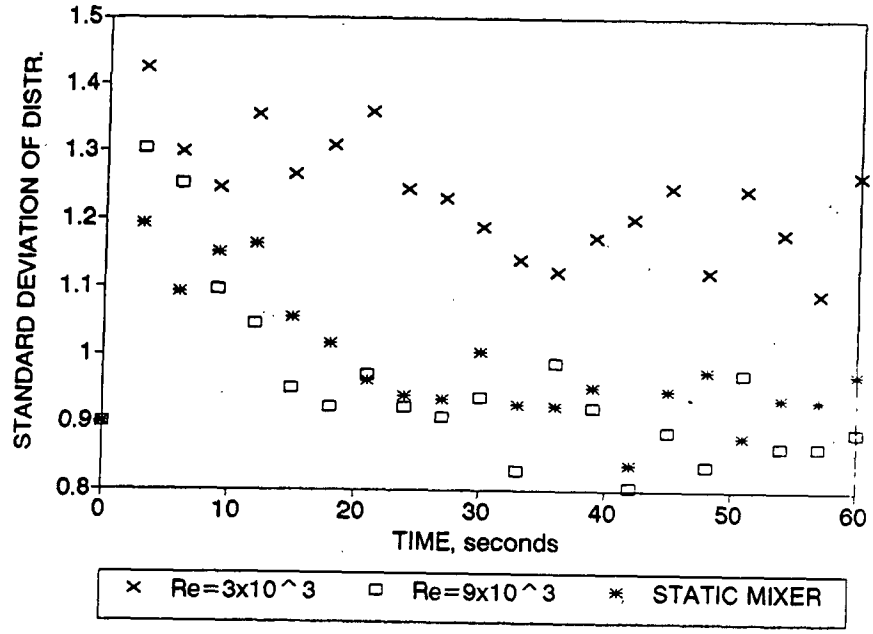

Figure 45. Electrophoretic mobility standard deviation of distribution for latex concentration 0.025 percent for three mixing conditions.

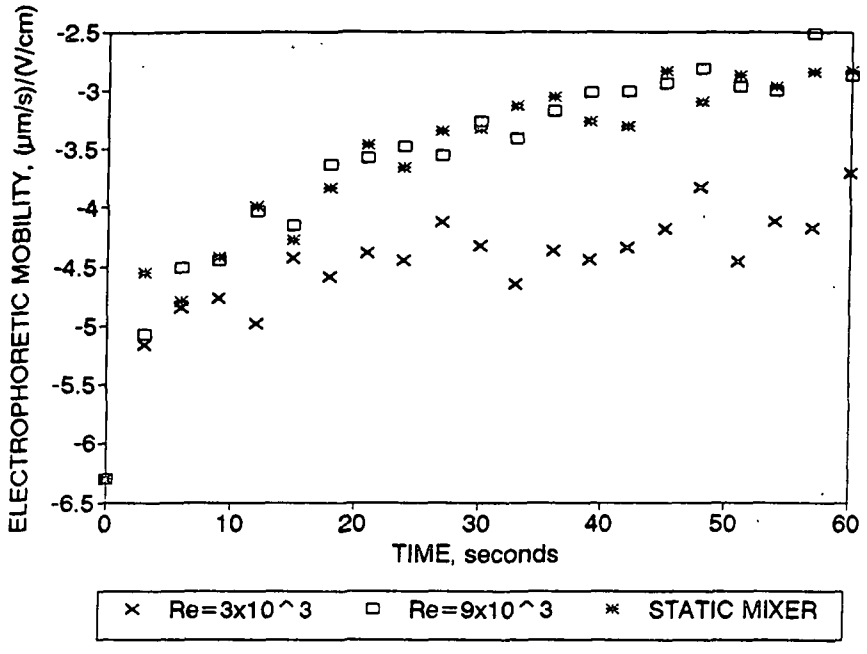

Figure 46. Electrophoretic mobility distribution average for latex concentration 0.005 percent for three mixing conditions.

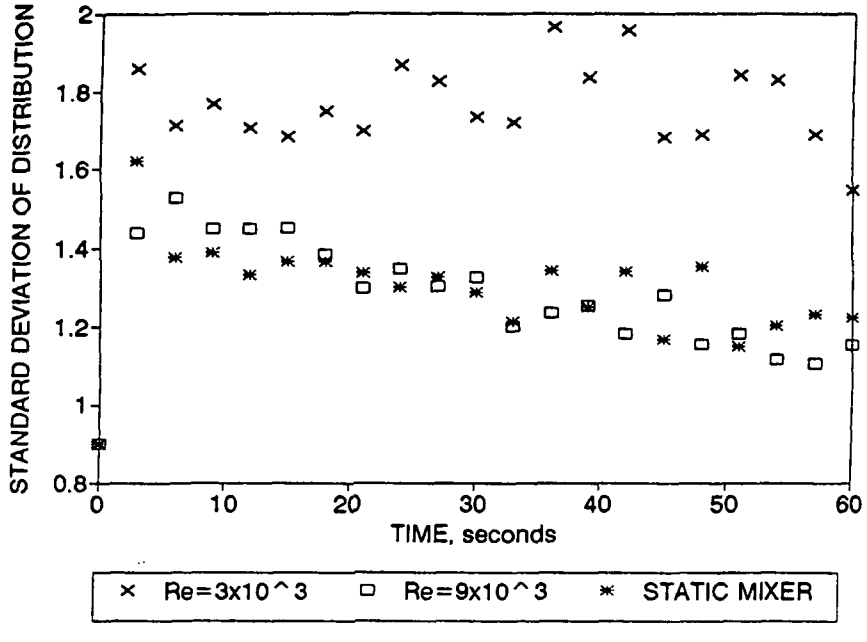

Figure 47. Electrophoretic mobility standard deviation of distribution for latex concentration 0.005 percent for three mixing conditions.

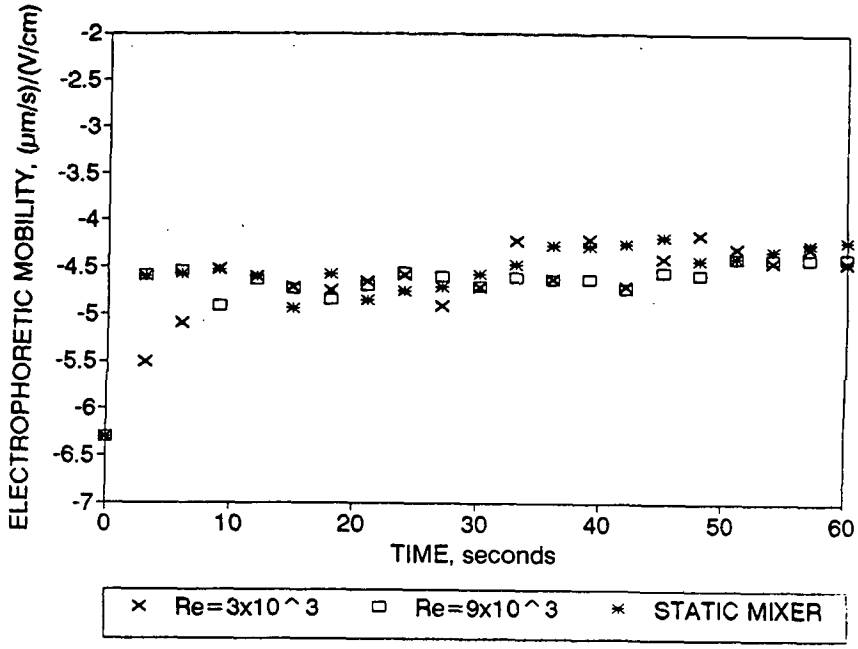

Figure 48. Electrophoretic mobility distribution average for latex concentration 0.001 percent for three mixing conditions.

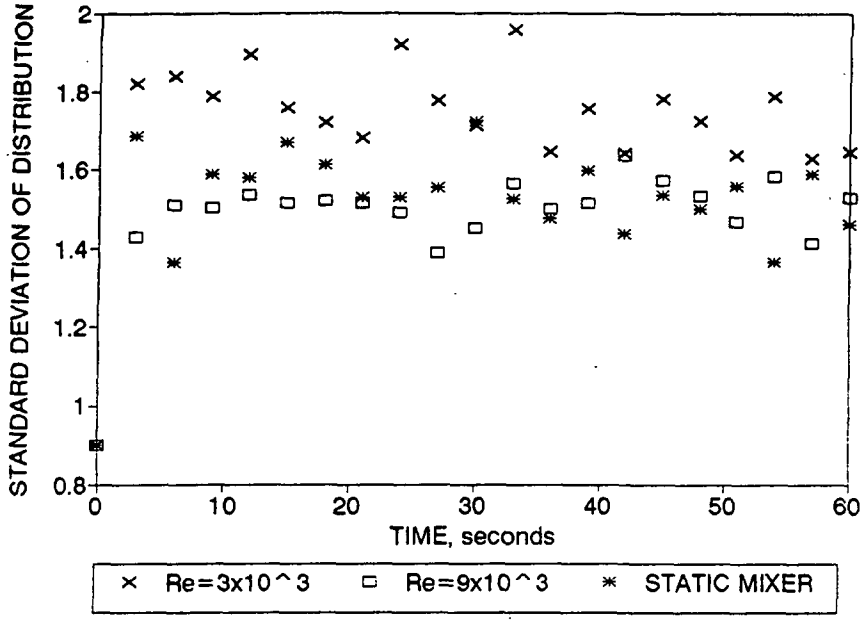

Figure 49. Electrophoretic mobility standard deviation of distribution for latex concentration 0.001 percent for three mixing conditions.

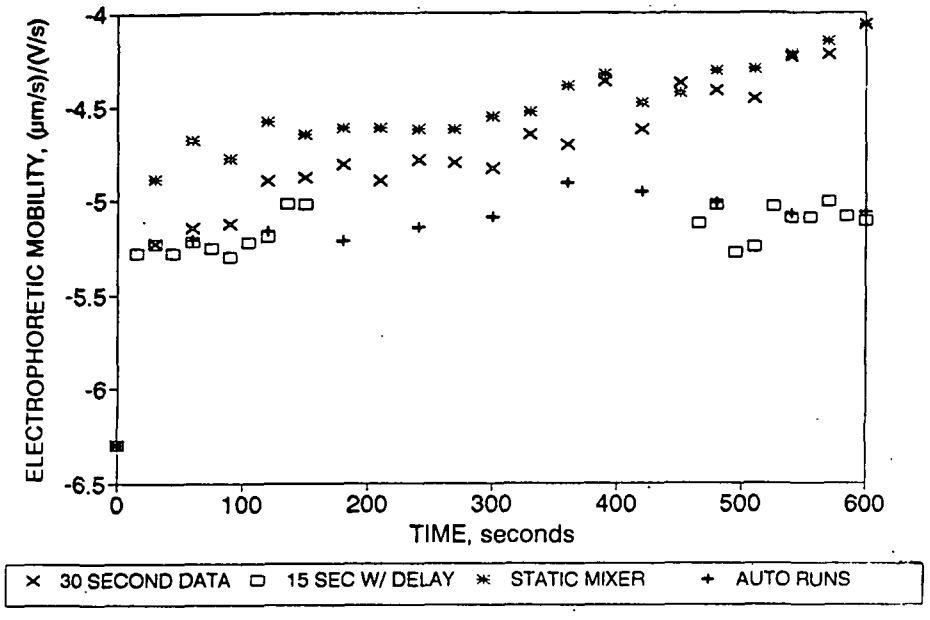

Figure 50. Electrophoretic mobility distribution average for latex concentration 0.0005 percent for three mixing conditions.

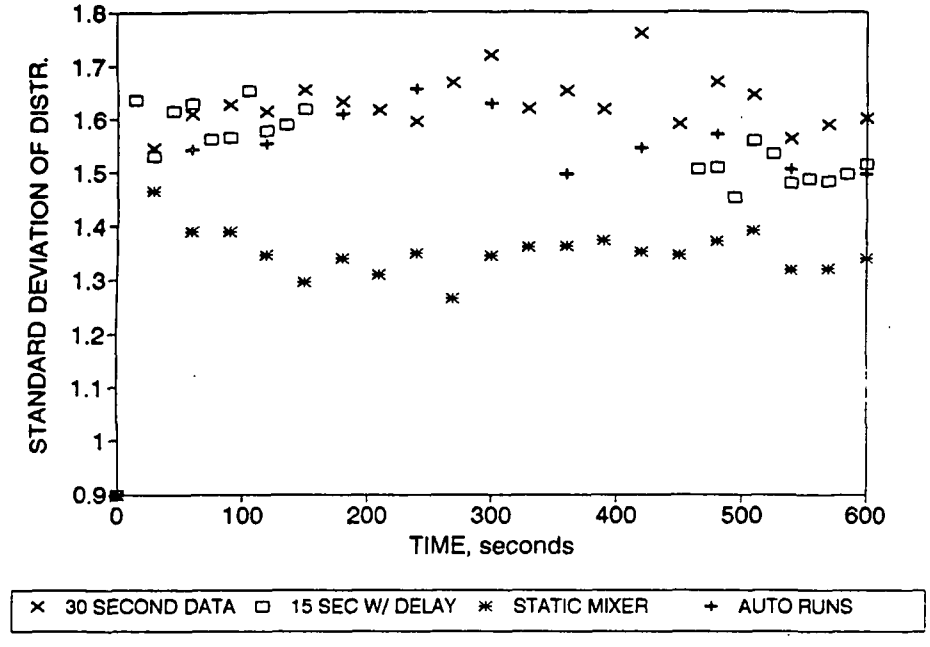

Figure 51. Electrophoretic mobility standard deviation of distribution for latex concentration 0.0005 percent for three mixing conditions.

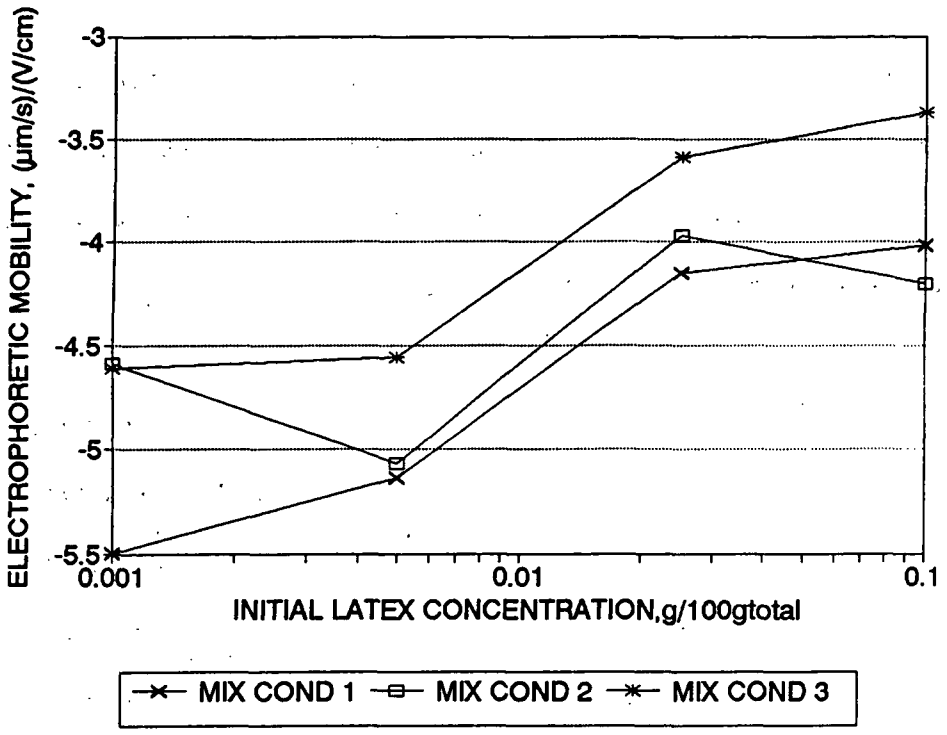

Figure 52. Electrophoretic mobility data taken at three seconds after dual-syringe injection versus concentration for three Y-junction configurations.

Figures 50 and 51 represent the lowest concentration measured, 0.0005 percent. The rate of change of EM was so low that a 10-minute experiment was performed on the low Reynolds number Y-junction (30-second data set) and with a static mixer junction. The static mixer gave a higher initial change and a more narrow EM distribution.

This slow rate of collision within the cell to reach an equilibrium EM enabled the study of the collision efficiency during cell voltage-induced movement. Two experiments were designed using the low Reynolds number injection rate: 1. Ten 15-second measurements were taken sequentially (150 seconds total run time); the cell voltage was then turned off for five minutes; the cell voltage was turned on for a measurement sequence of 10 every 15 seconds (the manual mode commands are outlined in Appendix V). The results

shown in Figures 50 and 51 are an average of 10 replicates. 2. A dual syringe injection was performed with the cell voltage off; at a predetermined time, chosen randomly, the cell voltage was turned on, and an automatic mode, 30-second measurement, was made. The data shown are an average of five measurements.

The results illustrate the effect of collisions during the electrophoretic mobility (EM) measurement. The initial slopes, given a constant mixing chamber, are reproducible regardless of the measuring technique. The subsequent slope, however, is dependent on the EM-induced collisions generated by the cell voltage. An interesting visual observation was made during the experiments using the large and small Y-junctions. For the low Reynolds number condition (the large Y-junction), the flow was observed to be near-laminar in the Y-junction. The cloudy-white latex solution did not mix with the clear polymer solution prior to entering the Zetasizer cell body.

Savitzky-Golay first derivative regressions were performed on the data sets in Figures 42 through 49. The results are presented in Figure 53 and Table 8. The high concentration data points were omitted from the regression to determine the kinetic parameters. The decision to omit these points was based on the nonlinearity of the curves when included and the problems with the Zetasizer operation when this concentration was measured (described above). We believe this is a reasonable decision. The curves for the three mixing conditions were similar in slope, with a higher rate constant for the high Reynolds number condition.

DYNAMIC DRAINAGE JAR EXPERIMENTS -- PHASE II

The final phase of experiments examined four RPM settings during polymer addition

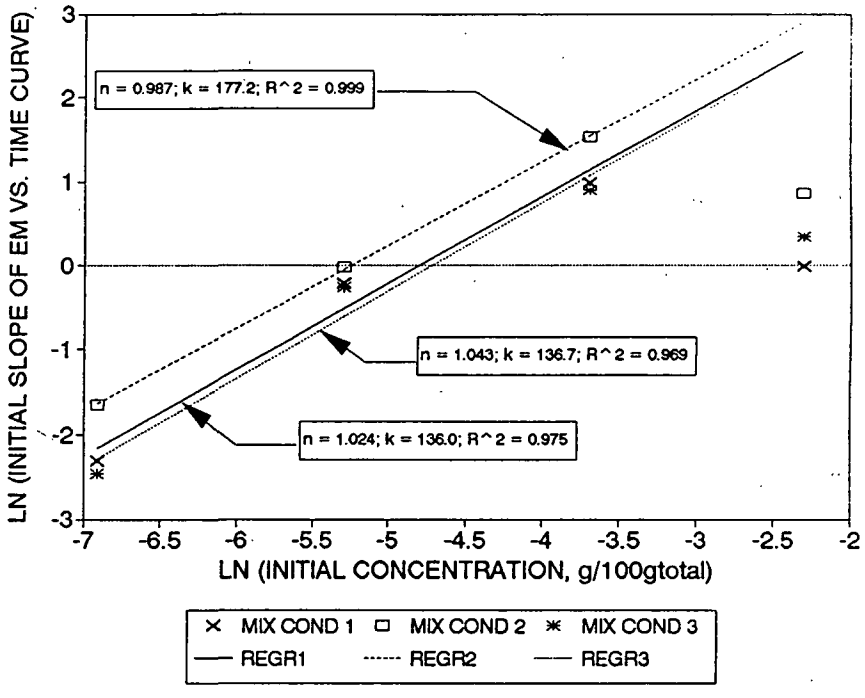

Figure 53. Determination of adsorption kinetics for three mixing conditions: initial slope of the EM versus time curve versus the initial latex concentration. Mixing conditions are defined as follows in Table 8.

Table 8. Definitions for mixing conditions described in this section and in Figure 53 giving parameters for curve regressions.

	Characteristics of Mixing	Reaction Order, n	Adsorption rate constant, k	Regression Coefficient, R^2
Mixing Condition 1	Re = 3×10^3	1.024	136.0	0.975
Mixing Condition 2	Re = 9×10^3	1.043	136.7	0.969
Mixing Condition 3	Static mixer in-line; larger size Y-junction used for Condition 1	0.987	177.2	0.999

to a DDJ; polymer dosages of 0, 1, and 2 #/T were used. The EM results, given in Figure 54, were independent of the addition mixing condition. The dosage results follow those found in earlier experiments. The distributions were influenced by the mixing conditions as seen in Figure 55. The standard deviations of these values were substantial; however, for both the 1 and 2 #/T dosage levels, we found a downward trend -- a more narrow distribution with higher levels of mixing.

Gravimetric retention results, in Figure 56, show an optimum retention was achieved at relatively low mixing levels. A regression curve (R^2 = 0.991) drawn through the 2 #/T dosage level data gives a maximum at 512 RPM. Thus, a certain level of inhomogeneous adsorption resulted in a higher retention than the relatively more uniform adsorption of the high RPM condition.

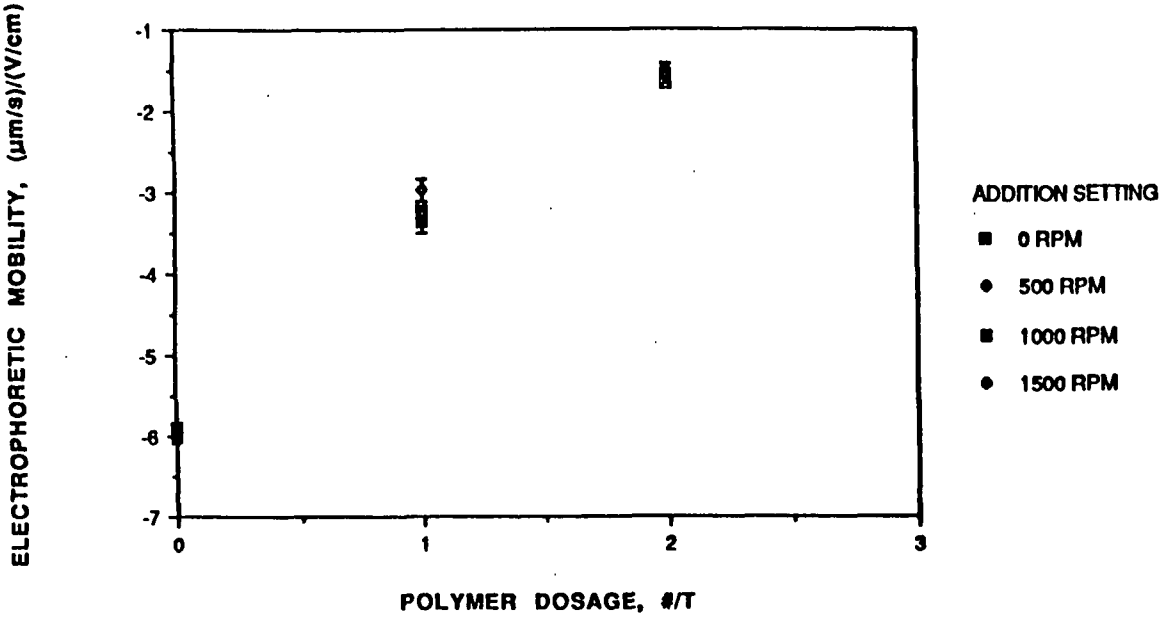

Figure 54. Electrophoretic mobility distribution average versus retention aid dosage for four dynamic drainage jar settings during the addition.

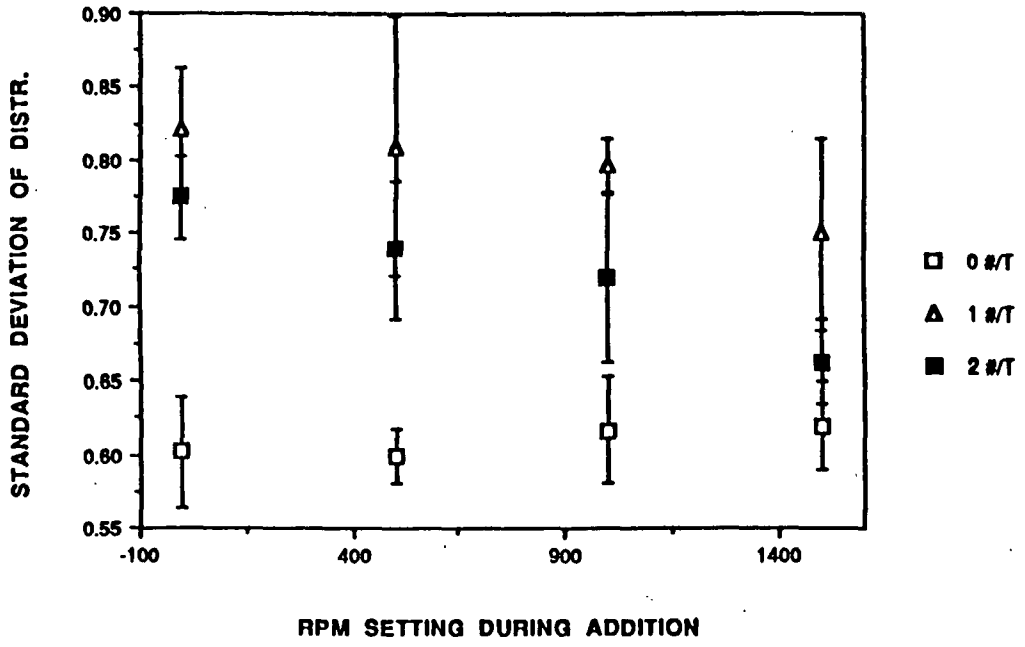

Figure 55. Standard deviation of the electrophoretic mobility distribution versus the dynamic drainage jar mixer setting during the addition for three retention aid dosages.

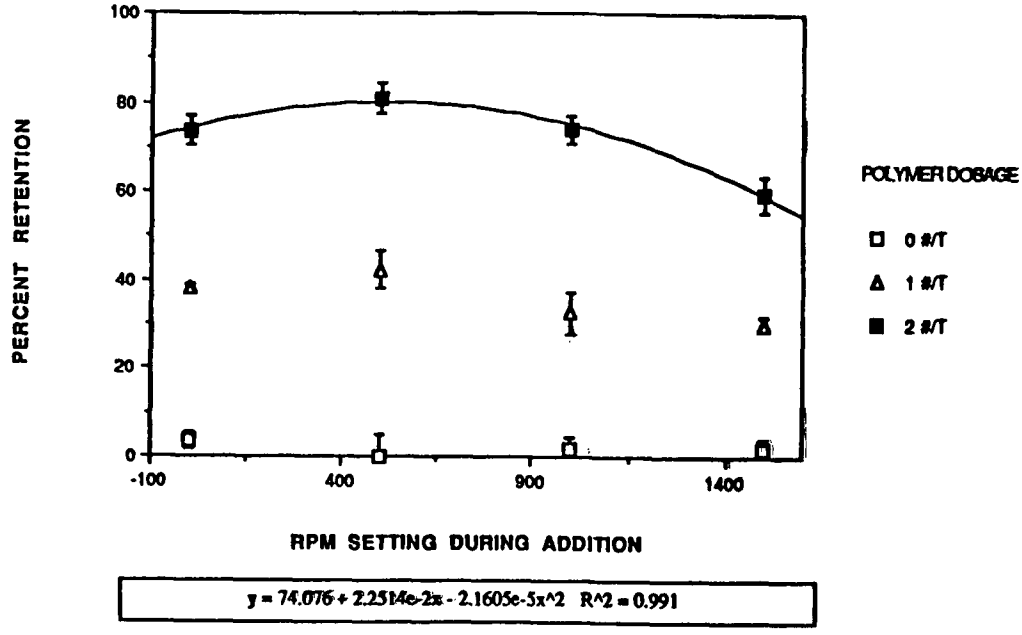

Figure 56. Percent retention as determined by gravimetric measurement versus dynamic drainage jar mixer setting during the addition for three retention aid dosages.

DISCUSSION OF RESULTS

We will divide the discussion into two segments: first, the jet dispersion and the significance of the results for pulp suspension flows and, secondly, the polymer adsorption studies with the resultant homogeneity and particle retention.

PIPELINE/JET DISPERSION

Unfortunately, the experiments of this study were not designed with fiber-turbulence interactions in mind, but were designed to study polymer adsorption as a function of mixing conditions. As a result, when we apply the results to fundamental issues of turbulent flow, the data and experimental techniques can only be taken as preliminary. Further work using more appropriate techniques and better instrumentation would be recommended.

In addition to the small data set, several complications exist in the experiments which limit their value. For example, the probe was intrusive, though equally so in both water and pulp. Mass transfer may also have been affected by the polymer in the injected jet as well as the turbulent structure of the pipe flow, as the polymer itself is a drag-reducing material at high Reynolds number. However, the effect of the polymer in the injection jet on the main pipe flow is expected to be essentially the same for both the water and pulp suspension flows. We have shown that the time for significant polymer adsorption to occur onto the fibers and thus be removed from the solution is much longer than the dwell time within the test section where conductivity measurements were made. Times to reach a state of 50 percent of equilibrium adsorption (plateau EM) were shown to be a minimum of one second, or three feet (12 pipe diameters) downstream from the injection. As a result, even if the polymer were affecting the turbulence, we do not expect polymer adsorption onto the furnish

to cause a significant difference in the suspension flow compared to the pure water flow.

The observation of higher turbulent dispersion in the fibrous suspension than in pure water seems counterintuitive for a drag-reducing flow. Drag reduction implies a decrease in turbulent momentum transfer, and a decrease in momentum transfer intuitively has been linked to a decrease in mass transfer. However, the literature, and this work, have raised several questions on the validity of this assumption. As mentioned above, the historical work of Bobkowicz and Gauvin[99] showed that radial dispersion in a turbulent pipe flow significantly increased in the presence of nylon fibers. There seemed to be no dependence on fiber diameter or length alone, but only on the aspect ratio, l/d. Subsequently, this work received criticism as being inconsistent with generally accepted beliefs of fiber turbulence damping. Possible reasons reported were that the flow was not fully turbulent and that there may have been particle interference with the sensing probe. We find no such grounds for criticism; the flow conditions were probably turbulent given the reported parameters and the evidence of dispersion. Also, particle interference does not explain a larger dispersion area measured by the thermistor probe.

Examination of velocity has often been used to deduce information about the turbulent mechanisms of a flow. Based on examinations of velocity profiles, others have concluded that the mechanisms of turbulence production in fiber suspensions are the same as those in Newtonian fluids. However, the results of Park et al.[110] discussed above show that examination of the longitudinal velocity profile alone may not reveal important changes in the turbulent structure. In their flow, the longitudinal turbulent velocity profile was virtually identical to that observed in Newtonian fluids, but the turbulence structure, and hence the mechanisms of turbulent production, showed significant changes.

Although some of the mechanisms of particle turbulence interactions in gas flows will differ from fiber-turbulence interactions in liquid flows, the interesting finding from the gas flow studies of Gore and Crowe[108] and Liljegren and Vlachos[112] is that particles can simultaneously cause drag reduction while inducing an increase in turbulent activity in the core of the pipe flow.

Based on the reviewed studies, the effect of particles on turbulence structure appears to be complex and not presently understood. Many authors have assumed that drag reduction in fiber suspensions is due to damping of turbulence, but this does not coincide with the experimental data. We have presented evidence of an altered turbulence structure by the observation that increased turbulent dispersion and decreased momentum transfer can occur simultaneously when fibers are added to a turbulent water flow. For drag reduction to occur, Reynolds stresses must be decreased; however, this need not require damping of turbulence, but rather a decoupling of the radial and longitudinal velocity fluctuations. How fibers might induce this decoupling has yet to be explained as much further work is required to validate these findings. Experimental data with a discussion of recent pertinent literature is presented which raises questions about the intuitive understanding of turbulent suspension flows. The primary thrust of this project, however, has involved the polymer adsorption during these different mixing conditions. Therefore, the main thrust of this discussion section will involve the adsorption findings we have presented in the Results Section.

POLYMER ADSORPTION

We will begin by summarizing the results from the different experimental phases. The initial Dynamic Drainage Jar (DDJ) experiments suggested that the level of mixing during polymer addition influenced the homogeneity of the resultant adsorption: the more

uniform adsorption resulted from the higher mixing level. The final electrophoretic mobility (EM), however, was not affected by the level of mixing. We found the same results in the final phase of DDJ experiments.

The flow loop conductivity data suggest that we were able to create different jet trajectories by adjusting the ratio of jet-to-pipeline velocities. The work of Sroka and Forney[123] have suggested altering the trajectory in order to optimize mixing efficiency: a delayed reaction rate, beyond 15 pipe diameters downstream, would be optimized by a near field trajectory which geometrically centers the injected jet along the pipe axis at some distance downstream; an intermediate reaction rate, between three and 15 pipe diameters downstream, would be optimized by setting near field geometry parameters to minimize the second moment at the desired far field location; and a faster reaction rate, occurring within three pipe diameters of injection, would be optimized by an impingement flow against the opposite wall. The flow loop experiments were capable of simulating each of these types of injection flow conditions.

The adsorption results showed that there were no differences in characteristics between the different flow loop mixing conditions. The data followed a characteristic polymer dosage curve; however, no significant differences were observed for EM nor adsorption homogeneity. Due to these results, we undertook an examination of adsorption kinetics under similar mixing conditions.

The Zetasizer IIC manual mode of operation allowed for a unique experimental opportunity. Initial findings suggested a strong dependency on adsorbent and adsorbate concentrations. By changing the latex concentration and maintaining a constant polymer

dosage, a first-order reaction was determined. The homogeneity of the adsorption during the reaction was discovered by examining the standard deviation of the distributions over the three-second interval data. A degree of homogeneity is defined by the standard deviation value. Three seconds after the introduction of untreated latex to the adsorbing polymer the EM distribution was broad. Beyond this point we see that the distribution becomes either more narrow or remains broad. The final state distribution width is dependent on the initial concentrations: the higher concentration resolves to a final, more narrow EM distribution, analogous to the distribution found when a higher level of mixing was used in DDJ experiments. Thus, a collision theory based on availability of particles (concentration) and level of shear (DDJ mixer setting or Y-junction Reynolds number) is supported.

Further work with the reaction kinetics examined three levels of mixing during the injection into the EM cell. Similar concentration-dependent results were obtained: a direct relationship was observed for the initial adsorption slope and for the initial and final adsorption homogeneity, with the initial latex particle concentration. The higher particle concentration yielded a higher initial adsorption rate, a broad intermediate adsorption condition, and a more narrow final condition. A low latex concentration resulted in a lower initial adsorption rate, a more broad intermediate adsorption condition, and a broad final condition.

The effect of the mixing condition played a role in the final state homogeneity. The higher mixing levels equated to a higher degree of homogeneity. A higher initial slope was obtained for the higher level of mixing; the lower level of mixing resulted in a more heterogeneous adsorption state throughout the time period measured (refer to Figures 43, 45, 47, and 49). An intermediate state characterized by a more broad EM distribution was

observed. We represent this intermediate state in Figures 57 and 58. A "good mixing condition" would represent a situation where particle or adsorbate concentration allowed for efficient collisions or a situation in which the level of mixing increased the collision efficiency. Either good mixing or poor mixing conditions would result in an intermediate relatively more broad distribution. We saw in some cases, such as 0.1 and 0.025 percent latex concentration with a high Reynolds number or in-line static mixer, that the final state distribution was comparable in width to that of untreated latex. A "poor mixing condition" represented in Figure 58 would maintain a broad distribution or heterogeneous adsorption state for its final state condition.

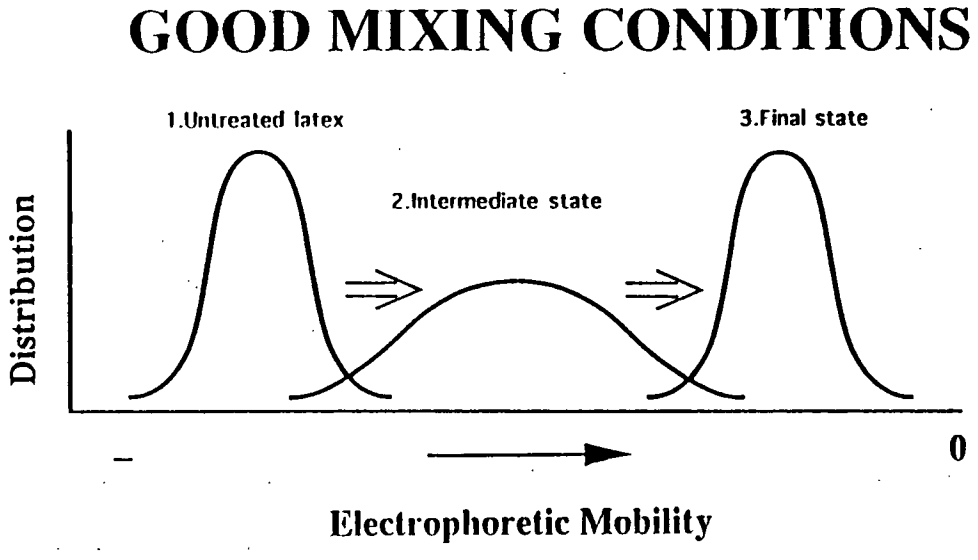

Figure 57. A representation of electrophoretic mobility distribution during adsorption of cationic material for a good mixing condition or a high particle/polymer concentration condition.

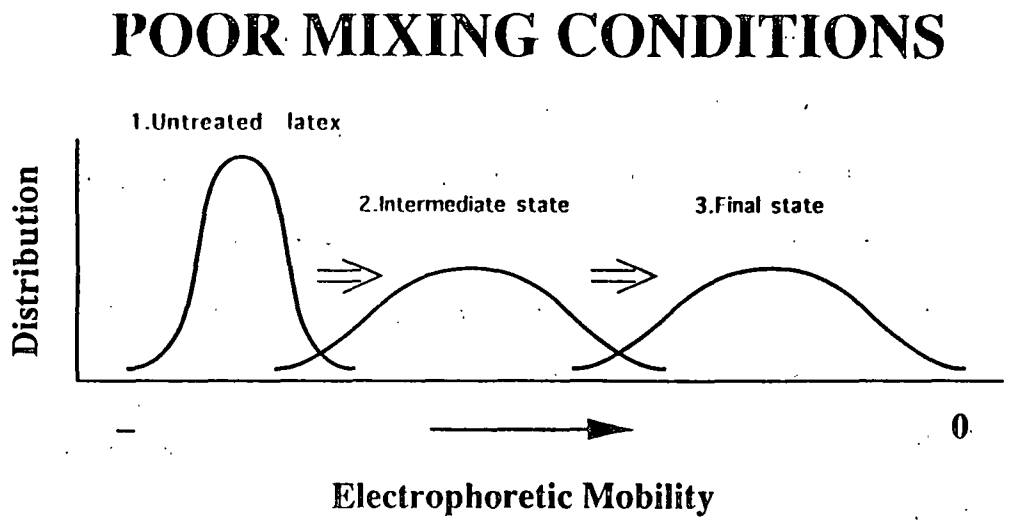

Figure 58. A representation of electrophoretic mobility distribution during adsorption of cationic material for a poor mixing condition or a low particle/polymer concentration condition.

Going from left to right in Figures 57 and 58, from the initial untreated state to a less negative EM after adsorption, we obtain a more broad intermediate distribution. The width of the intermediate distribution is also dependent on the level of mixing and the concentration, although it was always found to be more broad than the width of the untreated distribution. The reason for this more broad intermediate distribution may be explained by looking at a simplified, ideal case of spheres and polymer coils represented in Figure 59. The initial introduction of the coils to the spheres will result in a particular distribution dependent on the level of mixing. Further adsorption will be dependent on the presence of previously adsorbed polymer. A completely heterogeneous condition represented in Figure 59(b), Intermediate State, will result in a slightly more homogeneous situation as time progresses following the remainder of adsorption, as shown in Figure 59(b), Final State. The condition in Figure 59(a), Intermediate State, will become homogeneous following

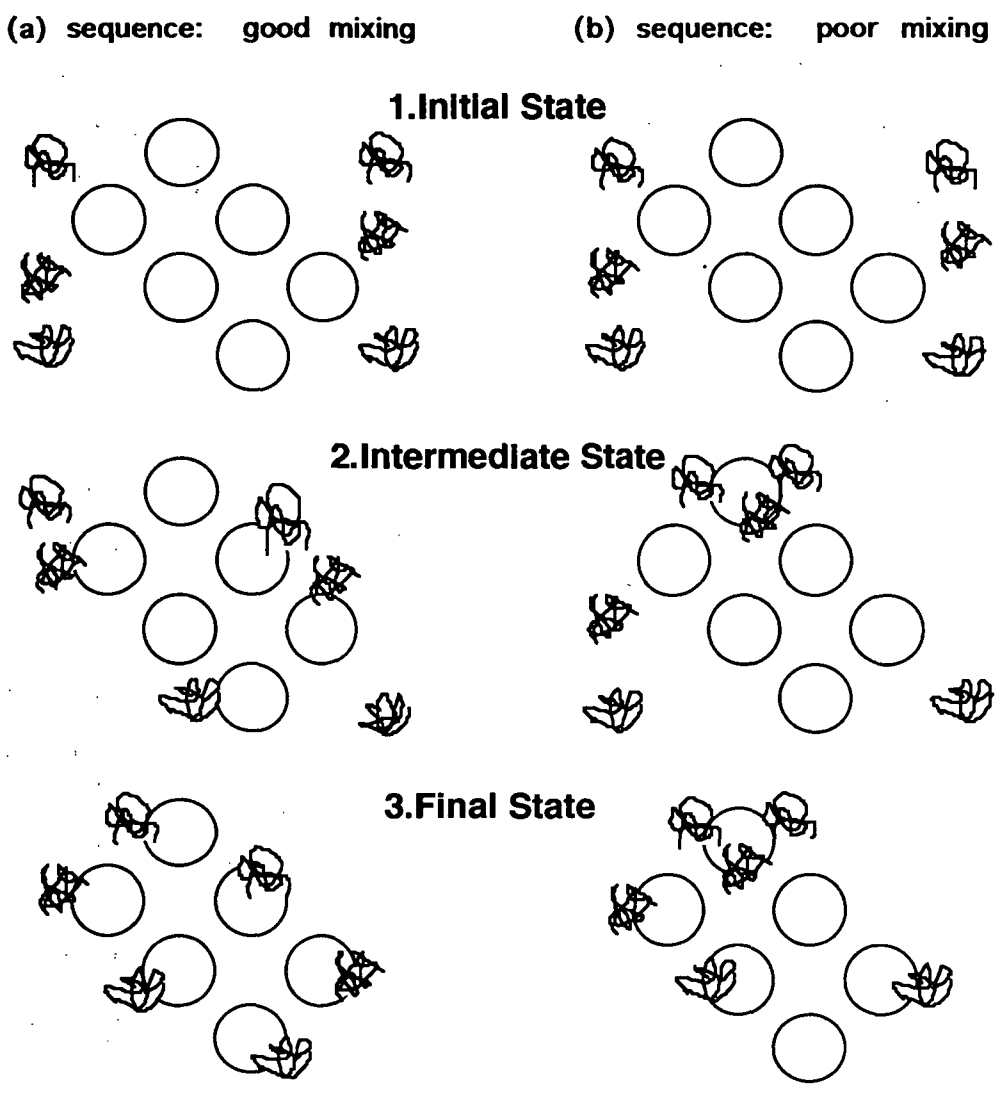

Figure 59. A simplified case representing the differences between extreme homogeneity and heterogeneity with the possible intermediate steps involved in each case.

complete adsorption, as shown in Figure 59(a), Final State.

We have not yet discussed the reasons why we did not detect differences in adsorption for the flow loop mixing conditions. An initial estimation would be that either the adsorption defining homogeneity occurred too quickly for deviations in the flow to create adsorption

differences, or that adsorption occurred too slowly for near field conditions to alter adsorption criteria. The flow loop conditions have been characterized as being significantly different at probe locations between 1D and 5D. The EM adsorption kinetic experiments have shown that, for the concentration of latex we used in the flow loop experiments, the adsorption continues to a plateau region in approximately nine to 11 seconds. For our flow loop condition, this would mean that adsorption continues downstream from 30 to 150 feet (for 3 and 15 fps flow rates) from the injection port. In many cases adsorption occurred well beyond the test section and within the sampling jar. From the kinetic work performed with the Zetasizer, the initial introduction of polymer should have influenced the final adsorption homogeneity state. The Reynolds number of the injection condition played a role in this adsorption criteria. For the low Reynolds number condition, the flow could be observed to be laminar within the Y-junction. This laminar condition during the initial introduction created an inhomogeneous state which persisted through the course of the experiment.

The downstream turbulence in the pipeline should not have affected the adsorption homogeneity. Figures 50 and 51 show that the charge electrodes in the electrophoresis cell create collisions. When the cell voltage was turned off, the collisions did not occur; however, the adsorption homogeneity was not affected. The initial introduction of cationic polymer and anionic spheres, as defined by the tube Reynolds number or the presence of a static mixer, defined the homogeneity (as seen by the static mixer and low Reynolds number data sets in Figure 51).

If in fact the mixing conditions were different during the initial state of adsorption, which should determine the final state of adsorption, we would see differences in the final state. Since we do not see differences in the final state of adsorption for the flow loop

experiments, we may consider that the initial adsorption, analogous to that which occurred in the Y-junction of the Zetasizer, occurred prior to deviations in the flow pattern with different velocity ratios. As the jet enters the pipeline flow, we see that the trajectory is bent at different locations in the cross section dependent on the momentum ratio of jet-to-pipe flow. The initial introduction, however, was defined by the single-port injection. Within one pipe diameter of the injection, the jet is not exposed to significantly different volumes of the pipe cross section due to trajectory considerations. The single port defined the initial and final adsorption homogeneity. Since the jet geometry was not significantly different within the first pipe diameter (0.0167 to 0.0833 seconds depending on the velocity), the homogeneity was significantly altered.

One indication that the flow conditions within one pipe diameter of the injection were not altered by the velocity ratio comes from the conductivity data presented above. If one assumes that the plume cross section is round from the injection port to 1D, calculating the half-height width from the data at 1D gives an indication of the exposure of the pipeline to the injected material at this short distance. Table 7 shows the half-height width values calculated from the conductivity data. These data suggest that the exposure within 1D of the injection port is independent of the port size and the velocity conditions. We have discussed above how the assumption of a round profile at 1D is inaccurate. However, one can visualize that the differences between the plume shapes within 1D are insignificant in affecting the adsorption. Within 1D the total volume of the pipeline exposed to the plume is approximately 3 percent (estimating the plume to be a cone segment 2 cm in diameter at the base, approximately 11.3 cm^2, and comparing it to pipeline volume from the port to 1D, 363.4 cm^2). The variations in this volumetric exposure are probably insignificant in affecting the adsorption.

We may say then that this discussion is the most significant finding from this research: that the adsorption continues to an equilibrium plateau, beyond 10 seconds after introduction, but the initial introduction mixing conditions define the adsorption homogeneity. A simplified model has been presented in Figures 57 and 58 to represent extreme cases of homogeneity and heterogeneity. We use this model to explain the adsorption characteristics which have been discovered by the various experimental techniques used in this research. Different mixing conditions during the initial introduction resulted in different states of adsorption homogeneity at constant average electrophoretic mobility.

CONCLUSIONS

The significant conclusions from this project are:

1. Polyelectrolyte adsorption uniformity has been quantified by electrophoretic mobility (EM) standard deviation data.

2. Laboratory mixing conditions have been found to alter the homogeneity of the EM distribution. The higher shear condition resulted in a more narrow distribution.

3. Polyelectrolyte adsorption kinetic experiments have quantified the rate of adsorption to be dependent on mixing condition and concentration of polymer and surface at constant polymer dosage. The higher Reynolds number condition and the higher concentration resulted in more uniform EM distribution.

4. Polymer adsorption homogeneity was not altered by the flow loop mixing conditions. Y-junction kinetic experiments have shown that the mixing in the junction affected the initial rate of adsorption and homogeneity and the equilibrium homogeneity. Therefore, it is suggested that the flow loop conditions, which created insignificant differences in the exposed volume in the first few pipe diameters downstream from the injection, were defined by the single-port injection.

5. An intermediate EM distribution was relatively more broad than the equilibrium distribution. The width of this distribution was dependent on the initial mixing conditions due to the homogeneity of the adsorption during the high adsorption rate step. During the

depletion step, characterized by decreasing rate of EM change, the polymer will more likely continue to adsorb based on collisions. The initial adsorption homogeneity, however, controlled the subsequent equilibrium homogeneity.

The significant finding from this thesis has been the quantification of adsorption homogeneity as determined by mixing conditions for several addition conditions. For some time workers have speculated that uniform mixing will result in homogeneous adsorption. One method which was developed in this project measured the electrophoretic mobility distribution with time during an adsorption process. The average electrophoretic mobility results support work which had been reported previously on the kinetics of polyelectrolyte adsorption. This thesis has presented unique data on the adsorption homogeneity which has shown that the mixing conditions, during cationic polyelectrolyte addition to an anionic particle solution, play a role in the uniformity of the adsorption.

SPECULATIONS ON SIGNIFICANCE OF RESULTS

Many techniques are used for introducing polyelectrolytes to adsorbent material. In the paper industry, dyes, coagulants, and flocculants are added to the papermaking furnish by such techniques as pipeline injection, pump inlet, mixing chest inlet, or quiescent tank dumping. Seldom is it considered whether the mixing condition during the addition has an effect on the product quality or uniformity. Multiport rings and internal wands have recently been introduced to enhance pipeline introduction of flocculants. But what is the effect of uniformity of mixing on the retention efficiency and end product uniformity?

A conclusion from this project has been that the higher level of mixing resulted in the most uniform adsorption. If one visualizes a uniform adsorption state, this condition would probably result in the most uniform flocculation state, both in the size of the flocced particles and in the number of particles per floc. This would be due to the adsorption state determining the mass distribution of flocculated material. A condition of nonuniform adsorption would result in a heterogeneous flocculation state. The formation of the sheet, or the distribution of floc sizes throughout the sheet, would be diminished.

A personal recount I witnessed at a mill emphasizes this point. A coagulant and clay were added in close proximity into a quiescent chest of papermaking furnish. It was shown that the resultant base sheet had a negative opacity response to retained ash. Clay-clay interfaces rather than clay-fiber interfaces were created by the poor addition conditions and resulted in an inefficient use of raw materials. The clay was being coagulated prior to being distributed throughout the furnish. The same can be said for pipeline injections; in many instances, a single side-port injection is used to introduce an adsorbing material. Yet are we

aware of the adsorption rate or the velocity ratio?

Parameters other than mixing conditions have been found to affect adsorption kinetics, such as hydrodynamic size of the particles and polymer molecule, polymer and particle concentration, and the magnitude of electrostatic forces. In these experiments, the adsorption time to reach a plateau level took never less than seven to 10 seconds. Yet, in many cases, a papermaking additive is not given this time to reach an adsorption equilibrium before the paper machine forming section. We must ask, what is the magnitude of effect on adsorption rate for these other parameters? And, if adsorption rate cannot be affected substantially by these parameters, how do we better utilize wet-end additives to allow equilibration to occur?

Many other pieces of information must be discovered before the entire picture of polymer adsorption, retention efficiency, and sheet formation is well understood. If a directed purpose of a manufacturing operation is to reduce system variation, then there are several things which can be accomplished by looking at individual unit process variations. This project has hopefully shed light on one cause of possibly substantial variation and inefficiency.

SUGGESTIONS FOR FUTURE RESEARCH

Considerable fundamental work in the area of adsorption kinetics and the role of mixing remains to be performed in order to comprehend the mechanics of polymer addition and optimization. The factors which are known to influence the rate of adsorption should be studied independently. A thorough evaluation of the result of perikinetic and orthokinetic collision conditions would be a considerable contribution especially when viewed in light of the valuable theoretical works of Gregory.

In order to make acceptable applications to the papermaking system, emphasis should be concentrated on the colloidal aspects and the chemistry of component interaction. We must realize that the fines and filler materials control the adsorption, subsequent retention, and wet web consolidation properties of the system; the parameters affecting these components should be elaborated upon. Also, since short contact times are prevalent from polymer addition to forming, the initial adsorption characteristics are truly of the most concern.

Further work with the Zetasizer, or similar instrument, may continue to elucidate the distribution of charge and the effect of polymer addition parameters. The techniques within this thesis will hopefully prove valuable for such endeavors.

ACKNOWLEDGEMENTS

I would like to thank the Institute of Paper Science and Technology (formerly The Institute of Paper Chemistry) and its member companies for providing the financial support to conduct this multidisciplinary research in a truly unique environment. I thank my Thesis Advisory Committee, comprised of Drs. Robert A. Stratton, Jeffrey D. Lindsay, and Frank M. Etzler. Their consistent guidance throughout the course of this thesis has made the endeavor both challenging and enjoyable. I would especially wish to acknowledge Dr. Stratton as counsel and friend. Bob's thoughtfulness as my A190 and thesis advisor has been far above the call of duty. Thank you Bob.

I thank Mead Corporation, Escanaba, Michigan, for donation of hardwood pulp to this thesis; also, Morton Thiokol Corporation, in particular, Dr. Morris Merchant and Mr. William Edwards for their generous donation of polystyrene latex. Appleton Papers Research thankfully allowed the use of their Leeds and Northrup particle size analysis device for latex size data.

Due to the fact that this project combined aspects of fluid mechanics and surface and colloid chemistry, there have been several people among the Institute staff who have greatly participated in its completion. Also, due to the Institute move from Appleton to Atlanta, the number of people who participated effectively doubled. I wish to thank all who assisted in some capacity. In particular, Bruce Andrews for operating the pilot paper machine, assisting in the design and initial operation of the flow loop system, and for sharing his vast engineering experience with anyone who would ask. Russ Tyler and the deceased Don Gilbert assisted greatly in the operation of the pilot paper machine as the pulp processing

procedure took four people working constantly. For this I am grateful. "DG", whose office was across the hall from mine in Appleton, is sorely missed.

Gerry Kloth, Paul Hannon, and Mike Kleiber helped to design the flow loop and computer data acquisition hardware. Data analysis was greatly assisted by Ted Jackson. Rodney Lane and Rich Mirabello put together the flow loop piping and electrical wiring. Marvin "Phat" Filz, Glen Winkler, and Paul Van Rossum built several items in the Appleton machine shop and offered endless advice on not only improved design, but also sexology, religion, and politics. Jack Hultman and Norm Colson assisted by offering their time and years of experience in the area of wet end chemistry. Walter Rantainen and Lynn Kroll measured quantitative fiber identification and fiber length analyses. Karen Vandenberg, Nancy Skifstad, Hart Phinney, and the entire library staff constantly assisted in photocopy services and library use. Gene Edwards, Lisa Juliani, Bob Davies, and Eric Podolski were consistently on hand for computer assistance. Other members of the faculty who offered encouragement, council, and expertise on this project - in particular Drs. Terrance Conners, Maclin Hall, Pierre Brodeur, Tom McDonough, Ron Dinus, and Mr. John Waterhouse - my sincere thanks. Finally, Angela Colar assisted greatly in the editorial analysis of this thesis. To all of these people and others who may have helped in the completion of this long and tortuous dissertation, may I offer my sincere thanks.

To my lovely wife and best friend Pam, who has steadfastly supported me in my endeavors and made life much more enjoyable, I thank you with all my heart. Your love has changed all my perspectives. Finally, to my parents Anna A. Luettgen and the deceased Dr. Andrew J. Luettgen, I dedicate this work. From the spiritually rich beginnings you offered, success will spawn. Papermaking in the family continues.

NOMENCLATURE

Symbols

a	- particle radius of curvature
A	- area
c	- molar concentration of electrolyte
c_j	- concentration of conductive material in jet stream
c_p	- concentration of conductive material in pipeline
C_1	- term to describe the three components of van der Waals forces
C_0	- initial concentration
d	- particle diameter
D	- diameter
e	- elementary charge
E	- applied potential
f	- fraction adsorbed (unless notes as a function of given variables)
f_p	- frequency of light pulses
G	- shear modulus
h	- annulus thickness
H	- Hamaker constant
ΔH	- head loss
k	- Boltzmann constant
k'	- rate constant
k_0	- specific conductance of the bulk electrolyte
k_1	- specific conductance of the particles
k_{12}	- rate constant
K	- apparent von Kármán constant
L	- pipe length
M	- resistance torque
M_W	- polymer molecular weight by intrinsic viscosity
n_i	- number of molecules (or particles) per unit volume
N_A	- Avagadro's number
N_0	- number of particles per unit volume
N_c	- particle number concentration
N_t	- particle concentration remaining at time, t
$N_{(turb)}$	- rate of coagulation resulting from turbulent agitation
$N_{(Br)}$	- rate of coagulation resulting from Brownian diffusion
N_{12}	- number of collisions between two particles per second per volume
P	- pressure
$\partial P/\partial \ell$	- longitudinal pressure gradient
r	- pipe radius
R	- cell radius
R_G	- polymer radius of gyration

NOMENCLATURE (Cont.)

s	- fringe spacing
t	- time
t_f	- characteristic flocculation time
t_A	- time to adsorb
T	- absolute temperature
u	- bulk fluid velocity
u_E	- electrophoretic mobility (EM)
u'	- longitudinal rms turbulent velocity component
U	- bulk pipeline velocity
v	- velocity
v'	- radial rms turbulent velocity component
V	- fluid velocity
V_{int}	- interaction energy
w'	- tangential rms turbulent velocity component
X	- position of zero electroosmotic flow
y	- distance from pipe wall

Dimensionless Groups

Re	- Reynolds number
ϕ	- friction factor
U^+	- reduced velocity
U^*	- reduced shear velocity
S^+	- dimensionless distance from the wall

Greek Symbols

α	- angle between incident laser beams
ß	- shear strain
γ	- shear rate
ϵ	- rate of turbulent energy dissipation per unit mass
ϵ_r	- dielectric constant
ϵ_o	- permittivity
ζ	- Zeta potential
η	- solution viscosity
κ	- inverse double-layer thickness
λ	- laser light wavelength
λ_L	- London retardation wavelength
Λ	- ratio of conductance terms in Henry equation for mobility
μ	- Newtonian fluid viscosity
ν	- kinematic viscosity

NOMENCLATURE (Cont.)

ρ	- density (charge density as in Eq. [8] and solution density as in Eq. [28]
σ	- collision efficiency factor
τ	- shear stress
$v_{E,}v$	- electrophoretic velocity, the velocity of surface relative to the stationary
ψ	- potential
ψ_o	- surface potential
ω	- angular velocity

Subscripts

a	- adsorption
A	- attractive
Br	- Brownian motion condition
d	- disruptive property
disp	- dispersive
eff	- effective
E	- electrophoresis
f	- fiber
F	- flocculation
int	- interaction
j	- jet
l	- latex
max	- maximum
o	- surface property
p	- pipeline
R	- repulsive
t	- at time, t
turb	- turbulent condition
w	- wall property
0	- initial condition, or bulk property

Abbreviations

A/D	- analog to digital converter
DDJ	- dynamic drainage jar
DMDAAC	- dimethyldiallylammonium chloride
EM	- electrophoretic mobility
ID	- pipe inner diameter
IPC	- The Institute of Paper Chemistry, 1929-1989, Appleton, Wisconsin
IPST	- Institute of Paper Science and Technology, Inc., 1989-, Atlanta, Georgia
LDA	- laser Doppler anemometry

NOMENCLATURE (Cont.)

LDV	- laser Doppler velocimeter
MT	- Morton Thiokol
PAM	- polyacrylamide
PEI	- polyethylemimine
PID	- proportional-integral-derivative
rms	- root-mean-square
%C	- percent consistency, or g solids per 100 g total

LITERATURE CITED

1. Gouy, G. J. Phys. 9(4):457(1910); Ann. Phys. 7(9):129(1917), as referenced in Adamson (22).

2. Chapman, D. L. Phil. Mag. 25(6):475(1913), as referenced in Adamson (22).

3. Stern, O. Z. Elektrochem 30:508(1924), as referenced in Adamson (22).

4. Overbeek, J. Th. G. Electrochemistry of the Double Layer, in Colloid Science, Vol 1, ed. by H. R. Kruyt, Elsevier, New York, 1952.

5. Shaw, D. J. Electrophoresis, Academic Press, 1969.

6. Dukhin, S. S.; Derjaguin, B. C. Surface and Colloid Science, ed. by E. Matijevic, Vol. 7, Wiley-Interscience, 1974.

7. Hunter, R. J. Zeta-potential in Colloid Science, Academic Press, 1981.

8. Swanson, J. W. Electrokinetic Properties of Cellulose, Course Compendium, Ch. 7, The Institute of Paper Chemistry, Appleton, Wisconsin (The IPC), 1982.

9. Strazdins, E. Factors affecting the electrokinetic properties of cellulose fibers. Tappi Journal 55(12):1691(1972).

10. Jaycock, M. J.; Pearson, J. L.; Counter, R.; Husband, F. W. Effect of cellulose fiber fines on the retention of fillers. J. Appl. Chem. Biotechnol. 26:370(1976).

11. Stratton, R. A.; Swanson, J. W. Electrokinetics in papermaking; a position paper. Tappi Journal 64(1):79(1981).

12. Overbeek, J. Th. G. Interpretation of electrokinetic phenomena. Trans. BPBIF Symp. Fiber-water Interactions in Papermaking, Vol. 1 (Oxford):85-106(1977).

13. Sennett, P.; Olivier, J. P. Colloidal dispersions, electrokinetic effects, and the concept of zeta-potential. Ind. Eng. Chem. 57(8):33(1965).

14. Black, A. P.; Smith, A. L. Determination of the mobility of colloidal particles by microelectrophoresis. J. Am. Water Works Assoc. 54:926(1962).

15. Herren, B. J.; Shafer, S. G.; Van Alstine, J.; Harris, J.; Snyder, R. S. Control of electro-osmosis in coated quartz capillaries. Journal Colloid Interface Science 115(1):46(1987).

16. Goulet, M. T. The effect of pulping, bleaching and refining processes on the electrokinetic properties of wood fibers. Doctoral Dissertation, The IPC, 1986.

17. Miller, C. E. An investigation of the effects of polymer partitioning on fines retention. Doctoral Dissertation, IPST, Atlanta, Georgia, 1989.

18. Kerekes, R. J.; Garner, R. G. Measurement of turbulence in pulp suspensions by laser anemometry. Trans. J. Pulp and Paper Science 8(3):TR53(1982).

19. Drain, L. E. The Laser Doppler Technique, Wiley-Interscience, New York, 1980.

20. Malvern Zetasizer IIC User Manual. Malvern Instruments, Malvern England. Issued November, 1986.

21. von Smoluchowski, M. Handbuch der Elektrizitat und des Magnetismus, Vol. 2. B. Graetz editor. Leipzig, Germany (1914), as referenced in Shaw (5).

22. Adamson, A. W. Physical Chemistry of Surfaces. Wiley-Interscience, New York, 1990.

23. Henry, D. C. Proc. Royal Soc. A258:319(1960), as referenced in Adamson (22), 1st Edition, 1967.

24. Derjaguin, B. V.; Landau, L. Acta Physicochim. USSR 14:633(1941), as referenced in Adamson (22).

25. Verwey, E. J. W.; Overbeek, J. T. G. Theory of the Stability of Lyophobic Colloids. Elsevier, Amsterdam, 1948.

26. van der Waals, J. D. Die Kontinuität des gasformigen und flüssigen Zustande. Ph.D. dissertation, Leyden, 1873, as referenced in Kruyt (4).

27. van Oss, C. J.; Chaudhury, M. K.; Good, R. J. Interfacial Lifshitz-van der Waals and polar interactions in macroscopic systems. Chemical Reviews 88:927-941(1988).

28. Keesom, W. H. Proc. R. Acad. Sci. Amsterdam 18:636(1915), as referenced in van Oss (27).

29. Debye, P. Phys. Z. 21:178(1920), as referenced in van Oss (27).

30. London, F. Z. Physik. 63:245(1930), as referenced in Kruyt (4).

31. LaMer, V. K.; Healy, T. W. Adsorption-flocculation reactions of macromolecules at the solid-liquid interface. Rev. Pure Appl. Chem. 13:112(1963).

32. Kasper, D. R. Theoretical and Experimental Investigations of the Flocculation of Charged Particles in Aqueous Solutions by Polyelectrolytes of Opposite Charge. Doctoral Dissertation, California Institute of Technology, Pasadena, CA, 1971.

33. Gregory, J. Rates of flocculation of latex particles by cationic polymers. Journal Colloid Interface Science 42(2):448(1973).

34. van de Ven, T. G. M. Effect of polymer bridging on selective shear flocculation. J. Colloid Int. Sci. 81(1):290-291(1981).

35. von Smoluchowski, M. Zur theorie der elecktrischen kataphorese und der oberflächenleitung. Physik. Zeitschr. 17:557(1916), as referenced in Kruyt (4).

36. von Smoluchowski, M. Zeitscrift F. physik. Chemie 92: 129(1917), as referenced in Kruyt (4).

37. van de Ven, T. G. M.; Mason, S. G. The microrheology of colloidal dispersions. J. Colloid Interface Sciences 57:505-546(1976).

38. Levich, V. G. Physicochemical Hydrodynamics. Prentice-Hall, New Jersey, 1962.

39. Stratton, R. A. Effect of agitation on polymer additives. TAPPI J. 66(3):141(1983).

40. Delichatsios, M. A.; Probstein, R. F. Coagulation in turbulent flow: theory and experiment. J. Colloid Int. Sci. 51:394-405(1975).

41. Brigham, K. M. The Role of Particle Size and Polymer Molecular Weight on the Adsorption of a Cationic Polyelectrolyte by and Subsequent to Flocculation of Pulp Fines. Doctoral Dissertation, The IPC, 1986.

42. Hesselink, F. Th. On the theory of polyelectrolyte adsorption: The effect on adsorption behavior of the electrostatic contribution to the adsorption free energy. Journal Colloid Interface Sciences 60:448-466(1977).

43. Cohen-Stuart, M. A.; Scheutjens, J. M. H. M.; Fleer, G. J. Polydispersity effects and the interpretation of polymer adsorption isotherms. J. Polym. Sci. Plym. Phys. 18:559-573(1980).

44. Papenhuijzen, J.; Fleer, G. J.; Bijsterbosch, B. H. Polyelectrolyte adsorption II. Comparison of experimental results for polystyrene sulfonate, adsorbed on polyoxymethylene crystals, with theoretical predictions. J. Colloid Interface Science 104(2):553-561(1985).

45. Norde, W.; MacRitchie, F.; Nowicka, G.; Lyklema, J. Protein adsorption at solid-liquid interfaces: reversibility and conformational aspects. J. Colloid Interface Sci. 112:447-456(1986).

46. Peterson, C.; Kwei, T. K. The kinetics of polymer adsorption onto solid surfaces. Journal of Physical Chemistry 65:1330-3(1963).

47. Kindler, W. A.; Swanson, J. W. Adsorption kinetics in the polyethylenimine-cellulose fiber system. Journal of Polymer Science 9(A-2):853-65(1971).

48. Abril Gonzalez, A.; Hernandez Castro, C. Adsorption of cationic polyelectrolyte by bleached bagasse chemical pulp; Adsorption kinetics. Investigacion Y Tecnica del Papel 23(89):521-31(1986).

49. Falk, M.; Ödberg, L.; Wågberg, L.; Risinger, G. Adsorption kinetics for cationic polyelectrolytes onto pulp fibers in turbulent flow. Colloids and Surfaces 40:115-124(1989).

50. Khlebstov, N. G.; Sirota, A. I.; Fomina, V. I.; Bypov, M. G. Use of an electrooptic method of study polymer-bearing disperse systems. Kolloidnyi Zhurnal 52(1):178-82(1990).

51. Neimo, L. Rate of adsorption of polyethylenimine by papermaking fibers and fillers. EUCEPA International Conference (Torremolinos, Spain) :391-407(1984).

52. Mahanta, D.; Chaliha, B. C.; Baruah, J. N. Adsorption kinetics of cationic polyacrylamide onto cellulose fibers. Colloids and Surfaces 25:101-9(1987).

53. Black, A. P.; Birkner, F. B.; Morgan, J. J. Destabilization of dilute clay suspensions with labeled polymers. J. AWWA 57:1547-1560(1965).

54. Somasundaran, P.; Sivakumar, A. Short term kinetics of polymer adsorption on glass substrate. Colloids and Surfaces 30:401-403(1988).

55. Pelssers, E. G. M.; Cohen Stuart, M. A.; Fleer, G. J. Kinetic aspects of polymer bridging: equilibrium flocculation and nonequilibrium flocculation. Colloids and Surfaces 38:15-25(1989).

56. Pefferkorn, E.; Elaissari, A. Adsorption-desorption processes in charged polymer/colloid systems: structural relaxation of adsorbed macromolecules. J. Colloid Interface Science 138(1):187-194(1990).

57. Dijt, H. C.; Cohen Stuart, M. A.; Hofman, J. E.; Fleer, G. J. Kinetics of polymer adsorption in stagnation point flow. Colloids and Surfaces 51:141-58(1990).

58. Baran, A. A.; Kocherga, I. I. Kinetics of polyethylene oxide adsorption by particles of coal and clay suspensions. Kolloidnyi Zhurnal 52(3):419-23(1990).

59. Lang, M. unpublished work, IPST, 1991.

60. Gregory, J.; Lee, S. Y. The effect of charge density and molecular mass of cationic polymers on flocculation kinetics in aqueous solution. Journal of Water SRT-Aqua 39(4):265-74(1990).

61. Wigsten, A. L.; Stratton, R. A. Polymer adsorption and particle flocculation in turbulent flow. In Polymer Adsorption and Dispersion Stability, Goddard, E. D. and Vincent, B., editors. ACS Symposium Series No. 240:429-44(1984).

62. Wågberg, L.; Lindström, T. Flocculation of cellulosic fibers by cationic polyacrylamides with different charge densities. Nordic Pulp and Paper Research Journal 2(4):152-160(1987).

63. Lindström, T.; Soremark, C. Adsorption of cationic polyacrylamides on cellulose. Journal of Colloid and Interface Science 55(2):305-12(1976).

64. Horn, D.; Melzer, J. Electrostatic and steric effects of cationic polymers adsorbed on cellulose fibers. Trans. Symp. Fiber-Water Interactions in Papermaking (Oxford), 1977.

65. Gregory, J. Polymer adsorption and flocculation in sheared suspensions. Colloids and Surfaces 31:231-253(1988).

66. Abson, D.; Brooks, D. F. Wet-end behavior of dry strength additives. TAPPI J. 68(1):76-8(1985).

67. Jankovics, L. Effect of agitation and molecular weight on polymer adsorption and deflocculation. Journal of Applied Polymer Science 9:545-552(1965).

68. Wågberg, L.; Lindström, T. Kinetics of polymer-induced flocculation of cellulosic fibers in turbulent flow. Colloids and Surfaces 27:29-42(1987).

69. Wågberg, L. Adsorption of Polyelectrolytes and Polymer-induced Flocculation of Cellulosic Fibers. Doctoral Dissertation, Royal Institute of Technology, Department of Paper Technology, Stockholm, Sweden, 1987.

70. Wågberg, L.; Ödberg, L.; Lindström, T.; Aksberg, R. Kinetics of adsorption and ion-exchange reactions during adsorption of cationic polyelectrolytes onto cellulosic fibers. J. Colloid Interface Science 123:287-295(1988).

71. Aksberg, R.; Einarson, M.; Berg, J.; Ödberg, L. Adlayer thickness of two cationic polyacrylamides adsorbed onto polystyrene latices. Langmuir 7:43-45(1991).

72. Döll, B. Particle destabilization in turbulent pipe flow. Water Science Tech. 21:435-442(1989).

73. Klute, R. Rapid mixing in coagulation/flocculation processes -- design criteria. Chemical Water and Wastewater Treatment 62:53-65(1985).

74. Franco, R. P. Flocculation in turbulent flow. A291 Report, The IPC, unpublished work, 1973.

75. Luettgen, C. O. A Study of a Retention Aid System Under Turbulent Shear. A190 Independent Research Report, The IPC, unpublished work, 1987.

76. Wågberg, L. A device for measuring the kinetics of flocculation following polymer addition in turbulent fiber suspensions. Svensk Papperstidning 88(7):R48-56(1985).

77. Saffman, P. G.; Turner, J. S. On the collision of drops in turbulent clouds. J. Fluid Mechanics 1:16(1956).

78. Wigsten, A. L. Polymer Adsorption and Flocculation of Particles in Turbulent Flow. Doctoral Dissertation, The IPC, Appleton, Wisconsin, 1983.

79. Duffy, G. G.; Titchener, A. L.; Lee, P. F. W.; Moller, K. The mechanisms of flow of pulp suspensions in pipes. Appita 29(5):363-370(1976).

80. Norman, B. G.; Moller, K.; Ek, R.; Duffy, G. G. Hydrodynamics of papermaking fibers in water suspension. Trans. BPBIF Symp. Fiber-water Interactions: 195-249(1977).

81. Robertson, A. A.; Mason, S. G. The flow characteristics of dilute fiber suspensions. TAPPI J. 40(5):326-334(1957).

82. Forgacs, O. L.; Robertson, A. A.; Mason, S. G. The hydrodynamic behavior of paper-making fibers. Pulp and Paper Mag. Can. 59:117-127(1958).

83. Duffy, G. G.; Moller, K.; Lee, P. F. W.; Milne, S. W. A. Design correlations for groundwood pulps and the effects of minor variables on pulp suspension flow. Appita 27(5):327-333(1974).

84. Durst, R. E.; Jenness, L. C. The flow properties of paper pulp stock, II. The relationship of shear value to pipe friction for soda kraft and groundwood slurries. TAPPI J. 38(4):193-198(1955).

85. Moller, K.; O'Sullivan, M. J. Annulus formation in plug flow of pulp suspensions. TAPPI J. 57(3):165(1974).

86. Hemström, G.; Moller, K.; Norman, B. Boundary layer studies in pulp suspension flow. TAPPI J. 59(8):115-118(1976).

87. Mih, W.; Parker, J. Velocity profile measurements and a phenomenological description of turbulent fiber suspension pipe flow. TAPPI J. 50(5):237-246(1967).

88. Lee, P. F. W.; Duffy, G. G. Velocity profiles in the drag-reducing regime of paper pulp suspensions in pipes. Svensk Papperstidning 74(24):829-834(1971).

89. Daily, J. W.; Bugliarello, G. Basic data for dilute fiber suspensions in uniform flow with shear. Tappi J. 44(7):497- 501(1961).

90. Bugliarello, G.; Daily, J. W. Rheological models and laminar shear flow of fiber suspensions. Tappi J. 44(12):881-885(1961).

91. Moller, K.; Duffy, G. G. An equation for predicting transition-regime pipe friction loss. TAPPI J. 61(1):63-66(1978).

92. Bobkowicz, A. J.; Gauvin, W. H. The turbulent flow characteristics of model fiber suspensions. Can. J. Chem. Eng. 43:87-91(1965).

93. Lee, P. F. W.; Duffy, G. G. An analysis of the drag reducing regime of pulp suspension flow. TAPPI J. 59(8):119-122(1976).

94. Kerekes, R. J. E. Turbulent Drag Reduction in Pipe Flow of Ideal Fiber Suspensions. Doctoral Dissertation, McGill University, Canada (1970), as referenced in Lee(93).

95. Radin, I.; Zakin, J. L.; Patterson, G. K. Drag reduction in solid-fluid systems. AIChE J. 21:358-371(1975).

96. Vaseleski, R. C.; Metzner, A. B. Drag reduction in turbulent flow of fiber suspensions. AIChE J. 20:301-306(1974).

97. Virk, P. S. Drag reduction fundamentals. AIChE J. 21:625-656(1975).

98. Daily, J. W.; Bugliarello, G.; Troutman, W. W. M.I.T. Hydrodynamics Lab. Tech. Report No. 35 (1959), as referenced in Lee (88).

99. Bobkowicz, A. J.; Gauvin, W. H. The effects of turbulence on the flow characteristics of model fiber suspensions. Chemical Engineering Science 22:229-241(1967).

100. Lee, P. F. W.; Duffy, G. G. Models for the drag reducing regime of pulp suspension flow. TAPPI Engineering Conf. Proc. :137-142(1975).

101. Sanders, H. T. An Investigation of Fiber Consistency Distributions in Turbulent Tube Flow. Doctoral Dissertation, The IPC, 1970.

102. Lee, P. F. W.; Duffy, G. G. Velocity profiles in the drag reducing regime of pulp suspension flow. Appita 30(3):219-226(1976).

103. Seely, T. Turbulent Tube Flow of Dilute Fiber Suspensions. Doctoral Dissertation, The IPC, Appleton, Wisconsin (1968).

104. Lee, P. F. W.; Duffy, G. G. An analysis of the drag reducing regime of pulp suspension flow. TAPPI J. 59(8):119-122(1976).

105. Lee, P. F. W.; Duffy, G. G. Relationships between velocity profiles and drag reduction in turbulent fiber suspension flow. AIChE J. 22(4):750-753(1976).

106. Goldstein, S. Proc. Cambridge Phil. Soc. 31(2):232(1935), as referenced in Lee (102).

107. Lee, P. F. W.; Duffy, G. G. Velocity profiles in the drag reducing regime of pulp suspension flow. Appita 30(3):219-226(1976).

108. Gore, R. A.; Crowe, C. T. Effect of particle size on modulating turbulent intensity. Int. J. Multiphase Flow 15(2):279-285(1989).

109. Hutchinson, P.; Hewitt, G.; Dukler, A. E. Deposition of liquid or solid dispersion from turbulent gas streams: a stochastic model. Chemical Engineering Science 26:419-439(1971).

110. Park, J. T.; Mannheimer, R. J.; Grimley, T. A.; Morrow, T. G. Pipe flow measurements of a transparent non-Newtonian slurry. J. Fluids Engineering 111:331-336(1989).

111. Ek, R. Int. Symp. of Paper Machine Headboxes. McGill University, Montreal, Canada :31(1979).

112. Liljegren, L. M.; Vlachos, N. S. Laser velocimetry measurements in a horizontal gas-solid pipe flow. Experiments in Fluids 9:205-212(1990).

113. McComb, W. D.; Chan, K. T. J. Laser-doppler amemometer measurements of turbulent structure in drag-reducing fiber suspensions. J. Fluid Mech. 152:455(1985).

114. Steen, M. Turbulence and Flocculation in Fiber Suspensions. Doctoral Dissertation, University of Trondheim, Norway, 1990.

115. Steen, M. On turbulence structure in vertical pipe flow of fibers suspensions. Nordic Pulp Paper Res. J. 4(4):244-252(1989).

116. Chilton, T. H.; Genereaux, R. P. AIChE Trans. 25:102(1930).

117. Forney, L. J.; Kwon, T. C. Efficient single-jet mixing in turbulent tube flow. AIChE J. 25(4):623-630(1979).

118. Forney, L. J.; Lee, H. C. Optimum dimensions for pipeline mixing at a T-junction. AIChE J. 28(6):980-987(1982).

119. O'Leary, C. D.; Forney, L. J. Optimization of in-line mixing at a 90° tee. Ind. Eng. Chem. Process Des. Dev. 24:332-338(1985).

120. Maruyama, T.; Suzuki, S.; Mizushina, T. Pipeline mixing between two fluid streams meeting at a T-junction. Int. Chem. Eng. 21(2):205(1981).

121. Maruyama, T.; Mizushina, T.; Watanabe, F. Optimum jet mixing in turbulent pipe flow. Int. Chem. Eng. 23(4):707(1983).

122. Forney, L. J. Jet Injection for Optimum Pipeline Mixing. Encyclopedia of Fluid Mechanics. Cheremisinoff, N., Ed., Gulf Publishing Company, Houston :661-690(1986).

123. Sroka, L. M.; Forney, L. J. Fluid mixing with a pipeline tee: theory and experiment. AIChE J. 35(3):406-414(1989).

124. Cozewith, C.; Busko, M. Design correlations for mixing tees. Ind. Eng. Chem. Res. 28:1521-1530(1989).

125. Ottewill, R. H.; Shaw, J. N. Kolloid Zh., 218:34(1967); as referenced in Shaw (5).

126. Mabire, F.; Audebert, R.; Quivoron, C. Synthesis and solution properties of water soluble copolymers based on acrylamide and quaternary ammonium acrylic comonomer. Polymer 25:1317-1322(1984).

127. Petäjä, Timo. A Fundamental Study of the Influence of Timing of Polyelectrolyte Dosages and Agitation on Retention with the Dual Polymer System. Doctoral Dissertation. University of Oulu, Finland, 1980.

128. Tosun, G. A study of micromixing in tee mixers. Ind. Eng. Chem. Res. 26:1184-1193(1987).

129. Luettgen, C. O.; Lindsay, J. D.; Stratton, R. A. Turbulent dispersion in pulp flow: preliminary results and implications for the mechanisms of fiber-turbulence interactions. AIChE Annual Meeting, Los Angeles, California, Paper No. 180f(1991).

130. Savitzky, A.; Golay, M. J. E. Smoothing and differentiation of data by simplified least squares procedures. Analytical Chemistry 36(8):1627-1639(1964).

LITERATURE CITED IN APPENDICES

131. Isenberg, I. H. Pulpwoods of the United States and Canada, Volume II -- Hardwoods. 3rd Edition, Revised by M. L. Harder and L. Louden, IPC, 1981.

132. Panshin, A. J.; de Zeeuw, C. Textbook of Wood Technology, Structure, Identification, Properties, and Uses of the Commercial Woods of the United States and Canada, 4th Edition, McGraw-Hill, 1980.

133. CRC Handbook of Chemistry and Physics. 67th Edition.

134. Prutton, Carl F.; Maron, Samuel, H. Fundamental Principles of Physical Chemistry, 2nd Edition, 1951, pg. 454.

APPENDIX I. FIBER LENGTH ANALYSIS OF PULP

The original pulp was tested for fiber length using the Kajaani FS-100. A population distribution is shown in Figure A1. The reduction of the fines fraction was facilitated using the pilot paper machine at IPC. A schematic is shown in Figure A2. A fine tissue was made on the machine so as to reduce fines retention by filtration. The machine was run at 2500 fpm, and the white water was sewered. The tissue came off the press section at approximately 30 percent solids and was stored in barrels in cold storage refrigeration (40°C) until needed for flow loop experiments. A one percent by weight formaldehyde solution was added for preservation. Table A1 lists the fiber length analysis work performed during the operation of the pilot machine to monitor the efficiency of fines removal.

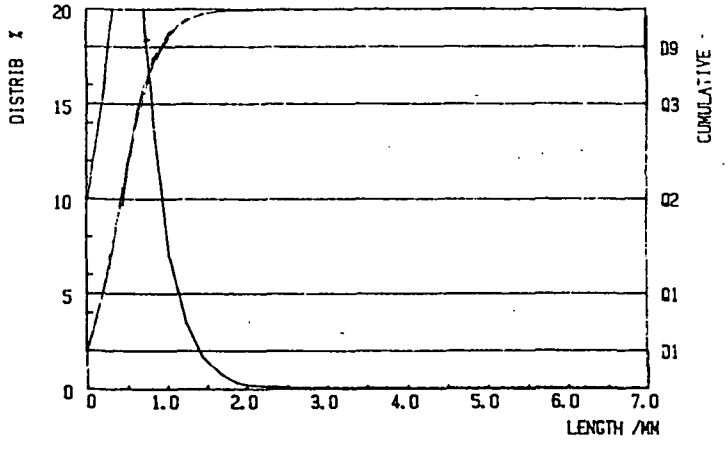

CHARACTERISTICS
TOTAL FIBERS 5977

CHAR	WEIGHTED	ARITHMETIC
D1	0.29	0.00
Q1	0.45	0.20
Q2	0.65	0.42
Q3	0.93	0.65
Q9	1.24	0.92
AV	0.74 1.00	0.51
X1	2.15	17.60 < 0.100

ANALYZED BY KAJAANI FS-100

Figure A1. Population distribution of original Escanaba pulp prior to fractionation.

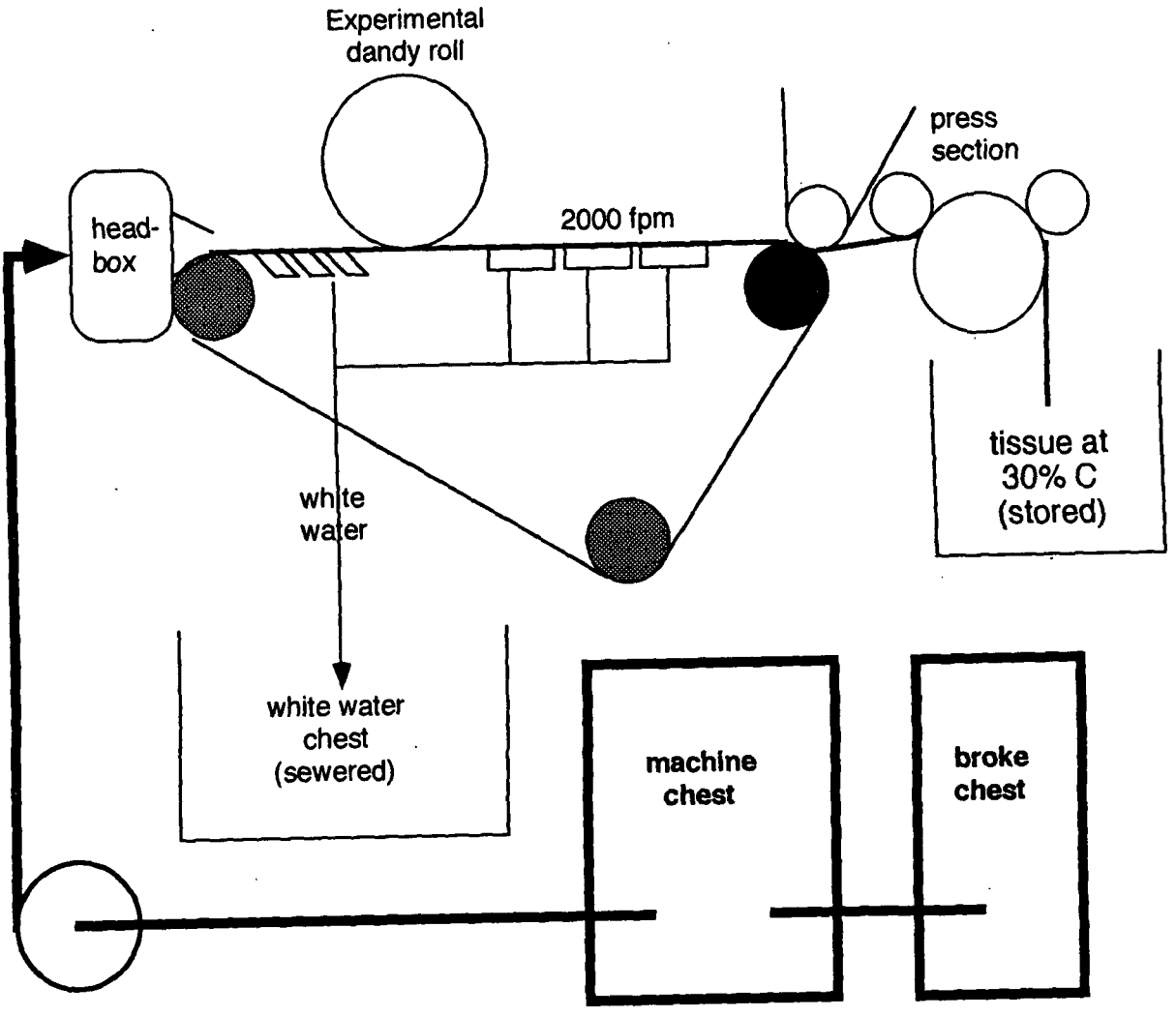

Figure A2. Schematic of pilot paper machine used for pulp fractionation.

Table A1. Results of Kajaani fiber length analysis of Escanaba pulp.

Sample	Numerical Average	Length Weighted Average	Weight Weighted Average	Weighted Percent Fines	Arithmetic Percent Fines
Pulp1	0.46mm	0.69mm	0.93mm	1.59	17.41
Pulp2	0.50	0.69	0.89	1.18	14.15
1/24/89					
#1	0.51	0.75	1.05	1.11	13.42
#2	0.51	0.72	0.94	1.04	11.94
#3	0.52	0.73	0.98	0.73	8.81
#4	0.53	0.73	0.95	0.68	8.37
#5	0.54	0.74	1.01	0.59	7.39
Final	0.54	0.74	1.01	0.40	4.85
1/25/89					
#1	0.52	0.73	1.01	0.69	8.19
Final	0.52	0.70	0.93	0.37	4.45
1/30/89					
Final	0.52	0.70	0.91	0.53	6.20
1/31/89					
Final	0.52	0.71	0.97	0.53	6.03
2/1/89					
Final	0.51	0.68	0.88	0.61	7.57
2/2/89					
Final	0.49	0.66	0.84	0.61	6.77
White Water Samples					
1/24/89	0.25	0.42	0.62	7.62	40.52
1/25/89	0.21	0.36	0.52	11.07	48.84

APPENDIX II. SPECIES IDENTIFICATION OF PULP

A species identification revealed the presence of mostly *Populus spp.*, with Basswood, Birch, Ash, and Maple. A study of what specific species would most probably be in a pulp from the Northern Michigan and Wisconsin regions has revealed the collection shown in Table A2. The majority of the information was obtained from data presented by Isenberg[131] and Panshin and deZeeuw.[132]

Table A2. A compilation of pulp wood species probably present in the "hardwood" dry lap pulp obtained from Mead, Escanaba.

Species	Typical Weight Weighted Fiber Length, mm(St.D.)[§]	Typical Fiber Diameter, μm[*]
Populus grandidentata Michx. (Bigtooth Aspen)	1.33(0.17)	23-40
Populus tremuloides Michx. (Trembling Aspen)	1.32(0.22)	N.M.
Betula alleghaniensis Britton (Yellow Birch)	1.38(0.17)	20-36
Betula papyrifera Marsh. (Paper Birch)	1.35(0.15)	N.M.
Betula populifolia Marsh. (Gray Birch)	1.26(0.14)	N.M.
Tilia americana L. (American Basswood)	1.21(0.17)	24-36
Tilia heterophylla Vent. (White Basswood)	1.34(0.18)	N.M.
Fraxinus americana L. (White Ash)	1.26(0.17)	22.73[‡]
Fraxinus nigra Marsh. (Black or Brown Ash)	1.27(0.17)	12-22
Fraxinus pennsylvanica Marsh. (Green Ash)	1.27(0.17)	N.M.
Acer rubrum L. (Red Maple)	0.92(0.12)	16-30
Acer saccharinum L. (Silver Maple)	0.76(0.13)	16-30
Acer saccharum Marsh. (Sugar Maple)	0.92(0.13)	16-30

[§] There may be some question as to whether each of these compiled values is a weight weighted fiber length average as the authors do not state in each case. Values however do fall in expected ranges for weight weighted lengths.

[*] The methods for measurement were not declared by the authors as they may be by wet or dry determinations.

[‡] Average fiber diameter at the 25 year ring.

APPENDIX III. LATEX CHARACTERIZATION

The latex used as an adsorption tracking material and thus a model filler particle in the stock was a polystyrene sphere donated by Morton Thiokol (Lytron® #2501). The particle size average and distribution were characterized by several instruments and methods. The manufacturer reported by Micromeritics FlowSizer HDC 5600 a mass distribution mean diameter of 407.0 nm with a standard deviation of 33.2 nm; 92.4 mass percent was reported to be between 317.0 and 473.3 nm.

In attempts to characterize the sample with the Zetasizer particle size cell, a broader distribution and a higher average were found; the average distribution mean was 0.47 μm, z average size of 0.45 μm with distributions described by 0.34 to 0.49 μm and 0.32 to 0.67 μm of 55.4 and 90.1 percent, respectively. Because of the discrepancy in size distribution data, alternative methods of characterization were examined.

Scanning Electron Microscope (SEM) photomicrographs were taken of the particles at 10,000X magnification in order to visualize the size homogeneity. Particle size was measured using SEM negatives and a Hewlett-Packard Dymec Imager with a method described by Miller.[17] Figure A3 shows a typical photomicrograph and, in particular, how particle agglomeration can cause distortion of the image diameter. Only isolated particles were measured by this method.

Two different methods were used to calculate the particle diameters from the projected images: 1) using the one micron scale on each micrograph, and 2) using a micrograph of a calibrated grid pattern. Both methods gave average particle size measurements much larger

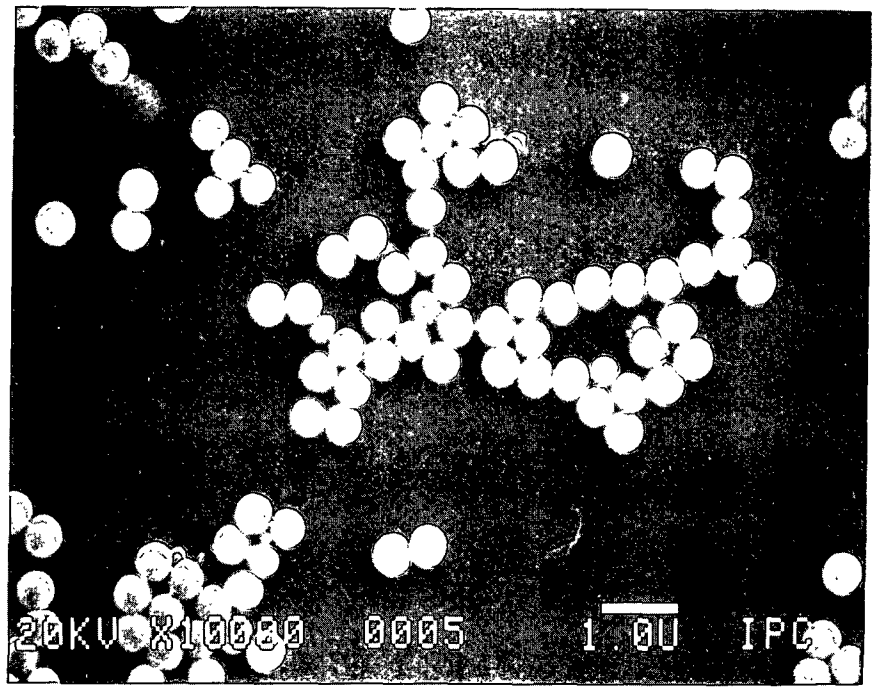

Figure A3. Scanning electron micrograph of Morton Thiokol latex, Lytron 2501.

than by the Micromeritics or Zetasizer instruments: 0.542 and 0.563 μm number average, respectively. This may be attributed to an apparent flattening of the particles due to high temperatures used in SEM sample preparation.

A final technique was used to characterize the latex particle size. The use of a Leeds and Northrup Microtrac (Model 7991-3) Particle Size Analyzer owned by Appleton Paper Research (Appleton, Wisconsin) was requested for this purpose. This instrument measures low-angle, forward scattering light from a laser beam projected through a stream of sample particles. The angular distribution of scattered light is said to be a function of particle size.

A multipoint optical filter detects the amount and direction of the light scattered by the particles which is analyzed by microcomputer to determine particle size distribution.

The median particle size measured by the Microtrac system was 0.405 μm. The volume mean diameter of the distribution was 0.455 μm; 68.0 percent fell between the 0.55 to 0.30 μm channels, and 93.0 percent between 0.80 and 0.20 μm. This would again suggest a broader distribution of particle diameters than reported by the Micromeritics instrument.

The various particle size instrument results are summarized in Table A3. The results suggest that the latex is suitable for Zetasizer mobility measurements due to the size and distribution, and for Dynamic Drainage Jar (DDJ) retention measurements due to the capability to model filler materials in a stock furnish.

Table A3. Results from various particle size analyses.

Micromeritics	
Mass distribution mean diameter	0.407 μm
Standard devation	0.033 μm
Between 317.0 and 473.3 nm	92.4 mass percent
Zetasizer	
Distribution mean (average of eight)	0.47 μm
Z average size	0.45 μm
Between 0.34 and 0.49 μm	55.4 percent
Between 0.32 and 0.67 μm	90.1 percent
Leeds and Northrup	
Median	0.405 μm
Volume mean diameter of distribution	0.455 μm
Between 0.30 and 0.55 μm	68.0 percent
Between 0.20 and 0.80 μm	93.0 percent

APPENDIX IV. ZETASIZER OPERATIONAL DATA

A standard polystyrene latex, Interfacial Dynamics #2-27-92, was measured on the Zetasizer IIC for electrophoretic mobility (EM) at the beginning of each operational day. Given good operational behavior, the standard gave a reproducible EM distribution average and standard deviation of the distribution. The mean EM distribution average was -4.376 (μm/s)/(Volt/cm) with a standard deviation of 0.0781 (μm/s)/(Volt/cm), and the mean standard deviation of the distribution was 0.5591 (μm/s)/(Volt/cm) with a standard deviation of 0.03432 (μm/s)/(Volt/cm). Figure A4 shows the EM and standard deviation values for the standard latex during the course of this project.

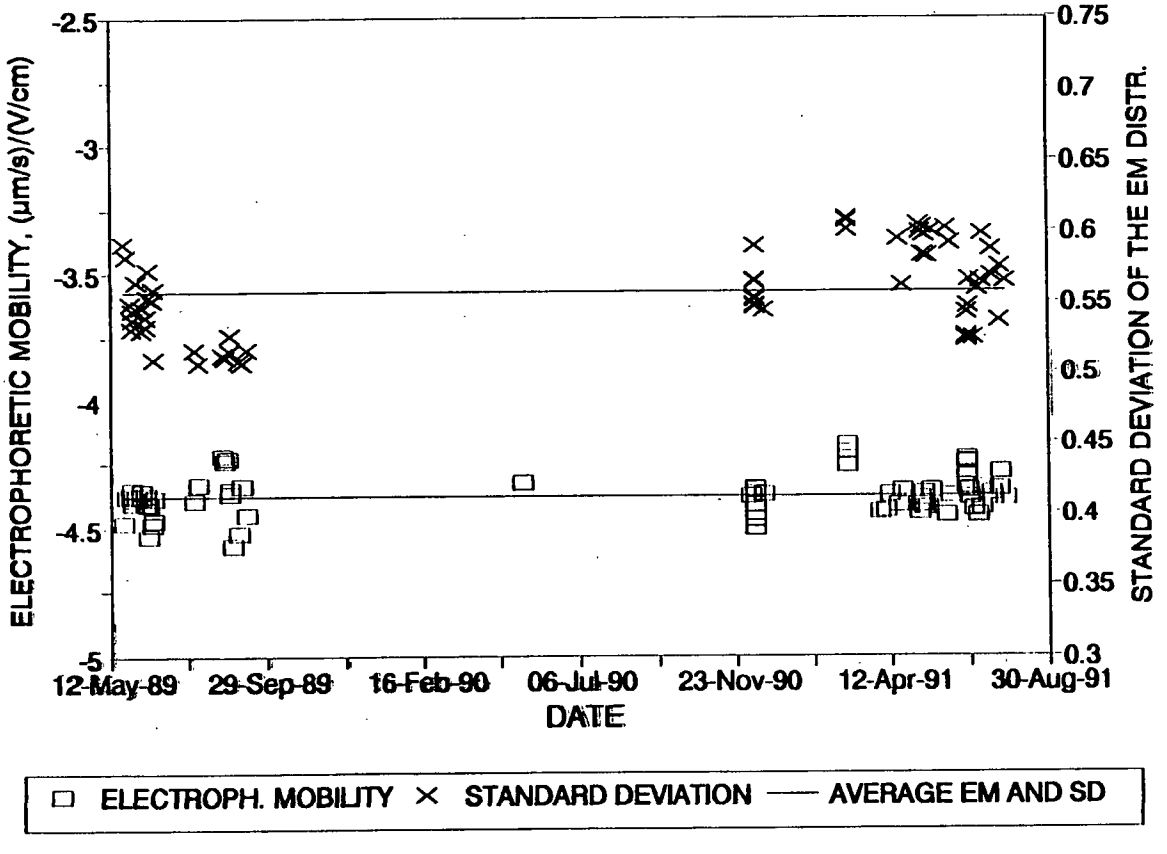

Figure A4. Electrophoretic mobility distribution average and standard deviation of the distribution as measured by the Zetasizer versus the date of operation. A standard latex, IDS #2-27-92, in 0.01 M KCl background electrolyte.

APPENDIX V. ZETASIZER MANUAL MODE PROCEDURES AND COMMANDS

Sample preparation: A latex solution master batch is prepared from the 49 percent solids solution as stored. The accurate solids content of this master batch is determined. Twenty tared aluminum weigh dishes are each filled with 5 to 20 grams of solution and placed in an oven for eight hours. They are removed and placed in a desiccator until cool, and reweighed. By this method, the average solids content of our master batch was determined to be 1.0716 percent.

All quantities of latex are pipetted by automatic pipette using a plastic disposable tip. Weights of retention aid and latex are determined by placing a tared plastic weigh dish on a balance and pipetting the material into the dish. Weights are taken in grams to five decimal places. Dilutions are made with a 0.01 M KCl solution. All solutions are stored in polypropylene containers with Nitrogen gas purging prior to sealing.

Zetasizer preparation: Prior to each run of the Zetasizer, a standard latex injection is made. An EM reading is taken at both stationary layers and at the center of the cell. This is to detect operational problems with the instrument. An injection is then made with untreated Morton Thiokol latex to test whether the EM and distribution fall within historical values. Finally, a dual injection is made in automatic mode in order to set the instrument operational parameters. The average EM from six measurements at alternating stationary layers tells us if we are close to a typical 1 #/T polymer dosage. We are now ready for manual mode dual injection.

Dual injection: The Zetasizer is switched to manual mode. The command "clb: mme

20,3,0" is typed. Syringes of latex and retention aid solutions are taken with the containers purged with Nitrogen gas before sealing. The two syringes are placed in the dual syringe device, attached to the Y-junction and placed on the Zetasizer port (see Figure 59). The end clamp on the opposite side of the cell is opened to allow transport of fluid through the cell without disturbing the instrument. The laser, photomultiplier, and cell voltage and modulator are all turned on. To prevent air from entering the cell and altering the results of the experiment, the syringes are slowly injected to evenly fill the Y-junction and entrance tube. When the tube is filled with liquid and there are no attached air bubbles, the rate of syringe injection increases. A three-second count is made to complete the injection. The dual syringe system is laid on the platform, and return is hit on the instrument keyboard. When the 60-second experiment is completed, the command "zer: loo 20: obb: dat "b:<filename>.exp": sav 1: next" is made which will save the 20 results to blocks numbered 1 through 20 in the named file. After a series of experiments are completed with each file containing up to 100 blocks of data, the commands that will print out the distributions and save the data in ASCII form for spreadsheet manipulation are "dat "b:<filename>.exp" followed by "zer: rsf "a:<filename>.asc": loo 100: loa 1: dct: fir: apr: next". Many of these commands had been explained by personal communication with Malvern.[21] The following explanations of these commands were obtained from the Zetasizer IIC manual.

dat - open data file; a data file is opened for access.

sav - save; save the data currently in store at the record location specified in the file.

loa - load; load the specified record from the file into store.

loo - loop; repeat the commands following, the specified number of times.

nex - next; the end of the loop commands.

dct - transform; perform the discrete cosine transform and further analysis steps on the current data in store.

apr - print analysis; the last result is printed in the standard presentation form.

exp - experiment; set duration of correlation run to number of seconds specified.

zer - zero; clear transform array summation store.

mme - measure a specified number of times for a specified number of seconds, adding each correlation function to buffer, and wait a specified number of seconds before preceding to the next.

clb - clear buffer; clear buffer of previously summed correlation functions.

obb - output buffer; output buffer block to correlation store for subsequent display/analysis/manipulation.

rsf - result file; set result file name.

fir - file result; will file blocks of result data in ASCII, in named file.

APPENDIX VI. RETENTION BY ABSORBANCE

A UV absorbance method was used to track white water concentration, and thus retention efficiency, in DDJ and flow loop experiments. A calibration curve was made by measuring the absorbance at a peak wavelength, typically at approximately 246.7 nm, for various latex concentrations. A sample from a DDJ was typically diluted with a known amount of background electrolyte to a concentration on this calibration curve. Two instruments were used for this procedure during the course of the project: in Appleton, experiments were conducted on a Perkin-Elmer 320 Spectrophotometer; in Atlanta, a Perkin-Elmer Lambda 4b UV/Vis Spectrophotometer was used. Thus, two calibration curves of very similar character were obtained. Figure A5 illustrates both curves.

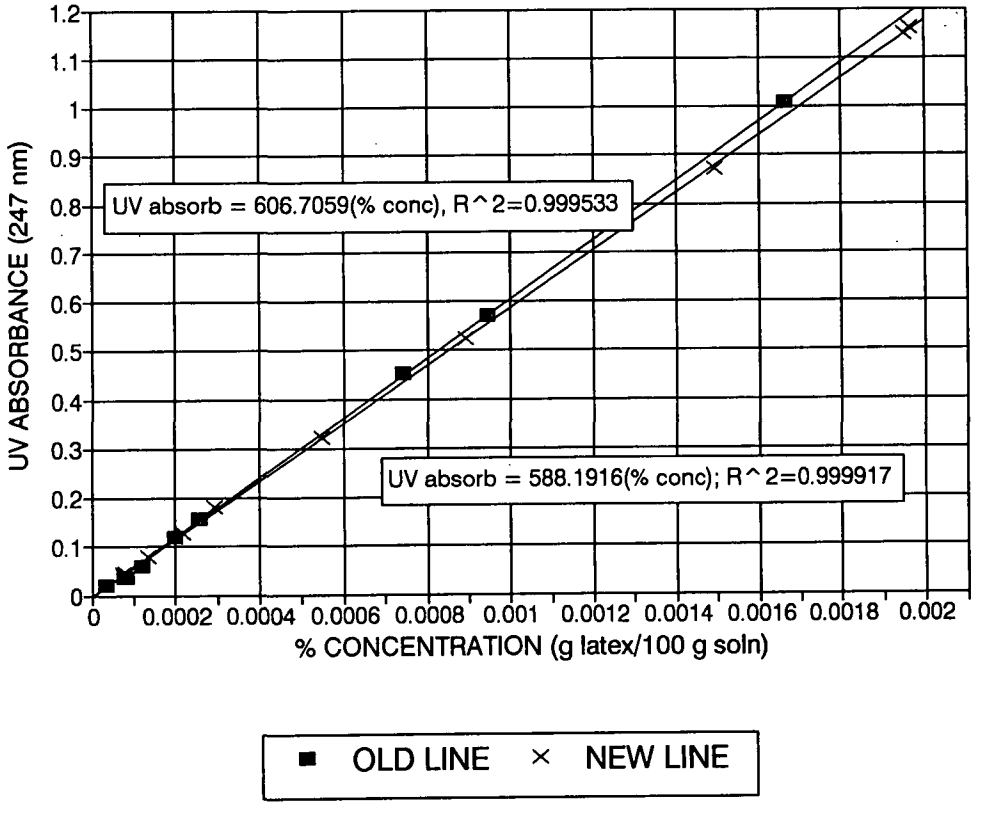

Figure A5. UV absorbance versus latex percent concentration for the two Spectrophotometers used in this project.

APPENDIX VII. RETENTION BY GRAVIMETRICS

Sample Calculation for Gravimetric Retention Determinations

Dynamic Drainage Jar Experiments:

Measured weights:
- wet weight in DDJ
- g polymer solution added to DDJ
- weigh dish tare$_{(x=1,2 \text{ and } 3)}$
- weigh dish and wet weight of white water sample$_{(x)}$
- weigh dish and oven dry weight$_{(x)}$

Calculations:
g KCl in pulp/latex sample in DDJ = wet weight in DDJ * concentration of salt in pulp/latex batch ÷ 100

g KCl in polymer added = g polymer solution added * concentration of KCl in polymer batch ÷ 100

$[KCl]_{DDJ}$ = (g $KCl_{pulp/latex}$ + g $KCl_{polymer}$) ÷ wet weight * 100

g KCl_x = $[KCl]_{DDJ}$ * wet weight in $dish_x$ ÷ 100

g $latex_x$ = dry weight in $dish_x$ - g KCl_x

$[latex \text{ in white water}]_x$ = g $latex_x$ ÷ wet weight in $dish_x$ * 100

% Retention = (concentration of latex in pulp/latex batch - $[latex]_x$) ÷ concentration of latex in pulp/ latex batch * 100

% Retention = $\sum$(% $Retention_x$) ÷ 3

Flow Loop Pipeline Injection Experiments:

Measured weights:

- percent fines content
- pounds per ton polymer dosage added to pipeline
- wet weight in DDJ
- weigh dish tare$_{(x=1,2, \text{ and } 3)}$
- weigh dish and wet weight of white water sample$_{(x)}$
- weigh dish and oven dry weight$_{(x)}$

Procedure:

1. Estimate fines content of pulp by taking sample of pulp before latex addition, running a DDJ on the sample and measuring gravimetrically the concentration of the white water. The solids in the weigh dishes will be the weight of fines through the DDJ 200 mesh screen plus the solids of the flow loop source water. Take three measurements of each batch of pulp for estimating fines content.

2. Measure the gravimetric retention of a pulp/latex batch without retention aid addition. The result (referred to as a blank) will be the weight of fines, latex and solids of the source water. Periodically measured the blank of a batch of pulp throughout each run.

3. The difference between these two measurements is the concentration of latex in the pulp/latex/water solids batch. This concentration is used as the headbox concentration in retention calculations.

4. The white water concentration of latex is calculated from the gravimetric measurements of white water solids minus the weight of fines and water solids measured in step 1.

Calculation:

% Retention = (concentration of latex in pulp/latex batch - $[latex]_x$) ÷ concentration of latex in pulp/latex batch * 100

% Retention = $\sum$(% $Retention_x$) ÷ 3

APPENDIX VIII. CALIBRATION OF POLYMER FEED ROTOMETER

Calibration of the rotometer was performed with a bucket and stopwatch method. The rotometer float was set to a predetermined level and the injection tube placed into a graduated cylinder for a certain length of time. Figure A6 shows the results of these tests. The calibration curve was determined from a linear regression analysis as:

$$GPM = 0.0144815 * SETTING,\ R^2 = 0.9964 \qquad \textbf{[A1]}$$

The high end of flow rates was more variable than the remainder of settings. The figure represents the operating range for the rotometer during experimentation.

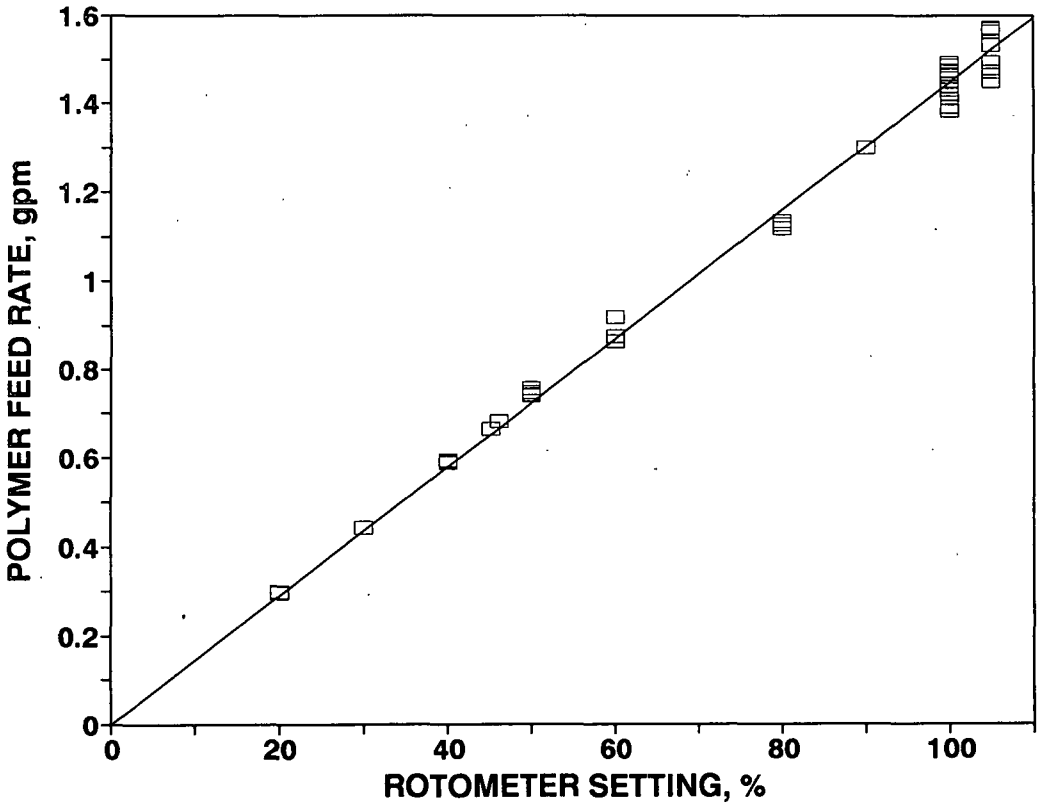

Figure A6. Rotometer calibration curve from stopwatch and graduated cylinder data.

APPENDIX IX. CALIBRATION OF CONDUCTIVITY METER

The on-line conductivity probe was calibrated using KCl solutions of known molarities. Data for KCl solutions were obtained from a CRC handbook[133] and physical chemistry texts including Prutton et al.[134]. The following equation was determined from regression analysis of the historical data:

$$\text{Conductivity[mmho/cm]} = 102.3188(\text{Molarity})^{0.91}\,\text{[mol/L]},\ R^2 = 0.9993 \qquad \textbf{[A2]}$$

With this equation, measured conductivities in the pipeline were converted to concentrations for the Effective Area calculations.

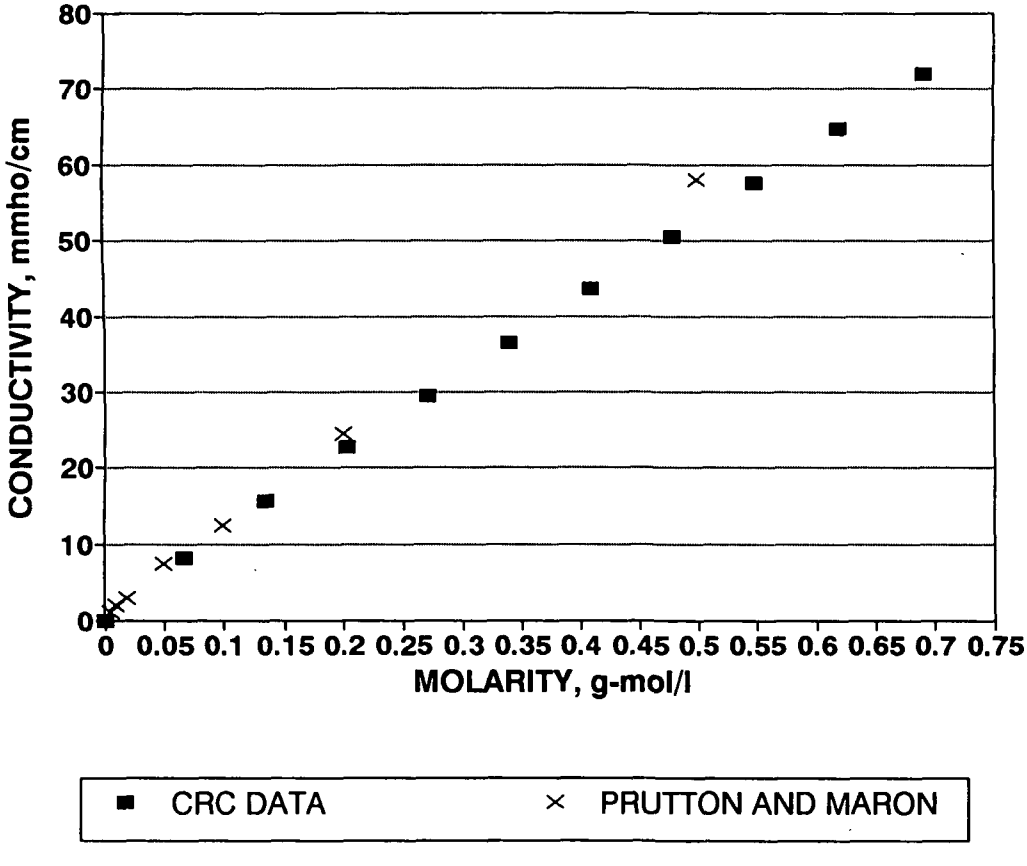

Figure A7. Standard conductivities of KCl solutions versus the molarity as obtained from the CRC Handbook of Chemistry and Physics and Prutton et al.

APPENDIX X. PID ALGORITHM

The Proportional-Integral-Derivative (PID) controller used for flow loop experiments was written in Turbo Pascal. The program used the input signal from the magnetic flowmeter, calculated the correct output, and sent the signal to the flow control valve. The Pascal code is included in the following pages. The levels of proportional, integral, and derivative control were determined by testing several integer values for speed to set-point and standard deviation around set-point once achieved. The objectives for control were 1. minimize raw material loss during the ramp to set-point, and 2. minimize the variation around set-point once achieved.

The first Pascal file is the root program, "d16pid_2.pas" which calls several units into the operation, including "tp4d16.tpu" and "tp4pid_1.tpu". These units in turn use several procedures and functions. For brevity, we include only those files which were modified or specifically written for this project. The main thrust of the programing is to take the input voltage, calculate an offset based on predetermined proportional, integral, and derivative parameters (proportional gain, reset minute and, derivative minute), and output a voltage signal to correct for the error. The unit tp4pid_1 specifically outputs to the monitor those parameters which are updating the output signal.

"d16pid_2.pas"

```
program d16pid_2(input,output);
uses crt, tp4d16, tp4pid_1;

const max_buffer = 1000;

var last_volts, volts, out_volt        : real;
```

```
    lsv,hsv,lsv_out,hsv_out,llim,hlim,
       set_gpm,setpnt,up              : real;
    pg, rm, dm                        : real;
    ne, se                            : real;
    valout, i                         : integer;
    base_adr, err_code, int_level, dma_level,
    board_num, dataval, chanlo        : integer;


begin
  lsv := 1.345;  hsv := 5.970;  lsv_out := 0.960;  hsv_out := 4.800;
  llim := 2;  hlim := 8;
  pg := 7; rm := 10; dm := 0;
  up := 1; {1 PID update per/sec}
  board_num := 0; int_level := 7;  dma_level := 1;
  chanlo := 0; base_adr := $300;
  d16_init(board_num,base_adr,int_level,dma_level,err_code);

  i := 0;
  se := 0;
  ne := 0;
  clrscr;
  writeln('Enter the target flow rate setpoint in gpm:  ');
  readln(set_gpm);
  setpnt :=  set_gpm / 745.946 * 5 + 1.345;
  writeln('The setpoint is =  ',setpnt:8:5);
  write('Press any key to exit program');
  up := 1;
  repeat
    begin
      i := 0;
      chanlo := i;
      d16_ains(board_num,chanlo,dataval,err_code);
      volts := dataval / 409.5; {convert to 0 - 10 V range}
      gotoxy(18,8);
      writeln('ADC units input = ',dataval:4,'       Volts = ',volts:5:3);
      calc_pid_1(volts,lsv_out,hsv_out,setpnt,pg,rm,dm,up,ne,se,valout);
      dataval := valout + 786;
      out_volt := dataval / 3931 * 4.8;
      gotoxy(16,22);
      writeln('DAC units output = ',dataval:4,'   Output Volts = ',out_volt:5:3);
      d16_aous(board_num,chanlo,dataval,err_code);
      writeln('DAC units output = ',dataval:4);
      write('Error Code = ',err_code:2);
      d16_print_error(err_code);
      end;
    delay(round(up * 1000)); {convert update period to msec}
  until keypressed or (err_code <> 0);
end.
```

"tp4pid_1.tpu"

```
Unit TP4PID_1;

INTERFACE
procedure calc_pid_1(current_val,lsv_out,hsv_out,setpoint, prop_gain,
                     reset_min, deriv_min, update_rate: real;
                var  new_error, sum_error: real;
                var  aot_count: integer);

IMPLEMENTATION

procedure calc_pid_1(current_val,lsv_out,hsv_out,setpoint, prop_gain,
                     reset_min, deriv_min, update_rate: real;
                var  new_error, sum_error: real;
                var  aot_count: integer);

const max_conv_num = 3145; min_conv_num = 0;
var  scan_min, aot_count_real, old_error, pid_calc,
    proport_cntrl, integ_cntrl, deriv_cntrl : real;
begin
     scan_min := update_rate/60;
     old_error := new_error;
     sum_error := sum_error + old_error;
     new_error := setpoint - current_val;
     proport_cntrl := new_error * prop_gain;
     deriv_cntrl   := prop_gain * deriv_min / scan_min *
                      (new_error - old_error);
     integ_cntrl   := sum_error * reset_min * prop_gain * scan_min;

     pid_calc      := proport_cntrl + integ_cntrl + deriv_cntrl;
     aot_count_real := max_conv_num * pid_calc / (hsv_out - lsv_out);

writeln('Current Value (Same as volts) = ',current_val:4:2);
writeln('Update Rate (up) = ',update_rate:2);
writeln('Scan Minutes = ',scan_min:6:4);
writeln('Old Error (oe) = ',old_error:6:4);
writeln('Sum Error (se) = ',sum_error:6:4);
writeln('New Error (ne) = ',new_error:6:4);
writeln('Proportional Control Factor (proport_cntrl) = ',proport_cntrl:10:4);
writeln('Integral Control Factor (integ_cntrl) = ',integ_cntrl:10:4);
writeln('Derivative Control Factor (deriv_cntrl) = ',deriv_cntrl:10:4);
writeln('Pid Calculation (pid_calc) = ',pid_calc:10:4);
writeln('Output Value (aot_count_real) = ',aot_count_real:10:4);

     if (aot_count_real > max_conv_num) or
      (aot_count_real < min_conv_num) then
     begin
       if aot_count_real > max_conv_num then aot_count_real := max_conv_num;
       if aot_count_real < min_conv_num then aot_count_real := min_conv_num;
```

```
    end;
    aot_count := round(aot_count_real);
end;

end.
```

"tp4d16.tpu"

```
UNIT tp4d16;

INTERFACE

uses DOS;

var xxx: integer;
type
d16_gv_type = record
                auto,
                basadr,
                c0cfg,
                ctltmp,
                dmalev,
                dof,
                dptr,
                fcnt,
                fptr,
                intlev,
                imr,
                memend,
                memoff,
                memseg,
                mode,
                oldmemoff,
                oldmemseg,
                opflg,
                starr,
                sof,
                vecadr,
                vofs,
                wcnt,
                muxconfig,
                dmaflg,
                ftt,
                intflg: integer;
                oldvec: pointer;
                c1dat,
                c2dat: word;
```

```
                ain_lb,
                ain_hb,
                mux_ctrl,
                din,
                aot0_lb,
                aot0_hb,
                aot1_lb,
                aot1_hb,
                d16_stat,
                d16_ctrl,
                cntr_enable,
                gain_cntrl,
                cntr0,
                cntr1,
                cntr2,
                cntr_ctrl: integer;

              end;

var
  d16_gv: array[0..3] of d16_gv_type;


procedure d16_print_error(error_num: integer);

procedure d16_calc_timer_values(var freq:  real;
                            var c1,c2: word);

function  d16_ain_fast(board:    integer;
                var err_code: integer): integer;

procedure  d16_set_pit_ratio(board: integer;
                        n1,n2: word;
                    var err_code:    integer);

procedure GetDMABuffer( size: word;
                    var dmapntr: pointer;
                    var errcode: integer);

procedure FreeDMABuffer(size: word;
                    dmapntr: pointer;
                    var errcode: integer);

procedure d16_init(board,
                base_adr,
                int_lev,
                dma_lev:  integer;
             var err_code: integer);

procedure D16_set_gain(board, gain_setting: integer; var err_code: integer);
```

```
procedure d16_set_mux(board,
                      low_lim,
                      high_lim: integer;
                   var err_code: integer);

procedure d16_read_mux(board:    integer;
                    var low_lim,
                        high_lim,
                        next_ch,
                        err_code: integer);

procedure d16_ain_inc_mux(board:    integer;
                      var ain_data,
                          ch_num,
                          err_code: integer);

procedure d16_ain_direct(board,
                         count,
                         trigger:  integer;
                       var target,
                         err_code: integer);

procedure  d16_ain_int(board,
                       count,
                       trigger,
                       cycle:    integer;
                    var target,
                       err_code: integer);

procedure  d16_ain_dma(board,
                       count,
                       trigger,
                       cycle:    integer;
                    var target,
                       err_code: integer);

procedure d16_dma_int_disable(board: integer; var err_code:integer);

procedure  d16_dma_int_status(board:    integer;
                        var op_type,
                            status,
                            count,
                            err_code: integer);

procedure d16_convert_data(volt_offset,
                           word_count: integer;
                        var source_adr,
                            data_adr,
                            chan_adr:   integer;
                            chan_flag:  integer;
```

```
                var err_code:   integer);

procedure  d16_set_cntr0_config(board,
                        config_num: integer;
                    var err_code:   integer);

procedure  d16_cset0(board,
                counter_data: word;
              var err_code:     integer);

procedure  d16_cins0(board,
                read_type: integer;
              var cntr_data: word;
              var err_code:  integer);

procedure  d16_bous(board,
                dot_out:  integer;
             var err_code: integer);

procedure  d16_bins(board:     integer;
             var din_in,
                err_code:  integer);

procedure  d16_aous(board,
                channel_num,
                dataval:   integer;
             var err_code:  integer);

procedure  d16_set_two_aot(board,
                    dataval0,
                    dataval1: integer;
                  var err_code: integer);

procedure  d16_ains(board,
                chanlo:   integer;
             var dataval,
                err_code: integer);

procedure d16_ainm(board,
                chanlo,
                mode,
                cycle,
                trigger,
                count:    integer;
             var rate:     real;
             var data_pntr,
                err_code: integer);

procedure d16_ainsc(board,
                chanlo,
```

```
                chanhi,
                mode,
                cycle,
                trigger,
                count:    integer;
            var rate:     real;
            var data_pntr,
                err_code: integer);

IMPLEMENTATION
const
    min_base_adr = $FF;
    max_base_adr = $3f0;
    min_int_lev = 2;
    max_int_lev = 7;
    dma_lev_1 = 1;
    dma_lev_2 = 3;
    int_dseg_save: integer = 0;
type
    regt = record
             ax,bx,cx,dx,bp,si,di,ds,es,flags:integer;
           end;

procedure d16_print_error(error_num: integer);
type line_type = string[80];
const  d16_error_messages: array[0..24] of line_type =

        (
{  0 }    'No error',
{  1 }    'Driver not initialized (use d8_init)',
{  2 }    'Board number out of range (0-3)',
{  3 }    'Base address out of range ($100 - $3F0)',
{  4 }    'Interrupt level out of range (2-7)',
{  5 }    'DMA level out of range (1,3)',
{  6 }    'Mux scan limits out of range',
{  7 }    'Mux channel out of range',
{  8 }    'Counter # out of range (0-2)',
{  9 }    'A/D timeout error (no EOC)',
{  10 }   'Counter divison ratio 0 or 1 in set_pit_ratio',
{  11 }   'Number of conversion out of range (1 - 32767)',
{  12 }   'Counter configuration # out of range',
{  13 }   'Digital output data out of range',
{  14 }   'D/A data out of range',
{  15 }   'D/A channel out of range (0,1)',
{  16 }   'Counter read operation out of range (0,1)',
{  17 }   'Cycle mode out of range',
{  18 }   'Insufficient Memory for DMA Buffer Request ',
{  19 }   'Trigger mode out of range (0,1)',
{  20 }   'DMA or interrupt operation already active',
{  21 }   'Trigger channel out of range (d8_ain_on_trigger)',
```

```
{ 22 }      'Trigger level out of range (-2048 - 2047)',
{ 23 }      'Trigger slope out of range (0,1)',
{ 24 }      'Mode out of range (0-2)'
                                    );
begin
  writeln(d16_error_messages[error_num]);
end;


function d16_check_eoc(board: integer): boolean;
var i: byte;
begin
  d16_check_eoc := true;
  with d16_gv[board] do
  begin
    i := 1;
    repeat
      i := i + 1;
    until ((port[d16_stat] and $80) <> $80) or (i > 100);
    if i > 100 then
    d16_check_eoc := false;
  end;
end;


procedure d16_calc_timer_values(var freq:  real;
                                var c1,c2: word);

const clock_freq = 1000000.0;
var   divisor : real;
      c1r,c2r: real;
begin
  divisor := clock_freq / freq;
  c1 := 1;
  repeat
    c1 := c1 + 1;
    c2r := divisor / c1;
  until c2r < maxint;
  c1r := c1;
  c2 := round(c2r);
  c2r := c2;
  freq := clock_freq / (c1r * c2r);
end;


function  d16_ain_fast(board:    integer;
                  var err_code: integer): integer;

var i: integer;
begin
```

```
  with d16_gv[board] do
  begin
    port[ain_lb] := $FF;
    i := 1;
    repeat
      i := i + 1;
    until ((port[d16_stat] and $80) <> $80) or (i > 100);
    if i > 100 then
      err_code := 9
    else
    d16_ain_fast := ((swap(port[ain_hb]) or port[ain_lb]) shr 4) - vofs;
  end;
end;

procedure  d16_set_pit_ratio(board: integer;
                             n1,n2: word;
                         var err_code:    integer);
begin
  err_code := 0;
  if (board < 0) or (board > 3) then err_code := 2
  else
  with d16_gv[board] do
  begin
    if ftt <> 1 then err_code := 1
    else
      if (n1 = 1) or (n1 = 0) or (n2 = 1) or (n2 = 0)  then
         err_code := 10
      else
      begin
        c1dat := n1; c2dat := n2;
        port[cntr_ctrl] := $b4;
        port[cntr_ctrl] := $74;
        port[cntr2] := lo(n2);
        port[cntr2] := hi(n2);
        port[cntr1] := lo(n1);
        port[cntr1] := hi(n1);
      end;
  end;
end;

{ Notice for Das-16G users.

A new procedure has been added for controlling the Das-16G gain:
The board parameter is the same as the board parameter for the other Das-16
routines.  The gain setting parameter can have a value of 0 to 3.  For the
Das-16G1 values of 0,1,2,3 will cause the gain of programmable amplifier to
be set at 1, 10, 100, and 500 respectively.  For the Das-16G2 values of
0,1,2,3 will cause the gain of the programmable amplifier to be set at 1,2,4
and 8 respectively.
}
```

```
procedure D16_set_gain(board, gain_setting: integer; var err_code: integer);
begin
  err_code := 0;
  if (board < 0) or (board > 3) then err_code := 2
  else
  with d16_gv[board] do
  begin
    if ftt <> 1 then err_code := 1
    else
      port[gain_cntrl] := gain_setting;
  end;
end;

procedure GetDMABuffer
  ( size: word;         {Size in bytes of buffer to allocate - Maximum
                        allowable value is 65521 bytes}
var dmapntr: pointer;  {Returns a generic pointer to the buffer}
var errcode: integer); {Returns 18 if insufficient memory}

{Make sure you call FreeDMABuffer when you are finished with the
 DMA buffer.  }

var TopOfHeap, tpntr: pointer;
    i,j,k,l: longint;
begin
  errcode := 0;
  if MaxAvail < size then
    errcode := 18
  else
  begin
    Mark(TopOfHeap);
    i := 16 * seg(TopOfHeap^) + ofs(TopOfHeap^);
    j := i + size;
    if (i div $10000) <> (j div $10000) then
    begin
      k := ((i div $10000)+1) * $10000;
      l := k - i;
      If MaxAvail < (l+size) then
        errcode := 18
      else
      begin
        GetMem(tpntr,l);
        GetMem(dmapntr,size);
        FreeMem(tpntr,l);
      end;
    end
    else
    begin
      GetMem(dmapntr,size);
    end;
```

```
  end;
  if dmapntr = nil then errcode := 18;
end;

procedure FreeDMABuffer
   (size: word;        {Size of buffer associated with dmapntr}
    dmapntr: pointer;  {Pointer allocated with GetDMABuffer}
var errcode: integer); {Returns 18 if pointer already NIL}

begin
  if (dmapntr = nil) then
    errcode := 18
  else
  begin
    FreeMem(dmapntr,size);
    errcode := 0;
  end;
end;


procedure d16_init(board,
                   base_adr,
                   int_lev,
                   dma_lev:  integer;
                var err_code: integer);

var temp_val: integer;
begin
  err_code := 0;
  if (board < 0) or (board > 3) then err_code := 2
  else
  if (base_adr < min_base_adr) or (base_adr > max_base_adr) then
    err_code := 3
  else
    If (int_lev < min_int_lev) or (int_lev > max_int_lev) then
      err_code := 4
    else
      if (dma_lev <> dma_lev_1) and (dma_lev <> dma_lev_2) then
        err_code := 5
      else
      begin
        with d16_gv[board] do
        begin
          intlev := int_lev;
          dmalev := dma_lev;

          ain_lb := base_adr + 0;
          ain_hb:= base_adr + 1;
          mux_ctrl:= base_adr + 2;
          din:= base_adr + 3;
```

```
        aot0_lb:= base_adr + 4;
        aot0_hb:= base_adr + 5;
        aot1_lb:= base_adr + 6;
        aot1_hb:= base_adr + 7;
        d16_stat:= base_adr + 8;
        d16_ctrl:= base_adr + 9;
        cntr_enable:= base_adr + 10;
        gain_cntrl := base_adr + 11;
        cntr0:= base_adr + 12;
        cntr1:= base_adr + 13;
        cntr2:= base_adr + 14;
        cntr_ctrl := base_adr +  15;

        if ($20 and port[d16_stat]) = $20  then
        begin
          muxconfig := 16;
          port[mux_ctrl] := $f0;
        end
        else
        begin
          muxconfig := 8;
          port[mux_ctrl] := $70;
        end;
        if (port[d16_stat] and $40 ) = $40 then
          vofs := 0 else vofs := 2048;
        port[d16_ctrl] := 0;
        port[cntr_enable] := 0;
        port[d16_stat] := 0;

        opflg := 0;
        dmaflg := 0;
        port[cntr_ctrl] := $30;
        ftt := 1;
        d16_set_pit_ratio(board,100,500,err_code);  {default timer setup}
        int_dseg_save := dseg;
      end;
    end;
end;


procedure d16_set_mux(board,
                      low_lim,
                      high_lim: integer;
                  var err_code: integer);

begin
  err_code := 0;
  if (board < 0) or (board > 3) then err_code := 2
  else
  with d16_gv[board] do
```

```
  begin
    if ftt <> 1 then err_code := 1
    else
    begin
      case muxconfig of
      16: if (low_lim < 0) or (low_lim > 15)
            or (high_lim > 15) or (high_lim < 0) then
             err_code := 6;
       8: if  (low_lim < 0) or (low_lim > 7)
             or (high_lim > 7) or (high_lim < 0) then
             err_code := 6;
      end;
      if err_code = 0 then
      begin
        port[mux_ctrl] := (high_lim shl 4) or low_lim;
      end;
    end;
  end;
end;

procedure d16_read_mux(board:    integer;
                  var low_lim,
                      high_lim,
                      next_ch,
                      err_code: integer);

var i,port_in: byte;
begin
  err_code := 0;
  if (board < 0) or (board > 3) then err_code := 2
  else
  with d16_gv[board] do
  begin
    if ftt <> 1  then err_code := 1
    else
        begin
          port_in := port[mux_ctrl];
          low_lim := port_in and $0F;
          high_lim := (port_in and $F0) shr 4;
          i := 1;
          repeat
            i := i + 1;
          until ((port[d16_stat] and $80) <> $80) or (i > 100);
          if i < 100 then
            next_ch := port[d16_stat] and $0f
          else
          begin
            next_ch := 0;
            err_code := 9;
          end;
```

```
      end;
  end;
end;

procedure d16_ain_inc_mux(board:    integer;
                      var ain_data,
                          ch_num,
                          err_code: integer);

var i: integer;
begin
  err_code := 0;
  if (board < 0) or (board > 3) then err_code := 2
  else
  with d16_gv[board] do
  begin
    if ftt <> 1 then err_code := 1
    else
    begin
      ctltmp := port[d16_ctrl];
      port[d16_ctrl] := ctltmp and $f4;
      inline($fa);
      port[ain_lb] := $ff;
      i := 1;
      repeat
        i := i + 1;
      until ((port[d16_stat] and $80) <> $80) or (i > 100);
      if i > 100 then
        err_code := 9
      else
      begin
        ain_data := (swap(port[ain_hb])) or port[ain_lb];
        ch_num := ain_data and $F;
        ain_data := (ain_data shr 4) - vofs;
        port[d16_ctrl] := ctltmp;
      end;
    end;
  end;
  inline($fb);
end;

procedure d16_ain_direct(board,
                         count,
                         trigger:  integer;
                      var target,
                         err_code: integer);

var  i, ofs_tmp, seg_tmp: integer;
begin
  err_code := 0;
```

```
  if (board < 0) or (board > 3) then err_code := 2
  else
  with d16_gv[board] do
  begin
    if ftt <> 1 then err_code := 1
    else
      if (count < 1) or (count > maxint) then err_code := 11
      else
      if  (trigger <> 0) and (trigger <> 1) then err_code := 19
      else
        begin
          ofs_tmp := ofs(target);
          seg_tmp := seg(target);
          port[d16_ctrl] := 0;
          i := 1;
          repeat
            i := i + 1;
          until ((port[d16_stat] and $80) <> $80) or (i > 100);
          if i > 100 then
            err_code := 9
          else
          begin
            port[d16_stat] := 0;
            port[mux_ctrl] := port[mux_ctrl];
            if trigger = 1 then
              repeat
              until ((1 and port[din]) = 1);
            port[d16_ctrl] := (trigger or $82);
            for i := 0 to count - 1 do
            begin
              repeat
              until (($10 and port[d16_stat]) = $10);
              memw[seg_tmp:ofs_tmp] := ((swap(port[ain_hb]) or port[ain_lb])
                                        shr 4) - vofs;

              port[d16_stat] := 0;
              ofs_tmp := ofs_tmp + 2;
            end;
          end;
        end;
  end;
end;


procedure d16_ain_int_handler0;
interrupt;
begin
xxx := xxx + 1;
  with d16_gv[0] do
  begin
```

```
    memw[memseg:memoff] := ((swap(port[ain_hb]) or port[ain_lb]) shr 4) - vofs;
    memoff := memoff + 2;
    wcnt := wcnt + 1;
    if wcnt = fcnt then
    begin
      if auto = 1 then
      begin
        memoff := starr;
        wcnt := 0;
      end
      else
      begin
        port[d16_ctrl] := 0;
        port[d16_stat] := 0;
        intflg := 0;
        SetIntVec(8+intlev,oldvec);
        port[$21] := imr;
      end
    end;
    port[d16_stat] := 0;
    port[$20] := $20;
  end;
end;

procedure d16_ain_int_handler1;
interrupt;
begin
  with d16_gv[1] do
  begin
    memw[memseg:memoff] := ((swap(port[ain_hb]) or port[ain_lb]) shr 4) - vofs;
    memoff := memoff + 2;
    wcnt := wcnt + 1;
    if wcnt = fcnt then
    begin
      if auto = 1 then
      begin
        memoff := starr;
        wcnt := 0;
      end
      else
      begin
        port[d16_ctrl] := 0;
        port[d16_stat] := 0;
        intflg := 0;
        SetIntVec(8+intlev,oldvec);
        port[$21] := imr;
      end
    end;
    port[d16_stat] := 0;
    port[$20] := $20;
```

```
  end;
end;


procedure  d16_ain_int(board,
                       count,
                       trigger,
                       cycle:    integer;
                   var target,
                       err_code: integer);

var temp, old_c1dat, old_c2dat,i,port_out:  integer;
    regs: registers;
begin
  xxx := 0;
  err_code := 0;
  if (board < 0) or (board > 1) then err_code := 2
  else
  with d16_gv[board] do
  begin
    if ftt <> 1 then err_code := 1
    else
      if (dmaflg or intflg) = 1 then err_code := 20
      else
        if (count < 1) or (count > maxint) then err_code := 11
        else
          if  (trigger <> 0) and (trigger <> 1) then err_code := 19
          else
            if (cycle <> 1) and (cycle <> 0) then err_code := 17
            else
            begin
              auto := cycle;
              old_c1dat := c1dat; old_c2dat := c2dat;
              d16_set_pit_ratio(board,$FFFF,$FFFF,err_code); {need to leave c1dat and d2dat
unchanged}
              port[d16_ctrl] := 0;
              port[d16_stat] := 0;
              wcnt := 0;
              fcnt := count;
              memoff := ofs(target); starr := ofs(target);
              memseg := seg(target);
              imr := port[$21];
              GetIntVec(8+intlev,oldvec);
              if board = 0 then
                SetIntVec(8+intlev,@d16_ain_int_handler0)
               else
                SetIntVec(8+intlev,@d16_ain_int_handler1);
              port[cntr_enable] := 1;
              if trigger = 1 then
                repeat
```

```
            until ((port[din] and 1) = 1);
          port[cntr_enable] := 0;
          port[$21] := ((1 shl intlev) xor $ff) and imr;
          port[d16_stat] := 0;
          port[d16_ctrl] := ((intlev shl 4) or $82) or trigger;
          memoff := ofs(target);
          temp := port[mux_ctrl];
          port[mux_ctrl] := temp;
          wcnt := 0;
          intflg := 1;
          opflg := 2;
          d16_set_pit_ratio(board,old_c1dat,old_c2dat,err_code);
        end;
  end;
end;


procedure d16_dma_int_handler0;
interrupt;
begin
  with d16_gv[0] do
  begin
    dmaflg := 0;
    port[d16_ctrl] := 0;
    port[d16_stat] := 0;
    SetIntVec(8+intlev,oldvec);
    port[$21] := imr;
    port[$20] := $20;
  end;
end;

procedure d16_dma_int_handler1;
interrupt;
begin
  with d16_gv[1] do
  begin
    dmaflg := 0;
    port[d16_ctrl] := 0;
    port[d16_stat] := 0;
    SetIntVec(8+intlev,oldvec);
    port[$21] := imr;
    port[$20] := $20;
  end;
end;



procedure  d16_ain_dma(board,
                       count,
                       trigger,
```

```
                cycle:    integer;
              var target,
                err_code: integer);

var i,old_c1dat, old_c2dat,
   port_num, port_int:      integer;
   port_out, port_in:       byte;
   regs: registers;
begin
  err_code := 0;
  if (board < 0) or (board > 1) then err_code := 2
  else
  with d16_gv[board] do
  begin
    if ftt <> 1 then err_code := 1
    else
      if (dmaflg or intflg) = 1 then err_code := 20
      else
        if (count < 1) or (count > maxint) then err_code := 11
        else
          if  (trigger <> 0) and (trigger <> 1) then err_code := 19
          else
            if (cycle <> 1) and (cycle <> 0) then err_code := 17
            else
            begin
              memseg := seg(target);
              wcnt := count;
              auto := cycle;

              port[$0a] := dmalev or $04;
              old_c1dat := c1dat; old_c2dat := c2dat;
              d16_set_pit_ratio(board,$FFFF,$FFFF,err_code);  {need to leave c1dat and d2dat
unchanged}
              port[d16_ctrl] := 0;
              port_out :=  ((2 + trigger) or (((auto shl 3) or intlev) shl 4)
                                xor $80) ;
              port[d16_ctrl] := port_out and 3;
              for i := 1 to 100 do ;     {delay}
              port[d16_stat] := 0;
              port[d16_ctrl] :=  port_out or $04;
              port[cntr_enable] := 1;
              if dmalev = 3 then
                port[$82] := memseg shr 12   {dma level 3}
              else
                port[$83] := memseg shr 12;   {dma level 1}
              port_int := memseg shl 4;
              port_num := dmalev shl 1;

              inline($fa);
              port[$0C] := lo(port_int);
```

```
            port[port_num] := lo(port_int);
            port[port_num] := hi(port_int);
            port_int := (wcnt shl 1) - 1;
            port[port_num + 1] := lo(port_int);
            port[port_num + 1] := hi(port_int);
            inline($fb);

            if auto = 1 then
              port[$B] := dmalev or $10 or $44
            else
              port[$b] := dmalev or $44;
            GetIntVec(8+intlev,oldvec);
            if board = 0 then
              SetIntVec(8+intlev,@d16_dma_int_handler0)
             else
              SetIntVec(8+intlev,@d16_dma_int_handler1);

            imr := port[$21] ;
            if auto = 0 then
              port[$21] := imr and ((1 shl intlev) xor $FF);
            if trigger = 1 then
            repeat
            until (port[din] and $01) = $01;
            port[cntr_enable] := 0;
            port_out := port[mux_ctrl];
            port[mux_ctrl] := port_out;
            port[$0a] := dmalev;
            d16_set_pit_ratio(board,old_c1dat,old_c2dat,err_code);
            opflg := 1;
            dmaflg := 1;
          end;
  end;
end;

procedure d16_dma_int_disable(board: integer; var err_code:integer);
var regs: registers;
begin
  if (board < 0) or (board > 1) then err_code := 2
  else
  with d16_gv[board] do
  begin
    port[$a] := dmalev or 4;
    port[$21] := port[$21] or (1 shl intlev);
    SetIntVec(8+intlev,oldvec);
    port[$21] := imr;
    opflg := 0;
    intflg := 0;
    dmaflg := 0;
  end;
end;
```

```
procedure  d16_dma_int_status(board:    integer;
                        var op_type,
                            status,
                            count,
                            err_code: integer);

var port_num, countl,counth: integer;
begin
  err_code := 0;
  if (board < 0) or (board > 1) then err_code := 2
  else
  with d16_gv[board] do
  begin
    case opflg of
    1: begin
         op_type := opflg;
         status := dmaflg;
         port_num := (dmalev shl 1) + 1;
         inline($fa);
         port[$0C] := 0;
         countl :=  port[port_num];
         counth := port[port_num];
         inline($fb);
         count := ((swap(counth) or countl) +1) shr 1;
         count := wcnt - count;
       end;
    2: begin
         op_type := 2;
         status := intflg;
         count  := wcnt + 1;
       end;

  else begin
         op_type := 0;
         status := 0;
         count := 0;
       end;
    end;
  end;
end;


procedure d16_convert_data(volt_offset,
                           word_count: integer;
                       var source_adr,
                           data_adr,
                           chan_adr:   integer;
                           chan_flag:  integer;
                       var err_code:   integer);
```

```
var i,byte_count,
    data_ofs, data_seg,
    chan_ofs, chan_seg,
    ofs_count, temp_val: integer;
begin
    err_code := 0;
    if word_count <= 0  then err_code := 11
    else
      begin
        byte_count := word_count shl 1;
        move(source_adr,data_adr,byte_count);
        if chan_flag <> 0 then
          move(source_adr,chan_adr,byte_count);
        data_ofs := ofs(data_adr);
        data_seg := seg(data_adr);
        for i := 0 to word_count - 1 do
        begin
          memw[data_seg:data_ofs] := (memw[data_seg:data_ofs]  shr 4) -
                                     volt_offset;
          data_ofs := data_ofs + 2;
        end;
        if chan_flag <> 0 then
        begin
          chan_ofs := ofs(chan_adr);
          chan_seg := seg(chan_adr);
          for i := 0 to word_count - 1 do
          begin
            memw[chan_seg:chan_ofs] := memw[chan_seg:chan_ofs]  and $f;
            chan_ofs := chan_ofs + 2;
          end;
        end;
      end;
end;


procedure  d16_set_cntr0_config(board,
                                config_num: integer;
                           var err_code:    integer);

begin
  if (board < 0) or (board > 3) then err_code := 2
  else
  with d16_gv[board] do
  begin
    if ftt <> 1 then err_code := 1
    else
      if (config_num < 0) or (config_num > 5) then
        err_code := 12
      else
      begin
```

```
      port[cntr_ctrl] := (config_num  or $18) shl 1;
      c0cfg := config_num;
    end;
  end;
end;

procedure  d16_cset0(board,
                     counter_data: word;
                 var err_code:     integer);
begin
  err_code := 0;
  if (board < 0) or (board > 3) then err_code := 2
  else
  with d16_gv[board] do
  begin
    if ftt <> 1 then err_code := 1
    else
    begin
      port[cntr_ctrl] := c0cfg;
      port[cntr0] := lo(counter_data);
      port[cntr0] := hi(counter_data);
    end;
  end;
end;

procedure  d16_cins0(board,
                     read_type: integer;
                 var cntr_data: word;
                 var err_code:  integer);

var cntr_data_l, cntr_data_h: integer;
begin
  err_code := 0;
  if (board < 0) or (board > 3) then err_code := 2
  else
  with d16_gv[board] do
  begin
    if ftt <> 1 then err_code := 1
    else
      if (read_type <> 0) and (read_type <> 1) then err_code := 16
      else
      begin
        if read_type = 1 then port[cntr_ctrl] := 0;
        cntr_data_l := port[cntr0];
        cntr_data_h := port[cntr0];
        cntr_data := swap(cntr_data_h) or cntr_data_l;
      end;
  end;
end;
```

```
procedure  d16_bous(board,
                    dot_out:  integer;
                var err_code: integer);
begin
  err_code := 0;
  if (board < 0) or (board > 3) then err_code := 2
  else
  with d16_gv[board] do
  begin
    if ftt <> 1 then err_code := 1
    else
      if (dot_out < 0) or (dot_out > 15) then  err_code :=13
      else
      begin
        port[din] := dot_out and $F;
      end;
  end;
end;


procedure  d16_bins(board:     integer;
               var din_in,
                   err_code:  integer);

begin
  err_code := 0;
  if (board < 0) or (board > 3) then err_code := 2
  else
  with d16_gv[board] do
  begin
    if ftt <> 1 then err_code := 1
    else
      begin
        din_in := port[din] and $F;
      end;
  end;
end;

procedure  d16_aous(board,
                    channel_num,
                    dataval:   integer;
               var err_code:  integer);

begin
  err_code := 0;
  if (board < 0) or (board > 3) then err_code := 2
  else
  with d16_gv[board] do
  begin
    if ftt <> 1 then err_code := 1
```

```
    else
      if (channel_num < > 0) and (channel_num < > 1) then err_code := 15
      else
        if (dataval < 0) or (dataval > 4095) then err_code := 14
        else
        begin
          dataval := dataval shl 4;
          case channel_num of
          0: begin
               port[aot0_lb] := lo(dataval);
               port[aot0_hb] := hi(dataval);
             end;
          1: begin
               port[aot1_lb] := lo(dataval);
               port[aot1_hb] := hi(dataval);
             end;
          end;
        end;
  end;
end;

procedure  d16_set_two_aot(board,
                           dataval0,
                           dataval1: integer;
                       var err_code: integer);
begin
  err_code := 0;
  if (board < 0) or (board > 3) then err_code := 2
  else
  with d16_gv[board] do
  begin
    if ftt < > 1 then err_code := 1
    else
        if (dataval0 < 0) or (dataval0 > 4095) or
          (dataval1 < 0) or (dataval1 > 4095) then err_code := 14
        else
        begin
          dataval0 := dataval0 shl 4;
          dataval1 := dataval1 shl 4;
               port[aot0_lb] := lo(dataval0);
               port[aot0_hb] := hi(dataval0);
               port[aot1_lb] := lo(dataval1);
               port[aot1_hb] := hi(dataval1);
        end;
  end;
end;


procedure  d16_ains(board,
                    chanlo:   integer;
```

```
            var dataval,
                err_code: integer);
begin
  err_code := 0;
  d16_set_mux(board,chanlo,chanlo,err_code);
  if err_code = 0 then
    d16_ain_inc_mux(board,dataval,chanlo,err_code);
end;

procedure d16_ainm(board,
                   chanlo,
                   mode,
                   cycle,
                   trigger,
                   count:    integer;
                 var rate:   real;
                 var data_pntr,
                   err_code: integer);

var c1dat,c2dat: word;
begin
 err_code := 0;
 if (board < 0) or (board > 3) or ((board > 1) and (mode > 0))
 then err_code := 2
 else
 if (mode < 0) or (mode > 2) then err_code := 24
 else
 begin
   d16_set_mux(board,chanlo,chanlo,err_code);
   if err_code = 0 then
   begin
     d16_calc_timer_values(rate,c1dat,c2dat);
     d16_set_pit_ratio(board,c1dat,c2dat,err_code);
     if err_code = 0 then
     begin
       case mode of
         0: d16_ain_direct(board, count,trigger,data_pntr,err_code);
         1: d16_ain_int(board,count,trigger,cycle,data_pntr,err_code);
         2: d16_ain_dma(board,count,trigger,cycle,data_pntr,err_code);
       end;
     end;
   end;
 end;
end;

procedure d16_ainsc(board,
                    chanlo,
                    chanhi,
                    mode,
                    cycle,
```

```
                trigger,
                count:    integer;
            var rate:     real;
            var data_pntr,
                err_code: integer);

var c1dat,c2dat: word;
begin
  err_code := 0;
  if (board < 0) or (board > 3) or ((board > 1) and (mode > 0))
  then err_code := 2
  else
  if (mode < 0) or (mode > 2) then err_code := 24
  else
  begin
    d16_set_mux(board,chanlo,chanhi,err_code);
    if err_code = 0 then
    begin
      d16_calc_timer_values(rate,c1dat,c2dat);
      d16_set_pit_ratio(board,c1dat,c2dat,err_code);
      if err_code = 0 then
      begin
        case mode of
          0: d16_ain_direct(board,count,trigger,data_pntr,err_code);
          1: d16_ain_int(board,count,trigger,cycle,data_pntr,err_code);
          2: d16_ain_dma(board,count,trigger,cycle,data_pntr,err_code);
        end;
      end;
    end;
  end;
end;


end.
```

APPENDIX XI. COMPUTER-AIDED DATA ANALYSIS TECHNIQUES

Several computer-aided data analysis techniques were used during the course of this project. This Appendix describes and lists some of the more vital programs which were developed during the course of the project for data analysis.

I. A LabCalc program written in Array Basic was utilized for transferring a binary file to a trace that may be read by LabCalc's peak frequency tracking parameters.

II. A SAS software program for generating and plotting a three-dimensional spline interpolation of an imported three-column ASCII data set.

III. A W.A.V.E. macro for reading a CODAS-generated data file, calculating the mean, root mean square, maximum and minimum conductivities, the Fourier Transform spectrum, the autocorrelation function and the Fourier of the autocorrelation, and writing the results to a floating point decimal, 32 bit binary file.

I. LabCalc program

```
free

dim length(1)
dim lngth_wfm(1)
dim ymean(1)
dim ymax(1)
dim ymin(1)
dim name(90), name1(90), name2(90)
dim line(90), line2(90)
dim valuex(20000)
dim valuey(20000)

string name - "dir a:\"
string name(7+i,7+i+5) = "*.BIN"
i = index0(name)
string name(i,i+15) = " >A:\z.tmp"
```

```
        dos $name
        string name = "A:\z.tmp"
        open "O", #1, $name
        onerror 100
        input #1, " ", $line

100     onerror 200
        input #1, " ", $line

        onerror -1
        ecnt = 0
        i = index0(line - 40)
        if i<index0(line) goto 300
        if line(3) > 95 goto 100
        i = index0(line - 32)
        j = index0(line)
        if j<i then i=j
        if i=0 or i > 8 goto 100

        q = index0(line - 32)
        string name1 = $line(0,q-1)
        z = index0(name1)

        string name2 = "A:\"
        string name2(3,3+z) = $name1
        string name2(3+z,7+z) = ".BIN"

        open "O", #2, $name2
        read #2, length, lngth_wfm, ymax, ymin

        i = length
        for j = 0 to i-1
        read #2, valuex(j)
        next j

        for k = 0 to i-1
        read #2, valuey(k)
        next k

        newspc trace(length)
        xadjust trace = valuex, valuey

        string line = "B:\"
        string line(3,3+z) = $name1
        string line(3+z,7+z) = ".spc"
        savespc $line
        close #2

        noshow
        goto 100
```

```
200   ecnt = ecnt+1
      if ecnt < 3 goto 100

300   onerror -1
      close #1
      kill $name
      end
```

II. SAS program

```
goptions gaccess='sasgastd>com2' dev=hp7470 gprolog='494e3b';
data d3data;
input x y z;
carda;
        0      0    6400
        3      0  98.272
        3   0.25  105.638
        3    0.5  107.061
        3   0.75  108.051
        3      1  110.409
        3   1.25  116.293
        3  1.318  121.715
        3    1.5  133.66
        3  1.568   137.01
        3   1.75  163.449
        3  1.818  200.782
        3  2.068  222.258
        3  2.318  294.329
        3  2.568  278.657
        3  2.818  236.448
        3  3.068  199.717
        9      0  93.4301
        9   0.25  104.864
        9    0.5  107.011
        9   0.75  107.494
        9      1  108.473
        9   1.25     134
        9  1.318  158.637
        9    1.5     155
        9  1.568  168.019
        9   1.75     163
        9  1.818  167.517
        9  2.068  188.657
        9  2.318  208.742
        9  2.568  242.546
        9  2.818   258.1
        9  3.068  255.731
```

```
        15      0  101.253
        15   0.25   121.37
        15    0.5  146.031
        15   0.75  168.974
        15      1  153.519
        15   1.25      167
        15  1.318  176.644
        15    1.5      159
        15  1.568  163.943
        15   1.75  153.037
        15  1.818  163.929
        15  2.068  179.163
        15  2.318  183.476
        15  2.568  203.988
        15  2.818  197.733
        15  3.068  185.005
;
run;
proc g3grid data = d3data out = data2;
grid x*y = z/spline;
run;
title1 's27m';
title2 'spline interpolation';
proc g3d data = data2;
plot x*y = z / rotate = 15 tilt = 55;
run;
```

III. W.A.V.E. macro

```
dir c:\
DIR labcalc\ascii
# PULLS IN A CODAS FILE AND CALCULATES THE FFT AND AUTO-FFT

show i
finit ( $2 )
frecv ( ystring )
the_length = val( ystring, yvalue )
xwave = 0.001..( the_length/1000 ); 0.001
xvalue = xwave:x
wfm = xy( xvalue, yvalue )
ymean = mean( yvalue )
wfm = wfm - ymean
delete ystring yvalue xwave xvalue

show i
fft1 = mag( dft( the_length, wfm ) )
```

```
ted = conv( wfm, rev( wfm ) )
tedfft = mag( dft( the_length, ted ) )

if $1 = 1
plot 1 wfm
plot 2 fft1
plot 3 ted
plot 4 tedfft
endif

fclose

DIR C:\
# TAKES THE DATA ABOVE AND SENDS IT TO A BINARY FILE

DIR labcalc\binary
finit ( $2 )
lengthvec = [ length( wfm ), length( fft1 ), length( tedfft ) ]

show i
fsendb( ymean, FLOAT )
fsendb( lengthvec, FLOAT )
fsendb( wfm:x, FLOAT )
fsendb( wfm:y, FLOAT )
fsendb( fft1:x, FLOAT )
fsendb( fft1:y, FLOAT )
fsendb( tedfft:x, FLOAT )
fsendb( tedfft:y, FLOAT )
fclose

show i
the_length = lengt( wfm )
the_max = max( wfm )
the_min = min( wfm )

show i
tedfft2 = mag( dft( length( ted ), ted ) )
length_ted = length( tedfft2 )

DIR C:\
# NOW WE SEND IT TO A FINAL BINARY FILE FOR READING INTO LABCALC

DIR labcalc
finit ( $2 )
fsendb( length_ted, FLOAT )
fsendb( the_length, FLOAT )
fsendb( ymean, FLOAT )
fsendb( the_max, FLOAT )
fsendb( the_min, FLOAT )
fsendb( tedfft2:x, FLOAT )
```

```
fsendb( tedfft2:y, FLOAT )
fclose

DIR C:\
delete the_length wfm ymean fft1 ted tedfft lengthvec
delete the_max the_min tedfft2 length_ted
```

APPENDIX XII. TABULATED CONDUCTIVITY DATA

Table A4. Tabulated conductivities as presented in Figures 24 through 28 and A8 through A60. The table shows the "DATE" code of the experiment; a "W" denotes an experiment with water flow. The "CODE" corresponds with the list given in Table 4 (Page 73). The next two columns give the location and position of the conductivity probe for the data set. The following columns are: length of the file, or the number of data points taken; the mean of the data set; the baseline conductivity of the water without injected material; the maximum and minimum data point of the set; the root-mean-square of the set; and finally, the result of subtracting the baseline from the mean, or the mean result of the injected polymer at that position.

DATE	CODE	LOC	POS	LENGTH	MEAN	BASELINE	MAX	MIN	RMS	MEAN-BL
JL3 W	B	1	1	1689	425.927	66.0387	225.77	-220.73	433.57	359.888
	B	1	2	1848	287.352	68.2818	228.95	-185.55	298.25	219.07
	B	1	3	1898	119.521	68.2818	328.68	-53.091	128.05	51.2392
	B	1	4	3280	73.9629	68.2818	141.34	-11.733	74.947	5.6811
	B	1	5	2503	67.9371	67.9371	6.0628	-4.8671	67.979	0
	B	1	6	1459	66.5321	66.5321	5.7879	-5.1421	66.575	0
	B	1	7	1042	68.8801	68.8801	5.9599	-4.9701	68.92	0
	B	2	1	1488	294.275	57.631	92.026	-137.67	297.03	236.644
	B	2	2	910	241.924	59.8589	100.57	-141.23	245.34	182.065
	B	2	3	1347	165.861	59.8589	165.44	-87.561	171.6	106.002
	B	2	4	1789	111.388	59.8589	98.612	-52.018	115.76	51.5291
	B	2	5	146	105.652	59.8589	62.649	-44.932	109	45.7931
	B	2	6	1063	74.3834	60.1559	80.517	-21.033	76.078	14.2275
	B	2	7	4147	59.6779	59.6779	65.122	-8.0479	60.033	0
	B	2	8	893	61.1861	61.1861	6.7939	-5.2561	61.238	0
	B	3	1	1066	221.737	64.3058	45.563	-53.137	222.71	157.431
	B	3	2	797	205.541	66.4386	66.359	-78.641	207.68	139.102
8	B	3	3	1178	177.696	66.4386	67.904	-84.356	179.7	111.257
	B	3	4	1779	141.507	66.4386	58.793	-56.317	143.14	75.0684
	B	3	5	1033	127.556	66.4386	67.244	-50.526	129.68	61.1174
	B	3	6	2066	82.2206	66.4386	60.979	-22.411	83.409	15.782
	B	3	7	1604	71.0266	64.8363	55.873	-13.937	71.904	6.1903
	B	3	8	2783	69.7638	66.4386	68.036	-9.9538	70.257	3.3252
	B	4	1	169	62.1427	62.1427	9.0273	-4.8427	62.202	0
	B	4	2	116	67.7805	67.7805	6.1595	-4.9305	67.829	0
	B	4	3	145	66.8837	66.8837	6.1363	-4.9637	66.934	0
	B	4	4	206	67.2455	67.2455	5.7745	-5.3255	67.294	0
	B	4	5	149	66.7005	66.7005	6.3195	-4.7805	66.75	0
	B	4	6	127	66.5164	66.5164	5.5736	-4.5966	66.565	0
	B	4	7	105	68.861	68.861	5.9991	-5.091	68.913	0
	B	4	8	575	74.0812	74.0812	6.3288	-5.6912	74.127	0
	B	5	1	253	54.8615	54.8615	5.5485	-6.3515	54.925	0
	B	5	2	103	59.4835	59.4835	5.4965	-5.4835	59.539	0

Table A4, continued

DATE	CODE	LOC	POS	LENGTH	MEAN	BASELINE	MAX	MIN	RMS	MEAN-BL
	B	5	3	150	60.7551	60.7551	6.0649	-4.9251	60.809	0
	B	5	4	169	62.4051	62.4051	6.2349	-4.7451	62.458	0
	B	5	5	137	61.8632	61.8632	5.8668	-6.0332	61.918	0
	B	5	6	128	60.6936	60.6936	6.1164	-4.8636	60.747	0
	B	5	7	124	61.1085	61.1085	5.7015	-5.2785	61.164	0
	B	5	8	199	62.3663	62.3663	6.2737	-5.6163	62.418	0
	B	6	1	236	55.8001	55.8001	6.1299	-4.8	55.862	0
	B	6	2	223	57.7761	57.7761	5.9739	-4.956	57.834	0
	B	6	3	206	58.1408	58.1408	5.6092	-5.3208	58.194	0
	B	6	4	284	60.0317	60.0317	5.5383	-6.3017	60.09	0
	B	6	5	2259	64.3959	64.3959	6.6441	-6.1059	64.449	0
	B	6	6	3536	66.0542	66.0542	35.946	-6.8515	66.169	0
	B	6	7	3952	72.5525	65.1503	36.748	-7.8925	72.694	7.4022
	B	6	8	2725	72.5545	59.7376	51.871	-7.3494	72.696	12.8169
	B	7	1	144	54.7185	54.7185	6.6015	-5.2985	54.78	0
	B	7	2	113	55.4582	55.4582	5.8618	-5.1182	55.517	0
	B	7	3	1509	59.3779	59.3779	16.592	-6.2979	59.444	0
	B	7	4	1689	63.7138	63.2069	19.576	-6.0538	63.793	0.5069
	B	7	5	2797	66.3674	65.8126	20.583	-5.9574	66.436	0.5548
	B	7	6	2641	70.3285	68.698	57.772	-7.1785	70.568	1.6305
	B	7	7	3842	71.7452	70.5044	33.555	-8.5952	71.865	1.2408
	B	7	8	3711	65.1917	63.5871	36.746	-7.8945	65.279	1.6046
JL6 W	D	1	1	3336	463.133	97.6314	275.87	-234.73	469.5	365.502
	D	1	2	3647	467.383	103.708	218.62	-145.28	473.33	363.675
	D	1	3	2423	349.049	104.6	338.75	-184.55	358.35	244.449
	D	1	4	2523	178.439	104.674	298.96	-66.939	187.2	73.765
	D	1	5	1408	114.868	112.702	101.83	-7.8678	115.17	2.166
	D	1	6	422	112.532	112.532	6.1678	-4.6322	112.56	0
	D	1	7	235	112.339	112.339	5.4613	-4.4387	112.37	0
	D	1	8	231	112.4	112.4	5.4	-4.5	112.43	0
	D	2	1	1834	355.209	98.3206	127.69	-130.71	358.55	256.888
	D	2	2	1798	352.625	98.3206	150.78	-169.13	356.12	254.304
	D	2	3	2011	299.688	98.3206	159.11	-161.59	304.05	201.367
	D	2	4	2414	232.147	98.3206	152.75	-116.35	237.49	133.826
	D	2	5	1843	165.404	108.747	208.8	-59.404	170.59	56.657
	D	2	6	1650	120.588	108.697	151.11	-16.388	122.09	11.891
	D	2	7	2474	109.275	108.697	40.425	-5.9747	109.34	0.578
	D	2	8	795	108.774	108.774	13.326	-5.4741	108.81	0
	D	3	1	2537	251.434	98.5823	75.866	-109.33	253.47	152.852
	D	3	2	2646	246.621	98.5823	100.38	-109.02	249.06	148.039
	D	3	3	1908	230.851	98.5823	86.549	-84.251	232.7	132.269
	D	3	4	1869	196.019	98.5823	79.981	-70.119	198.19	97.4367
	D	3	5	2107	161.193	98.5823	104.91	-53.293	163.65	62.6107
	D	3	6	1943	132.888	98.5823	96.412	-27.688	134.54	34.3057
	D	3	7	2129	119.824	109.859	68.976	-15.524	120.62	9.965
	D	3	8	4957	115.492	109.472	73.308	-11.192	115.99	6.02
	D	4	1	435	108.068	108.068	5.2324	-5.5676	108.1	0

Table A4, continued

DATE	CODE	LOC	POS	LENGTH	MEAN	BASELINE	MAX	MIN	RMS	MEAN-BL
	D	4	2	247	115.49	115.49	5.9101	-4.8899	115.52	0
	D	4	3	813	116.749	116.749	5.5506	-5.2495	116.77	0
	D	4	4	933	117.285	117.285	18.515	-47.155	117.32	0
	D	4	5	451	117.533	117.533	7.4674	-5.1326	117.56	0
	D	4	6	563	117.498	117.498	4.8021	-8.6979	117.52	0
	D	4	7	275	117.62	117.62	4.68	-5.22	117.65	0
	D	4	8	515	117.662	117.662	4.6381	-5.2619	117.69	0
	D	5	1	199	113.416	113.416	4.9839	-4.9161	113.44	0
	D	5	2	569	122.955	122.955	14.245	-19.855	122.98	0
	D	5	3	451	125.429	125.429	5.4712	-5.2288	125.45	0
	D	5	4	982	125.465	125.465	5.4345	-24.166	125.49	0
	D	5	5	1051	123.183	123.183	5.0172	-4.7828	123.21	0
	D	5	6	1123	123.954	123.954	5.1461	-5.5539	123.98	0
	D	5	7	1195	126.109	126.109	15.591	-7.7094	126.13	0
	D	5	8	4737	124.782	124.718	47.418	-14.482	124.81	0.064
	D	6	1	121	100.774	100.774	9.6261	-5.1339	100.81	0
	D	6	2	157	109.356	109.356	6.544	-5.4561	109.39	0
	D	6	3	146	111.622	111.622	9.7781	-4.9219	111.65	0
	D	6	4	153	118.657	118.657	9.1431	-4.6569	118.68	0
	D	6	5	2561	125.815	125.815	10.285	-5.3152	125.84	0
	D	6	6	3873	169.341	168.384	19.159	-7.4415	169.37	0.957
	D	6	7	2461	162.832	161.804	42.268	-19.332	162.9	1.028
	D	6	8	3675	189.399	176.954	101.2	-27.499	189.74	12.445
	D	7	1	523	111.549	111.549	5.7511	-5.049	111.58	0
	D	7	2	1875	118.281	118.281	17.119	-19.911	118.31	0
	D	7	3	601	119.326	119.326	7.8739	-5.6261	119.35	0
	D	7	4	3438	119.912	119.42	62.388	-12.512	119.96	0.492
	D	7	5	2785	120.409	119.418	60.991	-14.809	120.49	0.991
	D	7	6	3715	120.153	119.426	79.247	-14.553	120.24	0.727
	D	7	7	2115	120.208	119.404	42.192	-8.3081	120.28	0.804
	D	7	8	4220	118.433	117.654	79.167	-38.113	118.52	0.779
	F	1	1	1255	157.6688	117.373	96.131	-34.069	159.09	40.2958
	F	1	2	2035	227.5517	117.373	154.55	-83.152	231.84	110.179
	F	1	3	2277	347.3032	125.001	180.1	-154.8	352.34	222.302
	F	1	4	2189	417.925	125.001	155.78	-194.33	421.2	292.924
	F	1	5	3057	297.264	125.001	221.74	-143.46	304.46	172.263
	F	1	6	2688	158.147	131.893	210.75	-31.747	161.25	26.254
	F	1	7	3693	130.734	129.922	81.566	-7.1339	130.83	0.812
	F	1	8	3747	129.935	129.935	25.765	-6.3347	129.96	0
	F	3	1	2675	170.322	107.95	59.878	-47.322	171.32	62.372
	F	3	2	1857	190.6596	107.95	54.234	-35.166	190.71	82.7096
	F	3	3	2184	203.147	107.95	49.153	-50.047	203.65	95.197
	F	3	4	2996	204.161	107.95	52.539	-57.161	204.76	96.211
	F	3	5	2016	203.8559	110.421	54.644	-49.856	204.58	93.4349
	F	3	6	1930	196.149	109.01	66.751	-55.349	197.42	87.139
	F	3	7	1626	177.5446	107.95	66.755	-46.545	178.98	69.5946
	F	3	8	2126	159.4836	138.125	89.316	-38.184	161.29	21.3586

Table A4, continued

DATE	CODE	LOC	POS	LENGTH	MEAN	BASELINE	MAX	MIN	RMS	MEAN-BL
	F	4	1	675	109.8489	109.8489	5.8511	-5.5489	109.88	0
	F	4	2	755	117.9219	117.9219	6.2972	-5.1219	117.95	0
	F	4	3	915	120.201	120.201	5.8992	-5.5008	120.23	0
	F	4	4	771	120.468	120.468	5.6318	-5.7682	120.5	0
	F	4	5	866	120.983	120.983	6.1167	-6.2633	121.01	0
	F	4	6	939	120.515	120.515	5.5846	-4.8154	120.54	0
	F	4	7	1779	121.963	121.963	6.037	-5.363	121.92	0
	F	4	8	2058	124.656	123.565	26.334	-6.8657	124.51	1.091
	F	6	1	157	150.382	150.382	5.8185	-4.0815	150.4	0
	F	6	2	595	155.84	155.27	22.759	-5.0408	155.88	0.57
	F	6	3	1859	164.234	163.18	9.8656	-7.1344	164.26	1.054
	F	6	4	2354	202.815	201.58	37.685	-9.915	202.86	1.235
	F	6	5	2181	218.162	212.832	87.838	-10.862	218.34	5.33
	F	6	6	2794	231.4898	212.906	80.81	-15.19	231.86	18.5838
	F	6	7	3099	230.1674	174.369	91.133	-31.867	231.41	55.7984
	F	6	8	3539	318.8487	234.128	85.851	-55.949	320.04	84.7207
JL13 W	A	1	1	2219	366.435	107.665	139.97	-152.93	370.75	258.77
	A	1	2	1688	419.143	107.665	192.36	-170.94	422.64	311.478
	A	1	3	1476	391.126	107.665	190.57	-176.83	395.75	283.461
	A	1	4	1469	231.522	107.665	188.78	-125.62	239.62	123.857
	A	1	5	1329	114.984	107.665	86.916	-12.384	115.77	7.319
	A	1	6	791	106.237	106.237	8.7632	-13.567	106.27	0
	A	1	7	1138	105.566	105.566	9.4336	-12.066	105.59	0
	A	1	1	2038	410.059	98.3811	216.24	-201.56	416.32	311.678
	A	1	2	1699	429.948	110.728	178.35	-187.15	435.06	319.22
	A	1	3	1260	375.849	110.728	181.85	-180.25	382.38	265.121
	A	1	4	910	239.821	110.728	291.28	-106.82	250.34	129.093
	A	1	5	2313	120.571	110.728	135.93	-29.621	121.69	9.843
	A	1	6	1409	110.728	110.728	6.772	-6.928	110.76	0
	A	1	7	625	108.079	108.079	6.0211	-8.5489	108.11	0
	A	1	8	867	107.405	107.405	4.9948	-24.185	107.44	0
	A	2	1	1785	321.442	93.0908	113.76	-121.34	323.2	228.351
	A	2	2	928	293.494	93.0908	97.306	-118.19	297.48	200.403
	A	2	3	728	273.672	93.0908	88.128	-102.67	275.97	180.581
	A	2	4	699	242.212	93.0908	72.488	-94.212	244.73	149.121
	A	2	5	677	164.65	93.0908	86.75	-60.35	168.59	71.5592
	A	2	6	733	126.212	103.622	90.188	-26.112	128.22	22.59
	A	2	7	1208	105.568	103.747	52.632	-7.2176	105.72	1.821
	A	2	8	1357	104.201	104.201	14.699	5.00111	104.72	0
	A	3	1	2123	232.776	98.3495	66.524	-50.476	233.43	134.427
	A	3	2	1986	245.475	110.712	61.525	-63.175	246.79	134.763
	A	3	3	1322	217.361	110.712	50.939	-64.261	218.35	106.649
	A	3	4	1265	197.655	110.712	58.645	-57.455	199.41	86.943
	A	3	5	1304	173.47	110.712	61.33	-50.47	174.65	62.758
	A	3	6	1535	143.576	112.724	78.324	-31.776	144.79	30.852
	A	3	7	1326	125.442	113.635	55.158	-19.642	126.08	11.807
	A	3	8	1494	115.651	110.712	41.749	-23.621	115.94	4.939

Table A4, continued

DATE	CODE	LOC	POS	LENGTH	MEAN	BASELINE	MAX	MIN	RMS	MEAN-BL
	A	4	1	371	124.14	124.14	13.46	-4.4399	124.16	0
	A	4	2	932	102.753	102.753	5.847	-4.4328	102.78	0
	A	4	3	771	104.637	104.637	5.663	-4.6367	104.66	0
	A	4	4	426	113.02	113.02	4.9796	-5.3204	113.05	0
	A	4	5	531	103.637	103.637	5.7627	-4.4673	103.66	0
	A	4	6	771	102.924	102.924	5.6761	-12.304	102.95	0
	A	4	7	707	103.773	103.773	4.8275	-4.6025	103.8	0
	A	4	8	611	106.284	106.284	4.8155	-5.3845	106.31	0
	A	5	1	463	115.677	115.677	4.9233	-4.4767	115.7	0
	A	5	2	251	127.266	127.266	4.4339	-21.266	127.3	0
	A	5	3	427	129.157	129.157	5.9431	-11.957	129.18	0
	A	5	4	195	128.922	128.922	4.4785	-4.9215	128.94	0
	A	5	5	202	129.796	129.796	4.5045	-4.8955	129.82	0
	A	5	6	898	123.911	123.911	5.1893	-5.0107	123.93	0
	A	5	7	2282	113.983	113.983	33.117	-5.3827	114.02	0
	A	5	8	2233	114.764	113.594	54.536	-6.1644	114.9	1.17
	A	6	1	519	131.65	131.65	4.2497	-4.3503	131.67	0
	A	6	2	457	144.742	144.742	9.9584	-4.5416	144.76	0
	A	6	3	579	148.819	148.819	4.9813	-4.4187	148.84	0
	A	6	4	895	151.356	151.356	5.0441	-4.3559	151.37	0
	A	6	5	707	155.381	155.381	6.1188	-4.9812	155.4	0
	A	6	6	691	152.706	152.706	5.3941	-21.906	152.73	0
	A	6	7	733	149.078	137.278	7.3222	-21.778	149.1	11.8
	A	6	8	1433	154.577	131.349	40.223	-7.5766	154.7	23.228
	A	7	1	727	108.075	108.075	5.4252	4.77483	108.1	0
	A	7	2	719	117.118	117.118	10.982	-5.3179	117.15	0
	A	7	3	1302	118.073	118.073	5.7268	-4.5732	118.1	0
	A	7	4	1400	118.057	117.901	23.644	-33.537	118.09	0.156
	A	7	5	2320	119.976	119.259	32.824	-6.476	120.02	0.717
	A	7	6	3052	125.667	122.736	50.233	-8.6669	125.88	2.931
	A	7	7	2376	129.089	127.512	41.711	-6.989	129.19	1.577
	A	7	8	3212	138.727	135.47	36.273	-4.727	138.76	3.25696
JL14 W	B	1	1	1398	404.837	99.864	181.26	-197.14	410.95	304.973
	B	1	2	796	438.224	108.388	187.48	-183.92	441.94	329.836
	B	1	3	802	361.814	108.388	268.19	-171.31	369.19	253.426
	B	1	4	780	190.082	108.388	378.72	-76.282	199.51	81.694
	B	1	5	988	116.14	108.388	133.76	-12.74	117.02	7.752
	B	1	6	944	107.662	107.662	6.938	-5.0619	107.69	0
	B	1	7	646	106.906	106.906	5.0944	-5.2056	106.93	0
	B	1	8	723	106.555	106.555	5.4447	-4.8553	106.58	0
	B	2	1	1201	316.372	94.2195	100.63	-93.672	319.13	222.153
	B	2	2	824	315.364	105.429	102.44	-110.76	317.78	209.935
	B	2	3	1006	283.2755	105.429	123.32	-105.48	286.23	177.847
	B	2	4	841	231.486	105.429	142.32	-104.59	235.65	126.057
	B	2	5	927	160.792	105.429	149.11	-53.792	165.8	55.363
	B	2	6	1016	122.682	105.552	95.718	-21.682	124.41	17.13
	B	2	7	1388	107.166	105.108	60.334	-7.0656	107.32	2.058

Table A4, continued

DATE	CODE	LOC	POS	LENGTH	MEAN	BASELINE	MAX	MIN	RMS	MEAN-BL
	B	2	8	2039	105.306	105.306	22.494	-5.2057	105.34	0
	B	3	1	1292	226.97	107.586	63.13	-76.77	228.53	119.384
	B	3	2	1135	246.063	107.586	57.837	-82.063	247.28	138.477
	B	3	3	1429	216.471	107.586	65.429	-84.771	220.87	108.885
	B	3	4	960	193.163	107.586	80.537	51.5628	194.53	85.577
	B	3	5	999	162.148	107.586	68.352	-49.048	163.96	54.562
	B	3	6	1025	138.118	109.791	65.582	-33.618	139.69	28.327
	B	3	7	1412	120.466	107.586	78.934	-17.766	121.43	12.88
	B	3	8	1470	114.523	107.613	68.477	-11.823	115.03	6.91
	B	4	1	705	96.198	96.198	5.702	-4.688	96.228	0
	B	4	2	835	101.208	101.208	5.7919	-5.3881	101.24	0
	B	4	3	742	102.585	102.585	5.3151	-5.035	102.61	0
	B	4	4	877	102.919	102.919	5.8812	-4.5088	102.95	0
	B	4	5	793	103.1772	103.1772	5.6228	-4.7672	103.2	0
	B	4	6	504	103.1223	103.1223	5.6777	-4.7123	103.15	0
	B	4	7	790	103.1898	103.1898	5.6102	-4.7798	103.22	0
	B	4	8	614	103.4954	103.4954	5.3046	-5.0854	103.52	0
	B	5	1	698	132.8285	132.8285	4.4715	-4.2285	132.85	0
	B	5	2	598	138.1933	138.1933	5.1067	-4.3933	138.21	0
	B	5	3	970	139.0342	139.0342	5.1658	-4.3342	139.05	0
	B	5	4	696	137.8856	137.8856	4.5144	-4.0856	137.9	0
	B	5	5	761	138.4197	138.4197	4.8803	-4.6197	138.44	0
	B	5	6	802	134.6339	134.6339	4.3661	-4.2339	134.65	0
	B	5	7	829	131.0311	131.0311	4.4689	-5.0311	131.05	0
	B	5	8	1757	133.7845	133.7845	16.416	-5.1845	133.8	0
	B	6	1	757	134.1974	134.1974	3.9026	-3.7974	134.21	0
	B	6	2	870	140.2491	140.2491	4.7509	-3.8491	140.27	0
	B	6	3	495	141.7228	141.7228	5.0772	-4.4228	141.74	0
	B	6	4	459	140.8015	140.8015	4.1985	-4.4015	140.82	0
	B	6	5	991	142.5853	142.5853	5.0147	-4.4853	142.6	0
	B	6	6	1658	139.8888	137.826	14.611	-4.3888	139.91	2.06284
	B	6	7	1482	140.1773	129.184	36.823	-5.4773	140.23	10.9933
	B	6	8	1506	143.1955	125.964	44.105	-8.4955	143.39	17.2315
	B	7	1	758	95.19822	95.19822	5.8018	-4.5582	95.226	0
	B	7	2	885	101.4696	101.4696	5.5304	-4.7796	101.5	0
	B	7	3	1320	102.6321	102.6321	18.268	-5.0821	102.66	0
	B	7	4	1445	102.4127	102.4127	19.287	-4.8627	102.45	0
	B	7	5	1545	102.8828	102.03	27.517	-6.1928	102.96	0.8528
	B	7	6	1318	104.5789	102.486	36.121	-7.0289	104.72	2.09288
	B	7	7	1674	104.7443	103.589	50.656	-6.3343	104.86	1.15531
	B	7	8	2192	106.387	104.879	45.513	-6.287	106.51	1.508
JL15 W	C	1	1	1032	414.695	107.649	218.91	-194.6	420.21	307.046
	C	1	2	699	417.305	111.854	194.8	-199.8	423.1	305.451
	C	1	3	667	348.774	111.854	240.03	-197.67	357.51	236.92
	C	1	4	814	214.089	111.854	322.91	-98.389	225.9	102.235
	C	1	5	966	118.15	113.033	114.95	-10.25	118.75	5.117
	C	1	6	933	111.854	111.854	5.5458	-5.6542	111.88	0

Table A4, continued

DATE	CODE	LOC	POS	LENGTH	MEAN	BASELINE	MAX	MIN	RMS	MEAN-BL
	C	1	7	583	111.433	111.433	5.0669	-5.2331	111.46	0
	C	1	8	671	111.322	111.322	5.1776	-5.1224	111.35	0
	C	2	1	864	327.392	99.502	113.71	-96.892	330.06	227.89
	C	2	2	789	324.507	111.887	102.79	-129.41	327.27	212.62
	C	2	3	760	283.782	111.887	90.918	-112.88	286.74	171.895
	C	2	4	1036	232.376	111.887	157.82	-107.18	237.7	120.489
	C	2	5	996	182.018	111.887	162.38	-65.518	187.78	70.131
	C	2	6	1677	125.709	114.539	157.49	-17.809	127.78	11.17
	C	2	7	1676	113.338	112.206	86.062	-6.3384	113.49	1.132
	C	2	8	1428	111.887	111.887	9.8127	-4.8873	111.91	0
	C	3	1	997	252.708	104.948	62.392	-75.708	253.72	147.76
	C	3	2	1135	239.986	111.646	62.114	-64.786	241.28	128.34
	C	3	3	843	231.587	111.646	69.713	-59.787	233	119.941
	C	3	4	967	183.832	111.646	82.068	-60.432	185.96	72.186
	C	3	5	901	169.601	112.842	93.699	-50.501	171.61	56.759
	C	3	6	898	145.394	118.656	80.806	-35.794	147.29	26.738
	C	3	7	1068	120.607	113.2	67.593	-13.607	121.28	7.407
	C	3	8	1603	116.688	114.646	65.117	-9.6883	117.07	2.042
	C	4	1	515	97.3125	97.3125	4.5875	-4.9425	97.337	0
	C	4	2	227	103.101	103.101	5.699	-4.691	103.12	0
	C	4	3	685	103.739	103.739	5.0613	-4.4587	103.76	0
	C	4	4	484	103.826	103.826	4.9739	-4.5461	103.85	0
	C	4	5	567	104.147	104.147	4.6533	-4.8667	104.17	0
	C	4	6	478	103.955	103.955	4.8454	-4.6746	103.98	0
	C	4	7	464	104.024	104.024	4.7759	-3.9241	104.05	0
	C	4	8	516	104.32	104.32	5.2797	-4.2204	104.34	0
	C	5	1	498	117.215	117.215	4.4851	-4.1149	117.23	0
	C	5	2	658	125.6	125.6	3.8998	-3.9002	125.62	0
	C	5	3	562	125.521	125.521	3.9787	-3.8214	125.54	0
	C	5	4	616	122.505	122.505	4.3955	-4.2046	122.52	0
	C	5	5	557	119.58	119.58	4.7197	-3.8803	119.6	0
	C	5	6	740	105.674	105.674	4.8265	-4.6735	105.7	0
	C	5	7	763	104.698	104.698	5.8016	-4.5984	104.72	0
	C	5	8	1692	104.655	104.655	7.5452	-5.3718	104.68	0
	C	6	1	585	101.331	101.331	5.6687	-4.6413	101.36	0
	C	6	2	166	107.942	107.942	5.1577	-4.3423	107.96	0
	C	6	3	591	108.684	108.684	5.3156	-4.1844	108.71	0
	C	6	4	633	109.894	109.894	5.8055	-4.5945	109.92	0
	C	6	5	842	112.314	112.314	5.0863	-4.4137	112.34	0
	C	6	6	737	115.596	115.596	7.8039	-4.1961	115.12	0
	C	6	7	1378	115.079	108.714	22.221	-5.4795	115.12	6.365
	C	6	8	1303	123.42	106.804	69.98	-12.92	124.04	16.616
	C	7	1	704	89.2391	89.2391	5.7209	-5.4991	89.271	0
	C	7	2	638	95.2309	95.2309	5.7691	-4.5909	95.262	0
	C	7	3	1130	95.7842	95.7842	9.5159	-5.1442	95.816	0
	C	7	4	1145	96.0396	95.4236	41.26	-5.3996	96.119	0.616
	C	7	5	1739	96.0524	95.4655	21.348	-5.4124	96.098	0.5869

Table A4, continued

DATE	CODE	LOC	POS	LENGTH	MEAN	BASELINE	MAX	MIN	RMS	MEAN-BL
	C	7	6	1418	97.8118	95.4689	48.988	-7.1718	97.986	2.3429
	C	7	7	1325	97.8288	96.4139	55.871	-6.3188	98.029	1.4149
	C	7	8	1843	100.8985	97.5206	89.902	-8.5285	101.38	3.3779
	D	1	1	861	390.3166	97.6543	168.38	-183.42	396.21	292.662
	D	1	2	838	416.935	100.421	219.57	-195.44	422.61	316.514
	D	1	3	820	353.925	100.872	226.18	-208.63	363.18	253.053
	D	1	4	1089	199.613	100.252	261.49	-91.913	211.54	99.361
	D	1	5	1157	106.292	100.659	103.21	-11.452	106.91	5.633
	D	1	6	805	100.228	100.228	5.7724	-5.3876	100.26	0
	D	1	7	569	100.353	100.353	5.6469	-5.5131	100.38	0
	D	1	8	678	99.6155	99.6155	5.4845	-5.6255	99.646	0
	D	2	1	668	328.476	89.1334	78.724	-75.276	329.98	239.343
	D	2	2	701	319.654	101.2	119.25	-115.25	322.84	218.454
	D	2	3	721	273.802	100.985	121.4	-122.5	277.71	172.817
	D	2	4	705	216.248	100.79	135.35	-102.55	221.44	115.458
	D	2	5	1095	161.382	100.35	200.42	-63.112	167.33	61.032
	D	2	6	1173	116	102.108	185.9	-19.44	118.2	13.892
	D	2	7	1151	105.186	101.977	144.51	-8.6264	105.78	3.209
	D	2	8	1312	102.5199	102.206	19.68	-5.1098	102.56	0.3139
	D	3	1	999	239.357	91.95	71.143	-77.757	240.89	147.407
	D	3	2	947	224.509	102.13	71.391	-66.309	226.12	122.379
	D	3	3	844	210.702	102.13	77.498	-63.702	212.7	108.572
	D	3	4	924	185.915	102.13	72.385	-68.815	188.17	83.785
	D	3	5	853	155.001	102.13	93.899	-43.001	157.3	52.871
	D	3	6	884	126.302	100.13	84.098	-27.182	127.77	26.172
	D	3	7	1336	113.068	103.114	86.132	-14.798	113.93	9.954
	D	3	8	1240	107.117	101.012	69.823	-8.9071	107.54	6.105
	D	4	1	545	86.4658	86.4658	5.8143	-4.4558	86.499	0
	D	4	2	708	94.4007	94.4007	5.5793	-5.5507	94.43	0
	D	4	3	408	95.8798	95.8798	5.8202	-5.3098	95.909	0
	D	4	4	559	96.3452	96.3452	6.1548	-4.9252	96.374	0
	D	4	5	644	97.0364	97.0364	5.4636	-4.7564	97.063	0
	D	4	6	688	96.9632	96.9632	5.5368	-4.6832	96.989	0
	D	4	7	911	97.0479	97.0479	5.4521	-4.7679	97.074	0
	D	4	8	835	98.1065	98.1065	5.2935	-4.9765	98.132	0
JL16 W	D	1	1	652	300.54	99.0171	227.36	-138.94	307.69	201.523
	D	1	2	909	382.477	104.606	270.72	-188.98	380.23	277.871
	D	1	3	592	357.25	104.606	276.05	-197.45	367.51	252.644
	D	1	4	890	226.021	104.606	383.08	-121.52	243.89	121.415
	D	1	5	870	113.541	105.154	300.26	-13.341	115.88	8.387
	D	1	6	758	104.797	104.797	4.9028	-4.5972	104.82	0
	D	1	7	504	104.606	104.606	5.0939	-4.4062	104.63	0
	D	1	8	802	102.809	102.809	6.0908	-5.1792	102.83	0
	D	5	1	609	86.5113	86.5113	5.9387	-4.4314	86.541	0
	D	5	2	633	98.7103	98.7103	4.9897	-4.5403	98.736	0
	D	5	3	756	100.265	100.265	5.1349	-4.3651	100.59	0
	D	5	4	502	100.719	100.719	5.5812	-4.8188	100.74	0

Table A4, continued

DATE	CODE	LOC	POS	LENGTH	MEAN	BASELINE	MAX	MIN	RMS	MEAN-BL
	D	5	5	565	101.082	101.082	5.2176	-5.1824	101.11	0
	D	5	6	661	101.252	101.252	5.0479	-4.4821	101.28	0
	D	5	7	1341	101.461	101.461	5.639	-4.691	101.49	0
	D	5	8	2008	102.203	102.11	29.997	-5.4333	102.24	0.093
	D	6	1	851	86.2295	86.2295	5.3505	-4.1495	86.259	0
	D	6	2	573	97.096	97.096	4.904	-4.646	97.121	0
	D	6	3	521	99.0759	99.0759	5.4241	-4.0359	99.099	0
	D	6	4	610	99.676	99.676	5.7236	-4.6364	99.7	0
	D	6	5	964	100.14	100.14	19.96	-4.2403	100.17	0
	D	6	6	2501	100.758	100.758	17.642	-4.8577	100.78	0
	D	6	7	1505	103.014	94.763	27.486	-6.244	103.09	8.251
	D	6	8	1635	110.591	87.14	109.71	-12.102	111.59	23.451
	D	7	1	656	93.5284	93.5284	5.8316	-5.3984	93.558	0
	D	7	2	1378	97.9833	97.9833	19.517	-5.5333	98.019	0
	D	7	3	1311	98.7264	98.5533	12.774	-5.4164	98.76	0.1731
	D	7	4	1518	99.2559	98.6182	47.644	-5.9459	99.338	0.6377
	D	7	5	2205	99.63	98.5623	66.27	-6.3204	99.749	1.0677
	D	7	6	1721	101.638	97.5807	100.66	-7.3283	101.94	4.0573
	D	7	7	2514	101.116	97.8881	145.98	-7.8058	101.66	3.2279
	D	7	8	1566	101.917	97.5707	82.983	-9.4666	102.62	4.3463
	E	1	1	1295	106.335	102.786	34.565	-11.085	106.53	3.549
	E	1	2	935	146.679	104.016	57.221	-35.079	148.02	42.663
	E	1	3	975	260.642	104.016	115.66	-95.542	264.05	156.626
	E	1	4	992	292.18	104.016	115.12	-100.38	294.61	188.164
	E	1	5	891	267.774	104.016	118.93	-123.37	272.56	163.758
	E	1	6	745	153.355	104.016	142.75	-48.655	157.82	49.339
	E	1	7	805	116.585	106.302	70.015	-16.185	117.36	10.283
	E	1	8	2589	105.605	104.016	81.895	-6.9055	105.94	1.589
	E	2	1	873	117.418	91.0653	34.682	-22.168	117.83	26.3527
	E	2	2	1105	155.982	92.0641	61.718	-35.682	157.29	63.9179
	E	2	3	718	174.046	92.0641	55.654	-49.446	175.31	81.9819
	E	2	4	1093	197.02	92.0641	87.08	-67.32	198.81	104.956
	E	2	5	1238	209.129	92.0641	63.671	-52.629	210.31	117.065
	E	2	6	1005	205.909	92.0641	79.891	-79.609	207.71	113.845
	E	2	7	1168	170.215	93.064	86.285	-60.315	173.42	77.151
	E	2	8	1531	134.662	93.064	101.14	-34.262	136.88	41.598
	E	3	1	2023	128.987	99.2548	30.013	-21.687	129.36	29.7322
	E	3	2	997	142.251	101.187	33.149	-25.451	142.73	41.064
	E	3	3	1075	148.687	101.187	33.613	-19.787	148.95	47.5
	E	3	4	1891	155.24	101.187	43.461	-26.34	155.67	54.053
	E	3	5	1225	163.362	101.187	39.638	-24.162	163.73	62.175
	E	3	6	1141	165.911	101.187	35.389	-28.412	166.42	64.724
	E	3	7	1056	162.951	101.187	35.749	-48.751	163.84	61.764
	E	3	8	1190	129.775	101.187	56.025	-29.375	130.95	28.588
	E	4	1	638	95.4249	95.4249	4.9751	-5.3449	95.453	0
	E	4	2	551	96.7132	96.7132	6.2868	-4.9132	96.741	0
	E	4	3	788	96.9645	96.9645	5.1355	-4.3045	96.992	0

Table A4, continued

DATE	CODE	LOC	POS	LENGTH	MEAN	BASELINE	MAX	MIN	RMS	MEAN-BL
	E	4	4	935	97.0383	97.0383	5.0617	-6.0983	97.066	0
	E	4	5	1373	97.0938	97.0938	18.006	-7.8838	97.123	0
	E	4	6	1232	97.207	97.207	5.793	-20.927	97.236	0
	E	4	7	5611	100.227	92.8811	108.87	-29.977	100.49	7.3459
	E	4	8	4078	100.644	67.797	86.856	-27.814	101.01	32.847
	E	5	1	1124	87.6995	87.6995	33.401	-9.6895	87.737	0
	E	5	2	864	96.7638	96.7638	5.3363	-4.9638	96.788	0
	E	5	3	1022	98.2204	98.2204	4.7796	-11.59	98.246	0
	E	5	4	958	98.702	98.702	5.198	-12.072	98.726	0
	E	5	5	835	99.1757	99.1757	5.5243	-4.7857	99.2	0
	E	5	6	730	100.414	100.146	10.386	-5.164	100.45	0.268
	E	5	7	1967	150.019	90.831	95.881	-31.739	159.15	59.188
	E	5	8	1730	188.763	90.146	108.34	-27.063	190.68	98.617
	E	6	1	1628	83.107	83.107	28.492	-12.857	83.144	0
	E	6	2	768	95.8641	95.8641	5.4359	-4.0641	95.888	0
	E	6	3	2403	98.9478	98.2042	26.452	-20.938	99.02	0.7436
	E	6	4	2592	99.4645	98.6315	30.236	-18.875	99.533	0.833
	E	6	5	3323	100.766	99.1592	35.034	-15.866	100.87	1.6068
	E	6	6	2323	109.535	98.2042	58.965	-14.285	110.14	11.3308
	E	6	7	1347	140.658	98.2042	50.642	-28.688	141.79	42.4538
	E	6	8	1731	164.34	98.2042	63.96	-40.34	165.93	66.1358
	E	7	1	1330	96.2881	96.2881	11.912	-10.518	96.321	0
	E	7	2	1769	100.32	99.654	25.98	-10.24	100.38	0.666
	E	7	3	1758	101.956	98.0385	47.644	-17.916	102.31	3.9175
	E	7	4	1579	107.24	98.468	50.96	-16.3	107.71	8.772
	E	7	5	1271	112.511	98.0385	118.09	-34.501	113.85	14.4725
	E	7	6	1774	131.966	98.0385	97.434	-28.446	134	33.9275
	E	7	7	1860	136.046	108.521	83.354	-41.656	137.98	27.525
	E	7	8	2452	133.395	98.0385	69.605	-40.736	135.46	35.3565
	F	1	1	1069	121.241	103.147	37.259	-15.641	121.64	18.094
	F	1	2	1251	160.347	108.69	120.75	-39.347	162.47	51.657
	F	1	3	1314	219.683	108.69	117.72	-68.883	223	110.993
	F	1	4	1125	307.767	108.69	100.33	-115.27	310.11	199.077
	F	1	5	1175	267.197	108.69	133.2	-103.6	270.99	158.507
	F	1	6	972	190.644	108.69	155.26	-78.144	196.34	81.954
	F	1	7	1209	122.337	110.739	127.26	-15.837	123.55	11.598
	F	1	8	1780	109.413	108.69	69.487	-5.513	109.52	0.723
	F	2	1	1052	122.136	90.1298	32.964	20.7359	122.56	32.0062
	F	2	2	824	145.104	92.1361	55.996	-28.404	146.06	52.9679
	F	2	3	1244	158.081	92.1361	78.719	-35.381	159.18	65.9449
	F	2	4	1410	197.875	92.1361	91.825	-55.575	199.65	105.739
	F	2	5	1129	207.868	92.1361	63.932	-77.568	209.42	115.732
	F	2	6	1132	209.311	108.1358	81.189	-83.212	211.14	101.175
	F	2	7	1247	174.47	112.256	90.43	-64.57	177.38	62.214
	F	2	8	1214	126.922	113.136	114.98	-28.102	129.11	13.786
	F	3	1	1522	140.51	89.4554	20.49	-22.11	140.72	51.0546
	F	3	2	1218	146.443	89.4554	25.657	-25.443	146.72	56.9876

Table A4, continued

DATE	CODE	LOC	POS	LENGTH	MEAN	BASELINE	MAX	MIN	RMS	MEAN-BL
	F	3	3	1395	153.804	89.4554	31.896	-24.304	154.16	64.3486
	F	3	4	1260	158.202	89.4554	50.498	-29.602	158.71	68.7466
	F	3	5	1216	170.003	90.8842	44.697	-30.303	170.62	79.1188
	F	3	6	1064	173.061	95.5684	34.839	-45.261	173.59	77.4926
	F	3	7	1004	167.307	101.7894	39.693	-47.207	168.13	65.5176
	F	3	8	1075	147.439	111.9812	62.161	-44.339	149.1	35.4578
	F	4	1	882	90.3389	90.3389	5.0812	-4.2989	90.367	0
	F	4	2	628	97.6751	97.6751	5.4249	-4.8151	97.7	0
	F	4	3	641	98.879	98.879	5.021	-4.319	98.904	0
	F	4	4	542	99.4673	99.4673	5.3327	-4.0473	99.491	0
	F	4	5	752	99.632	99.632	5.168	-5.072	99.656	0
	F	4	6	896	99.736	99.736	5.0637	-5.1763	99.761	0
	F	4	7	1145	104.208	99.845	61.092	-7.9376	104.41	4.363
	F	4	8	1135	134.227	70.894	61.073	-7.9573	134.42	63.333
	F	5	1	723	102.888	102.888	5.3117	-4.9183	102.91	0
	F	5	2	492	107.834	107.834	4.6663	-4.7337	107.86	0
	F	5	3	631	104.686	104.686	5.2141	-5.0059	104.71	0
	F	5	4	647	104.486	104.486	5.4135	-4.8065	104.51	0
	F	5	5	774	104.253	104.253	5.6472	-4.5728	104.28	0
	F	5	6	1811	104.259	103.819	40.541	-5.4392	104.32	0.44
	F	5	7	1228	140.402	93.819	118.8	-10.722	141	46.583
	F	5	8	1291	170.038	90.869	111.26	-38.638	173.5	79.169
	F	6	1	221	106.594	106.594	5.0059	-4.3941	106.62	0
	F	6	2	1734	98.4752	98.4752	8.8248	-5.6152	98.515	0
	F	6	3	708	99.0859	99.0859	6.5141	-4.5259	99.116	0
	F	6	4	1358	98.463	98.2112	13.137	-5.603	98.498	0.2518
	F	6	5	1152	101.987	100.654	44.513	-8.2774	102.15	1.333
	F	6	6	1448	109.484	98.3583	89.016	-14.924	110.34	11.1257
	F	6	7	1464	124.32	86.3583	60.58	-28.05	125.56	37.9617
	F	6	8	1556	161.52	86.8524	53.78	-52.7	162.9	74.6676
	F	7	1	989	93.0169	93.0169	8.3831	-5.2669	93.05	0
	F	7	2	1504	98.7855	97.8981	28.115	-6.7755	98.869	0.8874
	F	7	3	1269	101.391	98.1631	31.509	-7.6808	101.56	3.2279
	F	7	4	1162	108.693	98.6111	51.507	-14.983	109.43	10.0819
	F	7	5	990	118.091	98.1631	90.609	-23.531	119.87	19.9279
	F	7	6	1107	138.767	98.1631	85.333	-42.497	141.76	40.6039
	F	7	7	1277	136.84	98.1631	87.76	-42.57	139.54	38.6769
	F	7	8	1092	142.95	98.1631	75.95	-41.55	145.14	44.7869
	G	1	1	1039	106.916	95.2281	33.284	-13.146	107.23	11.6879
	G	1	2	986	147.393	105.005	95.207	-41.593	149.1	42.388
	G	1	3	936	203.249	105.005	148.55	-71.649	206.58	98.244
	G	1	4	859	303.075	105.005	117.63	-107.78	305.63	198.07
	G	1	5	905	272.31	105.005	137.99	-115.71	276.11	167.305
	G	1	6	869	178.237	105.005	154.66	-70.737	183.87	73.232
	G	1	7	910	117.109	105.868	143.59	-16.509	118.58	11.241
	G	1	8	919	105.682	105.005	69.819	-5.8916	105.84	0.677
	G	2	1	605	125.802	92.5997	28.998	-26.872	126.42	33.2023

Table A4, continued

DATE	CODE	LOC	POS	LENGTH	MEAN	BASELINE	MAX	MIN	RMS	MEAN-BL
	G	2	2	948	144.643	92.5997	55.757	-33.644	145.6	52.0433
	G	2	3	876	164.249	92.5997	87.751	-40.349	165.78	71.6493
	G	2	4	1153	192.524	92.5997	87.076	-60.924	193.87	99.9243
	G	2	5	1061	219.125	92.5997	94.875	-65.125	220.49	126.525
	G	2	6	269	190.752	102.6744	67.948	-65.352	192.3	88.0776
	G	2	7	981	157.484	102.6744	105.22	-62.584	160.5	54.8096
	G	2	8	907	126.911	92.5997	103.59	-27.121	128.92	34.3113
	G	3	1	1237	132.945	94.5235	35.655	-21.945	133.32	38.4215
	G	3	2	1197	147.042	94.5235	48.258	-25.742	147.41	52.5185
	G	3	3	1190	156.301	94.5235	44.099	-29.001	156.87	61.7775
	G	3	4	977	165.762	94.5235	50.138	-27.262	166.33	71.2385
	G	3	5	904	175.842	104.8749	52.158	-42.542	176.43	70.9671
	G	3	6	920	177.419	106.784	53.981	-45.819	178.23	70.635
	G	3	7	902	167.417	104.8749	44.183	-59.917	168.48	62.5421
	G	3	8	895	156.313	116.8146	65.587	-48.813	157.81	39.4984
	G	4	1	405	95.0183	95.0183	5.5817	-4.6983	95.046	0
	G	4	2	583	101.552	101.552	5.1483	-5.2018	101.58	0
	G	4	3	749	102.922	102.922	5.4783	-4.8517	102.95	0
	G	4	4	892	103.379	103.379	5.0206	-4.4494	103.4	0
	G	4	5	755	103.514	103.514	5.7863	-4.584	103.54	0
	G	4	6	462	103.551	103.551	4.8486	-4.621	103.58	0
	G	4	7	1357	104.274	94.067	17.926	-5.344	104.31	10.207
	G	4	8	1100	157.993	95.307	111.41	-8.203	158.3	62.686
	G	5	1	700	106.684	106.684	5.116	-4.284	106.71	0
	G	5	2	441	114.136	114.136	4.564	-4.036	114.16	0
	G	5	3	616	115.933	115.933	4.467	-4.933	115.95	0
	G	5	4	871	116.486	116.486	4.814	-4.686	116.51	0
	G	5	5	1354	105.421	105.421	6.379	-4.821	105.44	0
	G	5	6	1769	106.132	105.566	52.168	-5.532	106.2	0.566
	G	5	7	1500	133.643	95.566	96.257	-13.043	134.4	38.077
	G	5	8	1139	157.546	95.566	117.05	-35.146	160.1	61.98
	G	6	1	260	115.487	115.487	4.913	-4.487	115.51	0
	G	6	2	684	126.684	126.684	6.616	-4.484	126.7	0
	G	6	3	869	133.028	132.567	20.072	-4.828	133.06	0.461
	G	6	4	1232	134.72	134.681	17.58	-4.82	134.74	0.039
	G	6	5	1039	136.92	133.85	76.38	-7.92	137.18	3.07
	G	6	6	1306	144.949	132.567	70.951	-14.149	147.6	12.382
	G	6	7	1276	170.831	112.784	82.969	-30.631	172.26	58.047
	G	6	8	1196	182.578	112.784	60.022	-46.678	183.99	69.794
	G	7	1	1290	98.9744	98.1631	21.426	-6.0644	99.028	0.8113
	G	7	2	906	104.254	103.522	16.146	-5.324	104.3	0.732
	G	7	3	899	105.166	103.138	34.234	-6.236	105.26	2.028
	G	7	4	1108	113.783	103.138	66.817	-13.993	114.51	10.645
	G	7	5	869	126.717	103.138	99.483	-26.117	129	23.579
	G	7	6	892	143.546	103.138	79.254	-38.646	145.89	40.408
	G	7	7	966	146.082	103.138	86.218	-44.582	148.86	42.944
	G	7	8	846	150.461	103.138	74.039	-44.661	152.7	47.323

Table A4, continued

DATE	CODE	LOC	POS	LENGTH	MEAN	BASELINE	MAX	MIN	RMS	MEAN-BL
	H	1	1	915	109.352	95.9922	43.248	-13.332	109.75	13.3598
	H	1	2	1120	141.768	104.551	93.132	-35.469	143.19	37.217
	H	1	3	1148	226.937	104.551	141.66	-85.437	230.15	122.386
	H	1	4	964	296.156	104.551	123.04	-115.26	298.94	191.605
	H	1	5	1124	269.841	104.551	163.06	-117.24	273.79	165.29
	H	1	6	1093	154.224	104.551	139.78	-51.324	158.02	49.673
	H	1	7	898	109.9	104.551	98.4	-10.45	110.35	5.349
	H	1	8	1674	104.895	104.782	36.605	-5.4451	104.94	0.113
	H	2	1	911	120.706	92.4078	29.294	-22.976	121.2	28.2982
	H	2	2	1087	146.773	92.4078	78.727	-36.173	148.13	54.3652
	H	2	3	782	173.98	92.4078	86.621	-47.08	175.53	81.5722
	H	2	4	912	205.568	92.4078	93.632	-60.668	207.23	113.16
	H	2	5	1013	226.667	92.4078	76.833	-69.767	228.3	134.259
	H	2	6	749	209.393	92.4078	107.81	-86.794	212.09	116.985
JL18 W	H	1	1	1111	106.613	99.2973	48.087	-12.573	106.94	7.3157
	H	1	2	988	136.284	102.071	91.119	-34.584	137.71	34.213
	H	1	3	1009	194.926	102.071	106.87	-66.726	198.05	92.855
	H	1	4	943	273.356	102.071	105.34	-98.956	275.87	171.285
	H	1	5	950	270.039	102.071	134.36	-133.24	274.01	167.968
	H	1	6	996	154.827	102.071	189.07	-58.827	160.5	52.756
	H	1	7	849	112.412	102.776	159.39	-14.952	113.85	9.636
	H	1	8	2141	102.44	102.071	53.16	-5.8397	102.5	0.369
	H	2	1	1051	116.252	93.1349	41.948	-23.072	116.77	23.1171
	H	2	2	769	131.627	93.1349	53.873	-27.327	132.47	38.4921
	H	2	3	937	151.154	93.1349	72.846	-31.454	152.28	58.0191
	H	2	4	1058	181.399	93.1349	114.4	-54.899	183.21	88.2641
	H	2	5	1385	206.412	93.1349	75.688	-61.912	207.91	113.277
	H	2	6	1268	183.262	93.1349	154.94	-81.062	185.57	90.1271
	H	2	7	856	155.418	93.1349	92.182	-74.518	159.21	62.2831
	H	2	8	915	121.36	93.1349	96.94	-34.761	124.01	28.2251
	H	3	1	1042	130.198	93.1349	28.002	-19.899	130.54	37.0631
	H	3	2	914	136.508	93.1349	44.692	-27.908	137.05	43.3731
	H	3	3	870	149.113	93.1349	50.087	-32.013	149.62	55.9781
	H	3	4	882	159.899	93.1349	47.001	-30.799	160.45	66.7641
	H	3	5	857	167.161	93.1349	43.139	-46.661	167.75	74.0261
	H	3	6	818	172.346	93.1349	45.654	-46.646	173.05	79.2111
	H	3	7	884	157.021	93.1349	48.279	-53.421	158.05	63.8861
	H	3	8	858	125.991	93.1349	48.909	-41.691	127.32	32.8561
	H	4	1	387	92.4137	92.4137	5.8963	-5.2138	92.445	0
	H	4	2	842	99.541	99.541	5.5588	-4.6512	99.569	0
	H	4	3	914	100.883	100.883	5.1168	-4.2832	100.91	0
	H	4	4	923	101.119	101.119	5.7813	-4.5187	101.15	0
	H	4	5	1012	101.037	101.037	4.9633	-4.4368	101.06	0
	H	4	6	1940	101.147	101.147	8.2529	-5.3972	101.17	0
	H	4	7	2209	101.629	101.506	22.371	-5.0294	101.66	0.123
	H	4	8	1201	135.048	101.506	103.55	-8.448	135.37	33.542
	H	5	1	509	94.2609	94.2609	4.9091	-4.5009	94.288	0

Table A4, continued

DATE	CODE	LOC	POS	LENGTH	MEAN	BASELINE	MAX	MIN	RMS	MEAN-BL
	H	5	2	546	98.842	98.842	5.458	-3.952	98.866	0
	H	5	3	514	101.452	101.452	5.4476	-4.8524	101.78	0
	H	5	4	650	101.995	101.995	4.9055	-4.5345	102.02	0
	H	5	5	1643	102.797	102.673	26.303	-5.3369	102.84	0.124
	H	5	6	1266	104.023	102.079	25.877	-6.5627	104.09	1.944
	H	5	7	1079	144.775	102.079	115.23	-15.605	146.06	42.696
	H	5	8	1131	167.625	102.079	119.68	-36.725	170.76	65.546
	H	6	1	904	88.3325	88.3325	5.7075	-4.5525	88.362	0
	H	6	2	729	99.1852	99.1852	10.215	-5.1452	99.213	0
	H	6	3	1312	101.004	100.942	7.5965	-4.4035	101.03	0.062
	H	6	4	899	103.786	101.531	30.414	-7.1864	103.93	2.255
	H	6	5	970	107.881	101.623	70.819	-11.281	108.36	6.258
	H	6	6	844	116.224	100.942	97.476	-18.764	117.31	15.282
	H	6	7	1507	152.23	100.942	70.47	-35.53	153.93	51.288
	H	6	8	974	172.07	100.942	55.63	-52.97	173.54	71.128
	H	7	1	1269	94.6832	94.129	32.717	-5.7732	94.74	0.5542
	H	7	2	1020	101.336	100.147	20.864	-6.4462	101.41	1.189
	H	7	3	937	106.531	100.147	54.169	-9.9311	106.93	6.384
	H	7	4	925	113.926	100.147	83.574	-15.617	114.83	13.779
	H	7	5	846	126.38	100.147	96.72	-28.07	128.48	26.233
	H	7	6	772	140.817	100.147	89.983	-42.507	143.24	40.67
	H	7	7	981	145.204	100.147	83.096	-47.744	147.47	45.057
	H	7	8	1153	148.942	100.147	80.158	-50.632	151.42	48.795
JL18 W	B	1	1	1210	404.818	91.248	178.78	-190.72	410.61	313.57
	B	1	2	882	405.341	103.512	206.26	-166.34	410.49	301.829
	B	1	3	1187	358.028	103.512	253.57	-182.43	365.27	254.516
	B	1	4	903	198.557	103.512	391.64	-88.957	210.49	95.045
	B	1	5	775	111.222	104.924	148.28	-11.862	112.36	6.298
	B	1	6	265	103.512	103.512	5.2883	-5.0017	103.54	0
	B	1	7	679	102.845	102.845	5.9547	-5.1953	102.87	0
	B	1	8	624	102.963	102.963	4.9368	-5.3132	102.99	0
	B	2	1	1002	308.956	98.042	107.34	-108.56	311.91	210.914
	B	2	2	1049	298.371	102.407	99.929	-115.97	300.72	195.964
	B	2	3	841	279.251	102.407	94.249	-84.851	281.41	176.844
	B	2	4	992	220.926	102.407	131.07	-105.33	225.4	118.519
	B	2	5	1045	157.886	102.407	129.91	-56.786	161.84	55.479
	B	2	6	913	125.791	103.051	131.21	-26.431	128.35	22.74
	B	2	7	1488	106.235	102.748	65.965	-8.5854	106.61	3.487
	B	2	8	1775	102.79	102.407	25.71	-5.1397	102.84	0.383
	B	3	1	2345	236.648	87.368	53.752	-98.748	238.32	149.28
	B	3	2	1178	231.594	106.152	49.406	-48.294	232.36	125.442
	B	3	3	1216	222.648	106.152	78.853	-71.848	223.98	116.496
	B	3	4	1315	194.12	106.152	60.28	-63.92	195.99	87.968
	B	3	5	1263	161.796	106.152	68.604	-44.496	163.7	55.644
	B	3	6	1113	133.202	106.152	62.998	-27.802	134.23	27.05
	B	3	7	1037	117.421	106.152	64.18	-15.521	118.1	11.269
	B	3	8	1087	110.07	106.152	49.23	-8.9699	110.32	3.918

Table A4, continued

DATE	CODE	LOC	POS	LENGTH	MEAN	BASELINE	MAX	MIN	RMS	MEAN-BL
	B	4	1	442	95.9557	95.9557	5.9443	-4.3057	95.983	0
	B	4	2	568	102.243	102.243	4.8573	-4.5927	102.27	0
	B	4	3	607	103.147	103.147	5.653	-4.6371	103.17	0
	B	4	4	549	103.144	103.144	5.6564	-4.6336	103.17	0
	B	4	5	777	102.966	102.966	4.9344	-4.4556	102.99	0
	B	4	6	903	102.769	102.769	5.1311	-4.2589	102.79	0
	B	4	7	891	102.541	102.541	5.3586	-4.8915	102.57	0
	B	4	8	926	102.653	102.653	5.2467	-4.1433	102.68	0
	B	5	1	468	95.3121	95.3121	4.8879	-4.5121	95.339	0
	B	5	2	395	101.462	101.462	5.6378	-4.6723	101.49	0
	B	5	3	539	102.582	102.582	5.3179	-4.9321	102.61	0
	B	5	4	586	102.794	102.794	5.1057	-5.1444	102.82	0
	B	5	5	523	102.932	102.932	4.9677	-4.4223	102.96	0
	B	5	6	512	103.066	103.066	5.7345	-4.5556	103.09	0
	B	5	7	812	101.545	101.545	5.5549	-4.7557	101.57	0
	B	5	8	1428	122.033	101.894	14.468	-5.2425	122.06	20.139
	B	6	1	417	93.2169	93.2169	5.2931	-4.9869	93.245	0
	B	6	2	672	102.619	102.619	5.2806	-4.1094	102.64	0
	B	6	3	718	107.484	107.484	4.7164	-4.6836	107.51	0
	B	6	4	601	108.215	108.215	4.8852	-4.6148	108.24	0
	B	6	5	627	110.724	110.724	4.8761	-4.5239	110.75	0
	B	6	6	1496	111.744	111.674	21.856	-5.5437	111.78	0.07
	B	6	7	981	123.537	122.77	32.363	-6.2369	123.6	0.767
	B	6	8	969	141.257	136.27	50.643	-9.3567	141.48	4.987
	B	7	1	1007	99.0349	99.0349	5.4651	-5.665	99.063	0
	B	7	2	837	102.401	102.401	5.4988	-4.7512	102.43	0
	B	7	3	939	103.788	103.285	17.817	-5.2785	103.83	0.503
	B	7	4	1310	103.772	103.486	11.028	-5.262	103.81	0.286
	B	7	5	1044	104.123	104.041	20.077	-6.4732	104.17	0.082
	B	7	6	1058	105.269	102.786	30.031	-5.9088	105.41	2.483
	B	7	7	1177	105.723	103.74	45.877	-7.2131	105.92	1.983
	B	7	8	1869	105.614	101.926	111.09	-7.9639	106.04	3.688
JL20	I	1	1	674	94.3194	94.3194	6.0806	-5.0894	94.352	0
	I	1	2	993	98.4514	98.4514	17.349	-12.651	98.493	0
	I	1	3	2731	99.85	99.85	7.4496	-5.4704	99.883	0
	I	1	4	2279	100.094	100.094	8.006	-5.7141	100.13	0
	I	1	5	2110	101.611	100.611	9.8887	-6.3713	101.65	1
	I	1	6	2064	106.41	100.611	15.39	-9.4497	106.47	5.799
	I	1	7	2131	128.584	83.728	29.816	-18.184	128.86	44.856
	I	1	8	1886	159.934	83.728	81.166	-37.234	161.34	76.206
	I	2	1	680	87.0625	87.0625	5.6075	-4.6925	87.095	0
	I	2	2	877	95.0912	95.0912	6.1088	-5.0012	95.121	0
	I	2	3	1156	96.4093	96.4093	5.6904	-5.4593	96.44	0
	I	2	4	953	96.7689	96.7689	6.2311	-4.9589	96.799	0
	I	2	5	1873	97.1352	97.1352	7.5648	-6.1852	97.166	0
	I	2	6	1450	98.5843	97.5472	24.116	-6.7743	98.65	1.0371
	I	2	7	1639	109.957	87.5641	24.413	-8.4372	110.05	22.3929

Table A4, continued

DATE	CODE	LOC	POS	LENGTH	MEAN	BASELINE	MAX	MIN	RMS	MEAN-BL
	I	2	8	1307	120.994	93.1404	29.406	-17.754	121.26	27.8536
	I	3	1	750	91.0049	91.0049	5.9555	-5.2049	91.037	0
	I	3	2	1207	95.0338	94.7424	7.9662	-5.8038	95.065	0.2914
	I	3	3	1171	96.3412	94.7424	10.059	-5.3912	96.376	1.5988
	I	3	4	2517	97.8832	94.7424	9.4168	-6.9332	97.923	3.1408
	I	3	5	1552	99.0659	90.4146	16.734	-7.2559	99.13	8.6513
	I	3	6	1838	99.67	84.8475	15.33	-7.0002	99.729	14.8225
	I	3	7	1547	104.216	86.7486	15.884	-10.697	104.32	17.4674
	I	3	8	2537	109.27	87.4561	21.13	-14.03	109.45	21.8139
	I	4	1	2348	89.4998	88.2389	58.9	-6.2698	89.719	1.2609
	I	4	2	1144	101.225	96.0986	48.075	-10.275	101.62	5.1264
	I	4	3	1089	118.642	96.0986	99.258	-25.122	121.02	22.5434
	I	4	4	1242	165.761	96.0986	93.339	-62.761	168.98	69.6624
	I	4	5	1305	202.947	96.0986	76.753	-82.847	204.67	106.848
	I	4	6	1055	200.104	96.0986	68.496	-57.704	201.45	104.005
	I	4	7	1111	168.524	99.0487	69.176	-40.724	169.61	69.4753
	I	4	8	1204	135.836	99.0487	48.664	-27.736	136.44	36.7873
	I	5	1	1289	143.071	89.9524	30.23	-27.271	143.45	53.1186
	I	5	2	963	157.069	91.8245	23.931	-22.37	157.34	65.2445
	I	5	3	1006	151.488	91.8245	30.412	-35.688	152.05	59.6635
	I	5	4	1006	157.356	91.8245	33.144	-32.056	157.89	65.5315
	I	5	5	1260	148.69	91.8245	40.91	-25.991	149.19	56.8655
	I	5	6	1098	127.988	91.8245	41.912	-21.588	128.65	36.1635
	I	5	7	1106	122.751	91.8245	55.749	-19.751	123.27	30.9265
	I	5	8	1264	115.09	94.4848	41.91	-14.69	115.37	20.6052
	I	6	1	2026	145.537	89.9524	11.463	-11.637	145.6	55.5846
	I	6	2	2385	145.817	91.8245	19.783	-20.517	145.95	53.9925
	I	6	3	1535	142.873	91.8245	21.027	-19.273	143.02	51.0485
	I	6	4	1624	137.363	91.8245	21.337	-18.963	137.54	45.5385
	I	6	5	1727	131.863	91.8245	23.437	-21.163	132.1	40.0385
	I	6	6	1460	125.732	91.8245	35.568	-18.432	125.95	33.9075
	I	6	7	1347	118.166	94.8774	19.934	-12.666	118.34	23.2886
	I	6	8	3145	113.728	93.8654	32.172	-11.628	113.89	19.8626
	I	7	1	4515	107.625	88.1259	47.637	-15.853	108.27	19.4991
	I	7	2	1857	114.821	88.1259	37.079	-17.861	115.23	26.6951
	I	7	3	1701	122.971	88.1259	27.229	-20.871	123.33	34.8451
	I	7	4	1687	123.37	88.1259	29.33	-21.27	123.77	35.2441
	I	7	5	2187	119.746	88.1259	37.254	-20.216	120.08	31.6201
	I	7	6	1903	114.404	88.1259	36.596	-14.004	114.75	26.2781
	I	7	7	1705	109.781	88.1259	22.319	-11.971	109.95	21.6551
	I	7	8	2560	112.664	88.1259	32.336	-25.154	112.86	24.5381
JL27	A	1	1	2137	412.232	95.2313	272.17	-249.53	423.3	317.001
	A	1	2	1458	363.532	95.2313	245.27	-187.83	372.26	268.301
	A	1	3	1882	195.722	95.2313	179.58	-100.21	205.68	100.491
	A	1	4	2984	138.249	95.2313	225.35	-82.01	148.43	43.0177
	A	1	5	2168	98.5697	89.5049	59.23	-19.08	98.898	9.0648
	A	1	6	3678	99.197	89.5049	32.803	-12.821	99.403	9.6921

Table A4, continued

DATE	CODE	LOC	POS	LENGTH	MEAN	BASELINE	MAX	MIN	RMS	MEAN-BL
	A	1	7	1746	107.789	107.789	6.1109	-5.5591	107.82	0
	A	1	8	1466	106.818	106.818	7.0818	-4.9182	106.85	0
	A	2	1	3429	245.894	113.175	278.01	-203.23	271.41	132.719
	A	2	2	2194	255.895	113.175	155.81	-107.6	259.63	142.72
	A	2	3	1335	254.015	113.175	142.09	-92.915	258.3	140.84
	A	2	4	1375	231.684	113.175	144.82	-85.884	235.53	118.509
	A	2	5	1168	173.666	113.175	142.53	-65.766	177.8	60.491
	A	2	6	2134	118.422	108.622	93.678	-19.992	119.57	9.8
	A	2	7	2276	104.556	104.413	32.644	-6.9862	104.64	0.143
	A	2	8	931	101.418	101.418	5.5819	-4.7181	101.45	0
	A	3	1	2827	220.749	84.8303	109.25	-131.79	223.93	135.919
	A	3	2	1782	149.37	84.8303	90.23	-75.91	153.38	64.5397
	A	3	3	1634	148.742	84.8303	77.058	-64.952	151.29	63.9117
	A	3	4	1335	128.607	84.8303	98.093	-52.567	131.78	43.7767
	A	3	5	1194	127.585	84.8303	60.415	-45.515	130	42.7547
	A	3	6	1313	96.7711	81.1408	91.229	-21.591	98.193	15.6303
	A	3	7	1539	100.856	81.1408	84.544	-25.676	102.73	19.7152
	A	3	8	2599	85.5869	81.8066	70.513	-13.847	86.073	3.7803
	A	4	1	752	107.913	107.913	5.1874	-5.2126	107.94	0
	A	4	2	552	112.689	112.689	4.7112	-5.7888	112.71	0
	A	4	3	312	114.217	114.217	4.8833	-4.6167	114.24	0
	A	4	4	534	114.668	114.668	5.3322	-5.0678	114.69	0
	A	4	5	507	114.837	114.837	5.1625	-5.2375	114.86	0
	A	4	6	485	114.894	114.894	5.1056	-5.2944	114.92	0
	A	4	7	690	115.114	115.114	4.8861	-4.6139	115.14	0
	A	4	8	473	114.957	111.957	5.0427	-4.4573	114.98	3
	A	5	1	1093	94.2943	94.2943	5.8057	-5.3344	94.324	0
	A	5	2	945	108.581	108.581	5.3185	-4.9815	108.61	0
	A	5	3	862	110.158	110.158	5.4421	-4.8579	110.18	0
	A	5	4	1502	110.78	110.78	4.8204	-4.5796	110.81	0
	A	5	5	2211	110.76	110.76	5.74	-4.56	110.78	0
	A	5	6	1071	110.473	110.473	5.1271	-4.2729	110.5	0
	A	5	7	1254	110.418	110.418	5.1823	-5.1177	110.44	0
	A	5	8	1275	110.723	103.847	5.7767	-4.5233	110.75	6.876
	A	6	1	1142	127.087	127.087	4.9125	-4.5875	127.11	0
	A	6	2	823	138.956	138.956	4.2441	-4.3559	138.97	0
	A	6	3	801	137.835	137.835	4.465	-4.135	137.85	0
	A	6	4	798	136.777	136.777	4.7226	-3.8774	136.79	0
	A	6	5	1501	171.943	171.943	6.5574	-7.2426	171.96	0
	A	6	6	1266	181.674	181.674	7.1258	-5.7743	181.69	0
	A	6	7	2421	196.136	181.614	43.464	-7.3357	196.17	14.522
	A	6	8	3456	189.992	178.542	39.308	-11.492	190.1	11.45
	A	7	1	756	117.92	117.92	4.5796	-4.8204	117.94	0
	A	7	2	1453	121.698	121.698	5.102	-4.298	121.72	0
	A	7	3	4193	123.009	123.009	21.891	-4.8086	123.04	0
	A	7	4	2340	124.523	123.125	56.577	-6.3231	124.64	1.398
	A	7	5	1972	123.6	123.046	15.3	-5.3998	123.64	0.554

Table A4, continued

DATE	CODE	LOC	POS	LENGTH	MEAN	BASELINE	MAX	MIN	RMS	MEAN-BL
	A	7	6	2851	123.67	123.076	22.93	-5.4704	123.71	0.594
	A	7	7	6867	124.367	123.323	58.433	-6.1666	124.48	1.044
	A	7	8	2954	125.33	123.75	62.67	-6.2299	125.47	1.58
	D	1	1	1207	314.042	94.2238	267.56	-135.84	319.39	219.818
	D	1	2	1042	367.043	101.696	205.96	-164.94	372.41	265.347
	D	1	3	1038	331.27	101.696	252.93	-157.37	337.65	229.574
	D	1	4	1304	232.81	101.696	305.99	-104.31	241.65	131.114
	D	1	5	1432	109.803	101.696	87.197	-11.303	110.35	8.107
	D	1	6	1094	101.653	100.117	5.4465	-4.8635	101.68	1.536
	D	1	7	193	101.557	101.557	4.6434	-4.7666	101.58	0
	D	2	1	984	266.363	N.M.	97.637	-92.463	268.74	266.363
	D	2	2	1487	270.615	N.M.	103.69	-107.02	272.78	270.615
	D	2	3	1118	254.381	N.M.	107.12	-83.081	256.41	254.381
JL30	D	2	1	1020	193.546	97.1935	71.754	-59.546	195.06	96.3525
	D	2	2	1109	204.013	100.147	89.687	-58.013	205.76	103.866
	D	2	3	889	193.39	100.147	120.91	-50.89	195.07	93.243
	D	2	4	843	183.734	100.147	87.566	-53.234	185.44	83.587
	D	2	5	1063	156.04	100.147	133.36	-50.44	158.6	55.893
	D	2	6	916	132.653	100.147	120.65	-36.484	135.18	32.506
	D	2	7	1273	104.048	100.147	120.95	-8.7381	104.62	3.901
	D	2	8	1527	99.852	99.852	6.6479	-5.4021	99.88	0
	D	3	1	912	167.759	100.929	30.641	-28.659	168.12	66.83
	D	3	2	777	172.444	100.929	44.756	-33.344	173.02	71.515
	D	3	3	1139	167.597	97.454	48.803	-45.697	168.25	70.143
	D	3	4	874	157.872	97.454	43.928	-33.372	158.46	60.418
	D	3	5	768	144.752	97.454	54.448	-37.453	145.64	47.298
	D	3	6	872	128.41	97.454	60.49	-26.21	129.36	30.956
	D	3	7	1110	111.891	97.454	60.709	-14.861	112.34	14.437
	D	3	8	973	105.837	100.929	40.163	-9.6669	106.14	4.908
	D	4	1	806	58.4955	58.4955	5.9045	-5.2555	58.545	0
	D	4	2	728	64.403	64.403	6.007	-4.293	64.444	0
	D	4	3	980	65.8728	65.8728	5.3972	-4.9028	65.913	0
	D	4	4	740	66.6543	66.6543	5.4757	-4.8343	66.694	0
	D	4	5	849	66.3852	66.3852	5.7448	-4.5652	66.426	0
	D	4	6	842	66.3588	66.3588	5.7712	-4.5388	66.398	0
	D	4	7	875	66.0081	66.0081	5.2619	-5.0381	66.048	0
	D	4	8	1064	65.9413	65.9413	6.1887	-4.9713	65.982	0
AU1	D	4	1	1273	247.88	247.88	7.72	-5.9801	247.9	0
	D	4	2	1376	261.421	261.421	7.9791	-7.5209	261.44	0
	D	4	3	920	264.751	264.751	8.0494	-6.5507	264.77	0
	D	4	4	759	267.135	267.135	8.2652	-6.3348	267.15	0
	D	4	5	1111	267.513	267.513	7.887	-6.7131	267.53	0
	D	4	6	889	268.045	268.045	7.3547	-6.4453	268.06	0
	D	4	7	966	268.224	268.224	7.976	-6.624	268.24	0
	D	4	8	876	264.707	264.707	7.1939	-6.5066	264.72	0
	D	5	1	838	107.037	107.037	4.963	-4.437	107.06	0
	D	5	2	756	111.138	111.138	5.1623	-4.2377	111.16	0

Table A4, continued

DATE	CODE	LOC	POS	LENGTH	MEAN	BASELINE	MAX	MIN	RMS	MEAN-BL
	D	5	3	781	107.337	107.337	4.663	-3.937	107.36	0
	D	5	4	803	107.937	107.937	4.9634	-4.5366	107.96	0
	D	5	5	762	109.462	109.462	5.1379	-4.2621	109.48	0
	D	5	6	850	109.914	109.914	5.5859	-4.7141	109.94	0
	D	5	7	2253	109.25	107.564	5.3502	-5.8498	109.27	1.686
	D	5	8	1953	110.485	97.881	17.915	-5.2851	110.52	12.604
	D	6	1	641	173.651	173.651	6.349	-5.751	173.67	0
	D	6	2	840	175.053	175.053	6.6467	-5.4533	175.07	0
	D	6	3	819	171.091	171.091	6.3088	-5.7912	171.11	0
	D	6	4	698	170.224	170.224	7.1762	-5.7238	170.24	0
	D	6	5	1051	166.504	166.504	12.596	-6.304	166.53	0
	D	6	6	1016	169.39	166.931	81.01	-8.3898	169.58	2.459
	D	6	7	907	169.268	162.3	75.132	-14.268	169.76	6.968
	D	7	1	692	82.4123	82.4123	5.5577	-4.7623	82.444	0
	D	7	2	748	86.5236	86.5236	6.6064	-4.5736	86.555	0
	D	7	3	1357	86.1125	86.1125	5.2975	-5.0225	86.142	0
	D	7	4	1331	86.3714	86.1033	33.429	-5.2814	86.423	0.2681
	D	7	5	1321	85.9974	85.4264	31.203	-5.7674	86.069	0.571
	D	7	6	1874	87.0594	85.4264	73.941	-6.8294	87.335	1.633
	D	7	7	1580	86.4958	85.4264	65.904	-7.1258	86.8	1.0694
	D	7	8	1720	86.9402	82.4123	112.76	-8.4302	87.418	4.5279
AU3	E	1	1	1934	94.5531	92.6519	31.147	-49.773	94.975	1.9012
	E	1	2	1686	108.537	92.6519	79.163	-23.277	109.48	15.8851
	E	1	3	1266	138.551	92.6519	57.149	-62.571	140.35	45.8991
	E	1	4	1113	196.918	92.6519	115.08	-58.018	201.5	104.266
	E	1	5	2097	213.058	92.6519	106.54	-70.908	215.98	120.406
	E	1	6	1788	154.403	92.1044	94.697	-58.613	157.92	62.2986
	E	1	7	2394	107.587	92.1044	62.913	-21.467	108.44	15.4826
	E	1	8	2052	89.0657	82.8188	63.334	-14.136	89.473	6.2469
	E	2	1	1296	104.543	96.6425	32.357	-33.923	104.97	7.9005
	E	2	2	1181	111.988	100.035	35.312	-16.388	112.36	11.953
	E	2	3	1404	117.208	100.035	58.492	-21.608	118.17	17.173
	E	2	4	1288	133.903	100.035	75.697	-35.403	135.25	33.868
	E	2	5	929	149.029	96.854	65.871	-34.929	150.36	52.175
	E	2	6	1051	156.547	96.854	78.553	-41.147	157.91	59.693
	E	2	7	1095	155.924	96.854	48.076	-32.024	156.85	59.07
	E	2	8	1453	143.523	96.854	71.777	-37.623	144.82	46.669
	E	3	1	3746	77.2759	73.284	36.424	-56.606	78.849	3.9919
	E	3	2	2155	104.671	93.157	49.529	-42.661	105.1	11.514
	E	3	3	2877	69.9787	50.4925	57.521	-30.359	71.264	19.4862
	E	3	4	2055	94.2858	68.284	64.214	-40.886	95.802	26.0018
	E	3	5	1727	175.162	133.317	72.838	-33.962	175.96	41.845
	E	3	6	1488	192.554	133.317	74.446	-52.154	193.71	59.237
	E	3	7	1588	177.103	133.317	80.397	-45.303	178.42	43.786
	E	3	8	2331	156.586	133.317	71.514	-21.586	157.38	23.269
	E	4	6	1489	95.7925	95.7925	5.8075	-4.5025	95.819	0
	E	4	7	2389	109.7663	95.7988	9.1337	-5.4763	109.8	13.9675

Table A4, continued

DATE	CODE	LOC	POS	LENGTH	MEAN	BASELINE	MAX	MIN	RMS	MEAN-BL
	E	4	8	2572	128.0464	95.7195	30.254	-6.7564	128.1	32.3269
	E	5	1	614	129.929	129.892	4.4713	-4.2287	129.95	0.037
	E	5	2	801	138.501	138.231	4.4994	-4.1006	138.52	0.27
	E	5	3	1550	140.645	140.645	6.6549	-4.5452	140.66	0
	E	5	4	1880	140.219	138.771	44.981	-5.019	140.29	1.448
	E	5	5	1137	141.055	136.7	75.145	-8.455	141.41	4.355
	E	5	6	999	142.428	135.801	80.672	-10.629	142.89	6.627
	E	5	7	1091	194.204	136.288	93.796	-21.604	195.17	57.916
	E	5	8	1652	195.027	136.288	88.973	-50.528	197.19	58.739
	E	6	1	872	91.7448	91.7448	5.5752	-4.7648	91.775	0
	E	6	2	661	134.584	134.584	4.9159	-4.5841	134.6	0
	E	6	3	541	134.678	134.678	4.8216	-3.7784	134.7	0
	E	6	4	677	132.344	132.335	4.5555	-4.0445	132.36	0.009
	E	6	5	924	137.652	121.386	4.9484	-4.4516	137.67	16.266
	E	6	6	2316	136.244	118.752	16.756	-4.8441	136.27	17.492
	E	6	7	1465	151.573	120.815	77.727	-11.873	152.19	30.758
	E	6	8	1465	154.098	107.366	92.102	-23.298	155.82	46.732
	E	7	1	739	88.3494	88.3094	5.5206	-4.8094	88.379	0.04
	E	7	2	1629	93.988	92.9948	13.712	-5.278	94.024	0.9932
	E	7	3	1942	98.2672	94.4978	83.433	-8.6972	98.713	3.7694
	E	7	4	3366	100.948	94.265	75.652	-10.518	101.63	6.683
	E	7	5	1436	128.876	94.9773	101.92	-34.146	131.37	33.8987
	E	7	6	1371	129.134	92.2367	139.87	-34.124	131.54	36.8973
	E	7	7	1925	134.3	98.0808	99.1	-44.73	137.43	36.2192
	E	7	8	4734	139.142	98.0808	89.058	-44.412	141.12	41.0612
	H	1	1	1243	87.8187	86.6767	24.181	-5.9987	87.883	1.142
	H	1	2	1374	93.8241	90.9954	41.376	-6.8441	93.956	2.8287
	H	1	3	1355	99.4009	90.9954	71.999	-11.561	99.875	8.4055
	H	1	4	986	105.796	90.9954	66.404	-16.226	106.67	14.8006
	H	1	5	1058	119.547	90.9954	75.053	-30.837	121.13	28.5516
	H	1	6	1850	135.726	90.9954	88.174	-43.576	137.88	44.7306
	H	1	7	1259	143.106	90.9954	81.694	-50.096	145	52.1106
	H	1	8	1393	142.349	90.9954	749.85	-48.479	144.29	51.3536
	H	2	1	1141	88.8752	83.263	24.825	-7.9152	89.011	5.6122
	H	2	2	989	106.836	95.028	67.164	-18.996	107.39	11.808
AU4	H	1	1	1562	98.8958	97.0477	35.404	-7.1258	99.001	1.8481
	H	1	2	783	114.77	100.125	50.93	-16.2	115.35	14.645
	H	1	3	633	153.926	100.125	99.274	-42.626	155.8	53.801
	H	1	4	722	233.095	100.125	122.91	-75.095	235.41	132.97
	H	1	5	724	253.037	100.125	133.56	-95.837	256.34	152.912
	H	1	6	806	176.673	110.864	158.33	-75.373	181.77	65.809
	H	1	7	632	112.199	106.992	92.701	-21.179	113.51	5.207
	H	1	8	1627	100.951	100.125	47.749	-5.7812	101.03	0.826
	H	2	1	850	98.5923	91.246	39.908	-11.922	98.877	7.3463
	H	2	2	815	114.027	92.9851	59.273	-17.157	114.49	21.0419
	H	2	3	921	130.771	92.899	76.529	-28.771	131.72	37.872
	H	2	4	892	151.882	93.0011	75.818	-42.282	152.99	58.8809

Table A4, continued

DATE	CODE	LOC	POS	LENGTH	MEAN	BASELINE	MAX	MIN	RMS	MEAN-BL
	H	2	5	865	177.894	93.0132	73.606	-54.694	179.15	84.8808
	H	2	6	823	187.407	99.101	72.693	-53.907	188.73	88.306
	H	2	7	839	162.025	99.101	81.975	-53.125	163.85	62.924
	H	2	8	826	129.543	99.101	80.457	-34.243	131.23	30.442
	H	3	1	881	116.015	99.101	22.485	-16.605	116.21	16.914
	H	3	2	896	128.423	101.854	38.077	-23.023	128.78	26.569
	H	3	3	773	132.128	101.854	29.272	-20.828	132.45	30.274
	H	3	4	918	145.014	101.854	41.086	-27.714	145.4	43.16
	H	3	5	871	152.809	101.854	34.991	-24.509	153.18	50.955
	H	3	6	778	156.26	105.654	42.84	-34.46	156.72	50.606
	H	3	7	877	154.405	105.654	40.395	-35.205	154.95	48.751
	H	3	8	1158	144.385	105.654	51.316	-37.885	145.29	38.731
	H	4	6	742	144.083	144.083	4.617	-3.883	144.1	0
	H	4	7	1256	144.828	144.148	25.972	-4.6281	144.85	0.68
	H	4	8	938	158.393	134.356	68.307	-8.883	158.58	24.037
	H	5	8	1052	199.35	152.12	69.15	-52.351	200.93	47.23
AU7	H	5	3	726	151.517	151.517	5.1828	-5.0172	151.54	0
	H	5	4	1008	180.318	180.318	7.0819	-5.7181	180.34	0
	H	5	5	1573	177.506	177.112	40.594	-6.3061	177.54	0.394
	H	5	6	830	178.366	169.245	37.134	-7.1657	178.42	9.121
	H	5	7	1124	201.439	169.245	93.161	-21.839	202.33	32.194
	H	5	8	965	229.543	169.245	119.56	-46.543	231.62	60.298
	H	6	1	879	111.619	111.619	4.181	-4.319	111.64	0
	H	6	2	1446	123.854	123.713	12.447	-3.7535	123.87	0.141
	H	6	3	1094	127.6	127.52	22.3	-4.9001	127.63	0.08
	H	6	4	1419	131.161	129.407	27.239	-5.061	131.21	1.754
	H	6	5	1042	136.544	129.407	56.856	-9.6436	136.8	7.137
	H	6	6	1093	142.331	125.479	70.369	-18.231	143.23	16.852
	H	6	7	1095	145.175	125.479	65.825	-28.775	146.28	19.696
	H	6	8	4063	167.888	125.479	59.312	-46.388	168.78	42.409
	H	7	1	507	87.8468	87.8468	5.8432	-6.9268	87.881	0
	H	7	2	1232	88.934	88.934	24.366	-5.464	88.98	0
	H	7	3	881	96.089	94.4241	49.611	-6.649	96.27	1.6649
	H	7	4	1131	99.3859	94.4241	56.514	-9.0959	99.724	4.9618
	H	7	5	1660	109.371	94.4241	87.429	-18.231	110.45	14.9469
	H	7	6	1190	121.767	94.4241	83.533	-28.927	123.35	27.3429
	I	1	6	1287	115.54	84.9537	78.66	-30.36	117.14	30.5863
	I	1	7	1126	140.418	84.9537	82.782	-52.688	142.34	55.4643
	I	1	8	1450	140.381	84.9537	75.119	-47.541	142.14	55.4273
AU8	I	1	2	1156	90.6055	90.6055	5.1445	-5.1155	90.634	0
	I	1	3	1020	92.025	92.025	5.435	-39.875	92.061	0
	I	1	4	1324	92.7857	92.7857	8.1143	-5.5857	92.814	0
	I	1	5	1806	94.5771	94.5771	8.0229	-5.6671	94.614	0
	I	1	6	1863	110.989	95.0402	10.911	-9.6388	111.03	15.9488
	I	1	7	2337	144.059	85.5557	32.741	-11.729	144.24	58.5033
	I	1	8	1566	150.116	87.1741	39.784	-19.216	150.52	62.9419
	I	2	1	1261	74.6707	74.6707	15.949	-41.331	75.109	0

Table A4, continued

DATE	CODE	LOC	POS	LENGTH	MEAN	BASELINE	MAX	MIN	RMS	MEAN-BL
	I	2	2	1675	86.6198	86.6198	5.7102	-5.3998	86.649	0
	I	2	3	1218	88.2555	88.2555	5.7845	-4.4755	88.285	0
	I	2	4	1500	88.9211	88.9211	5.9789	-5.1412	88.95	0
	I	2	5	1876	88.9964	88.9964	6.7536	-20.596	89.029	0
	I	2	6	1706	89.8092	89.8092	9.3609	-5.1692	89.843	0
	I	2	7	1406	119.764	89.5284	8.5562	-5.1238	119.8	30.2356
	I	2	8	1557	122.001	89.4675	21.699	-7.3609	122.09	32.5335
	I	3	1	1419	78.2914	78.2914	20.879	-55.211	78.943	0
	I	3	2	1645	86.9426	86.1148	10.518	-5.7226	86.984	0.8278
	I	3	3	2283	87.8261	87.1393	19.874	-5.7561	87.864	0.6868
	I	3	4	2185	87.7316	86.4218	24.268	-9.9316	87.809	1.3098
	I	3	5	2414	88.295	78.753	20.305	-13.055	88.421	9.542
	I	3	6	2152	90.0912	78.1596	23.609	-7.1612	90.165	11.9316
	I	3	7	1985	89.3849	77.4218	35.415	-17.565	89.561	11.9631
	I	3	8	1876	93.0371	77.4218	23.263	-9.2571	93.184	15.6153
	I	4	1	736	79.5958	79.5958	5.8942	-4.3558	79.629	0
	I	4	2	1553	86.6915	86.4967	12.479	-4.6215	86.725	0.1948
	I	4	3	1760	90.8174	88.3069	77.583	-7.0374	91.108	2.5105
	I	4	4	1648	83.8613	78.8054	67.739	-38.291	94.392	5.0559
	I	4	5	1855	133.771	78.8054	84.229	-45.711	136.3	54.9656
	I	4	6	1562	166.573	88.9374	77.227	-63.873	168.51	77.6356
	I	4	7	1466	182.622	88.9374	61.978	-61.122	184.08	93.6846
	I	4	8	1835	165.929	88.9374	70.171	-39.229	167.15	76.9916
	I	5	1	1916	179.135	176.868	48.265	-9.0348	179.25	2.267
	I	5	2	1221	192.559	176.868	62.241	-12.159	192.9	15.691
	I	5	3	1263	205.915	176.868	47.985	-27.215	206.6	29.047
	I	5	4	1630	227.361	176.868	53.04	-45.261	228.03	50.493
	I	5	5	1238	227.467	176.868	42.733	-36.767	227.96	50.599
	I	5	6	1246	205.498	166.456	45.702	-32.098	206.12	39.042
	I	5	7	1083	204.383	170.542	41.017	-29.083	204.78	33.841
	I	5	8	1104	192.234	166.456	52.266	-19.534	192.52	25.778
	I	6	1	1211	156.645	144.182	15.155	-16.445	156.76	12.463
	I	6	2	1029	163.28	140.392	29.12	-26.48	163.55	22.888
	I	6	3	1407	159.462	136.451	32.038	-22.662	159.82	23.011
	I	6	4	1056	161.822	136.451	33.978	-24.222	162.3	25.371
	I	6	5	1260	152.604	137.779	39.796	-20.104	153.01	14.825
	I	6	6	1314	146.112	126.178	46.288	-14.412	146.41	19.934
	I	6	7	1645	124.315	105.16	26.185	-14.015	124.6	19.155
	I	6	8	1461	109.954	96.056	24.246	-8.2543	110.03	13.898
	I	7	1	1635	116.597	98.6688	37.303	-20.847	117.19	17.9282
	I	7	2	2786	124.682	105.451	52.319	-23.782	125.41	19.231
	I	7	3	1198	124.409	105.451	46.992	-20.85	125.06	18.958
	I	7	4	1890	124.213	105.451	29.687	-19.013	124.56	18.762
	I	7	5	2154	120.829	105.451	30.471	-15.629	121.15	15.378
	I	7	6	1806	115.377	105.451	24.824	-10.177	115.52	9.926
	I	7	7	1482	116.099	105.451	31.001	-10.899	116.27	10.648
	I	7	8	2048	117.362	105.451	23.738	-10.462	117.46	11.911

Table A4, continued

DATE	CODE	LOC	POS	LENGTH	MEAN	BASELINE	MAX	MIN	RMS	MEAN-BL
	A	1	1	1843	346.298	92.137	179.5	-148	350.78	254.161
	A	1	2	919	343.512	94.0537	156.59	-118.61	347.96	249.458
	A	1	3	1721	344.42	94.0537	130.88	-122.12	348.31	250.366
	A	1	4	1301	221.276	94.0537	176.22	-71.676	226.5	127.222
	A	1	5	1896	109.376	94.0537	62.424	-20.466	110.32	15.3223
	A	1	6	1828	92.858	87.1023	14.842	-46.688	92.99	5.7557
	A	1	7	1477	81.0855	81.0855	7.8245	-6.7055	81.129	0
	A	2	1	1255	272.868	127.47	91.332	-62.568	274.09	145.398
	A	2	2	1093	261.906	127.9	111.69	-75.506	263.99	134.006
	A	2	3	1040	246.532	127.9	67.068	-62.932	248.64	118.632
	A	2	4	915	211.267	127.9	102.53	-58.267	213.28	83.367
	A	2	5	1039	168.159	126.12	107.14	36.4593	170.64	42.039
	A	2	6	1171	149.722	126.12	103.38	-23.222	151	23.602
	A	2	7	2003	93.7649	86.6071	117.44	-17.675	94.562	7.1578
	A	2	8	942	80.6284	80.6284	7.4316	-5.3884	80.671	0
	A	3	1	980	232.092	119.847	46.609	-71.392	233.35	112.245
	A	3	2	999	176.65	125.68	69.25	-46.95	178.65	50.97
	A	3	3	1059	182.587	125.68	66.213	-53.487	184.05	56.907
	A	3	4	1155	165.575	122.12	73.825	-37.375	166.83	43.455
	A	3	5	1173	152.373	122.12	86.127	-30.073	153.86	30.253
	A	3	6	1065	129.547	91.378	62.853	-14.947	130.21	38.169
	A	3	7	1625	111.589	95.688	50.811	-10.689	111.84	15.901
	A	3	8	2168	89.0778	80.4747	41.722	-12.128	89.195	8.6031
	A	4	1	662	79.2647	79.2647	5.3753	-4.8847	79.296	0
	A	4	6	1070	87.4596	87.4596	5.7304	-4.5296	87.488	0
	A	4	7	1887	86.7224	86.7224	15.878	-4.6524	86.751	0
	A	4	8	1027	86.3313	86.3313	5.1487	-5.1113	86.36	0
	A	5	6	745	98.8983	98.8983	4.5017	-5.7083	98.922	0
	A	5	7	1109	94.3447	94.3447	6.5553	-5.4347	94.37	0
	A	5	8	1662	94.3969	78.4612	9.0031	-4.6269	94.423	15.9357
	A	6	6	734	103.193	103.193	4.507	-4.023	103.21	0
	A	6	7	2164	104.556	92.815	62.144	-6.2356	104.81	11.741
	A	6	8	1513	125.932	93.696	53.968	-7.6125	126.09	32.236
	A	7	1	933	109.743	109.743	4.8567	-4.5433	109.76	0
	A	7	2	1082	91.8575	91.8575	15.843	-4.6575	91.886	0
	A	7	3	822	118.461	118.461	4.6388	-3.8612	118.48	0
	A	7	4	1218	120.329	120.055	7.8706	-4.0294	120.35	0.274
	A	7	5	1476	121.059	120.156	9.7414	-3.9586	121.08	0.903
	A	7	6	2770	121.366	120.069	8.6336	-4.2664	121.38	1.297
	A	7	7	2802	122.156	121.3	20.644	-5.056	122.19	0.856
	A	7	8	2846	124.22	122.427	93.78	-5.42	124.39	1.793
AU9	A	7	1	772	127.58	127.58	3.8196	-3.8804	127.6	0
	A	7	2	1187	127.61	127.61	6.3896	-3.9105	127.63	0
	A	7	3	2014	127.5	127.5	7.2998	-4.7003	127.52	0
	A	7	4	1592	125.91	125.795	14.09	-4.0101	125.93	0.115
	A	7	5	2536	125.205	124.76	23.395	-5.0052	125.24	0.445
	A	7	6	1816	122.937	120.158	97.764	-7.0365	123.39	2.779

Table A4, continued

DATE	CODE	LOC	POS	LENGTH	MEAN	BASELINE	MAX	MIN	RMS	MEAN-BL
	A	7	7	1497	125.346	123.878	41.254	-5.146	125.42	1.468
	A	7	8	5666	126.475	123.878	19.525	-4.5746	126.49	2.597
	D	1	1	1257	273.989	83.1347	208.61	-121.09	279.41	190.854
	D	1	2	1103	320.944	88.4838	218.36	-177.54	326.99	232.46
	D	1	3	1321	295.546	88.4838	300.45	-128.95	302.07	207.062
	D	1	4	1369	220.109	88.4838	373.29	-112.81	230.96	131.625
	D	1	5	1872	97.4784	91.0877	152.42	-11.608	98.508	6.3907
	D	1	6	1237	88.9425	85.1345	17.558	-4.7925	88.979	3.808
	D	1	7	958	88.4838	88.4838	30.016	-5.1838	88.52	0
	D	1	8	529	88.6054	88.6054	4.9946	-4.4554	88.638	0
	D	2	1	1013	224.618	85.2846	156.68	-75.218	227.18	139.333
	D	2	2	1323	212.47	87.3097	125.03	-99.07	215.29	125.16
	D	2	3	1146	194.075	87.3097	103.93	-75.575	196.81	106.765
	D	2	4	1346	156.119	87.3097	120.38	-53.919	159.44	68.8093
	D	2	5	1464	117.617	87.3097	148.58	-60.937	121.14	30.3073
	D	2	6	1596	90.6228	87.3097	136.08	-8.1828	91.219	3.3131
	D	2	7	1704	87.6095	85.2011	29.191	-12.04	87.669	2.4084
	D	3	1	1151	201.77	96.461	52.43	-39.47	202.61	105.309
	D	3	2	1033	192.771	98.963	48.529	-68.271	193.71	93.808
	D	3	3	943	182.235	98.963	69.365	-46.535	183.64	83.272
	D	3	4	1124	164.173	98.963	70.127	-50.073	165.71	65.21
	D	3	5	1211	141.407	98.963	70.693	-46.087	142.86	42.444
	D	3	6	1016	117.102	98.963	67.498	-30.372	118.65	18.139
	D	3	7	1278	99.319	94.124	70.681	-16.879	100.5	5.195
	D	3	8	1326	89.7711	88.461	47.629	-7.3311	89.968	1.3101
	D	4	7	1203	83.487	83.487	5.823	-9.637	83.519	0
	D	4	8	1199	82.7171	82.7171	5.7329	-4.5771	82.727	0
	D	5	5	823	67.2511	67.2511	5.7389	-16.591	67.293	0
	D	5	6	985	66.0188	66.0188	5.2512	-5.0488	66.059	0
	D	5	7	1269	65.7157	64	5.5543	-11.616	65.758	1.7157
AU12	D	5	5	1289	121.749	121.749	26.851	-12.849	121.77	0
	D	5	6	1026	129.969	129.969	4.8311	-33.199	129.99	0
	D	5	7	1765	126.274	126.274	13.726	-4.4741	126.29	0
	D	5	8	2663	125.203	124.934	42.397	-7.7034	125.23	0.269
	D	6	5	750	130.836	130.836	3.9644	-3.8356	130.85	0
	D	6	6	1905	129.625	129.529	30.175	-5.2254	129.65	0.096
	D	6	7	2289	131.258	129.923	62.242	-10.258	131.35	1.335
	D	6	8	2237	132.428	124.815	128.47	-11.428	133.06	7.613
	D	7	1	1315	105.432	105.432	6.0681	-4.3319	105.46	0
	D	7	2	1470	108.853	108.853	5.2468	-13.813	108.88	0
	D	7	3	1455	103.124	103.124	7.4764	-20.174	103.15	0
	D	7	4	1832	103.043	102.731	29.157	-8.8628	103.09	0.312
	D	7	5	2410	102.578	102.099	21.022	-27.408	102.62	0.479
	D	7	6	1701	95.5155	93.0274	114.59	-53.046	95.764	2.4881
	D	7	7	1794	94.1709	92.9258	65.529	-7.0409	94.442	1.2451
	D	7	8	1777	94.6229	91.9393	157.68	-8.2229	95.174	2.6836
	H	1	1	1461	88.6121	82.0051	23.688	-51.462	88.757	6.607

Table A4, continued

DATE	CODE	LOC	POS	LENGTH	MEAN	BASELINE	MAX	MIN	RMS	MEAN-BL
	H	1	2	1334	109.847	88.2728	56.954	-22.577	110.54	21.5742
	H	1	3	1638	164.689	90.4564	121.31	-63.589	167.44	74.2326
	H	1	4	1617	236.871	90.4564	127.73	-103.77	239.46	146.415
	H	1	5	1245	245.07	90.4564	122.13	-120.67	248.68	154.614
	H	1	6	1524	162.211	90.4564	143.69	-67.171	166.19	71.7546
	H	1	7	1371	100.524	97.1542	130.18	-15.844	101.79	3.3698
	H	1	8	2042	88.842	88.2728	54.558	-5.892	88.926	0.5692
AU13	H	2	1	1436	93.1973	80.9793	33.903	-14.347	93.539	12.218
	H	2	2	1097	109.961	83.0141	56.439	-18.111	110.61	26.9469
	H	2	3	2707	125.618	94.5134	76.282	-32.898	126.55	31.1046
	H	2	4	1348	151.21	94.5134	77.59	-46.41	152.67	56.6966
	H	2	5	1284	176.791	94.5134	75.409	-45.991	178	82.2776
	H	2	6	1429	180.418	94.5134	83.882	-53.018	181.48	85.9046
	H	2	7	1361	154.092	94.5134	115.81	-65.312	156.09	59.5786
	H	2	8	1538	120.227	94.5134	120.67	-30.977	121.89	25.7136
	H	3	1	1612	101.723	86.0154	37.777	-52.333	102.02	15.7076
	H	3	2	1277	116.508	86.0154	35.092	-25.528	117.03	30.4926
	H	3	3	1355	125.542	91.5143	36.458	-29.362	126.02	34.0277
	H	3	4	1768	132.344	91.5143	49.656	-30.144	132.97	40.8297
	H	3	5	1847	139.331	91.5143	47.869	-52.681	139.99	47.8167
	H	3	6	1682	147.517	91.5143	60.483	-42.718	148.03	56.0027
	H	3	7	1618	141.949	91.5143	50.451	-48.369	142.93	50.4347
	H	3	8	1422	133.311	95.8489	74.689	-48.391	134.86	37.4621
	H	4	5	1217	82.5877	82.5877	5.8023	-24.528	82.621	0
	H	4	6	1286	83.0377	83.0377	5.3523	-8.5177	83.068	0
	H	4	7	3582	82.6773	81.4202	41.223	-5.5573	82.717	1.2571
	H	4	8	2346	87.607	84.2919	96.993	-12.217	87.871	3.3151
	H	5	4	1085	122.521	122.521	4.8787	-3.8213	122.54	0
	H	5	5	1386	121.774	120.176	46.326	-8.2737	121.81	1.598
	H	5	6	1179	121.014	101.97	46.186	-8.4138	121.13	19.044
	H	5	7	1640	134.018	101.97	83.482	-17.918	135.05	32.048
	H	5	8	1742	165.929	101.97	95.371	-36.329	167.88	63.959
	H	6	1	1617	88.2114	88.2114	5.3686	-5.8914	88.241	0
	H	6	2	2294	98.328	97.0909	16.872	-65.398	98.364	1.2371
	H	6	3	1274	100.811	99.3379	21.389	-4.6306	100.85	1.4731
	H	6	4	1309	102.415	99.879	24.985	10.5646	102.48	2.536
	H	6	5	1175	106.882	99.3379	58.618	-11.562	107.31	7.5441
	H	6	6	1339	116.597	99.3379	55.003	-21.277	117.58	17.2591
AU14	H	6	1	911	102.915	102.915	4.6846	-13.525	102.94	0
	H	6	2	1601	111.603	111.493	15.097	-7.5027	111.63	0.11
	H	6	3	1251	112.095	112.018	10.305	-9.6946	112.12	0.077
	H	6	4	1526	110.355	109.389	31.145	-6.2552	110.44	0.966
	H	6	5	1211	110.141	106.323	68.659	-8.641	110.45	3.818
	H	6	6	1353	119.004	106.323	51.996	-20.065	119.92	12.681
	H	6	7	1357	128.224	91.0154	53.176	-34.494	129.52	37.2086
	H	6	8	1609	146.312	101.514	59.388	-43.912	147.31	44.798
	H	7	1	1556	76.3928	76.3295	14.737	-5.2228	76.441	0.0633

Table A4, continued

DATE	CODE	LOC	POS	LENGTH	MEAN	BASELINE	MAX	MIN	RMS	MEAN-BL
	H	7	2	1699	82.368	81.353	30.432	-8.598	82.458	1.015
	H	7	3	1617	85.0359	81.353	70.367	-61.606	85.326	3.6829
	H	7	4	1354	87.3102	81.353	57.59	-10.07	87.758	5.9572
	H	7	5	1589	103.884	81.353	71.917	-26.644	105.76	22.531
	H	7	6	1640	119.581	81.353	92.219	-40.601	121.57	38.228
	H	7	7	1512	118.307	81.353	67.493	-44.517	119.83	36.954
	H	7	8	1656	129.953	81.353	74.847	-44.903	131.53	48.6
	E	1	1	1920	92.8798	91.9288	11.22	-13.9	92.939	0.951
	E	1	2	973	107.296	96.9411	31.604	-17.036	107.58	10.3549
	E	1	3	1322	153.12	105.684	78.58	-41.12	154.38	47.436
	E	1	4	2746	226.51	105.684	91.19	-78.11	228.66	120.826
	E	1	5	1399	247.991	105.684	77.509	-71.791	249.63	142.307
	E	1	6	1512	153.521	105.684	95.579	-51.122	155.62	47.837
	E	1	7	2280	110.288	105.684	97.112	-19.159	111.14	4.604
	E	1	8	2993	95.8976	95.8976	6.5024	-4.7676	95.926	0
	E	1	1	1889	90.7072	87.4887	22.093	-10.857	90.865	3.2185
	E	1	2	2628	116.249	87.4887	71.251	-25.989	117.41	28.7603
	E	1	3	2103	172.884	87.4887	123.92	-61.784	175.55	85.3953
	E	1	4	1550	245.893	87.4887	111.71	-77.493	248.07	158.404
	E	1	5	1802	244.441	87.4887	102.76	-105.54	247.33	156.952
	E	1	6	2139	229.374	87.4887	139.53	-82.674	233.21	141.885
	E	2	1	1329	95.1481	89.2443	22.852	-35.258	95.481	5.9038
	E	2	3	1352	125.03	97.7774	51.17	-26.09	125.69	27.2526
	E	2	5	1903	168.81	105.936	64.69	-45.61	169.91	62.874
	E	2	6	2179	193.131	119.5464	81.169	-80.331	194.6	73.5846
	E	2	7	1403	155.836	119.5464	63.764	-49.936	157.57	36.2896
	E	2	8	1272	122.122	103.483	60.178	-24.912	122.9	18.639
	E	3	1	1710	96.5853	89.4959	28.415	-17.605	96.92	7.0894
	E	3	2	1542	98.7953	93.9251	46.105	-17.215	99.389	4.8702
	E	3	3	3703	114.677	92.0708	65.023	-27.887	115.51	22.6062
	E	3	4	3093	131.389	92.0708	75.211	-33.319	132.37	39.3182
	E	3	5	2170	136.283	92.0708	65.917	-41.683	137.25	44.2122
	E	3	6	1823	136.288	90.564	54.612	-36.478	137.07	45.724
	E	3	7	1662	138.741	90.564	59.459	-47.271	140.2	48.177
	E	3	8	2347	126.863	90.564	74.137	-43.943	128.55	36.299
	E	4	6	1152	92.2905	92.2905	4.9196	-16.781	92.318	0
	E	4	7	1172	93.3348	93.3348	7.3652	-5.6748	93.363	0
	E	4	8	1222	99.4897	93.3348	9.8103	-37.08	99.527	6.1549
	E	5	5	1057	108.008	108.008	4.7918	-4.7082	108.03	0
	E	5	6	2099	108.901	107.812	51.699	-33.391	109	1.089
	E	5	7	1463	113.243	90.184	50.757	-9.943	113.59	23.059
	E	5	8	2340	132.404	90.184	87.196	-28.304	134.02	42.22
	E	6	5	1587	104.721	96.456	63.569	-8.3812	105.17	8.265
	E	6	6	1595	120.67	96.424	78.73	-19.331	121.97	24.246
	E	6	7	1540	137.362	99.335	63.738	-32.552	138.8	38.027
	E	6	8	1712	139.58	99.335	81.72	-38.88	141.29	40.245
	E	7	1	2088	86.9982	85.7807	26.702	-9.7582	87.074	1.2175

Table A4, continued

DATE	CODE	LOC	POS	LENGTH	MEAN	BASELINE	MAX	MIN	RMS	MEAN-BL
	E	7	2	3155	92.5022	91.792	29.898	-10.922	92.591	0.7102
	E	7	3	3751	96.1923	92.8656	61.808	-8.5323	96.522	3.3267
	E	7	4	1852	98.8423	93.6655	68.658	-15.522	99.314	5.1768
	E	7	5	3856	110.089	93.83	111.21	-23.299	111.46	16.259
	E	7	6	2121	132.449	93.83	87.151	-36.979	134.55	38.619
	E	7	7	1987	129.387	93.83	78.913	-48.687	131.69	35.557
	E	7	8	4815	132.282	93.83	106.41	-38.552	134.46	38.452
AU21	I	1	1	715	95.0653	95.0653	5.0347	-6.4053	95.095	0
	I	1	2	1119	99.0648	99.0648	5.4352	-5.1348	99.091	0
	I	1	3	715	100.769	100.769	5.4307	-4.2093	100.8	0
	I	1	4	899	101.86	101.86	5.24	-5.3	101.89	0
	I	1	5	1958	103.34	102.389	8.1596	-11.17	103.37	0.951
	I	1	6	2929	105.44	101.86	12.16	-11.51	105.49	3.58
	I	1	7	3380	114.237	101.86	43.763	-13.237	114.39	12.377
	I	1	8	2073	137.69	101.86	58.91	-27.99	138.34	35.83
	I	2	1	688	86.2256	86.2256	6.8244	-7.2256	86.272	0
	I	2	2	877	98.66	98.66	5.84	-4.73	98.687	0
	I	2	3	1907	100.699	100.699	5.5012	-5.0188	100.73	0
	I	2	4	1071	101.156	101.156	53.044	-5.4762	101.18	0
	I	2	5	2192	101.796	101.796	8.8037	-6.1163	101.83	0
	I	2	6	1836	102.055	101.284	6.8445	-5.4955	102.08	0.771
	I	2	7	2923	103.086	102.044	15.414	-6.526	103.12	1.042
	I	2	8	1582	110.876	103.149	38.324	-16.066	111.13	7.727
	I	3	1	1328	78.4134	78.4134	9.3666	-19.603	78.474	0
	I	3	2	1159	86.4871	86.4871	7.4429	-7.4871	86.52	0
	I	3	3	1748	87.8408	87.5406	6.9692	-5.3209	87.874	0.3002
	I	3	4	2233	88.5301	88.0726	24.67	-6.0101	88.566	0.4575
	I	3	5	1439	89.6905	87.9223	11.31	-11.561	89.74	1.7682
	I	3	6	2007	94.9845	87.9879	18.616	-7.7146	95.086	6.9966
	I	3	7	2116	95.7561	88.6539	30.144	-8.4862	95.87	7.1022
	I	3	8	1780	98.8615	86.411	29.639	-10.716	99.022	12.4505
	I	4	1	2190	124.216	123.471	26.784	-5.7164	124.25	0.745
	I	4	2	1318	134.385	124.092	94.716	-14.085	135.41	10.293
	I	4	3	2177	168.805	124.092	98.096	-68.705	170.82	44.713
	I	4	4	1514	187.919	124.092	99.081	-58.919	190.88	63.827
	I	4	5	1853	216.482	124.092	63.518	-71.682	217.56	92.39
	I	4	6	1629	229.72	136.724	65.281	-68.22	230.78	92.996
	I	4	7	1435	168.93	136.724	75.67	-45.53	169.96	32.206
	I	4	8	1397	146.009	136.724	45.891	-27.009	146.54	9.285
	I	5	1	1309	138.736	121.247	26.264	-23.736	139.19	17.489
	I	5	2	965	168.82	124.56	37.48	-24.02	169.19	44.26
	I	5	3	1107	225.27	176.014	37.73	-36.07	225.6	49.256
	I	5	4	1300	227.76	176.014	39.94	-37.26	228.32	51.746
	I	5	5	1190	219.346	176.014	42.254	-33.246	219.85	43.332
	I	5	6	1559	205.149	172.898	49.451	-24.349	205.51	32.251
	I	5	7	1338	186.171	172.898	28.029	-14.071	186.29	13.273
	I	5	8	1855	180.963	174.628	26.237	-9.7627	181.02	6.335

Table A4, continued

DATE	CODE	LOC	POS	LENGTH	MEAN	BASELINE	MAX	MIN	RMS	MEAN-BL
	I	6	1	1600	144.407	139.59	16.193	-11.007	144.47	4.817
	I	6	2	1356	164.001	139.59	23.299	-18.801	164.26	24.411
	I	6	3	1161	168.308	139.59	23.392	-24.008	168.58	28.718
	I	6	4	877	160.027	132.583	25.773	-20.727	160.27	27.444
	I	6	5	1153	158.384	132.583	36.016	-21.084	158.82	25.801
	I	6	6	1096	148.823	132.583	28.277	-13.923	149	16.24
	I	6	7	1235	143.499	132.835	33.301	-12.299	143.7	10.664
	I	6	8	1139	143.247	132.583	34.453	-11.248	143.4	10.664
	I	7	1	1457	116.516	108.757	24.784	-36.636	116.74	7.759
	I	7	2	1588	129.815	117.376	34.385	-22.715	130.27	12.439
	I	7	3	1378	131.548	120.862	49.252	-22.648	132.16	10.686
	I	7	4	1357	130.619	120.862	38.781	-17.419	131.07	9.757
	I	7	5	3020	131.735	120.862	28.856	-17.635	132.03	10.873
	I	7	6	4296	125.098	119.953	38.202	-15.398	125.33	5.145
	I	7	7	1637	122.465	116.891	24.135	-13.565	122.69	5.574
	I	7	8	1571	121.633	114.267	24.067	-11.933	121.78	7.366
S27	K	1	1	1392	178.982	133.076	69.418	-46.882	180.72	45.906
	K	1	2	1352	251.264	133.076	107.34	-84.164	254.13	118.188
	K	1	3	1187	371.249	133.076	151.85	-104.45	374.97	238.173
	K	1	4	1071	445.152	133.076	145.25	-133.75	448.12	312.076
	K	1	5	1125	355.538	133.076	158.76	-145.64	360.55	222.462
	K	1	6	2340	227.724	133.076	189.48	-82.524	231.72	94.648
	K	1	7	1732	154.631	128.379	42.169	-27.831	155.5	26.252
	K	1	8	1972	125.377	112.19	29.423	-16.077	125.77	13.187
	K	2	1	1091	168.567	113.421	68.433	-46.067	171.27	55.146
	K	2	2	1080	175.132	113.421	156.37	-55.332	179.73	61.711
	K	2	3	1139	244.453	114.536	66.947	-63.354	245.99	129.917
	K	2	4	1062	267.815	114.536	96.085	-81.515	269.57	153.279
	K	2	5	1003	255.849	114.536	108.95	-82.649	250.33	141.313
	K	2	6	896	255.788	134.942	90.712	-92.988	258.52	120.846
	K	2	7	1112	187.93	134.942	120.87	-51.43	190.96	52.988
	K	2	8	1211	142.78	114.536	110.92	-30.78	144.85	28.244
	K	3	1	1046	189.753	151.121	38.547	-37.553	190.37	38.632
	K	3	2	1129	224.556	151.121	50.144	-41.756	225.49	73.435
	K	3	3	1102	241.389	151.121	73.511	-59.489	242.74	90.268
	K	3	4	1011	237.596	132.991	59.204	-44.896	236.46	104.605
	K	3	5	840	231.901	132.991	89.099	-44.701	232.82	98.91
	K	3	6	929	208.959	132.991	73.041	-48.557	210.18	75.968
	K	3	7	873	204.851	132.991	55.849	-55.251	206.12	71.86
	K	3	8	1070	178.279	132.991	96.421	-43.579	180.85	45.288
	K	4	1	599	98.4382	98.4382	4.7618	-3.9682	98.461	0
	K	4	2	642	103.931	103.931	4.5688	-4.2113	103.95	0
	K	4	3	871	201.473	201.473	6.7265	-6.3735	201.49	0
	K	4	4	838	225.588	225.588	7.1119	-10.388	225.61	0
	K	4	5	635	232.928	232.928	6.7724	-6.4276	232.95	0
	K	4	6	730	233.276	233.276	7.2241	-5.8759	233.29	0
	K	4	7	880	237.698	237.698	6.3021	-6.798	237.72	0

Table A4, continued

DATE	CODE	LOC	POS	LENGTH	MEAN	BASELINE	MAX	MIN	RMS	MEAN-BL
	K	4	8	1466	238.972	231.761	16.428	-12.472	239	7.211
	K	5	1	882	181.166	181.166	6.0338	-6.2662	181.19	0
	K	5	2	792	179.068	179.068	6.3323	-5.8677	179.09	0
	K	5	3	923	183.265	183.265	11.835	-5.6646	183.28	0
	K	5	4	826	186.745	186.745	6.5548	-38.045	186.77	0
	K	5	5	1036	189.46	189.46	6.4399	-5.7601	189.48	0
	K	5	6	1440	193.33	187.777	73.47	-7.03	193.43	5.553
	K	5	7	855	204.881	169.251	140.62	-15.981	205.88	35.63
	K	5	8	1107	226.982	169.251	122.92	-45.083	229.5	57.731
	K	6	1	612	146.125	146.125	5.1755	-4.4245	146.14	0
	K	6	2	912	160.169	160.169	6.0313	-5.3688	160.19	0
	K	6	3	775	162.814	162.814	5.9861	-5.4139	162.83	0
	K	6	4	973	161.776	156.368	31.524	-6.9765	161.87	5.408
	K	6	5	9101	167.573	156.875	112.33	-33.773	168.58	10.698
	K	6	6	698	173.893	156.875	86.807	-19.093	174.84	17.018
	K	6	7	875	190.851	156.875	79.449	-32.551	192.29	33.976
	K	6	8	878	215.241	156.875	92.659	-44.641	217.08	58.366
	K	7	1	1388	117.264	114.729	20.936	-14.064	117.3	2.535
	K	7	2	1859	108.062	105.461	22.238	-15.342	108.11	2.601
	K	7	3	1398	110.144	106.228	44.656	-6.0439	110.26	3.916
	K	7	4	1428	115.429	107.087	57.771	-10.429	116.04	8.342
	K	7	5	1306	121.572	107.111	107.63	-16.572	123.08	14.461
	K	7	6	1406	136.588	108.54	116.21	-28.988	138.92	28.048
	K	7	7	1070	135.067	108.54	87.633	-39.268	137.7	26.527
	K	7	8	1238	144.59	108.54	109.11	-36.99	147.29	36.05
	L	1	1	892	126.937	116.022	47.964	-17.637	127.3	10.915
	L	1	2	722	152.355	119.101	88.145	-30.755	153.66	33.254
	L	1	3	686	189.508	119.101	92.192	-53.908	192.02	70.407
	L	1	4	1094	259.699	119.101	147.9	-101.4	264.02	140.598
	L	1	5	1112	379.828	131.241	161.57	-124.43	383.09	248.587
	L	1	6	875	404.28	131.241	164.92	-186.78	409.55	273.039
	L	1	7	911	315.949	131.241	236.85	-107.75	322.08	184.708
	L	1	8	1045	236.941	131.241	149.66	-79.541	239.99	105.7
	L	2	1	789	104.771	93.9865	31.729	-15.551	105.21	10.7845
	L	2	2	812	133.879	110.093	55.021	-24.579	134.67	23.786
	L	2	3	850	166.826	110.093	95.574	-40.026	168.74	56.733
	L	2	4	877	189.773	110.093	78.127	-46.973	196.5	79.68
	L	2	5	745	207.477	110.093	54.923	-51.777	208.76	97.384
	L	2	6	785	245.451	110.093	69.749	-56.251	247.06	135.358
	L	2	7	817	242.54	120.412	82.46	-74.14	244.61	122.128
	L	2	8	941	204.954	120.412	105.65	-77.154	208.35	84.542
	L	3	1	831	122.216	104.084	32.584	-20.717	122.84	18.132
	L	3	2	1943	149.05	116.455	146.55	-41.45	151.17	32.595
	L	3	3	980	150.381	116.455	96.319	-38.381	153.13	33.926
	L	3	4	1097	163.178	116.455	85.222	-52.978	165.13	46.723
	L	3	5	1015	187.796	116.455	79.004	-53.096	189.13	71.341
	L	3	6	770	208.556	116.455	94.344	-44.756	210.43	92.101

Table A4, continued

DATE	CODE	LOC	POS	LENGTH	MEAN	BASELINE	MAX	MIN	RMS	MEAN-BL
	L	3	7	763	196.991	116.455	60.909	-47.491	198.41	80.536
	L	3	8	840	196.968	116.455	93.432	-58.768	199.37	80.513
	L	4	1	854	125.117	125.117	4.3829	-3.5171	125.13	0
	L	4	2	670	132.455	132.455	4.0454	-3.8546	132.47	0
	L	4	3	673	134.098	134.098	4.1022	-3.7978	134.11	0
	L	4	4	634	135.188	135.188	4.8117	-7.4883	135.2	0
	L	4	5	436	135.781	135.781	4.2186	-3.6814	135.8	0
	L	4	6	945	136.874	104.143	6.6258	-6.5742	136.89	32.731
	L	4	7	1051	244.767	104.861	58.133	-10.968	245.06	139.906
	L	4	8	1267	315.673	104.861	253.13	-77.473	326.8	210.812
	L	5	1	572	119.03	119.03	4.2705	-4.4296	119.05	0
	L	5	2	892	132.406	132.406	4.8942	-3.8058	132.42	0
	L	5	3	867	132.412	132.412	5.788	-3.812	132.43	0
	L	5	4	1148	135.597	129.988	62.103	-6.997	135.84	5.609
	L	5	5	1370	133.888	129.787	50.712	-6.1885	134.01	4.101
	L	5	6	1302	159.833	129.787	177.27	-20.333	162.11	30.046
	L	5	7	1435	206.562	129.787	161.04	-44.462	210.95	76.775
	L	5	8	1120	287.198	132.426	122.2	-103.5	290.91	154.772
	L	6	1	914	113.694	110.657	31.507	-6.0935	113.8	3.037
	L	6	2	1178	126.558	122.105	28.242	-14.558	126.66	4.453
	L	6	3	968	131.929	125.1	84.971	-10.329	132.28	6.829
	L	6	4	1079	158.98	125.1	74.52	-30.38	160.5	33.88
	L	6	5	1030	172.43	125.1	62.87	-39.43	174.16	47.33
	L	6	6	834	194.665	125.1	87.835	-54.665	197.28	69.565
	L	6	7	731	215.282	125.1	90.018	-58.682	217.33	90.182
	L	6	8	955	234.679	125.1	90.721	-73.779	236.5	109.579
	L	7	1	1021	112.262	106.281	28.538	-8.1624	112.5	5.981
	L	7	2	675	123.037	103.044	66.763	-22.437	124.42	19.993
	L	7	3	715	126.673	103.751	71.927	-25.173	128.1	22.922
	L	7	4	956	185.399	103.751	112	-65.6	189.28	81.648
	L	7	5	736	188.804	103.751	99.896	-57.604	191.88	85.053
	L	7	6	844	227.51	103.751	89.09	-64.81	229.66	123.759
	L	7	7	679	222.16	103.751	76.74	-77.26	223.49	118.409
	L	7	8	585	227.928	103.751	66.872	-68.728	230	124.177
	J	1	1	1541	98.2262	98.2262	7.5738	-16.876	98.274	0
	J	1	2	1395	106.224	106.224	15.377	-15.254	106.29	0
	J	1	3	1178	108.603	108.603	5.9969	-4.5031	108.63	0
	J	1	4	1001	110.506	107.738	7.5938	-5.5062	110.54	2.768
	J	1	5	2019	119.332	109.862	71.368	-11.732	119.49	9.47
	J	1	6	2980	167.151	108.603	83.749	-26.451	168.29	58.548
	J	1	7	1498	270.508	108.603	119.59	-90.308	273.13	161.905
	J	1	8	1772	276.69	108.603	119.51	-102.59	279.24	168.087
	J	2	1	928	91.9248	91.9248	16.575	-21.945	92.002	0
	J	2	2	848	106.46	106.46	5.5403	-4.9597	106.49	0
	J	2	3	1194	109.445	106.794	11.255	-6.2446	109.48	2.651
	J	2	4	1135	115.817	108.615	26.783	-10.017	116	7.202
	J	2	5	897	120.281	108.615	29.319	-14.482	120.57	11.666

Table A4, continued

DATE	CODE	LOC	POS	LENGTH	MEAN	BASELINE	MAX	MIN	RMS	MEAN-BL
	J	2	6	1009	137.67	108.615	44.23	-23.07	138.2	29.055
	J	2	7	1104	148.69	98.276	45.91	-24.09	149.3	50.414
	J	2	8	1718	159.182	98.276	63.418	-33.682	160.43	60.906
	J	3	1	1104	108.695	100.329	18.105	-12.475	108.87	8.366
	J	3	2	3007	104.112	103.925	28.888	-29.763	104.69	0.187
	J	3	3	1269	112.956	107.876	25.244	-13.236	113.09	5.08
	J	3	4	2048	107.325	97.4422	46.575	-12.855	107.62	9.8828
	J	3	5	1209	118.91	107.12	27.99	-13.91	119.19	11.79
	J	3	6	1926	133.08	107.12	87.32	-26.38	133.85	25.96
	J	3	7	1719	136.02	107.12	77.38	-21.42	136.67	28.9
	J	3	8	1535	143.786	107.12	46.914	-20.486	144.25	36.666
	J	4	1	802	164.724	164.724	5.8761	-5.5239	164.74	0
	J	4	2	883	170.864	166.915	8.4364	-6.4637	170.89	3.949
	J	4	3	985	151.053	147.541	7.2473	-4.9527	151.07	3.512
	J	4	4	1653	183.801	153.916	118.8	-47.301	186	29.885
	J	4	5	1157	251.858	153.916	149.64	-74.258	255.92	97.942
	J	4	6	1921	309.183	153.916	123.82	-117.58	312.33	155.267
	J	4	7	1140	327.565	153.916	156.14	-84.365	330.31	173.649
	J	4	8	1290	281.318	153.916	139.88	-104.12	283.47	127.402
	J	5	1	1400	130.503	127.539	14.697	-4.5029	130.54	2.964
	J	5	2	1091	178.451	130.471	77.85	-32.351	179.66	47.98
	J	5	3	1011	208.426	130.471	94.174	-53.626	210.7	77.955
	J	5	4	1165	241.309	130.471	84.991	-77.709	243.2	110.838
	J	5	5	1079	252.82	130.471	79.58	-76.12	254.07	122.349
	J	5	6	1162	242.736	130.471	103.66	-54.636	244.23	112.265
	J	5	7	944	218.523	143.618	102.98	-57.123	220.91	74.905
	J	5	8	905	196.55	143.618	87.35	-42.95	197.89	52.932
	J	6	1	1213	147.714	126.634	28.086	-24.414	148.07	21.08
	J	6	2	787	173.145	133.536	60.355	-40.145	174.08	39.609
	J	6	3	818	178.713	133.536	48.687	-40.513	179.46	45.177
	J	6	4	1290	189.294	133.536	46.006	-32.694	189.66	55.758
	J	6	5	818	182.191	133.536	40.809	-32.591	182.68	48.655
	J	6	6	908	172.984	133.536	38.716	-59.284	173.45	39.448
	J	6	7	1017	165.224	133.536	57.776	-30.524	165.95	31.688
	J	6	8	959	151.327	133.536	49.873	-48.127	151.95	17.791
	J	6	1	1163	166.14	N.M.	28.06	-25.34	166.44	166.14
	J	6	2	1307	218.558	N.M.	56.142	-37.458	219.04	218.558
	J	6	3	967	221.447	N.M.	42.753	-39.547	221.98	221.447
	J	6	4	1073	201.233	N.M.	55.067	-37.633	202.04	201.233
	J	6	5	1005	188.662	N.M.	47.538	-32.962	189.38	188.662
	J	6	6	1080	189.502	N.M.	55.398	-35.602	190.36	189.502
	J	6	7	1557	176.631	N.M.	48.169	-28.831	177.15	176.631
	J	6	8	1563	165.119	N.M.	69.281	-25.119	165.62	165.119
	J	7	3	1198	111.595	101.619	42.305	-15.375	111.86	9.976
	J	7	4	1256	132.205	111.67	40.995	-21.105	132.69	20.535
	J	7	5	1170	137.767	111.67	54.633	-24.967	138.33	26.097
	J	7	6	981	147.031	111.67	54.169	-26.331	147.8	35.361

Table A4, continued

DATE	CODE	LOC	POS	LENGTH	MEAN	BASELINE	MAX	MIN	RMS	MEAN-BL
	J	7	7	911	150.182	111.67	52.818	-45.982	151.43	38.512
	J	7	8	4306	154.115	111.67	82.085	-34.315	154.94	42.445
	M	1	1	414	96.7515	96.7515	5.5485	-9.8115	96.776	0
	M	1	2	1124	103.8	103.8	4.3996	-4.9304	103.82	0
	M	1	3	1104	105.174	105.174	4.8262	-4.5738	105.19	0
	M	1	4	1167	106.13	105.933	7.2699	-4.7301	106.15	0.197
	M	1	5	1233	108.439	105.933	9.1614	-6.1387	108.47	2.506
	M	1	6	1197	114.182	105.933	23.018	-8.4819	114.26	8.249
	M	1	7	1529	131.077	105.933	46.223	-16.878	131.46	25.144
	M	1	8	2546	160.122	105.933	84.478	-42.522	161.95	54.189
	M	2	1	819	91.9436	91.9436	5.2264	-5.0036	91.971	0
	M	2	2	606	103.125	103.125	5.9751	-5.9549	103.15	0
	M	2	3	627	105.037	104.702	8.3633	-4.4367	105.06	0.335
	M	2	4	856	105.56	105.476	6.1401	-4.1599	105.58	0.084
	M	2	5	1369	106.527	105.898	11.073	-5.1268	106.56	0.629
	M	2	6	1176	108.972	106.303	14.628	-6.6721	109.03	2.669
	M	2	7	1477	112.449	107.023	39.251	-22.959	112.68	5.426
	M	2	8	1209	122.92	106.254	35.58	-18.12	123.18	16.666
	M	3	1	2524	99.513	92.5701	42.787	-21.953	99.88	6.9429
	M	3	2	1239	119.132	105.984	28.368	-23.672	119.58	13.148
	M	3	3	2077	123.146	105.984	48.654	-35.746	124.54	17.162
	M	3	4	1688	135.506	105.984	48.394	-42.806	136.68	29.522
	M	3	5	1308	130.445	105.984	45.555	-27.745	131.18	24.461
	M	3	6	1422	128.959	105.984	29.541	-24.159	129.17	22.975
	M	3	7	1262	136.797	105.984	41.303	-17.497	137.4	30.813
	M	3	8	2032	129.973	105.984	54.627	-32.373	130.99	23.989
	M	4	1	1168	195.537	138.114	140.26	-62.537	201.47	57.423
	M	4	2	1065	231.219	148.715	170.18	-86.319	236.86	82.504
	M	4	3	1027	272.383	148.451	141.02	-126.68	277.07	123.932
	M	4	4	986	287.653	148.215	101.85	-89.953	289.91	139.438
	M	4	1	1621	237.131	111.405	120.87	-117.83	241.77	125.726
	M	4	2	1528	269.341	111.405	168.76	-139.74	274.02	157.936
	M	4	3	1462	266.631	111.405	111.77	-94.431	269.34	155.226
	M	4	4	1106	217.288	111.405	92.112	-78.388	219.77	105.883
	M	4	5	1407	196.492	111.405	115.51	-57.592	198.86	85.087
	M	4	6	1370	145.898	111.405	90.202	-36.798	147.2	34.493
	M	4	7	1039	134.328	111.405	68.572	-25.228	135.22	22.923
	M	4	8	1207	119.453	107.068	67.247	-18.053	119.88	12.385
	M	5	1	954	250.036	158.473	34.664	-55.736	250.65	91.563
	M	5	2	915	252.331	158.473	82.669	-69.031	254.27	93.858
	M	5	3	940	237.196	158.473	72.204	-52.197	238.24	78.723
	M	5	4	814	204.237	158.473	58.263	-43.137	205.75	45.764
	M	5	5	917	184.67	158.473	76.13	-30.37	185.62	26.197
	M	5	6	849	164.092	158.473	50.708	-19.192	164.49	5.619
	M	5	7	775	164.585	157.084	49.315	-16.285	165.09	7.501
	M	5	8	914	155.441	152.192	21.859	-7.9406	155.5	3.249
	M	6	1	1049	181.134	171	17.466	-16.634	181.25	10.134

Table A4, continued

DATE	CODE	LOC	POS	LENGTH	MEAN	BASELINE	MAX	MIN	RMS	MEAN-BL
	M	6	2	994	193.525	163.491	38.275	-32.425	194.07	30.034
	M	6	3	953	199.689	163.191	47.511	-37.79	200.55	36.498
	M	6	4	806	189.624	163.191	45.376	-28.724	190.26	26.433
	M	6	5	1270	175.436	150.945	52.164	-31.436	176.31	24.491
	M	6	6	1055	180.598	150.842	32.002	-19.098	180.89	29.756
	M	6	7	911	180.608	144.951	56.692	-22.508	181.18	35.657
	M	6	8	1016	173.007	142.262	63.893	-36.607	174.46	30.745
	M	7	1	835	221.377	152.228	34.323	-48.377	222.02	69.149
	M	7	2	897	243.145	152.228	61.155	-59.845	244.24	90.917
	M	7	3	961	218.056	152.228	69.144	-66.356	219.6	65.828
	M	7	4	858	219.405	152.228	49.895	-61.705	221.09	67.177
	M	7	5	827	190.623	152.228	67.677	-50.023	192.71	38.395
	M	7	6	996	161.837	152.228	42.763	-28.037	162.68	9.609

APPENDIX XIII. PLOTS OF CONDUCTIVITY DATA AND POSITION

The following pages utilize the data from Appendix XII to show graphically the dispersions into the pipeline under different mixing conditions. The first set of graphs are from the vertical probe locations; the second set includes the horizontal probe data.

The baseline conductivities have been subtracted for these graphs. In each graph, we represent the probe data and show the cross-sectional position with zero on the X-axis representing the wall at the same azimuthal position as the injection port. These graphs illustrate the dispersion of the jet as we get farther away from the port.

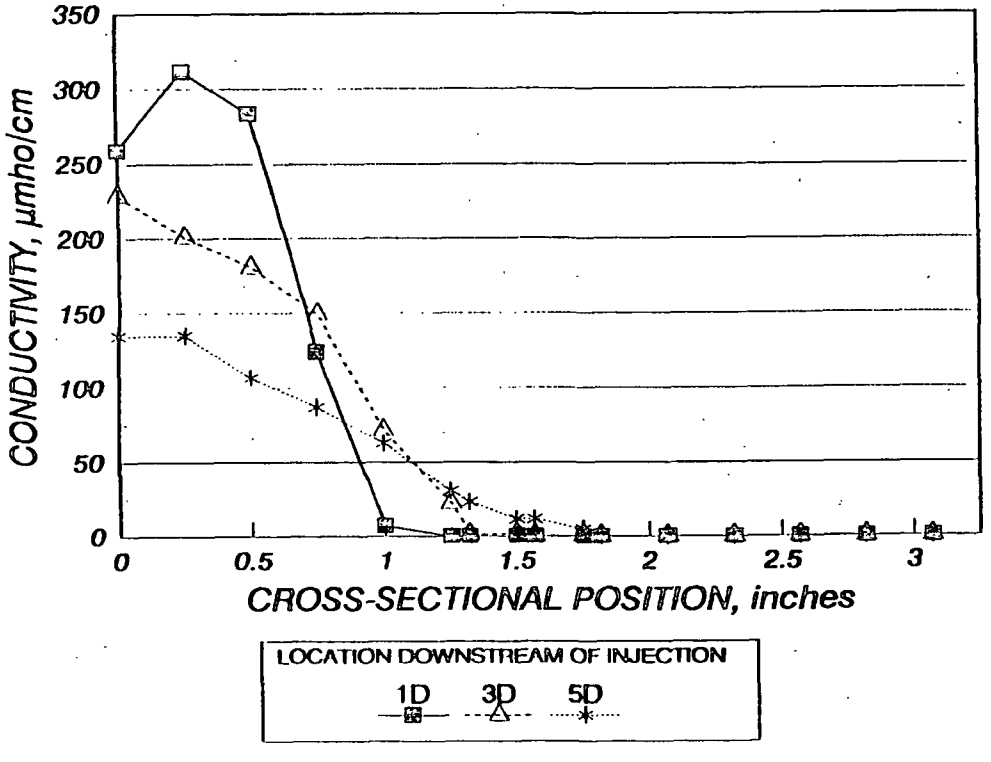

Figure A8. Three cross-sectional views downstream from an injection port showing the dispersion into a pipeline water flow for velocity condition A.

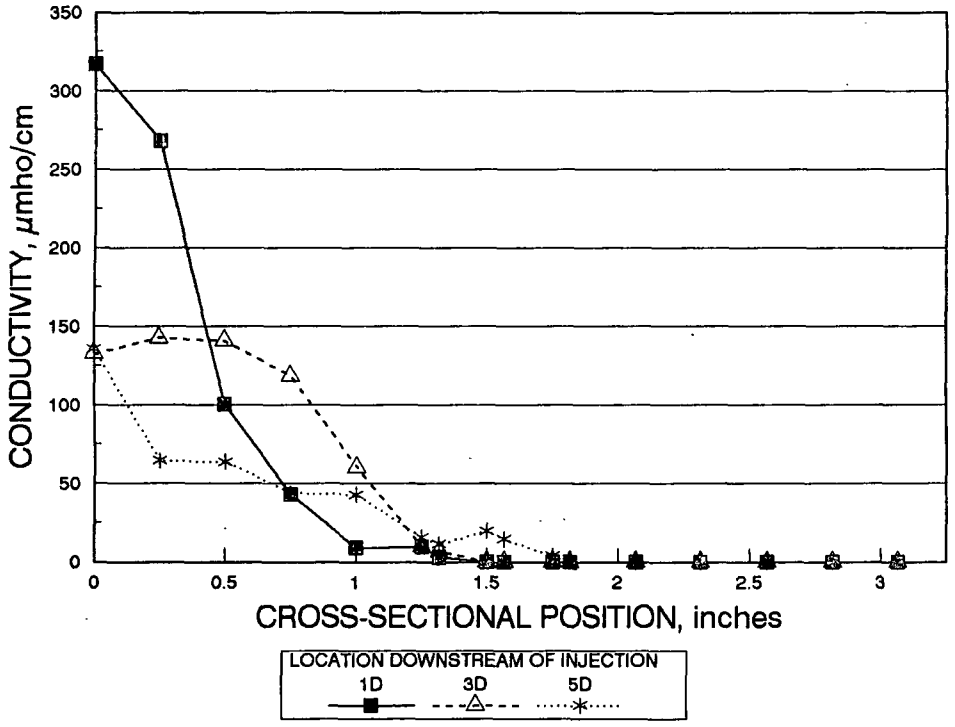

Figure A9. Three cross-sectional views downstream from an injection port showing the dispersion into a pipeline pulp flow for velocity condition A.

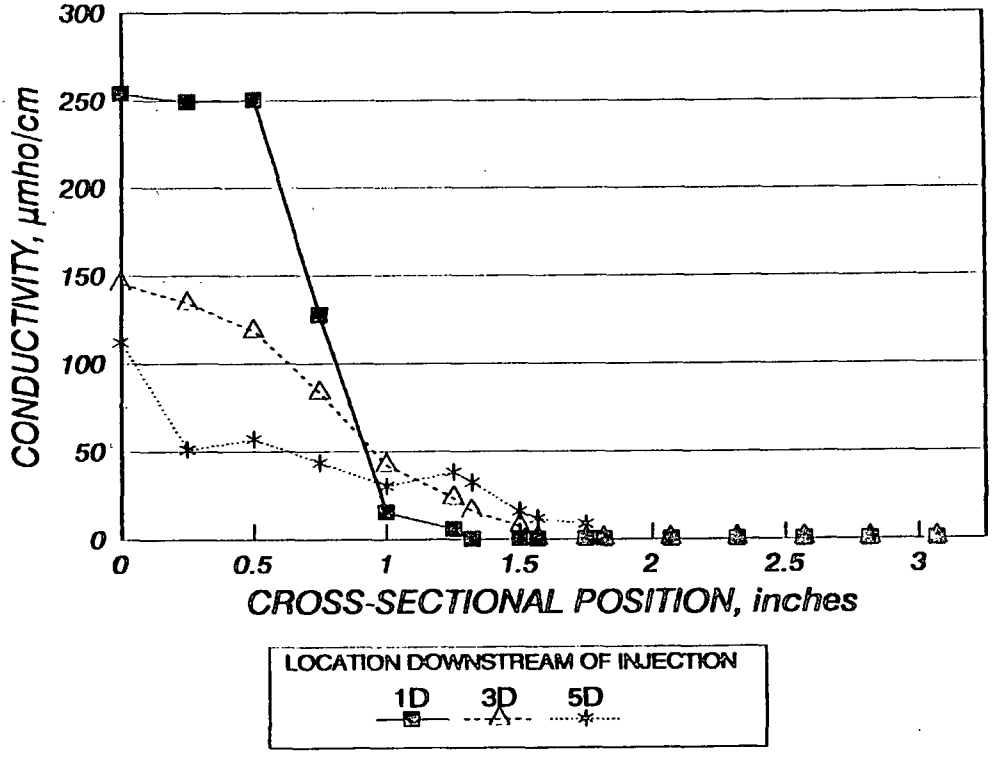

Figure A10. Three cross-sectional views downstream from an injection port showing the dispersion into a pipeline pulp flow for velocity condition A.

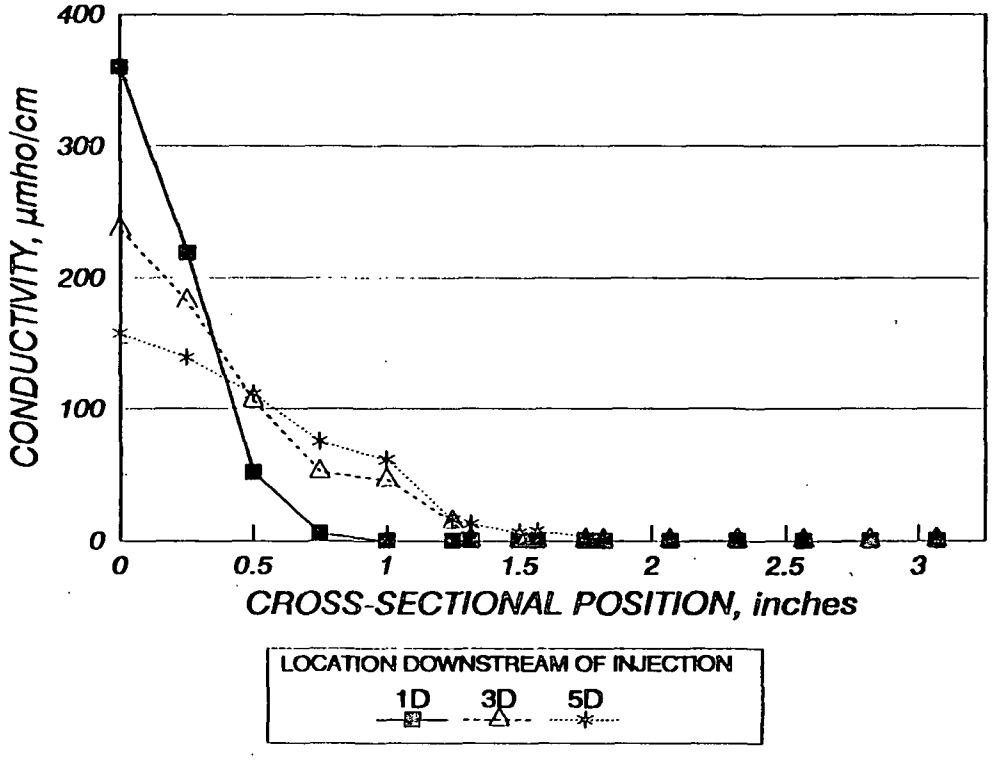

Figure A11. Three cross-sectional views downstream from an injection port showing the dispersion into a pipeline water flow for velocity condition B.

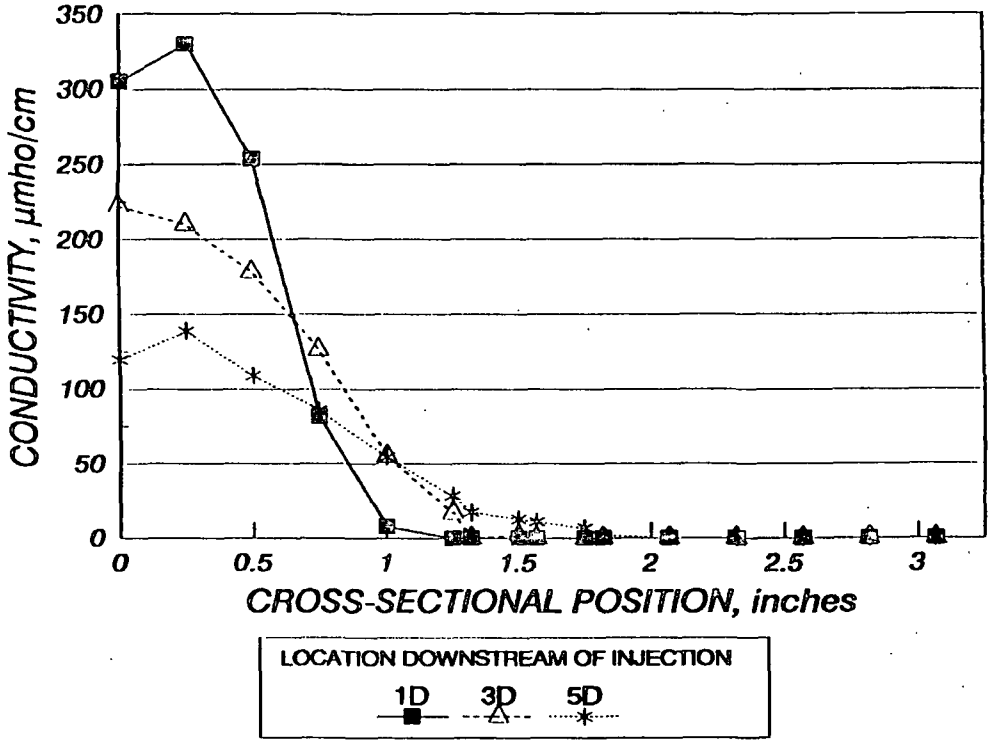

Figure A12. Three cross-sectional views downstream from an injection port showing the dispersion into a pipeline water flow for velocity condition B.

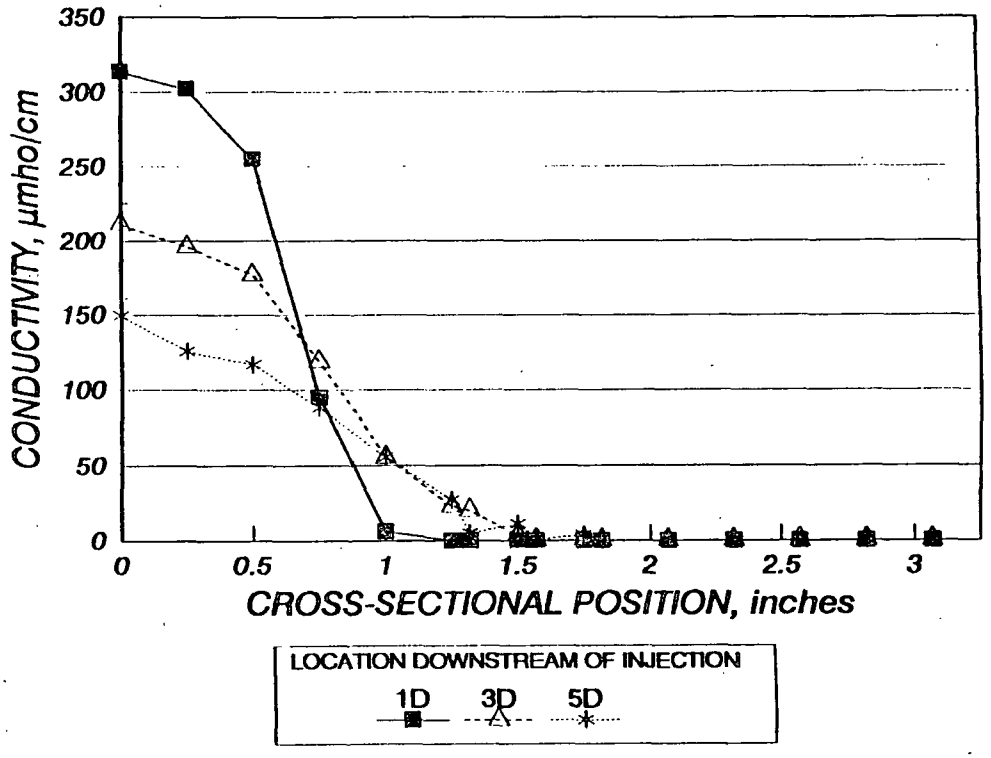

Figure A13. Three cross-sectional views downstream from an injection port showing the dispersion into a pipeline water flow for velocity condition B.

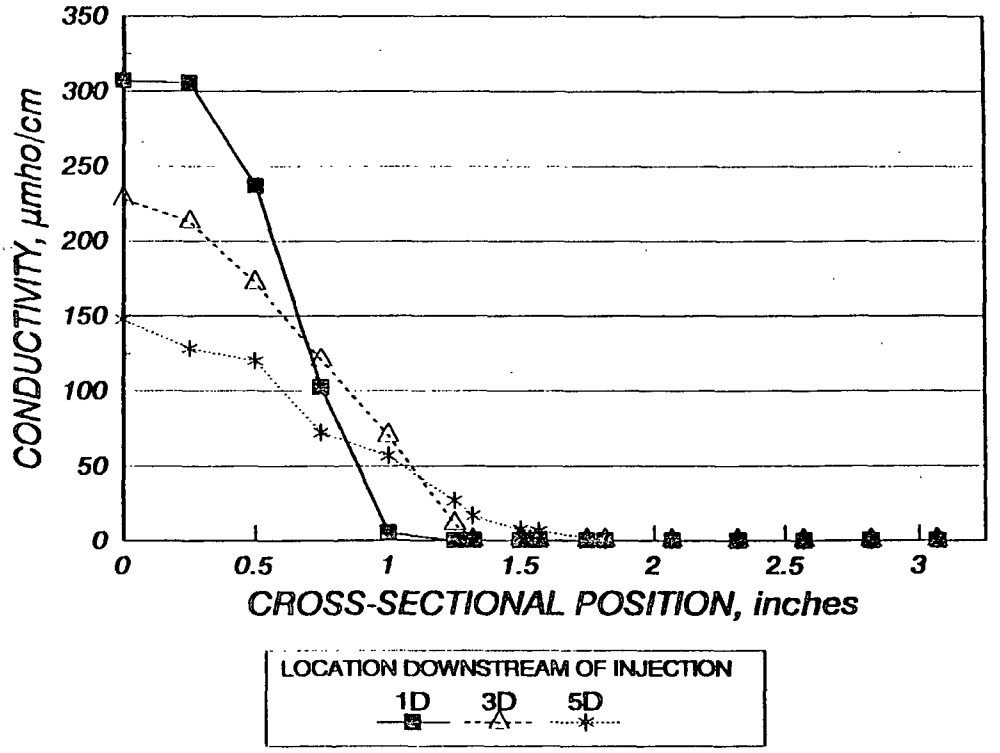

Figure A14. Three cross-sectional views downstream from an injection port showing the dispersion into a pipeline water flow for velocity condition C.

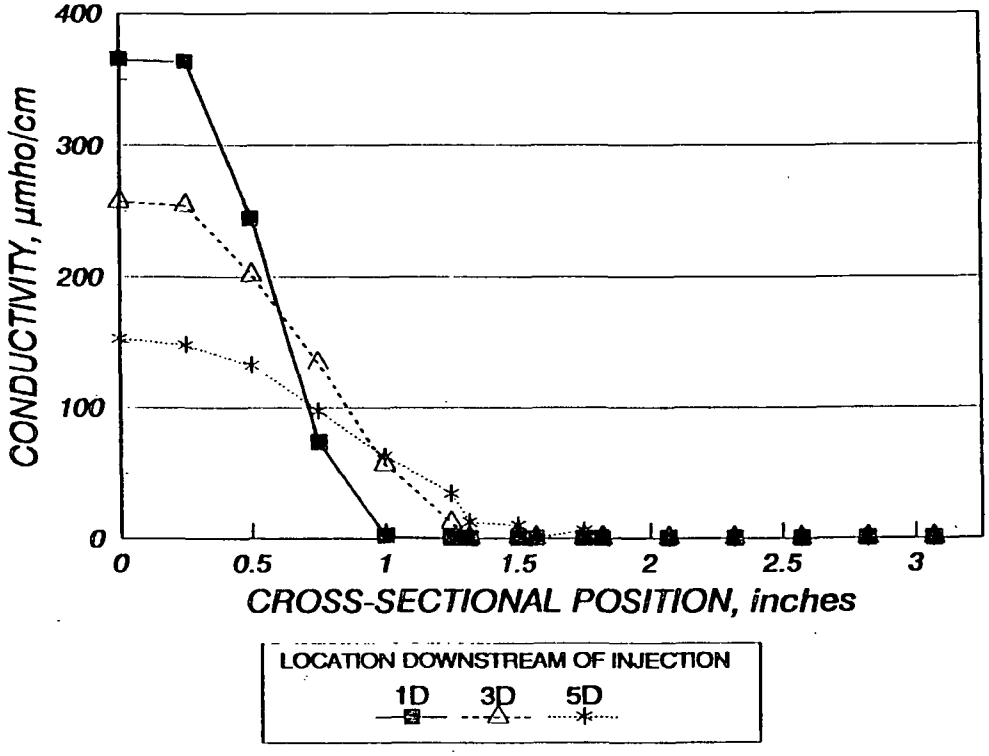

Figure A15. Three cross-sectional views downstream from an injection port showing the dispersion into a pipeline water flow for velocity condition D.

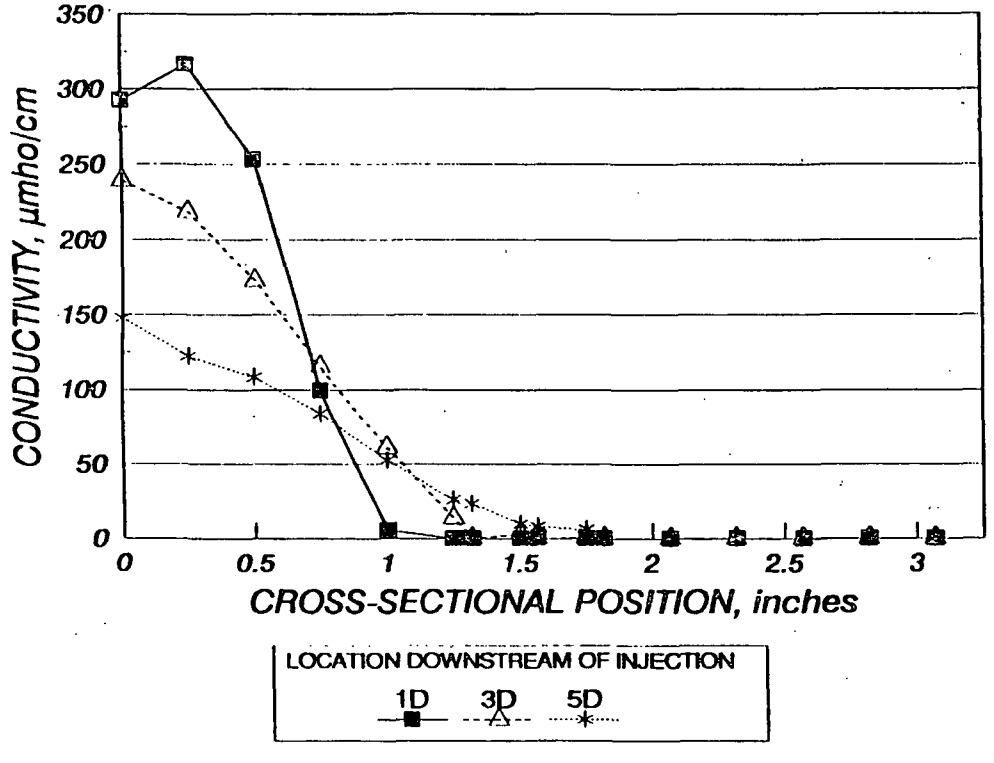

Figure A16. Three cross-sectional views downstream from an injection port showing the dispersion into a pipeline water flow for velocity condition D.

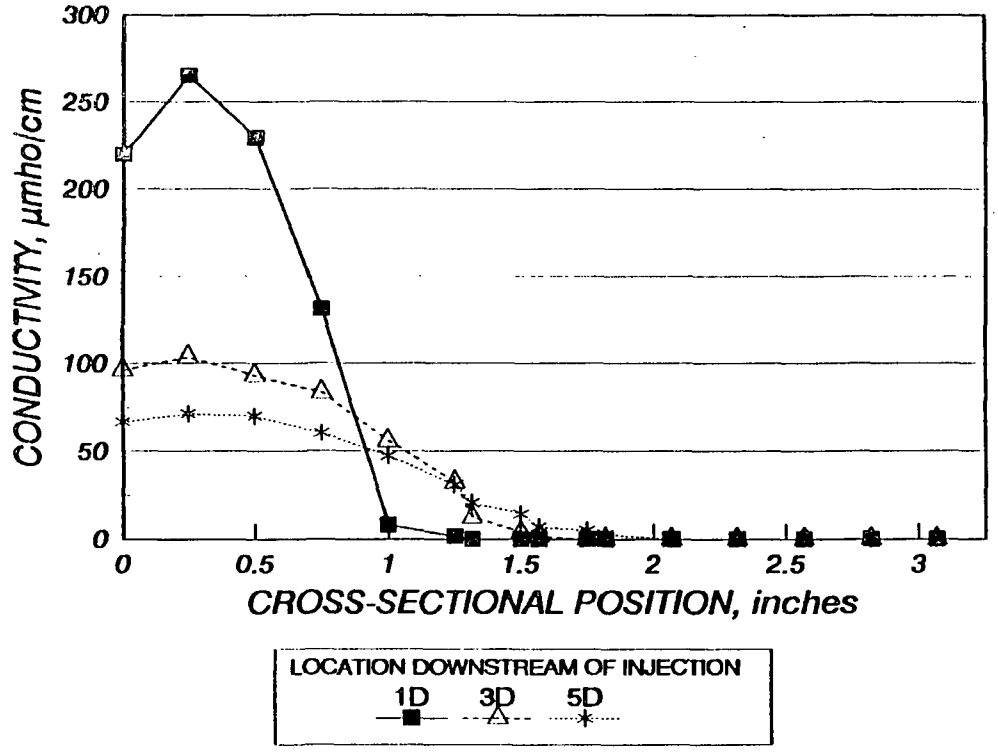

Figure A17. Three cross-sectional views downstream from an injection port showing the dispersion into a pipeline pulp flow for velocity condition D.

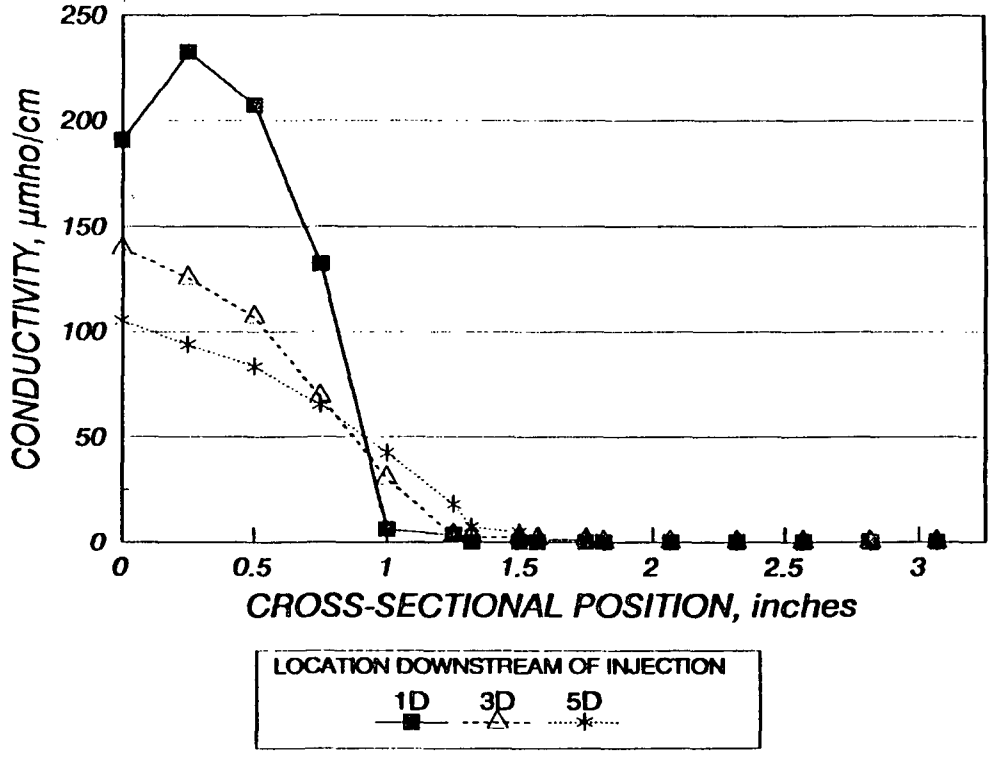

Figure A18. Three cross-sectional views downstream from an injection port showing the dispersion into a pipeline pulp flow for velocity condition D.

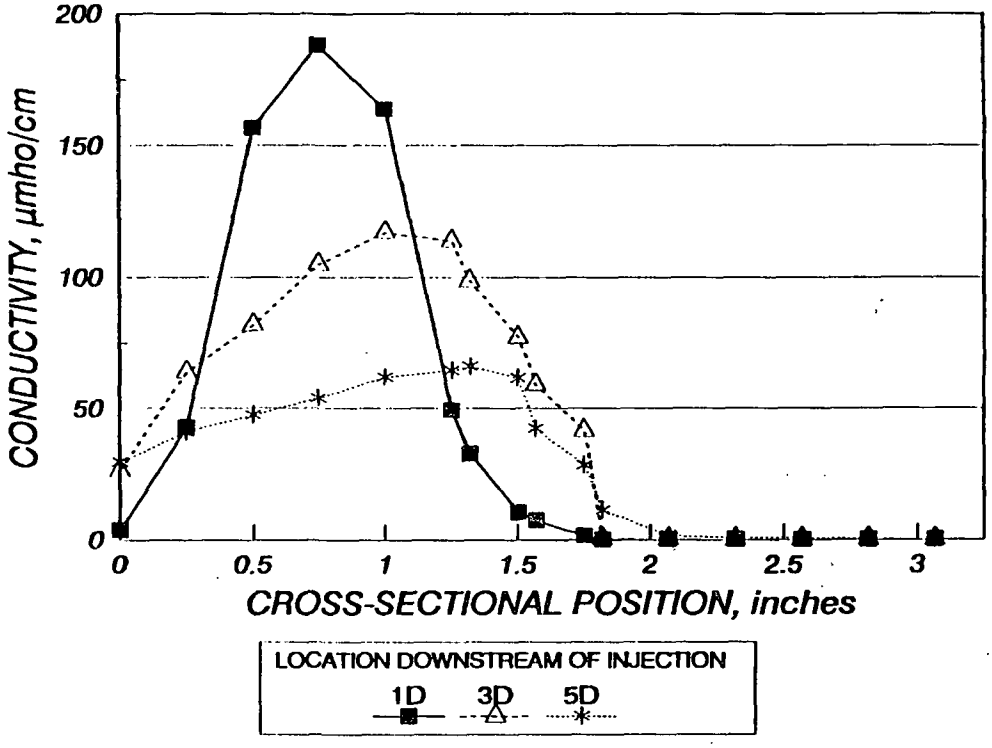

Figure A19. Three cross-sectional views downstream from an injection port showing the dispersion into a pipeline water flow for velocity condition E.

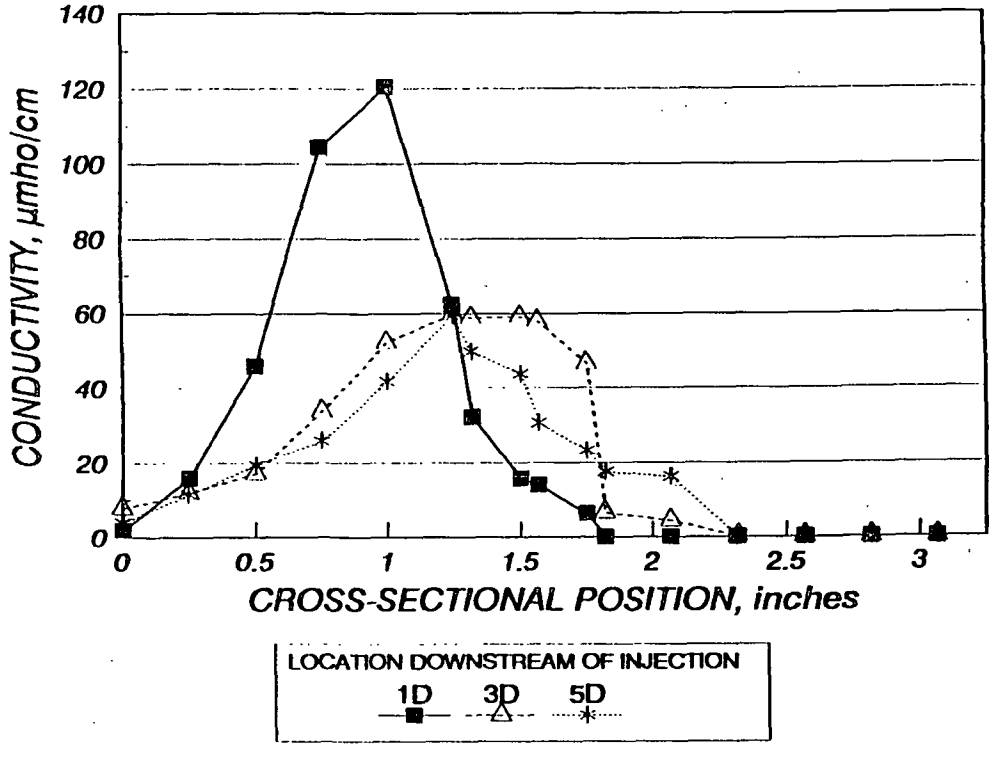

Figure A20. Three cross-sectional views downstream from an injection port showing the dispersion into a pipeline pulp flow for velocity condition E.

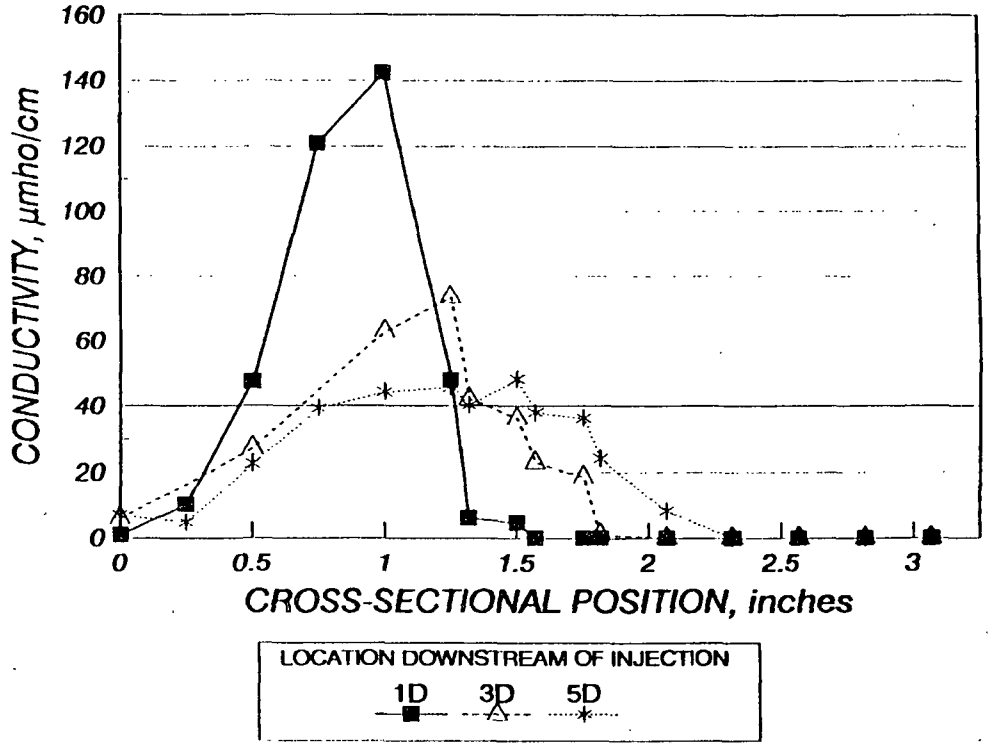

Figure A21. Three cross-sectional views downstream from an injection port showing the dispersion into a pipeline pulp flow for velocity condition E.

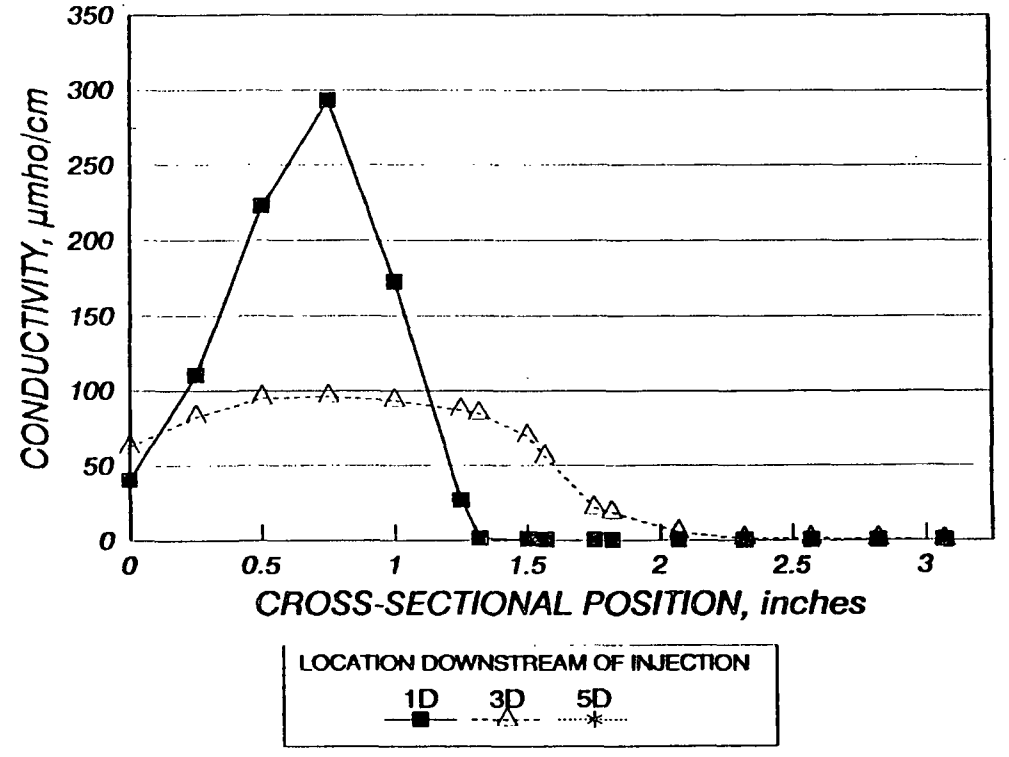

Figure A22. Three cross-sectional views downstream from an injection port showing the dispersion into a pipeline water flow for velocity condition F.

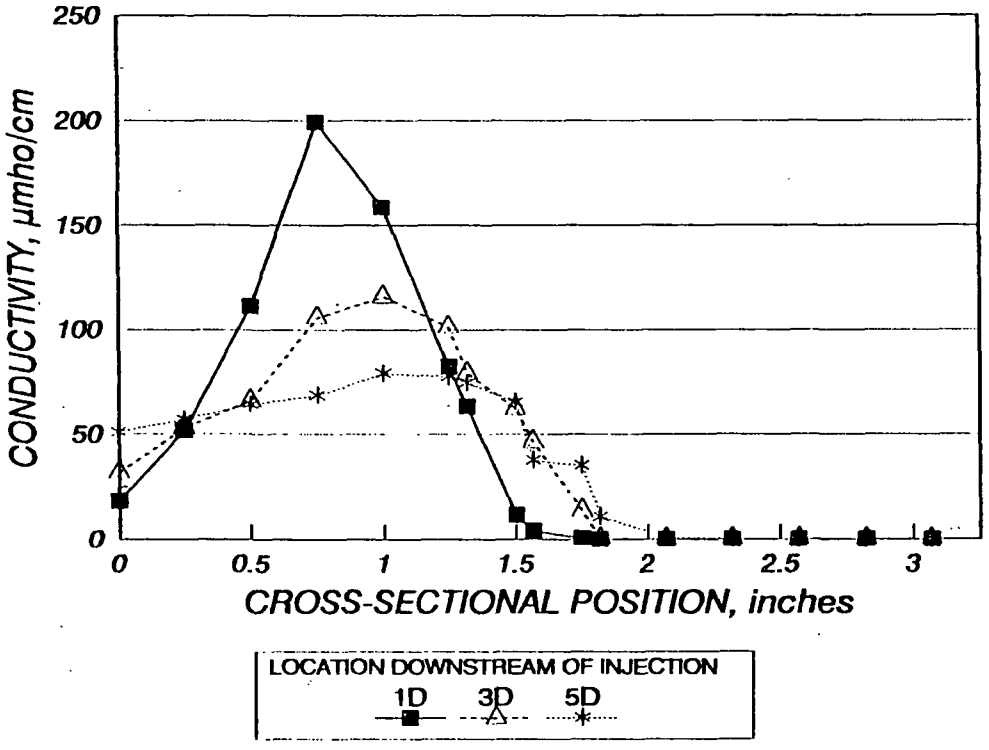

Figure A23. Three cross-sectional views downstream from an injection port showing the dispersion into a pipeline water flow for velocity condition F.

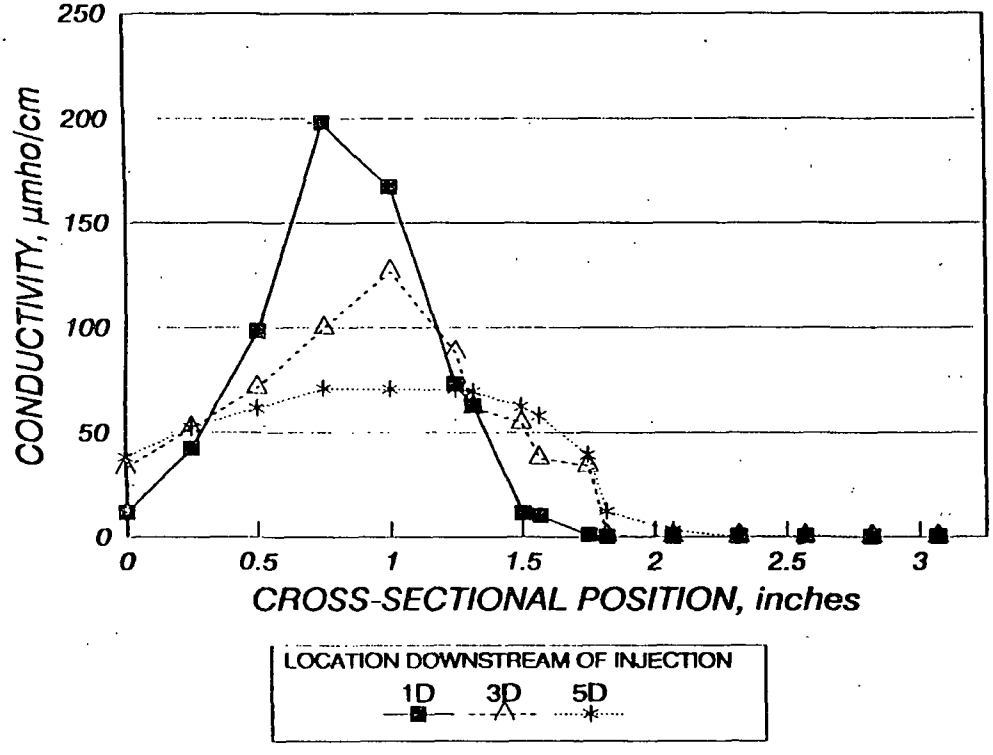

Figure A24. Three cross-sectional views downstream from an injection port showing the dispersion into a pipeline water flow for velocity condition G.

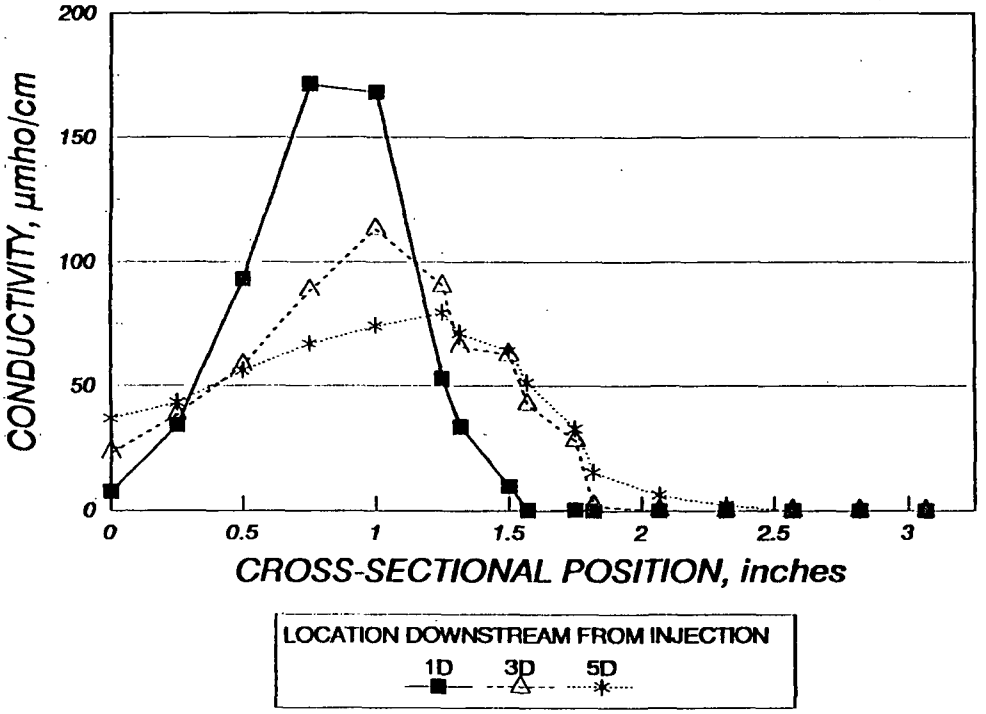

Figure A25. Three cross-sectional views downstream from an injection port showing the dispersion into a pipeline water flow for velocity condition H.

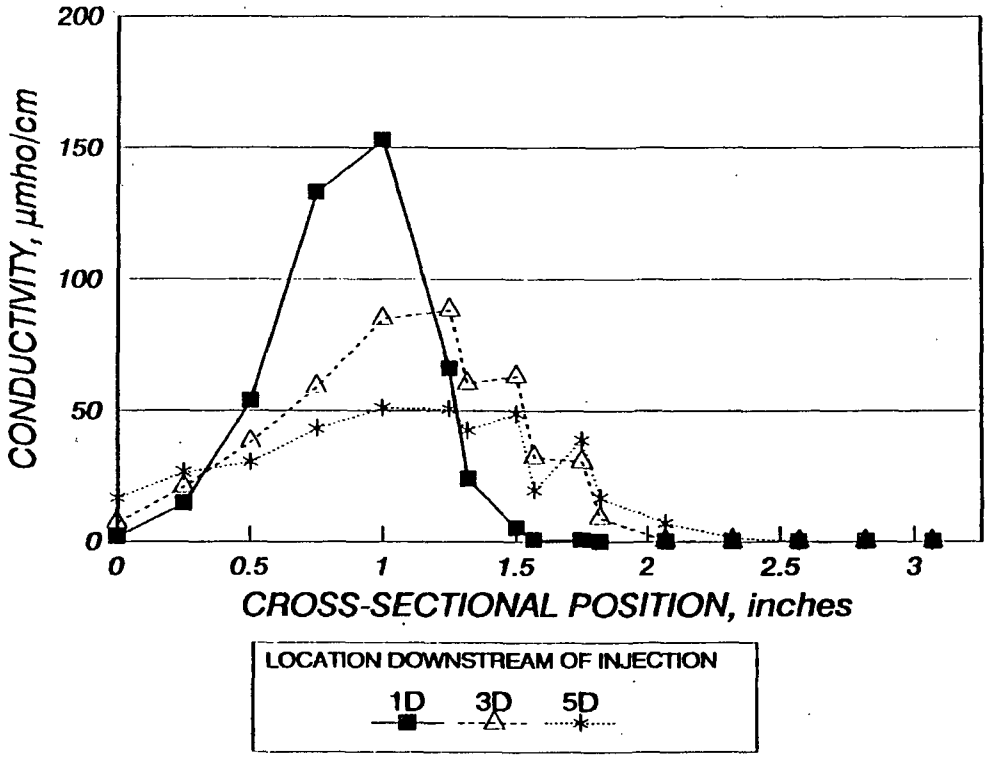

Figure A26. Three cross-sectional views downstream from an injection port showing the dispersion into a pipeline pulp flow for velocity condition H.

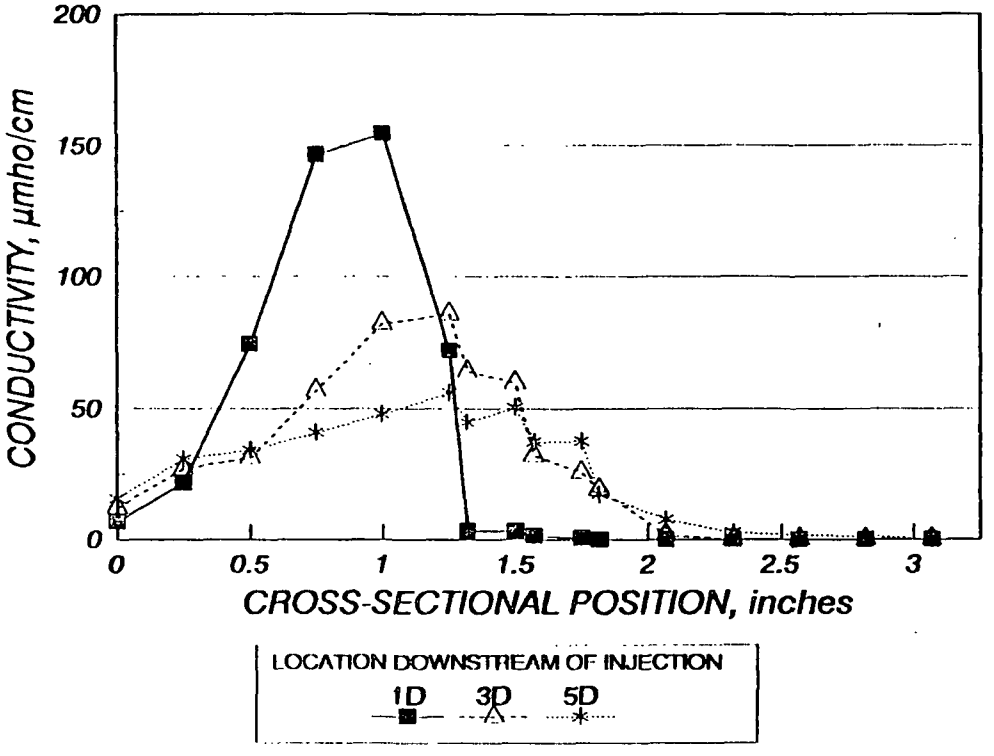

Figure A27. Three cross-sectional views downstream from an injection port showing the dispersion into a pipeline pulp flow for velocity condition H.

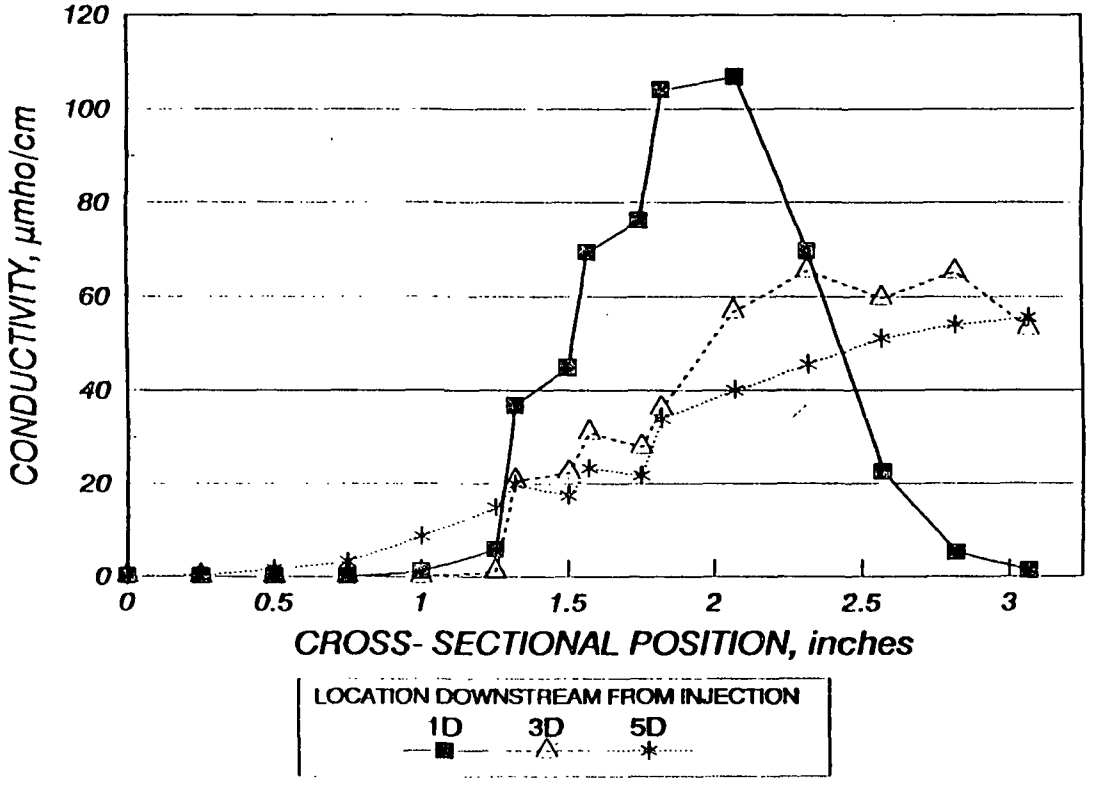

Figure A28. Three cross-sectional views downstream from an injection port showing the dispersion into a pipeline water flow for velocity condition I.

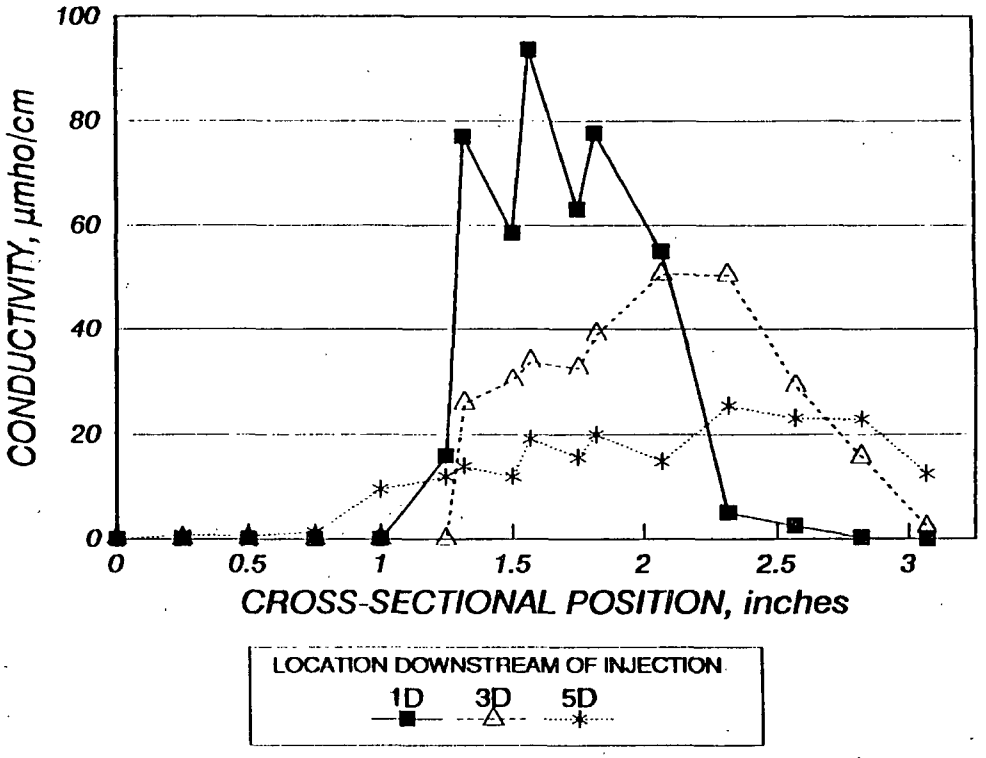

Figure A29. Three cross-sectional views downstream from an injection port showing the dispersion into a pipeline pulp flow for velocity condition I.

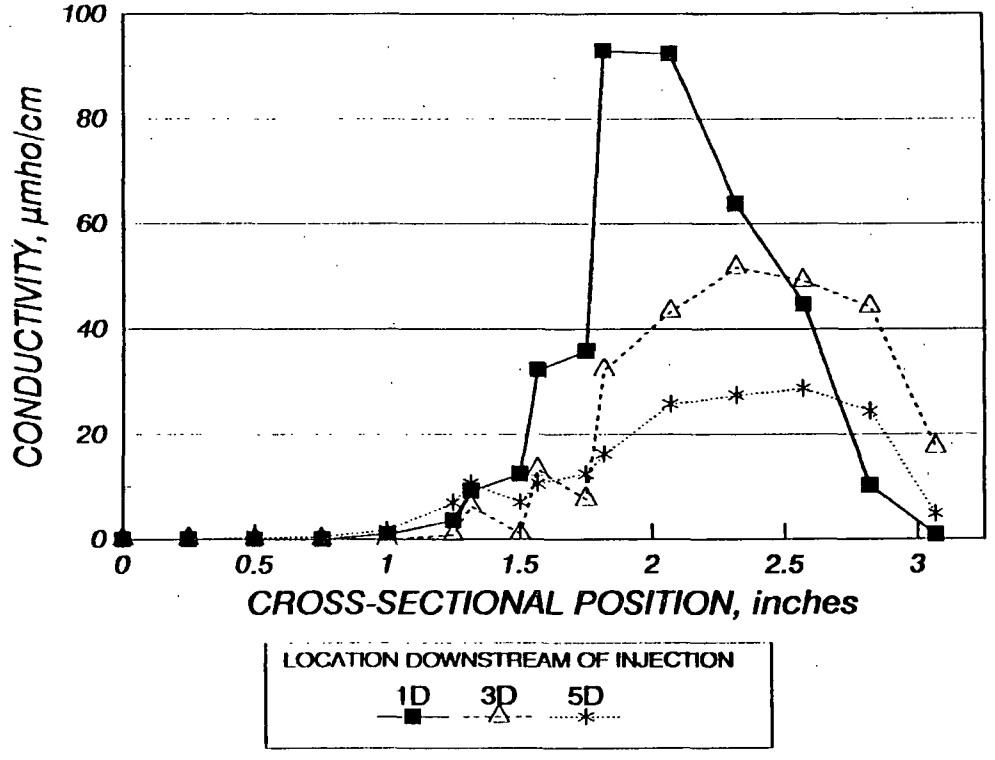

Figure A30. Three cross-sectional views downstream from an injection port showing the dispersion into a pipeline pulp flow for velocity condition I.

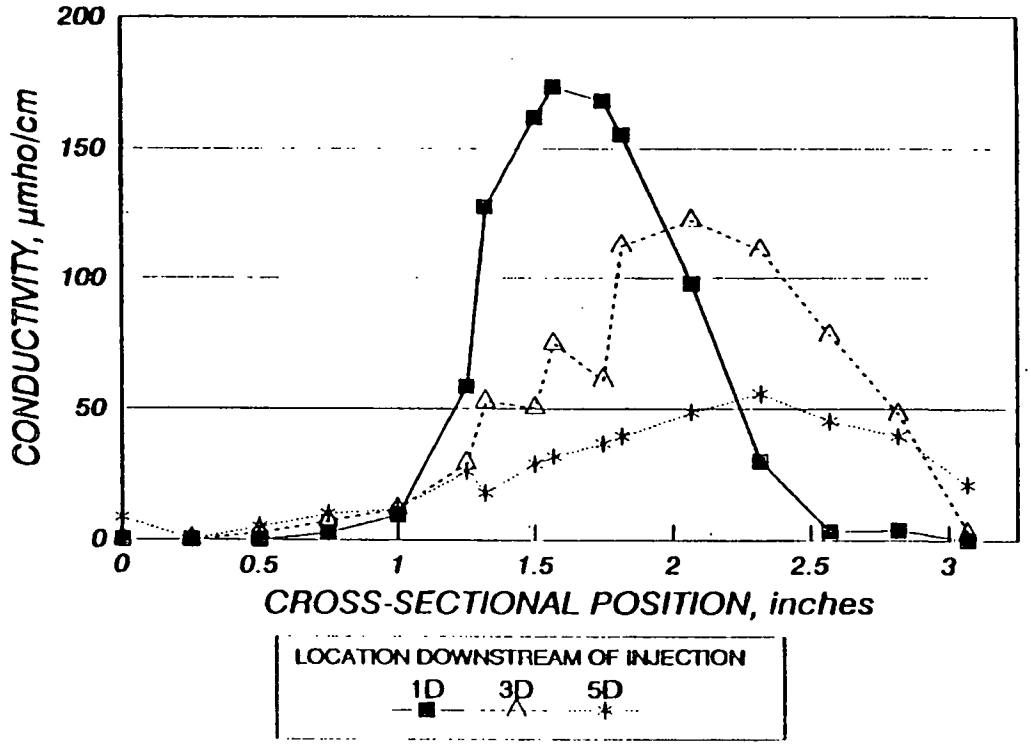

Figure A31. Three cross-sectional views downstream from an injection port showing the dispersion into a pipeline pulp flow for velocity condition J.

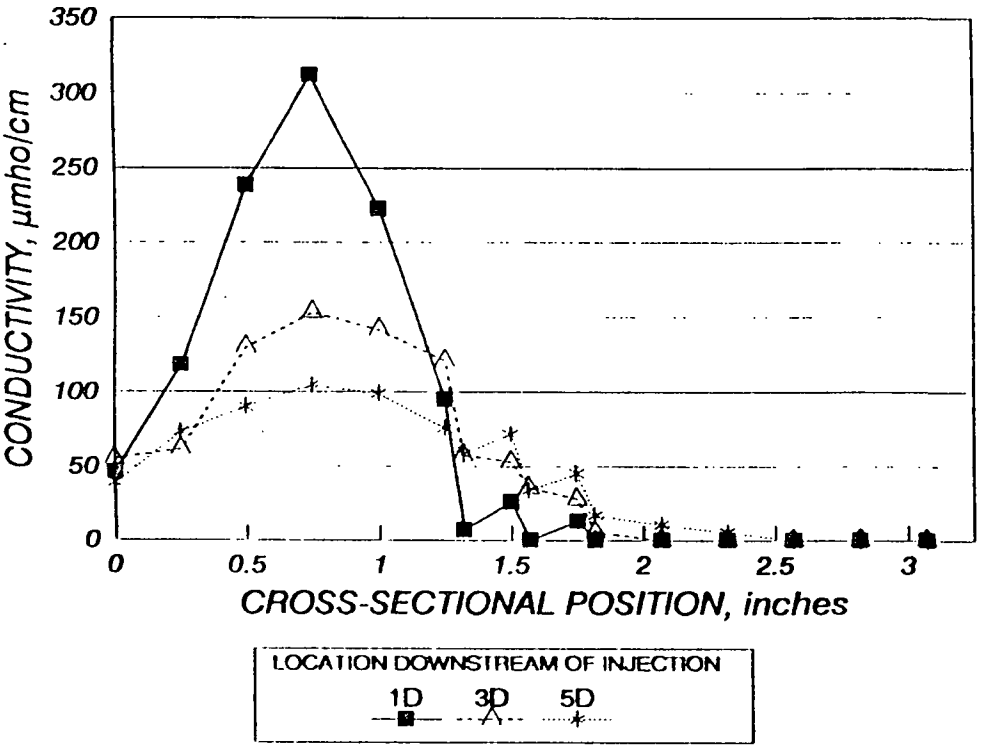

Figure A32. Three cross-sectional views downstream from an injection port showing the dispersion into a pipeline pulp flow for velocity condition K.

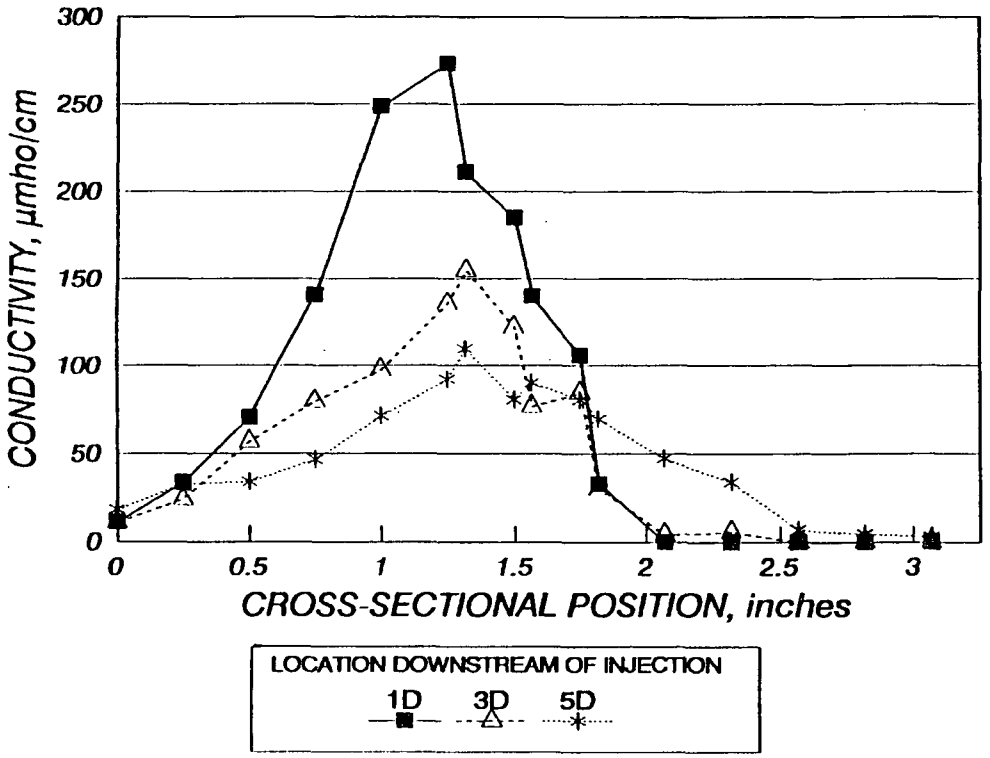

Figure A33. Three cross-sectional views downstream from an injection port showing the dispersion into a pipeline pulp flow for velocity condition L.

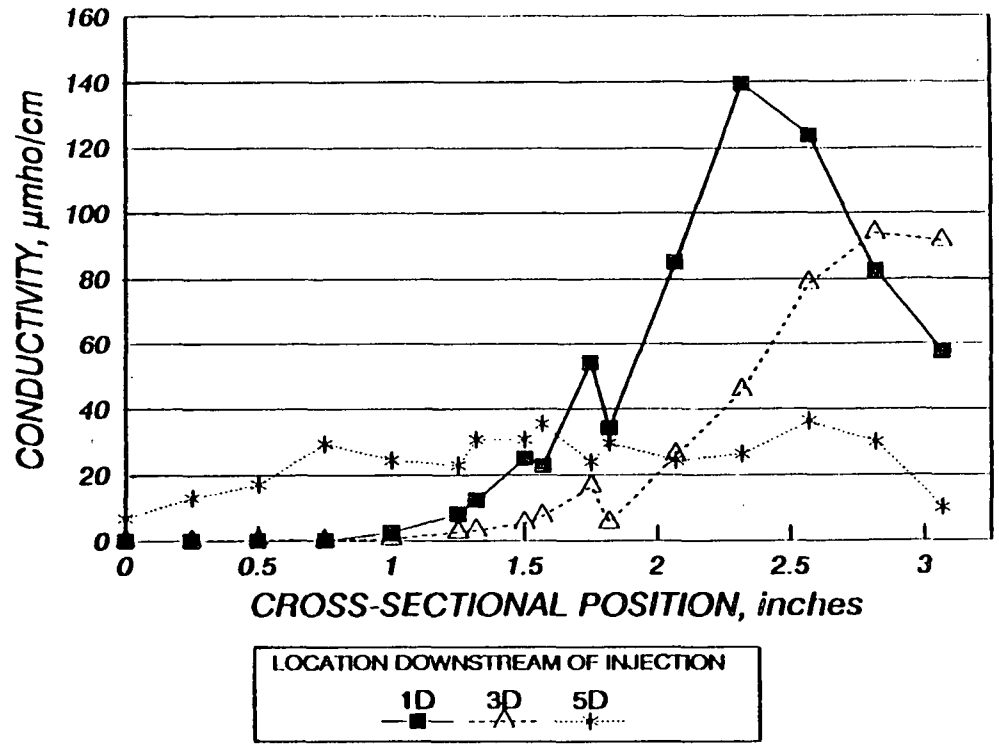

Figure A34. Three cross-sectional views downstream from an injection port showing the dispersion into a pipeline pulp flow for velocity condition M.

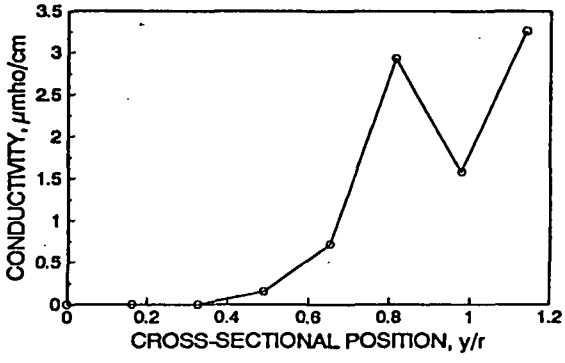

Figure A35. Horizontal probe data for water flow condition A.

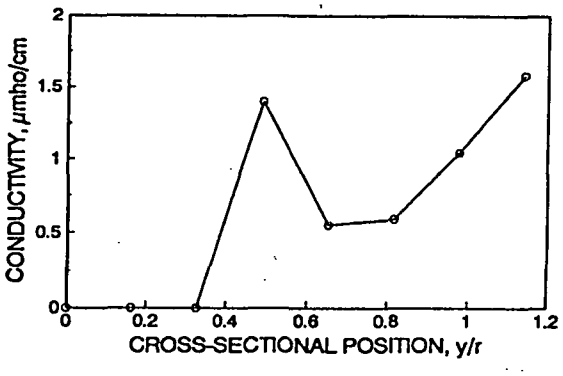

Figure A36. Horizontal probe data for pulp flow condition A.

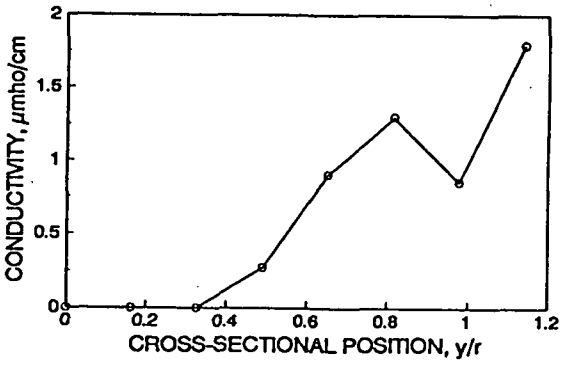

Figure A37. Horizontal probe data for pulp flow condition A.

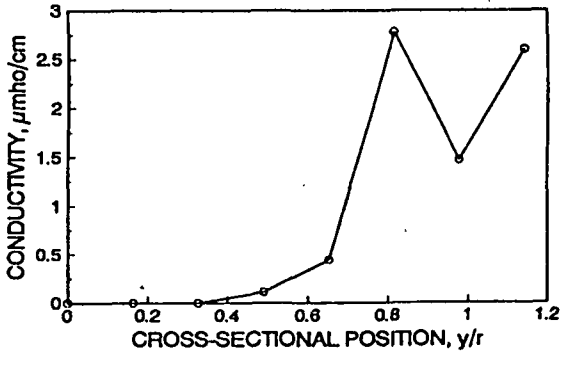

Figure A38. Horizontal probe data for pulp flow condition A.

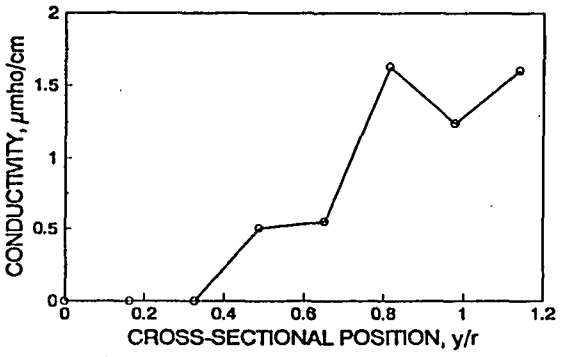

Figure A39. Horizontal probe data for water flow condition B.

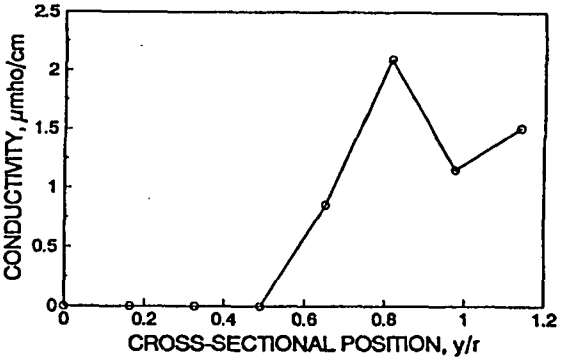

Figure A40. Horizontal probe data for water flow condition B.

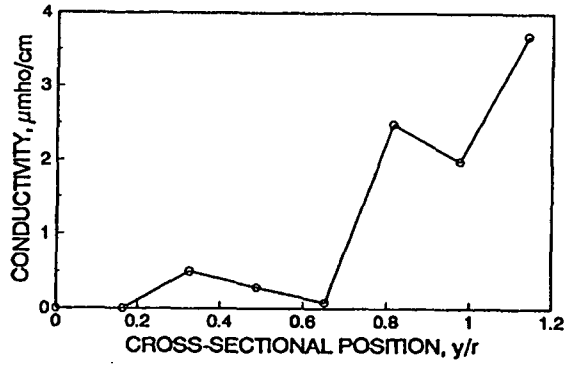

Figure A41. Horizontal probe data for water flow condition B.

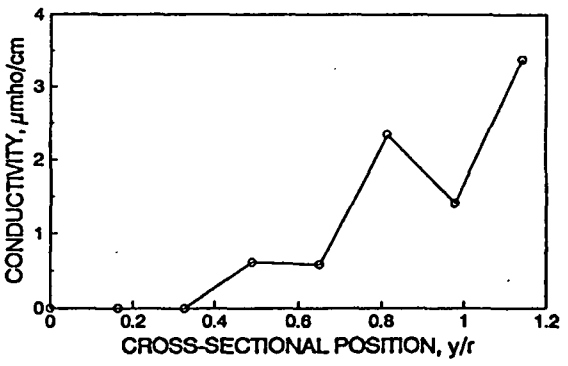

Figure A42. Horizontal probe data for water flow condition C.

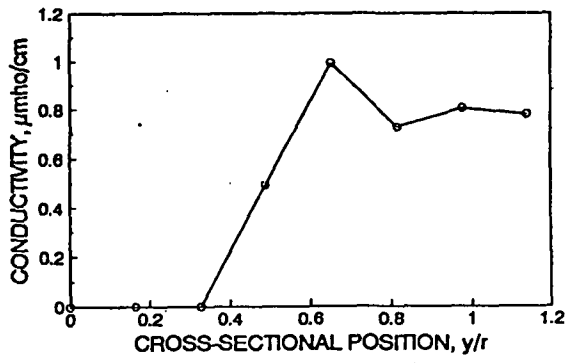

Figure A43. Horizontal probe data for water flow condition D.

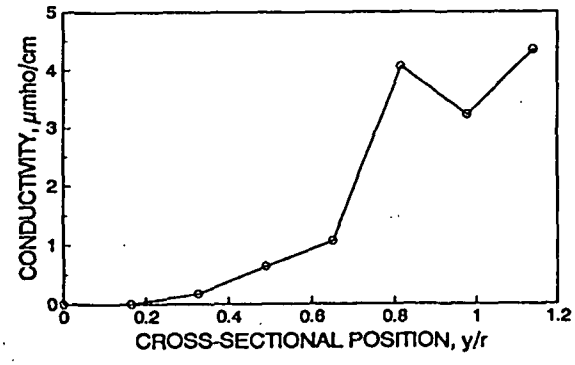

Figure A44. Horizontal probe data for water flow condition D.

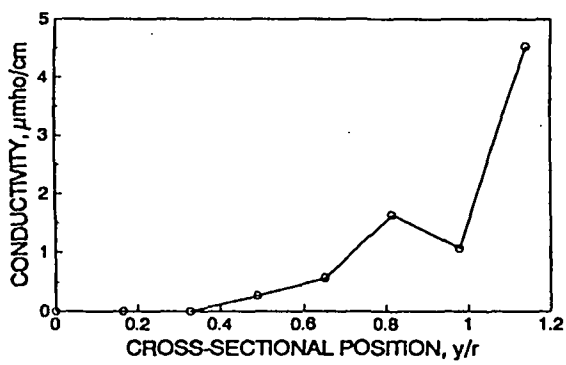

Figure A45. Horizontal probe data for pulp flow condition D.

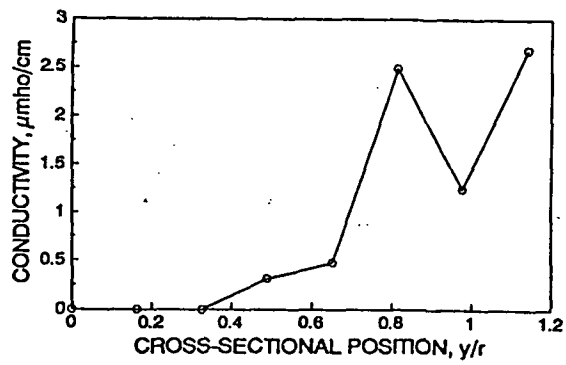

Figure A46. Horizontal probe data for water flow condition E.

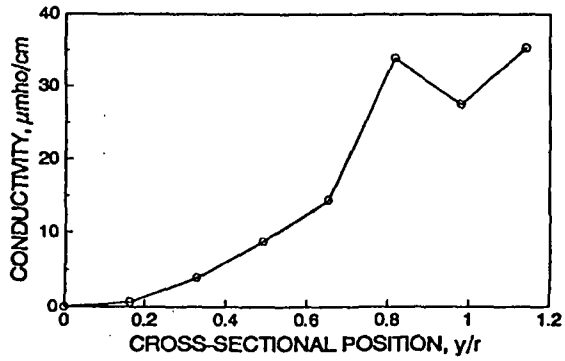

Figure A47. Horizontal probe data for pulp flow condition E.

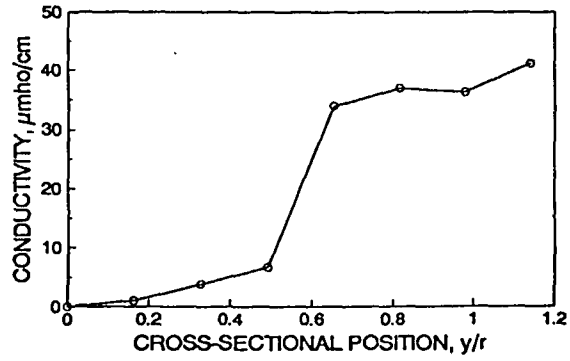

Figure A48. Horizontal probe data for pulp flow condition E.

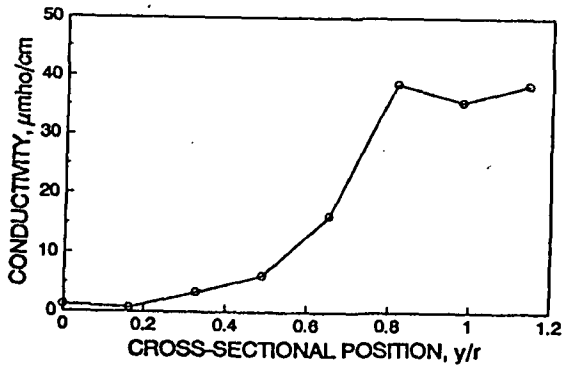

Figure A49. Horizontal probe data for water flow condition F.

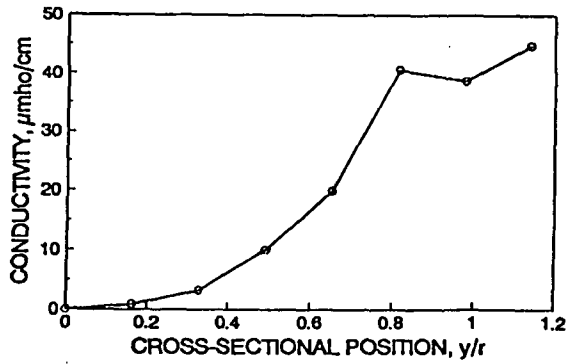

Figure A50. Horizontal probe data for water flow condition G.

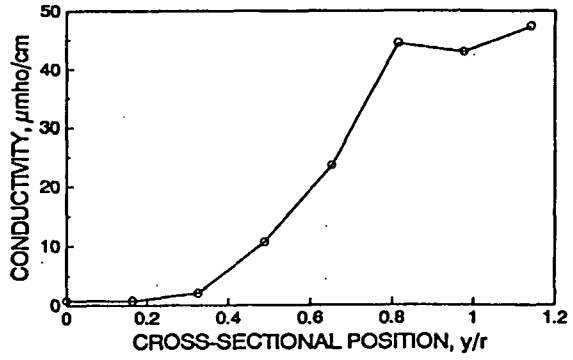

Figure A51. Horizontal probe data for water flow condition H.

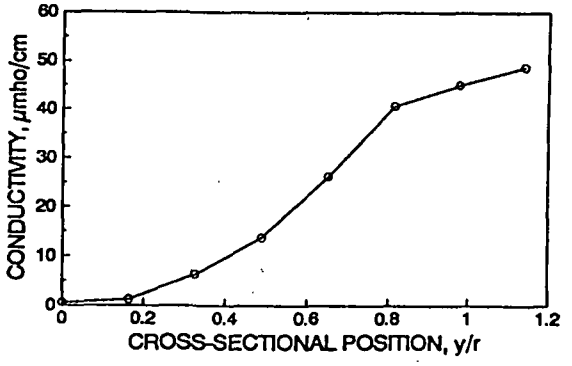

Figure A52. Horizontal probe data for pulp flow condition H.

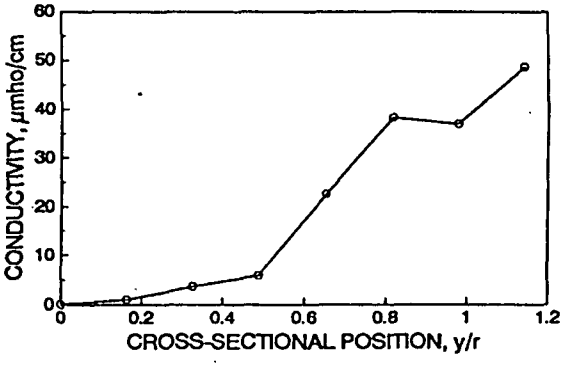

Figure A53. Horizontal probe data for pulp flow condition H.

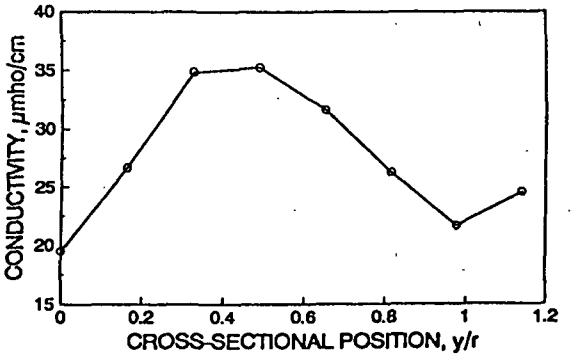

Figure A54. Horizontal probe data for water flow condition I.

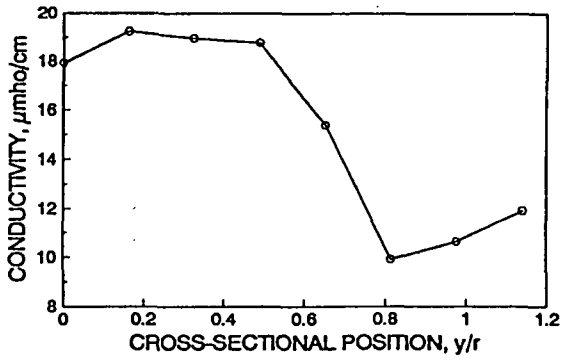

Figure A55. Horizontal probe data for pulp flow condition I.

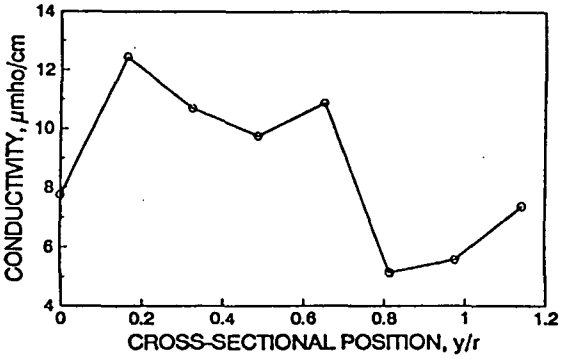

Figure A56. Horizontal probe data for pulp flow condition I.

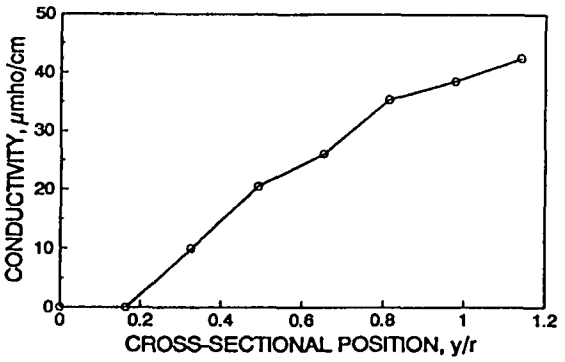

Figure A57. Horizontal probe data for pulp flow condition J.

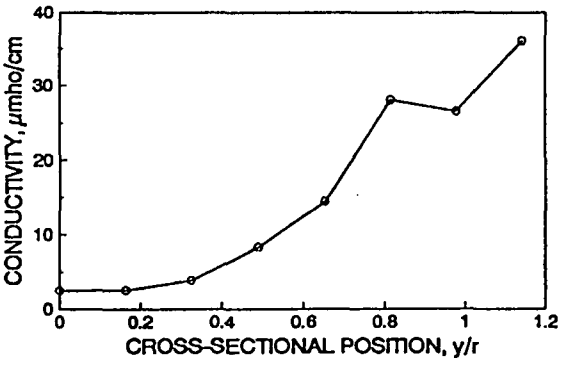

Figure A58. Horizontal probe data for pulp flow condition K.

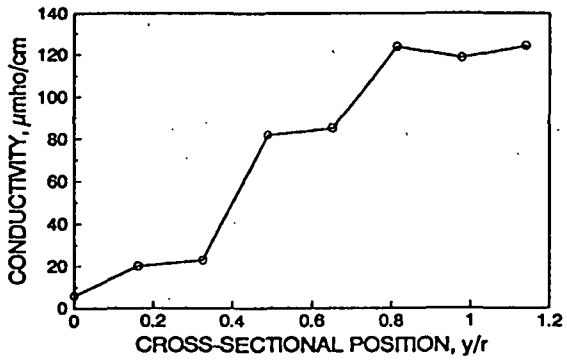

Figure A59. Horizontal probe data for pulp flow condition L.

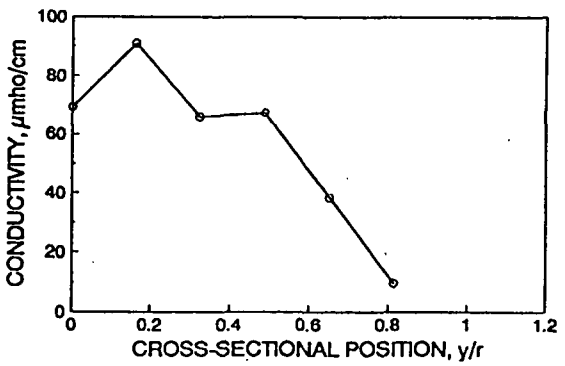

Figure A60. Horizontal probe data for pulp flow condition M.

APPENDIX XIV. EXPERIMENTAL DATA

Table A5. Electrophoretic mobility versus pH for the Morton Thiokol latex. The data have been plotted in Figure 13. The table shows experimental values for the EM distribution mean, and the average and standard deviations of these values.

pH	EM	Average EM	Stand. Dev. of Average EM
4.07	-3.81	-3.8	0.069761
	-3.71		
	-3.88		
5.09	-4.69	-4.616	0.084048
	-4.54		
	-4.58		
	-4.74		
	-4.53		
6	-5.4	-5.364	0.051614
	-5.43		
	-5.32		
	-5.29		
	-5.38		
6.5	-5.78	-5.865	0.068007
	-5.85		
	-5.97		
	-5.86		
6.73	-5.78	-5.845	0.046098
	-5.84		
	-5.91		
	-5.85		
7.5	-6.02	-6.085	0.047697
	-6.06		
	-6.12		
	-6.14		
8.55	-5.99	-6.01	0.01633
	-6.01		
	-6.03		
8.87	-6.06	-5.9725	0.108714
	-5.99		

Table A5, continued

	-5.79		
	-6.05		
9.12	-6	-6.035	0.035
	-6.07		
9.19	-6.08	-6.04333	0.026247
	-6.03		
	-6.02		
9.49	-5.94	-5.94	0
9.93	-5.94	-5.96333	0.032998
	-6.01		
	-5.94		

Table A6. Experimental data from the first phase of Dynamic Drainage Jar experiments. The data have been plotted in Figures 22 and 23.

HIGH RPM SETTING		LOW RPM SETTING		ACTUAL POLYMER DOSAGE, #/T
AVE SD	AVE EM	AVE SD	AVE EM	
0.73541	-5.32			0
0.74	-5.915			0
0.74	-5.845			0
		0.732458	-5.76	0
		0.749255	-5.785	0
		0.73751	-5.76	0
		0.7412	-5.855	0
		0.7391	-5.79	0
		0.7315	-5.865	0
0.73971	-5.91			0
0.637215	-4.21			0.508225
0.542655	-2.79			1.01964
		0.575645	-2.53	0.988356
		0.59706	-2.79	1.01106
0.53404	-2.52			1.023374

Table A6, continued

HIGH RPM SETTING		LOW RPM SETTING		ACTUAL POLYMER DOSAGE, #/T
AVE SD	AVE EM	AVE SD	AVE EM	
0.38665	-1.51			1.52536
0.3691	-0.66			2.053558
		0.45126	-0.58	2.021121
		0.4521	-0.145	1.965284
		0.4492	-0.125	1.975493
0.419555	-0.095			1.95251
0.405838	0.051667			2.014108
		0.50318	-0.18	1.958551
0.38254	-0.025			1.952725
		0.4642	-0.71	1.998299
		0.47152	-0.265	2.019579
0.36435	-0.41			1.987513
0.35036	-0.095			2.620976
0.33952	0.475			2.901217
		0.39021	0.58	3.034889
		0.405445	0.485	2.999265
0.34801	0.55			2.995025
0.33443	0.87			4.019488
0.33357	0.98			5.147242
		0.41589	0.85	4.848225
		0.359405	1.3	5.022112
0.303015	1.255			8.283474
0.31799	1.31			8.083426
		0.446455	1.4333333	7.832766

Table A7. Data from flow loop experiments. The data have been plotted in Figures 34 and 35.

EXPERIMENT	EM DISTRIBUTION MEAN	DISTRIBUTION STANDARD DEV.	MEAN EM	MEAN SD
			STAND. DEV. OF MEAN	STAND. DEV. OF SD
BLANK	-3.925	0.778505	**-3.99806**	**0.689441**
BLANK	-5.31	0.61572	**0.863814**	**0.08251**
BLANK	-2.97	0.716015		
BLANK	-4.59	0.66551		
BLANK	-2.455	0.53764		
BLANK	-3.68	0.719395		
BLANK	-4.635	0.62808		
BLANK	-3.19	0.74658		
BLANK	-3.84	0.720015		
BLANK	-3.105	0.77557		
BLANK	-3.72	0.77007		
BLANK	-3.13	0.7261		
BLANK	-5.305	0.564995		
BLANK	-4.445	0.720115		
BLANK	-3.625	0.78495		
BLANK	-3.63	0.78592		
BLANK	-5.265	0.557965		
BLANK	-5.145	0.596795		
A	-2.365	0.520305	**-1.96563**	**0.495808**
A	-1.925	0.5399	**0.291542**	**0.03805**
A	-2.46	0.551955		
A	-1.765	0.48925		
A	-1.71	0.43491		
A	-2.095	0.450395		
A	-1.62	0.48901		
A	-1.785	0.490735		
D	-1.83	0.54977	**-1.8625**	**0.526783**
D	-1.54	0.5202	**0.234014**	**0.045118**
D	-2.39	0.53408		
D	-1.805	0.515605		

Table A7, continued

EXPERIMENT	EM DISTRIBUTION MEAN	DISTRIBUTION STANDARD DEV.	MEAN EM	MEAN SD
			STAND. DEV. OF MEAN	STAND. DEV. OF SD
D	-2	0.44602		
D	-1.73	0.62		
D	-1.74	0.51667		
D	-1.865	0.51192		
E	-1.85	0.534185	**-1.82167**	**0.503883**
E	-1.625	0.51188	**0.246486**	**0.017799**
E	-2.33	0.51039		
E	-1.675	0.477375		
E	-1.84	0.49296		
E	-1.61	0.49651		
H	-1.72	0.49521	**-1.89333**	**0.500351**
H	-2.005	0.4771	**0.252334**	**0.023345**
H	-2.355	0.52095		
H	-1.635	0.492065		
H	-1.98	0.540645		
H	-1.665	0.476135		
I	-2.085	0.54409	**-2.02333**	**0.501524**
I	-1.89	0.46872	**0.280218**	**0.041686**
I	-1.535	0.53979		
I	-2.165	0.453485		
I	-2.46	0.544925		
I	-2.005	0.458135		
J	-1.32	0.3993	**-1.35**	**0.361649**
J	-1.48	0.34144	**0.090277**	**0.028707**
J	-1.23	0.3786		
J	-1.37	0.327255		
K	-1.285	0.38868	**-1.28125**	**0.348839**
K	-1.15	0.32376	**0.124317**	**0.025004**
K	-1.21	0.33209		
K	-1.48	0.350825		

Table A7, continued

EXPERIMENT	EM DISTRIBUTION MEAN	DISTRIBUTION STANDARD DEV.	MEAN EM	MEAN SD
			STAND. DEV. OF MEAN	STAND. DEV. OF SD
L	-1.015	0.29229	**-0.9825**	**0.31893**
L	-0.95	0.34557	**0.0325**	**0.02664**
M	-0.995	0.313675	**-1.02**	**0.310628**
M	-1.045	0.30758	**0.025**	**0.003048**

Table A8. Experimental data for gravimetric retention determinations for flow loop experiments. The data has been plotted in Figure 36.

EXPERIMENT	MEASURED GRAVIMETRIC RETENTION	MEAN GRAVIMETRIC RETENTION	STANDARD DEVIATION OF MEASUREMENTS
BLANK	0.5102		
BLANK	-1.0245		
BLANK	0.94842		
BLANK	-1.1321		
BLANK	0.7272		
BLANK	1.65347		
BLANK	0.915		
BLANK	-0.54235		
BLANK	1.1251		
BLANK	0.6324		
BLANK	0.5223		
BLANK	-0.79115		
BLANK	-1.9423		
BLANK	-0.845		
BLANK	-2.142		
BLANK	-2.458		
BLANK	-1.09		
BLANK	0.80931	0.282	1.201
A	10.036		

Table A8, continued

EXPERIMENT	MEASURED GRAVIMETRIC RETENTION	MEAN GRAVIMETRIC RETENTION	STANDARD DEVIATION OF MEASUREMENTS
A	11.1302		
A	17.1417		
A	9.00756		
A	15.2356		
A	18.9441		
A	12.019		
A	19.386	14.113	3.833
D	16.937		
D	11.006		
D	22.336		
D	6.7012		
D	24.898		
D	9.738		
D	20.351		
D	8.2808	15.031	6.537
E	13.012		
E	11.891		
E	12.972		
E	14.218		
E	11.519		
E	12.48	12.682	0.873
H	13.917		
H	16.08		
H	10.699		
H	18.026		
H	9.382		
H	10.91	13.169	3.114
I	16.458		
I	20.5849		
I	9.9684		
I	21.8854		
I	7.489		
I	6.1323	13.753	6.215

Table A8, continued

EXPERIMENT	MEASURED GRAVIMETRIC RETENTION	MEAN GRAVIMETRIC RETENTION	STANDARD DEVIATION OF MEASUREMENTS
J	28.481		
J	26.7105		
J	20.5841		
J	18.0364	23.453	4.286
K	28.948		
K	27.41		
K	29.0258		
K	27.3202	28.176	0.812
L	34.278		
L	47.974	41.126	6.848
M	37.993		
M	41.193	39.593	1.600

Table A9. Electrophoretic mobility and standard deviation data for the untreated Morton Thiokol latex in 0.01 M KCl solution showing the effect of the vibration resistant material on the stability of the measurement. The data have been plotted in Figures 37 and 38.

TIME, sec	0.005% Latex Concentration		0.025% Latex Concentration		0.0025% Latex Concentration		0.005% with vibration reduction	
	EM	SD of EM	EM	SD of EM	EM	SD of EM	EM	SD of EM
3	-5.407	2.1541	-6.286	2.0179	-5.731	1.7527	-6.17045	0.9308
6	-5.861	2.1019	-5.977	1.4058	-5.433	1.9886	-6.05545	0.8873
9	-6.16	1.943	-5.987	1.8042	-5.525	1.9395	-6.18845	0.8664
12	-6.431	2.258	-6.147	1.4365	-6.126	1.3649	-6.34845	0.8877
15	-6.54	1.8449	-6.036	1.7139	-5.841	0.9317	-6.20545	0.9913
18	-6.329	1.8741	-5.978	1.5157	-6.184	1.5128	-6.22745	0.7806
21	-6.046	2.2463	-6.365	1.114	-5.58	1.9231	-6.50245	0.9359
24	-6.087	1.974	-6.205	1.5479	-5.939	1.4147	-6.09645	0.8227
27	-6.268	2.1981	-6.041	1.9542	-5.97	1.6479	-6.44945	0.8732
30	-6.23	2.0822	-6.031	1.8106	-5.899	2.2017	-6.44045	0.9505
33	-5.479	2.1058	-6.239	1.7016	-5.216	2.0829	-6.28245	0.9028
36	-6.065	2.3288	-6.065	1.5235	-5.585	1.8343	-6.36845	0.9006
39	-5.314	1.956	-6.279	1.7197	-6.039	1.68	-6.33345	1.0512
42	-6.002	2.1789	-6.153	1.5141	-5.989	1.3358	-6.34645	0.8762
45	-6.27	2.226	-6.3	2.1371	-6.168	1.3682	-6.34345	0.901
48	-6.207	2.0418	-6	1.4728	-5.797	1.8402	-6.39445	0.9168
51	-6.063	1.8551	-6.115	1.6066	-5.237	1.4086	-6.33545	1.0052
54	-5.713	2.1177	-6.246	1.7202	-5.772	1.9551	-6.41345	0.8475
57	-6.161	2.1181	-6.391	1.6271	-5.467	2.3903	-6.20245	0.8456
60	-5.784	1.9915	-5.956	1.8692	-6.149	1.4621	-6.30545	0.8906
Column averages	-6.0208	2.0798	-6.1398	1.6606	-5.7824	1.7018	-6.3005	0.9032
Column σ	0.3262	0.1376	0.1367	0.2309	0.2947	0.3448	0.1168	0.0616

Table A10. Data from adsorption kinetics experiments using the Malvern Zetasizer IIC manual mode of operation.

(a) Initial experiments with five concentrations. Data have been plotted in Figures 39 and 40. The data presented here were averages of 10 replicates.

TIME, sec	MEAN EM	STAND. DEV. OF EM DISTRIBUTION MEAN	MEAN STANDARD DEVIATION	STAND. DEV. OF STANDARD DEVIATION
Concentration of latex = 0.05 percent				
0	-6.3	0	0.9	0
3	-4.2375	0.613845	1.228313	0.545836
6	-3.54863	0.378534	1.414663	0.360594
9	-3.22013	0.346042	1.480288	0.444667
12	-2.79413	0.397741	1.336125	0.232751
15	-2.93225	0.314371	1.292463	0.220696
18	-2.91975	0.411138	1.242638	0.138922
21	-3.03525	0.518254	1.369325	0.424103
24	-3.028	0.42007	1.221138	0.198526
27	-3.0355	0.458525	1.337588	0.238747
30	-2.88813	0.408943	1.24355	0.289468
33	-2.74825	0.100571	1.147525	0.272483
36	-2.83	0.286922	1.1513	0.164559
39	-2.874	0.337266	1.393925	0.524024
42	-2.8435	0.403713	1.378425	0.264091
45	-2.86125	0.286705	1.38215	0.335768
48	-2.84913	0.323402	1.424725	0.447478
51	-2.73638	0.404905	1.20945	0.113182
54	-2.626	0.437922	1.188263	0.125888
57	-2.76063	0.386256	1.033163	0.344931
60	-2.69388	0.349165	1.370263	0.259087
Concentration of latex = 0.025 percent				
0	-6.3	0	0.9	0
3	-3.9464	0.333107	1.64516	0.17418
6	-3.0364	0.151686	1.41314	0.30494
9	-2.6746	0.161911	1.2303	0.301072
12	-2.4064	0.541909	1.56326	0.400324

Table A10(a), continued

TIME, sec	MEAN EM	STAND. DEV. OF EM DISTRIBUTION MEAN	MEAN STANDARD DEVIATION	STAND. DEV. OF STANDARD DEVIATION
15	-2.3716	0.291833	1.36788	0.232114
18	-2.5212	0.389915	1.2791	0.20443
21	-2.427	0.590422	1.55436	0.397644
24	-2.347	0.414793	1.10864	0.149137
27	-2.5836	0.312275	1.30524	0.272023
30	-2.4796	0.409727	1.15618	0.228746
33	-2.4766	0.241632	1.1418	0.300262
36	-2.403	0.320954	1.22058	0.293753
39	-2.7904	0.28088	1.33248	0.148255
42	-2.5354	0.280299	1.34338	0.143146
45	-2.3962	0.402095	1.32368	0.171622
48	-2.115	0.469285	1.28536	0.185436
51	-2.6822	0.260386	1.10846	0.241009
54	-2.8896	0.183835	1.08296	0.091551
57	-2.495	0.812425	1.33694	0.287599
60	-2.73	0.568289	1.22684	0.246493
Concentration of latex = 0.01 percent				
0	-6.3	0	0.9	0
3	-5.406	0.920941	1.769525	0.512813
6	-5.24025	0.874304	1.796225	0.883447
9	-5.039	0.412994	1.274675	0.222209
12	-4.69788	0.605617	1.603525	0.383753
15	-4.65513	0.908743	1.500725	0.336927
18	-4.46638	0.778916	1.273988	0.317688
21	-4.13063	0.988511	1.665838	0.387951
24	-4.052	0.934887	1.578625	0.556552
27	-4.05163	0.758039	1.667838	0.623078
30	-3.50875	0.527988	1.968588	0.785542
33	-3.64688	0.595256	1.302238	0.408319
36	-3.9265	0.689331	1.334238	0.29258
39	-3.56138	0.972023	1.49405	0.595948

Table A10(a), continued

TIME, sec	MEAN EM	STAND. DEV. OF EM DISTRIBUTION MEAN	MEAN STANDARD DEVIATION	STAND. DEV. OF STANDARD DEVIATION
42	-3.54963	0.798198	1.524338	0.281475
45	-3.59688	0.871776	1.827363	0.682541
48	-3.39138	0.428459	1.7939	0.58071
51	-3.17213	0.512147	1.420575	0.781813
54	-3.54888	0.722726	1.59695	0.549408
57	-3.22338	0.872106	1.55615	0.390531
60	-3.14788	0.298304	1.398013	0.391144
Concentration of latex = 0.005 percent				
0	-6.3	0	0.9	0
3	-5.669	0.235565	1.8064	0.232617
6	-4.988	0.170452	1.4509	0.166433
9	-4.47967	0.152299	1.5313	0.047741
12	-4.18967	0.307676	1.2851	0.129996
15	-4.24733	0.354224	1.549533	0.108025
18	-3.944	0.222544	1.2524	0.2276
21	-4.11167	0.284882	1.3884	0.184633
24	-3.55233	0.378409	1.371867	0.208337
27	-3.65567	0.05478	1.491367	0.10386
30	-3.958	0.199772	1.306867	0.317174
33	-3.829	0.147339	1.453833	0.16472
36	-3.60533	0.0858	1.339367	0.049368
39	-3.945	0.096916	1.1504	0.10599
42	-3.309	0.05572	1.121033	0.331773
45	-3.38367	0.388127	1.342133	0.262103
48	-3.504	0.32672	1.505267	0.234287
51	-3.43467	0.472977	1.279067	0.216232
54	-3.22433	0.701153	1.337833	0.174475
57	-3.09	0.25843	1.275367	0.185927
60	-3.45033	0.267266	1.343367	0.105781

Table A10(a), continued

TIME, sec	MEAN EM	STAND. DEV. OF EM DISTRIBUTION MEAN	MEAN STANDARD DEVIATION	STAND. DEV. OF STANDARD DEVIATION
Concentration of latex = 0.001 percent				
0	-6.3	0	0.9	0
3	-5.817	0.285375	1.64308	0.169428
6	-5.765	0.476981	1.73002	0.169962
9	-5.5568	0.49713	1.74666	0.131312
12	-5.5196	0.231966	1.54568	0.289346
15	-5.3934	0.298112	1.46304	0.121095
18	-5.0208	0.265841	1.46252	0.204432
21	-5.3218	0.439344	1.46868	0.340851
24	-5.1164	0.235134	1.43286	0.202379
27	-4.9148	0.211958	1.46054	0.210928
30	-4.561	0.303669	1.5977	0.189352
33	-4.6068	0.43852	1.51162	0.24132
36	-4.3604	0.220092	1.4081	0.24416
39	-4.9804	0.547195	1.4771	0.292019
42	-4.726	0.230082	1.7028	0.324219
45	-4.2914	0.381179	1.56134	0.44305
48	-4.5168	0.196348	1.34206	0.298883
51	-4.1296	0.369621	1.48864	0.240039
54	-4.2048	0.56823	1.50596	0.157571
57	-4.231	0.359265	1.52946	0.405406
60	-4.0534	0.511538	1.3508	0.290381

(b) Final time to equilibrium experiments showing latex concentration of 0.10 percent, as presented in Figures 42 and 43, with three types of mixing: 1. a larger tube size with Reynolds number of 3×10^3, 2. a smaller tube size with Reynolds number of 9×10^3, and 3. the smaller tube size with an in-line static mixer. The data shown were taken from 10 replicates.

TIME, sec	MEAN EM	STAND. DEV. OF EM DISTRIBUTION MEAN	MEAN STANDARD DEVIATION	STAND. DEV. OF STANDARD DEVIATION
REYNOLDS NUMBER = 3×10^3				
0	-6.3	0	0.9	0
3	-4.01547	0.886268	1.171566	0.277753
6	-3.56709	0.525271	1.267376	0.284111
9	-3.30231	0.764644	1.085199	0.250624
12	-3.14773	0.500911	1.250271	0.359078
15	-3.1317	0.421221	1.122535	0.293769
18	-2.87936	0.357341	1.088116	0.283593
21	-2.80243	0.330639	1.077569	0.251679
24	-2.98479	0.317853	1.135964	0.148091
27	-3.12387	0.25378	1.187518	0.104301
30	-2.79995	0.219748	1.020151	0.314458
33	-2.93341	0.322646	1.10393	0.302606
36	-2.94993	0.275531	1.144345	0.322291
39	-2.97883	0.255739	1.055977	0.318664
42	-2.78879	0.206868	1.162166	0.302807
45	-3.08505	0.305	1.243829	0.269054
48	-2.73963	0.243336	1.296635	0.33785
51	-2.87503	0.262454	1.234964	0.416128
54	-2.86395	0.258887	1.10904	0.257649
57	-2.84388	0.313509	1.318966	0.27838
60	-2.82816	0.31941	1.138758	0.371891
REYNOLDS NUMBER = 9×10^3				
0	-6.3	0	0.9	0
3	-4.19906	1.194682	1.255546	0.400927
6	-3.57712	0.971133	0.943321	0.232452
9	-2.97382	0.736166	0.966286	0.298028
12	-2.85847	0.399615	0.84243	0.279038

Table A10(b), continued

TIME, sec	MEAN EM	STAND. DEV. OF EM DISTRIBUTION MEAN	MEAN STANDARD DEVIATION	STAND. DEV. OF STANDARD DEVIATION
15	-2.81884	0.359284	0.889228	0.185971
18	-2.70028	0.210027	0.908604	0.166367
21	-2.92825	0.298578	1.005281	0.289537
24	-2.47112	0.332415	0.783374	0.221951
27	-2.63622	0.316335	0.905431	0.244285
30	-2.71644	0.412004	0.802254	0.108605
33	-2.76029	0.334224	0.87437	0.18027
36	-2.63531	0.339436	0.91955	0.197434
39	-2.6342	0.328509	0.901135	0.172304
42	-2.63636	0.364765	0.895473	0.142989
45	-2.67437	0.403323	0.885537	0.171373
48	-2.5331	0.247564	0.846233	0.117244
51	-2.44502	0.309667	0.843178	0.185718
54	-2.4976	0.22384	0.80891	0.094273
57	-2.60264	0.283574	0.831551	0.142795
60	-2.60772	0.278829	0.90725	0.175993
WITH IN-LINE STATIC MIXER				
0	-6.3	0	0.9	0
3	-3.36911	0.471345	1.125514	0.243536
6	-3.07963	0.490819	1.010195	0.142182
9	-3.05546	0.342085	1.048441	0.108463
12	-2.9082	0.282023	0.985599	0.102524
15	-2.82117	0.263666	1.112212	0.139139
18	-2.87441	0.220246	1.005285	0.268495
21	-2.86352	0.325701	1.063329	0.276056
24	-2.76392	0.312785	0.946099	0.120664
27	-2.80462	0.27891	0.959793	0.168667
30	-2.79413	0.320051	0.944994	0.154186
33	-2.79158	0.309828	1.006318	0.195585
36	-2.90021	0.331007	0.997597	0.14093
39	-2.74806	0.384896	0.918558	0.162715

Table A10(b), continued

TIME, sec	MEAN EM	STAND. DEV. OF EM DISTRIBUTION MEAN	MEAN STANDARD DEVIATION	STAND. DEV. OF STANDARD DEVIATION
42	-2.73436	0.406573	0.82686	0.165534
45	-2.63138	0.30069	0.922787	0.17633
48	-2.66933	0.273643	0.957814	0.17109
51	-2.93252	0.296215	0.910844	0.179088
54	-2.66637	0.330386	0.980258	0.139951
57	-2.75962	0.299513	0.9391	0.139974
60	-2.81	0.307375	0.95978	0.156675

(c) Final time to equilibrium experiments showing latex concentration of 0.025 percent, as presented in Figures 44 and 45, with three types of mixing: 1. a larger tube size with Reynolds number of 3×10^3, 2. a smaller tube size with Reynolds number of 9×10^3, and 3. the smaller tube size with an in-line static mixer. The data shown were taken from 10 replicates.

TIME, sec	MEAN EM	STAND. DEV. OF EM DISTRIBUTION MEAN	MEAN STANDARD DEVIATION	STAND. DEV. OF STANDARD DEVIATION
REYNOLDS NUMBER = 3×10^3				
0	-6.3	0	0.9	0
3	-4.14918	0.722896	1.424572	0.125819
6	-3.39622	0.425866	1.298348	0.210608
9	-3.28153	0.511509	1.245982	0.161343
12	-3.32562	0.50872	1.355323	0.378464
15	-3.08389	0.333688	1.26558	0.263989
18	-3.1973	0.282943	1.308785	0.252539
21	-3.02743	0.443306	1.35958	0.321321
24	-2.84095	0.486364	1.245414	0.283087
27	-2.81715	0.341287	1.232644	0.255172
30	-2.94847	0.254881	1.19022	0.231843
33	-2.96534	0.39836	1.140637	0.194412
36	-2.97687	0.359479	1.122588	0.201871
39	-2.87677	0.194751	1.174083	0.319699

Table A10(c), continued

TIME, sec	MEAN EM	STAND. DEV. OF EM DISTRIBUTION MEAN	MEAN STANDARD DEVIATION	STAND. DEV. OF STANDARD DEVIATION
42	-2.79698	0.388587	1.201274	0.460857
45	-2.8073	0.301769	1.247357	0.329792
48	-2.82952	0.240779	1.123009	0.19736
51	-2.86223	0.42128	1.245264	0.13607
54	-2.67958	0.370566	1.181674	0.370661
57	-2.94291	0.264703	1.091705	0.251244
60	-2.84052	0.326259	1.266968	0.305544
REYNOLDS NUMBER = 9×10^3				
0	-6.3	0	0.9	0
3	-3.96888	0.723819	1.304751	0.287429
6	-3.16402	0.413806	1.252537	0.272766
9	-2.96422	0.503987	1.097197	0.319046
12	-2.94854	0.475909	1.046021	0.23514
15	-2.88012	0.655712	0.950742	0.204837
18	-2.75507	0.417205	0.922991	0.228186
21	-2.77581	0.56536	0.97	0.216784
24	-2.60014	0.657076	0.922739	0.168938
27	-2.83301	0.532065	0.908391	0.274697
30	-2.67369	0.554804	0.937681	0.226066
33	-2.51382	0.458672	0.827877	0.23932
36	-2.69712	0.602758	0.988268	0.26585
39	-2.65254	0.482842	0.921685	0.249988
42	-2.64446	0.58042	0.804071	0.206684
45	-2.73269	0.502359	0.885931	0.210319
48	-2.70533	0.582511	0.836292	0.207424
51	-2.73542	0.625728	0.972604	0.34303
54	-2.62056	0.542074	0.864067	0.195095
57	-2.69781	0.508684	0.865081	0.276571
60	-2.68406	0.812928	0.886944	0.301957

Table A10(c), continued

TIME, sec	MEAN EM	STAND. DEV. OF EM DISTRIBUTION MEAN	MEAN STANDARD DEVIATION	STAND. DEV. OF STANDARD DEVIATION
WITH IN-LINE STATIC MIXER				
0	-6.3	0	0.9	0
3	-3.59041	0.40636	1.192552	0.156448
6	-3.37179	0.524172	1.092064	0.218144
9	-3.10288	0.392549	1.150114	0.176691
12	-2.90546	0.55008	1.162446	0.299281
15	-2.74841	0.481783	1.054893	0.359127
18	-2.78692	0.363349	1.017305	0.259704
21	-2.70229	0.313675	0.961876	0.261892
24	-2.65108	0.354503	0.938376	0.318381
27	-2.60784	0.362158	0.934235	0.369812
30	-2.70432	0.351924	1.003376	0.243037
33	-2.64659	0.453743	0.926085	0.317483
36	-2.70236	0.410912	0.923766	0.263751
39	-2.54311	0.362606	0.951964	0.279666
42	-2.70093	0.338181	0.836609	0.245052
45	-2.62557	0.38806	0.945417	0.337474
48	-2.72518	0.259203	0.975445	0.291616
51	-2.95166	0.27863	0.878679	0.21819
54	-2.88338	0.289311	0.935104	0.174211
57	-2.60411	0.290749	0.933533	0.21667
60	-2.76006	0.359061	0.97262	0.287273

(d). Final time to equilibrium experiments showing latex concentration of 0.005 percent, as presented in Figures 46 and 47, with three types of mixing: 1. a larger tube size with Reynolds number of 3×10^3, 2. a smaller tube size with Reynolds number of 9×10^3, and 3. the smaller tube size with an in-line static mixer. The data shown were taken from 10 replicates.

TIME, sec	MEAN EM	STAND. DEV. OF EM DISTRIBUTION MEAN	MEAN STANDARD DEVIATION	STAND. DEV. OF STANDARD DEVIATION
REYNOLDS NUMBER = 3×10^3				
0	-6.3	0	0.9	0
3	-5.16359	0.655893	1.858881	0.556447
6	-4.84615	0.430183	1.711544	0.292212
9	-4.7616	0.64553	1.767206	0.367861
12	-4.97791	0.659986	1.706101	0.27576
15	-4.42745	0.580318	1.682627	0.363875
18	-4.58494	0.782607	1.748887	0.20046
21	-4.39136	0.706115	1.697193	0.413063
24	-4.44265	0.759839	1.865993	0.40981
27	-4.12572	0.625519	1.828057	0.404058
30	-4.32172	0.607705	1.733889	0.476589
33	-4.64776	0.716392	1.719793	0.37957
36	-4.36222	0.850526	1.963245	0.560072
39	-4.43398	0.824763	1.83735	0.290127
42	-4.33596	0.860448	1.957127	0.430908
45	-4.18344	1.138262	1.68192	0.407921
48	-3.82253	0.61622	1.690561	0.436136
51	-4.4519	0.603291	1.84141	0.412285
54	-4.11278	1.001908	1.829623	0.552057
57	-4.17581	1.220532	1.689501	0.427018
60	-3.69687	0.729323	1.549142	0.477322
REYNOLDS NUMBER = 9×10^3				
0	-6.3	0	0.9	0
3	-5.06484	1.249606	1.439407	0.560744
6	-4.50898	0.453423	1.529119	0.279121
9	-4.44833	0.44666	1.449412	0.245123
12	-4.0322	0.764941	1.448712	0.35831

Table A10(d), continued

TIME, sec	MEAN EM	STAND. DEV. OF EM DISTRIBUTION MEAN	MEAN STANDARD DEVIATION	STAND. DEV. OF STANDARD DEVIATION
15	-4.14958	0.335677	1.449901	0.295923
18	-3.63133	0.470589	1.382665	0.275396
21	-3.57757	0.518575	1.299707	0.279533
24	-3.48048	0.480536	1.347236	0.323123
27	-3.56094	0.668253	1.305118	0.276943
30	-3.26469	0.790662	1.326682	0.337539
33	-3.41258	0.785313	1.201404	0.292095
36	-3.17935	0.664755	1.237219	0.297322
39	-3.02152	0.438236	1.258048	0.421662
42	-3.00964	0.675162	1.184682	0.293621
45	-2.94121	0.579701	1.284936	0.475314
48	-2.8199	0.489106	1.156217	0.281648
51	-2.96655	0.589224	1.18502	0.254996
54	-3.00238	0.690866	1.118096	0.257136
57	-2.52103	0.313684	1.107165	0.210789
60	-2.868	0.58166	1.155416	0.402522
WITH IN-LINE STATIC MIXER				
0	-6.3	0	0.9	0
3	-4.55713	0.668567	1.619209	0.438
6	-4.79522	0.243635	1.375635	0.315423
9	-4.42217	0.34382	1.387621	0.221276
12	-3.98972	0.250734	1.332796	0.222959
15	-4.2701	0.38039	1.367536	0.347929
18	-3.83386	0.403682	1.367613	0.321361
21	-3.46563	0.364201	1.335755	0.333297
24	-3.65983	0.619998	1.302751	0.379111
27	-3.35005	0.45805	1.325539	0.427786
30	-3.32892	0.779711	1.290072	0.407174
33	-3.13365	0.58986	1.214486	0.26673
36	-3.06385	0.54242	1.343945	0.491669
39	-3.26849	0.874389	1.251799	0.276512

Table A10(d), continued

TIME, sec	MEAN EM	STAND. DEV. OF EM DISTRIBUTION MEAN	MEAN STANDARD DEVIATION	STAND. DEV. OF STANDARD DEVIATION
42	-3.30605	0.669708	1.342046	0.362036
45	-2.8394	0.391389	1.170353	0.320918
48	-3.10347	0.662285	1.353085	0.504516
51	-2.86663	0.545018	1.15093	0.246698
54	-2.96709	0.811883	1.204939	0.458987
57	-2.84591	0.582325	1.234037	0.339193
60	-2.82685	0.733464	1.225643	0.341937

(e) Final time to equilibrium experiments showing latex concentration of 0.001 percent, as presented in Figures 48 and 49, with three types of mixing: 1. a larger tube size with Reynolds number of 3×10^3, 2. a smaller tube size with Reynolds number of 9×10^3, and 3. the smaller tube size with an in-line static mixer. The data shown were taken from 10 replicates.

TIME, sec	MEAN EM	STAND. DEV. OF EM DISTRIBUTION MEAN	MEAN STANDARD DEVIATION	STAND. DEV. OF STANDARD DEVIATION
REYNOLDS NUMBER = 3×10^3				
0	-6.3	0	0.9	0
3	-5.49851	0.408489	1.819622	0.482813
6	-5.09991	0.335731	1.838495	0.408276
9	-4.5216	0.701321	1.786841	0.147548
12	-4.60624	0.66776	1.895416	0.523774
15	-4.72489	0.927817	1.75655	0.396518
18	-4.75466	0.57749	1.720707	0.534538
21	-4.65741	0.76975	1.681226	0.336419
24	-4.5848	1.087286	1.919222	0.39669
27	-4.91544	0.710226	1.777723	0.339519
30	-4.72488	0.706934	1.712957	0.58208
33	-4.20973	0.773374	1.957623	0.588276
36	-4.63101	0.754339	1.645822	0.408094
39	-4.20818	0.594444	1.755475	0.517338

Table A10(e), continued

TIME, sec	MEAN EM	STAND. DEV. OF EM DISTRIBUTION MEAN	MEAN STANDARD DEVIATION	STAND. DEV. OF STANDARD DEVIATION
42	-4.71753	0.665862	1.642326	0.644251
45	-4.41502	0.713039	1.778868	0.543597
48	-4.1532	0.815559	1.725318	0.411798
51	-4.29514	0.928434	1.638347	0.449893
54	-4.44493	0.73196	1.786912	0.363825
57	-4.28249	0.494516	1.631166	0.275541
60	-4.44854	0.350848	1.644717	0.366913
REYNOLDS NUMBER = 9×10^3				
0	-6.3	0	0.9	0
3	-4.59131	0.749995	1.429749	0.30366
6	-4.54991	0.358944	1.509358	0.283548
9	-4.92489	0.468452	1.502764	0.231698
12	-4.6384	0.556699	1.535566	0.240417
15	-4.73327	0.563803	1.516124	0.132754
18	-4.84472	0.159176	1.521135	0.239337
21	-4.70614	0.52306	1.515344	0.282608
24	-4.56442	0.518701	1.490514	0.19011
27	-4.61405	0.445107	1.387939	0.234973
30	-4.71396	0.559665	1.450784	0.217932
33	-4.6191	0.331466	1.566786	0.171679
36	-4.63885	0.465434	1.499843	0.170673
39	-4.62518	0.388939	1.516512	0.220115
42	-4.73478	0.330143	1.635786	0.148224
45	-4.5525	0.442291	1.574115	0.215102
48	-4.579	0.332995	1.532655	0.218409
51	-4.41294	0.31074	1.468915	0.22393
54	-4.41521	0.390357	1.58274	0.259836
57	-4.40908	0.305115	1.414501	0.22657
60	-4.40646	0.334718	1.53122	0.195413

Table A10(e), continued

TIME, sec	MEAN EM	STAND. DEV. OF EM DISTRIBUTION MEAN	MEAN STANDARD DEVIATION	STAND. DEV. OF STANDARD DEVIATION
WITH IN-LINE STATIC MIXER				
0	-6.3	0	0.9	0
3	-4.61012	0.751872	1.68583	0.38953
6	-4.58012	0.775225	1.363416	0.250188
9	-4.53879	0.635219	1.588707	0.246937
12	-4.60465	0.782499	1.58034	0.358693
15	-4.93933	0.774707	1.668172	0.232828
18	-4.5782	0.758787	1.613835	0.387284
21	-4.85278	0.635262	1.531816	0.219714
24	-4.7596	0.570958	1.530006	0.194019
27	-4.72638	0.631331	1.554884	0.208859
30	-4.58202	0.607502	1.723054	0.469009
33	-4.47728	0.438	1.525893	0.249388
36	-4.2668	0.316544	1.475579	0.317133
39	-4.28085	0.399053	1.597231	0.318341
42	-4.25887	0.448632	1.436841	0.331392
45	-4.17827	0.364815	1.53588	0.320303
48	-4.42352	0.2557	1.501948	0.261003
51	-4.39938	0.342647	1.558512	0.282366
54	-4.31397	0.331114	1.367016	0.259723
57	-4.2439	0.38107	1.591676	0.261483
60	-4.21938	0.36063	1.460844	0.188104

(f) Final time to equilibrium experiments showing latex concentration of 0.0005 percent, as presented in Figures 50 and 51, with four sets of experiments using the larger tube size: 1. a 30-second automatic mode setting, 2. 15-second manual mode experiment with a five-minute gap when the cell voltage was switched off, 3. an automatic mode experiment with an in-line static mixer, and 4. individual 30-second automatic mode experiments performed at specific times after the injection. The data shown were taken from 10 replicates.

TIME, sec	MEAN EM	St. D. OF EM DISTR. MEAN	MEAN STANDARD DEVIATION	STAND. DEV. OF STANDARD DEVIATION
30 SECOND MANUAL MODE EXPERIMENTS				
0	-6.3	0	0.9	0
30	-5.22526	0.579764	1.544679	0.401138
60	-5.14279	0.38977	1.608742	0.512077
90	-5.12521	0.530518	1.625895	0.561434
120	-4.893	0.396056	1.611816	0.442237
150	-4.87247	0.498629	1.654184	0.566728
180	-4.80742	0.478154	1.629563	0.532763
210	-4.89495	0.779665	1.615579	0.489921
240	-4.78332	0.728725	1.593411	0.350406
270	-4.79847	0.902884	1.667516	0.618401
300	-4.82837	0.669632	1.719163	0.525528
330	-4.64542	0.581266	1.618711	0.539126
360	-4.70047	0.892223	1.652326	0.567973
390	-4.36516	0.621172	1.617826	0.57005
420	-4.61763	0.83338	1.759753	0.674603
450	-4.377	0.74508	1.590663	0.423578
480	-4.41137	0.639648	1.6691	0.582669
510	-4.45705	0.61773	1.644026	0.61325
540	-4.23395	0.639117	1.563047	0.575824
570	-4.22553	0.650974	1.588326	0.615628
600	-4.06411	1.97987	1.601295	0.337458
15 SECOND MANUAL MODE EXPERIMENTS WITH FIVE MINUTE DELAY				
0	-6.3	0	0.9	0
15	-5.2785	0.312515	1.635733	0.309902
30	-5.23417	0.383592	1.530867	0.339809
45	-5.28017	0.350442	1.61405	0.347044
60	-5.21492	0.361539	1.629233	0.088121

Table A10(f), continued

TIME, sec	MEAN EM	St. D. OF EM DISTR. MEAN	MEAN STANDARD DEVIATION	STAND. DEV. OF STANDARD DEVIATION
75	-5.25492	0.431015	1.560558	0.159409
90	-5.30025	0.446446	1.56485	0.271451
105	-5.22092	0.275189	1.651392	0.212526
120	-5.19133	0.309545	1.575742	0.347199
135	-5.01525	0.514235	1.58795	0.291401
150	-5.01884	0.38984	1.617625	0.269632
465	-5.12325	0.568271	1.505942	0.227747
480	-5.02467	0.525077	1.509125	0.273891
495	-5.27646	0.559661	1.452046	0.204365
510	-5.24546	0.622771	1.557923	0.230873
525	-5.03208	0.448664	1.534392	0.24898
540	-5.094	0.473571	1.480292	0.315338
555	-5.09246	0.554054	1.487454	0.201997
570	-5.00523	0.452333	1.482731	0.315346
585	-5.08031	0.64624	1.4952	0.187726
600	-5.10538	0.68289	1.514977	0.253449
30 SECOND MANUAL MODE EXPERIMENTS WITH STATIC MIXER PLACED IN-LINE				
0	-6.3	0	0.9	0
30	-4.886	0.036341	1.4656	0.145992
60	-4.675	0.087086	1.388533	0.158779
90	-4.777	0.199446	1.389667	0.025969
120	-4.577	0.058691	1.344967	0.090464
150	-4.64767	0.065525	1.295567	0.085171
180	-4.61267	0.250139	1.339733	0.057911
210	-4.617	0.081662	1.308467	0.031235
240	-4.61867	0.07176	1.349233	0.114805
270	-4.62067	0.090981	1.265567	0.037504
300	-4.55133	0.191061	1.3433	0.016362
330	-4.52633	0.220853	1.3607	0.037867
360	-4.38767	0.702002	1.3615	0.108704
390	-4.32833	0.145882	1.373433	0.104572

Table A10(f), continued

TIME, sec	MEAN EM	St. D. OF EM DISTR. MEAN	MEAN STANDARD DEVIATION	STAND. DEV. OF STANDARD DEVIATION
420	-4.48133	0.051861	1.351267	0.051369
450	-4.42967	0.091696	1.346233	0.039976
480	-4.311	0.258369	1.371667	0.078832
510	-4.30333	0.161496	1.391	0.059772
540	-4.223	0.086595	1.317867	0.026114
570	-4.15233	0.080467	1.3192	0.05977
600	-4.071	0.15903	1.340867	0.02458
AUTOMATIC MODE EXPERIMENTS TAKEN AT SPECIFIC TIMES AFTER INJECTION				
0	-6.3	0	0.9	0
60	-5.204	0.53	1.5413	0.0686
120	-5.161	0.359	1.553	0.2301
180	-5.2115	0.0775	1.60775	0.03735
240	-5.1444	0.644	1.6558	0.1073
300	-5.0855	0.2645	1.6283	0.0032
360	-4.9054	0.266	1.49575	0.09745
420	-4.9505	0.1795	1.5448	0.03
480	-5.0105	0.4285	1.5709	0.0353
540	-5.069	0.739	1.5054	0.0267
600	-5.0585	0.2755	1.4958	0.1894

Table A11. Experimental data from the second phase of Dynamic Drainage Jar experiments. The data on the right have been plotted in Figures 54 and 55.

RUN NO.	RPM	POLYMER DOSAGE	EM-1	EM-2	%WIDTH -1	%WIDTH -2	SD-1	SD-2	AVE EM	AVE SD	AVG EM	AVG SD
4	0	0	-5.95	-5.99	9.9	9.6	0.58905	0.57504	-5.97	0.582045	SD OF EM	SD OF SD
6	0	0	-5.94	-6.04	11.2	10.3	0.66528	0.62212	-5.99	0.6437		
11	0	0	-6.02	-6.09	9.3	8.9	0.55986	0.54201	-6.055	0.550935		
13	0	0	-6	-6.01	10.7	10.3	0.642	0.61903	-6.005	0.630515	-6.005	0.601799
1	500	0	-5.99	-5.94	9.8	9.9	0.58702	0.58806	-5.965	0.58754	0.031425	0.037275
7	500	0	-5.94	-6.01	9.8	9.9	0.58212	0.59499	-5.975	0.588555		
10	500	0	-6.12	-6.15	10.2	10.4	0.62424	0.6396	-6.135	0.63192		
16	500	0	-6.02	-6.04	9.9	9.7	0.59598	0.58588	-6.03	0.59093	-6.02625	0.599736
3	1000	0	-5.77	-5.85	10.7	10	0.61739	0.585	-5.81	0.601195	0.067488	0.018622
5	1000	0	-5.82	-5.97	10.4	10.1	0.60528	0.60297	-5.895	0.604125		
9	1000	0	-6.06	-6	9.5	9.9	0.5757	0.594	-6.03	0.58485		
14	1000	0	-5.91	-5.98	11.3	11.5	0.66783	0.6877	-5.945	0.677765	-5.92	0.616984
2	1500	0	-5.76	-5.78	9.9	10.4	0.57024	0.60112	-5.77	0.58568	0.079765	0.035852
8	1500	0	-5.84	-5.96	11	10.1	0.6424	0.60196	-5.9	0.62218		
12	1500	0	-5.85	-6.07	10.2	10.1	0.5967	0.61307	-5.96	0.604885		
15	1500	0	-5.93	-6.03	11.2	11.1	0.66416	0.66933	-5.98	0.666745	-5.9025	0.619873
20	0	1	-3.46	-3.25	24.1	24.7	0.83386	0.80275	-3.355	0.818305	0.081968	0.029984
22	0	1	-3.49	-3.24	26	25	0.9074	0.81	-3.365	0.8587		
27	0	1	-3.49	-3.31	20.7	23.7	0.72243	0.78447	-3.4	0.75345		
29	0	1	-3.31	-3.34	23.9	27.5	0.79109	0.9185	-3.325	0.854795	-3.36125	0.821313
17	500	1	-3.49	-3.5	20.1	21.5	0.70149	0.7525	-3.495	0.726995	0.02678	0.042229
23	500	1	-3.45	-3.52	23.4	25	0.8073	0.88	-3.485	0.84365		
26	500	1	-3.26	-3.31	21.8	22.5	0.71068	0.74475	-3.285	0.727715		
32	500	1	-3.27	-2.93	28.9	31.9	0.94503	0.93467	-3.1	0.93985	-3.34125	0.809553
19	1000	1	-3.27	-3.41	24	24.3	0.7848	0.82863	-3.34	0.806715	0.162534	0.088957
21	1000	1	-3.34	-3.3	24.1	24.6	0.80494	0.8118	-3.32	0.80837		
28	1000	1	-3.22	-3.1	23.6	24.8	0.75992	0.7688	-3.16	0.76436		
30	1000	1	-3.12	-3.26	25.7	25	0.80184	0.815	-3.19	0.80842	-3.2525	0.796966
18	1500	1	-3.22	-3.2	26	25.7	0.8372	0.8224	-3.21	0.8298	0.078541	0.018838
24	1500	1	-2.95	-2.9	25.4	26.2	0.7493	0.7598	-2.925	0.75455		
25	1500	1	-2.86	-2.96	25.2	27.5	0.72072	0.814	-2.91	0.76736		
31	1500	1	-2.82	-2.87	23.2	22.3	0.65424	0.64001	-2.845	0.647125	-2.9725	0.749709
33	1500	1	-2.83	-2.99	31.6	33.3	0.89428	0.99567	-2.91	0.944975	0.140379	0.065713
37	0	2	-1.69	-1.61	45.5	52.5	0.76895	0.84525	-1.65	0.8071		
39	0	2	-1.69	-1.58	45.4	52.5	0.76726	0.8295	-1.635	0.79838		
44	0	2	-1.65	-1.72	43.9	44	0.72435	0.7568	-1.685	0.740575		
46	0	2	-1.61	-1.69	47.3	43.9	0.76153	0.74191	-1.65	0.75172	-1.655	0.774444
34	500	2	-1.66	-1.31	39.7	53.1	0.65902	0.69561	-1.485	0.677315	0.018371	0.028735
40	500	2	-1.83	-1.13	46	65.6	0.8418	0.74128	-1.48	0.79154		
43	500	2	-1.75	-1.47	42.4	46.2	0.742	0.67914	-1.61	0.71057		
49	500	2	-1.53	-1.24	51	62.6	0.7803	0.77624	-1.385	0.77827	-1.49	0.739424
36	1000	2	-1.53	-1.33	46.5	51.9	0.71145	0.69027	-1.43	0.70086	0.079922	0.04721
38	1000	2	-1.69	-1.62	43.6	42.9	0.73684	0.69498	-1.655	0.71591		
45	1000	2	-1.59	-1.64	44.8	35.9	0.71232	0.58876	-1.615	0.65054		
47	1000	2	-1.44	-1.76	57.7	44.7	0.83088	0.78672	-1.6	0.8088	-1.575	0.719028
35	1500	2	-1.57	-1.75	43.9	39.3	0.68923	0.68775	-1.66	0.68849	0.086096	0.057204
41	1500	2	-1.66	-1.54	40.9	42.3	0.67894	0.65142	-1.6	0.66518		
42	1500	2	-1.42	-1.69	47.5	40.8	0.6745	0.68952	-1.555	0.68201		
48	1500	2	-1.46	-1.45	41.5	43.3	0.6059	0.62785	-1.455	0.616875	-1.5675	0.663139
											0.074875	0.028033

Table A12. Gravimetric retention data for the final stage DDJ experiments. The data have been plotted in Figure 56.

RPM	ACTUAL POLYMER DOSAGE, lbs./T	PERCENT RETENTION	AVERAGE AND ST. DEV. OF PERCENT RETENTION
0	0	0.494729	
0	0	4.862319	
0	0	5.38374	3.49541
0	0	3.240851	1.904148
500	0	2.294051	
500	0	-5.17735	
500	0	7.110902	0.169597
500	0	-3.54922	4.876332
1000	0	1.403887	
1000	0	-2.14051	
1000	0	4.244805	1.779492
1000	0	3.609793	2.496763
1500	0	0.899214	
1500	0	-0.92256	
1500	0	4.545619	1.987553
1500	0	3.427941	2.137268
0	0.993584	39.15869	
0	0.971667	37.20778	
0	1.004888	36.70798	37.9748
0	0.992391	38.82474	1.038886
500	0.983353	49.0509	
500	0.968714	40.97243	
500	1.002111	41.41299	42.30008
500	1.000792	37.76399	4.14425
1000	0.99959	33.17812	
1000	0.991841	29.39336	
1000	0.989005	28.0476	32.70475
1000	0.983666	40.19992	4.718474
1500	0.996059	29.82611	
1500	0.992616	29.86692	
1500	0.974007	32.53494	30.17396
1500	0.99064	28.46787	1.474812
0	2.01379	74.63886	
0	1.993567	79.06733	
0	1.994466	71.30068	73.74256
0	1.975284	69.96338	3.514311
500	2.007737	82.34535	
500	1.971757	85.85059	
500	2.020369	77.01761	80.93051
500	2.010828	78.5085	3.44187
1000	1.99163	71.94179	

Table A12, continued

RPM	ACTUAL POLYMER DOSAGE, lbs./T	PERCENT RETENTION	AVERAGE AND ST. DEV. OF PERCENT RETENTION
1000	1.976465	77.52385	
1000	1.994744	70.00148	73.98625
1000	2.000785	76.47789	3.113725
1500	2.002243	55.11605	
1500	2.011751	59.03676	
1500	1.970843	57.92765	59.56937
1500	2.009375	66.19703	4.084632

APPENDIX XV. STATISTICAL ANALYSIS

The data presented in Figure 24, standard deviation of electrophoretic mobility versus the polymer dosage for two mixing conditions in early Dynamic Drainage Jar experiments, were analyzed as to whether the data sets are significantly different. A chi-squared test was performed testing the hypothesis that the sample standard deviations were not equal. Since the data sets were unpaired, the method used was to take the data from 2 lbs./Ton dosage and compare the mean values. Table A13 presents this data.

Table A13. Data for standard deviation of EM distribution for two levels of mixing during the polymer addition at 2 lbs./Ton dosage level.

	750 RPM	1500 RPM
	0.45126	0.3691
	0.4521	0.419555
	0.4492	0.405838
	0.50318	0.38254
	0.4642	0.36435
	0.47152	
Mean Standard Deviation	**0.46524**	**0.38828**
Mean Variance	**0.21645**	**0.15076**

We wish to test the sample data such that

$$\overline{S_1} \neq \overline{S_2}$$

Taking the null hypothesis,

$$H_o: \quad \sigma \neq \sigma_o$$

and the alternative hypothesis,

$$H_o: \quad \sigma = \sigma_o$$

the chi-squared test takes $\chi^2_{\alpha,n-1}$ and compares with

$$\chi^2 = \frac{(n-1)S^2}{\sigma_o^2}$$

Since $\chi^2 = 7.18$, we find that $\alpha = 0.20$.